UNIVERSIDADE DO PORTO
FACULDADE DE ENGENHARIA

# Chiral Separation by Simulated Moving Bed Chromatography

*Luís Manuel Santos Pais*

May 1999

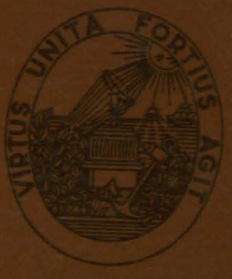

# Chiral Separation by Simulated Moving Bed Chromatography



A dissertation presented to the
Faculdade de Engenharia da Universidade do Porto
for the degree of Doctor in Chemical Engineering

by

Luís Manuel Santos Pais



May 1999

Laboratory of Separation and Reaction Engineering
School of Engineering, University of Porto
Porto, Portugal

# Agradecimentos
# Acknowledgments

Aos meus orientadores, Professor Alírio Rodrigues e Professor José Miguel Loureiro, pela oportunidade concedida, acompanhamento científico, dedicação e amizade demonstradas ao longo deste trabalho.

Ao *LSRE* (*Laboratory of Separation and Reaction Engineering*), na pessoa do Professor Alírio Rodrigues, pelas condições técnicas disponibilizadas.

A todos os professores do *LSRE*, pela simpatia e ajuda. Em particular, ao Professor José Carlos Lopes e colaboradores, pelo apoio prestado na utilização dos meios informáticos.

À colega Vera Mata, pelo acompanhamento nos estudos de SEM. Ao Avelino Da Silva, pela fotografia da instalação.

A todos os colegas do *LSRE* pela amizade, espírito de camaradagem e entreajuda demonstradas ao longo da minha permanência neste laboratório.

À Escola Superior de Tecnologia e de Gestão do Instituto Politécnico de Bragança (*ESTiG*), na pessoa do Professor Rolando Dias, pelas facilidades e apoio concedido. Agradeço também ao saudoso Professor Alcínio Miguel, ex-director da *ESTiG*, a cuja memória presto sentida homenagem.

A todos os colegas da *ESTiG*, pela amizade. Um especial obrigado a todos aqueles que me ajudaram na utilização dos meios informáticos da Escola.

À família e amigos, pelo apoio e com um pedido de desculpas pelo tempo roubado.

A todos os elementos do júri, pela sua disponibilidade na apreciação deste trabalho.

To Professor Roger-Marc Nicoud, Jean Blehaut and Frédéric Charton (*Novasep*) and Professor J. Kinkel (*Merck* and *Georg-Simon-Ohm Fachhochschule*) for helpful discussions and preparation of the chiral packings.

Financial support from the European Union under the BRITE-EURAM Programme (Contract No. BRE2-CT92-0337) is gratefully acknowledged.

*À Filomena*

*Chromatography is essentially a diluting machine.*

Daniel Tondeur

in *Dynamics of Fixed-Bed Adsorbers*,
A.E. Rodrigues *et al.* (eds.),
*Adsorption: Science and Technology*,
Kluwer Academic Publishers, 1989.

# Abstract

The general objective of this work is the study of the behaviour of the Simulated Moving Bed (SMB) processes, with applications to chiral separations. Briefly, SMB chromatography allows the continuous injection and separation of binary mixtures. The simulated countercurrent contact between the solid and liquid phases maximizes the mass transfer driving force, leading to a significant reduction in mobile and stationary phases consumption when compared with elution chromatography.

The problem of modeling a SMB separation process is analyzed by two different strategies: one, by simulating the system directly, taking into account its intermittent behaviour (the SMB model); other by representing its operation in terms of a true countercurrent system (TMB model). From the comparative study, we conclude that the prediction of the performance of a SMB operation, and so its flow-rate optimization, can be safely done by using the TMB approach.

The effect of the model parameters and operating variables on the SMB performance is analyzed in terms of four parameters: purity, recovery, solvent consumption, and adsorbent productivity. This work shows the influence of the switch time interval, recycling flow-rate, and inlet and outlet flow-rates. Also studied is the influence of axial dispersion and mass transfer resistance on the SMB performance. We conclude that the mass transfer resistance can reduce significantly the possible set of operating conditions that lead to the desired separation. Moreover, mass transfer resistance can affect the SMB operating conditions, being this influence emphasized when a higher purity requirement is desired.

The experimental operation of a Simulated Moving Bed unit was implemented in a *Licosep 12-26* SMB pilot unit (*Novasep, France*), available at the *LSRE*. Two chiral systems were considered: the bi-naphthol and the chiral epoxide enantiomers.

For the bi-naphthol system purities and recoveries higher than 95% were obtained for both extract and raffinate with an adsorbent productivity of 68 grams of racemic mixture processed per day and per liter of bed. The solvent consumption was 1.2 liter per gram of racemic mixture processed.

For the chiral epoxide system, a first set of experimental runs led to purities and recoveries higher than 90%. A productivity of 52 grams of racemic mixture per day and per liter of bed was achieved, with a solvent consumption of 0.4 liter of mobile phase per gram of racemic mixture processed. In a second set of experimental runs, we obtained 98% pure extract and raffinate, with a productivity of 34 grams per day and per liter of bed, and a solvent consumption of 1.3 liter per gram.

The experimental results obtained in the *Licosep 12-26* SMB pilot unit are reported in terms of process performance, steady-state internal concentration profiles, and transient evolution of the concentration of both species in the extract and raffinate streams. The simulation packages developed in this work are used to predict the SMB behaviour in reasonable agreement with the experimental results.

# Resumo

O objectivo deste trabalho consistiu no estudo do processo de leito móvel simulado (*Simulated Moving Bed*, SMB) com aplicações a separações quirais. Resumidamente, a cromatografia de SMB permite a injecção e separação contínua de misturas binárias. A simulação do contacto em contracorrente entre as fases sólida e líquida maximiza a força motriz de transferência de massa, permitindo uma diminuição significativa do consumo das fases móvel e estacionária comparativamente com a cromatografia de eluição.

O problema da modelização de um processo de separação por SMB foi analisado recorrendo a duas estratégias alternativas: uma, por simulação directa do sistema, levando em consideração o seu comportamento intermitente (o modelo SMB); a outro por representação da sua operação em termos de um sistema equivalente em contracorrente (o modelo TMB, *True Moving Bed*). Por estudo comparativo destas duas estratégias concluíu-se que o desempenho da operação do SMB, e assim a optimização das suas condições de operação, pode ser avaliada de forma segura por utilização do modelo TMB.

A influência dos parâmetros do modelo e das variáveis de operação no desempenho do SMB foi analisada recorrendo a quatro parâmetros: pureza, recuperação, consumo de solvente e produtividade do adsorvente. Este trabalho mostra o efeito do período de rotação, caudal de reciclo e caudais de entrada e saída. Foi também estudada a influência da dispersão axial e resistência à transferência de massa no desempenho do SMB. Concluiu-se que a resistência à transferência de massa pode reduzir significativamente o domínio de condições de operação que permitem uma desejada separação. Mais, a resistência à transferência de massa pode alterar as condições óptimas de operação do SMB, sendo esta influência particularmente importante quando se pretendem purezas elevadas.

A operação experimental de um leito móvel simulado foi efectuada na unidade piloto de SMB *Licosep 12-26* (*Novasep, França*), disponível no *LSRE*. Foram estudados dois sistemas: a separação de enantiómeros do bi-naftol e de um epóxido quiral.

Para o sistema bi-naftol, foram obtidas purezas e recuperações superiores a 95% no extrato e refinado. A produtividade do adsorvente foi de 68 gramas de mistura racémica processada por dia e por litro de leito, sendo o consumo de solvente de 1,2 litros por grama de mistura racémica processada.

Para o sistema do epóxido quiral, um primeiro conjunto de experiências conduziu a recuperações e purezas superiores a 90%. A produtividade do adsorvente foi de 52 gramas de mistura racémica processada por dia e por litro de leito, com um consumo de solvente de 0,4 litros por grama de mistura racémica processada. Num segundo conjunto de experiências foram obtidas purezas de 98% para extracto e refinado, com uma produtividade de 34 gramas por dia e litro de leito e um consumo de solvente de 1,3 litros por grama.

Os resultados experimentais obtidos na unidade piloto de SMB *Licosep 12-26* foram representados em termos do desempenho do processo, perfis internos de concentração e evolução transiente da concentração de ambos os componentes nas correntes de extrato e refinado. O simulador desenvolvido neste trabalho foi utilizado na previsão da operação do SMB, em concordância razoável com os resultados experimentais obtidos.

# Résumé

Le but générique de ce travail est l'étude des procédés à Lit Mobile Simulé (*Simulated Moving Bed*, SMB), avec des applications à la séparation de composés chiraux. En bref, la chromatographie à SMB permet l'injection continue et la séparation de mélanges binaires. Le contact à contre-courant simulé entre les phases solide et liquide rend maximale la force directrice de transfert de masse, conduisant à une réduction appréciable de la consommation des phases liquide et solide en comparaison avec la chromatographie d'élution.

Le problème de la modélisation d'un procédé de séparation à SMB est attaqué selon deux stratégies différentes: l'une, fondée sur la simulation directe du système, en tenant compte de son comportement intermitant (le modèle SMB); l'autre, partant de la représentation de son opération en termes d'un vrai système à contre-courant (le modèle TMB, *True Moving Bed*). D'après une étude comparative, nous sommes arrivés à conclure que la prévision de la performance d'une opération SMB, et donc son optimisation par rapport au débit, peut être faite en sécurité avec l'approche TMB.

L'effet des paramètres du modèle et des variables opératoires sur la performance du SMB est discutée selon quatre paramètres: la pureté, le taux de récupération, la consommation de solvant et la productivité de l'adsorbant. Ce travail montre l'influence de la période de rotation, des débits de recyclage, d'alimentation et de soutirage. L'influence de la dispersion axiale et de la résistance au transfert de masse sur la performance du SMB sont également étudiées. Nous concluons que la résistance au transfert de matière peut réduire significativement le domaine de conditions opératoires où l'on obtient la séparation souhaitée. En plus, la résistance au transfert de matière peut changer les meilleures conditions d'opération à SMB, et cet effet est particulièrement important lorsqu'on exige une plus grande pureté.

L'opération expérimentale d'une unité à SMB a été menée à bien avec un système pilote *Licosep 12-26* (*Novasep, France*), installé au *LSRE*. Deux systèmes chiraux ont été choisis: le binaphtol et les enantiomères d'un epoxide chiral.

Pour le binaphtol, des puretés et des taux de récupération au dessus de 95% ont été obtenus tant pour l'extrait que pour le raffiné, avec une productivité de l'adsorbant de 68 grammes de mélange racémique par jour et par litre de lit. La consommation de solvant a été de 1,2 litres par gramme de mélange racémique processé.

Pour l'epoxide chiral, un premier ensemble d'essais a conduit à des puretés et des taux de récupération au dessus de 90%. La productivité de 52 grammes de mélange racémique par jour et par litre de lit a été atteinte, avec une consommation de solvant de 0,4 litre de phase mobile par gramme de mélange racémique traité. Sur un deuxième groupe d'essais, nous avons réussi à atteindre des extraits et raffinés purs à 98% , avec une productivité de l'adsorbant de 34 grammes par jour et par litre de lit, et une consommation de solvant de 1,3 litres par gramme.

Les résultats expérimentaux obtenus sur le SMB *Licosep 12-26* ont été rapportés en termes de la performance du procédé, des profils de concentrations internes dans l'état stationnaire et de l'évolution transitoire de la concentration de toutes les deux espèces aux courants d'extrait et de raffiné. Les paquets de simulation développés pendant ce travail ont été utilisés pour la prévision du comportement du SMB avec un accord raisonnable avec les données experimentales.

# Table of Contents

# List of Figures

## Chapter 2 Simulated Moving Bed: Principles and Applications



## Chapter 3 Simulated Moving Bed Strategies of Modeling

## Chapter 5 Experimental Operation of a Simulated Moving Bed

# Appendices

# List of Tables

## Chapter 2 Simulated Moving Bed: Principles and Applications



## Chapter 3 Simulated Moving Bed Strategies of Modeling

## Chapter 4 Simulation and Optimization of a Simulated Moving Bed



## Chapter 5 Experimental Operation of a Simulated Moving Bed

## Appendices

# List of Symbols

| | |
|---|---|
| $A_c$ | Cross section area of a SMB column, $cm^2$ |
| $b$ | Adsorption isotherm parameter, $l_{fluid}/g$ |
| $c$ | Fluid phase concentration, g/l |
| $D_L$ | Axial dispersion coefficient, $cm^2/s$ |
| $D_c$ | Diameter of a SMB column, cm |
| $D_m$ | Molecular diffusivity, $cm^2/s$ |
| $D_{pe}$ | Effective diffusivity, $cm^2/s$ |
| $d_p$ | Particle diameter, μm |
| $H$ | Plate height, μm |
| $K$ | Initial slope of the adsorption isotherm (considering the adsorbent as homogeneous particles), $l_{fluid}/l_{particle}$ |
| $K_p$ | Initial slope of the adsorption isotherm considering only the adsorbent solid (excluding pores), $l_{fluid}/l_{solid}$ |
| $k$ | Mass transfer coefficient (used in the LDF model for homogeneous particles), $s^{-1}$ |
| $k_{pe}$ | Mass transfer coefficient (used in the LDF model for porous particles), $s^{-1}$ |
| $L$ | Length, cm |
| $L_c$ | Length of a SMB column, cm |
| $M$ | Molecular weight of the solvent, g/mol |
| $m$ | Adsorption isotherm parameter, $l_{fluid}/l_{particle}$ |
| $m$ | Flow-rate ratio, defined in *Equation 4.18* |
| $NCOL$ | Total number of columns in the SMB system |
| $N_s$ | Number of columns per section in the SMB system |
| $PR$ | Adsorbent productivity, grams/ day $l_{bed}$ |
| $PUR$ | Raffinate Purity |

| | |
|---|---|
| $PUX$ | Extract Purity |
| $Pe$ | Peclet number |
| $Q$ | Adsorption isotherm parameter, $g/l_{particle}$ |
| $Q$ | Volumetric liquid flow-rate in the TMB, $cm^3/min$ |
| $Q^*$ | Volumetric liquid flow-rate in the SMB, $cm^3/min$ |
| $Q_s$ | Solid flow-rate, $cm^3_{solid}/min$ |
| $Q_T$ | Total inlet or outlet flow-rates, $cm^3/min$ |
| $q$ | Average adsorbed phase concentration, $g/l_{particle}$ |
| $q^*$ | Adsorbed phase concentration in equilibrium with $c$, $g/l_{particle}$ |
| $RCR$ | Raffinate recovery |
| $RCX$ | Extract recovery |
| $R_p$ | Particle radius, μm |
| $SC$ | Solvent consumption, l/g |
| $T$ | Temperature, C |
| $t$ | Time variable, s |
| $t$ | Retention time, s |
| $t^*$ | Switch time interval, s |
| $t_d$ | Average dead time in the *Licosep 12-26* operation, s |
| $u_s$ | Interstitial solid velocity in the TMB operation, cm/s |
| $V$ | Molar volume of the solute at its normal boiling temperature, $cm^3/mol$ |
| $V_c$ | Column volume, $cm^3$ |
| $V_T$ | Total volume of the adsorbent bed, $cm^3$ |
| $v$ | Interstitial fluid velocity in the TMB operation, cm/s |
| $v^*$ | Interstitial fluid velocity in the SMB operation, cm/s |
| $x$ | Dimensionless axial coordinate |
| $z$ | Axial coordinate, cm |

## *Greek Symbols*

| | |
|---|---|
| $\alpha$ | Selectivity factor |
| $\alpha$ | Number of mass transfer units |
| $\beta$ | Safety margin (linear systems) |
| $\Gamma$ | Dimensionless parameter (defined in *Equation 4.2*) |
| $\gamma$ | Ratio between fluid and solid interstitial velocities in the TMB operation |

| | |
|---|---|
| $\gamma^*$ | Ratio between fluid and solid interstitial velocities in the SMB operation |
| $\varepsilon$ | Bed porosity |
| $\varepsilon_p$ | Particle porosity |
| $\varepsilon_T$ | Total porosity |
| $\eta$ | Solvent viscosity, cP |
| $\theta$ | Dimensionless time variable |
| $\lambda$ | Adsorption isotherm parameter, defined in *Equation 4.39* |
| $\tau$ | Tortuosity factor |
| $\Phi$ | Objective function of the optimization procedure |
| $\phi$ | Association factor of the solvent |
| $\psi$ | Coefficient in *Equation 5.4* |
| $\omega$ | Roots of the quadratic *Equation 4.38* |

## *Subscripts and Superscripts*

| | |
|---|---|
| $A$ | Less retained component |
| $B$ | More retained component |
| $E$ | Eluent |
| $F$ | Feed |
| $i$ | Component index ($i = A,B$) |
| $j$ | Section index ($j = I,II,III,IV$) |
| $k$ | Column index ($k = 1,2,...,NCOL$) |
| $R$ | Raffinate |
| $RF$ | Recycling flow-rate |
| $X$ | Extract |

## *List of Abbreviations*

| | |
|---|---|
| LDF | Linear driving force |
| SMB | Simulated Moving Bed |
| SMB4 | Simulated Moving Bed with 4 columns |
| SMB8 | Simulated Moving Bed with 8 columns |
| SMB12 | Simulated Moving Bed with 12 columns |
| TMB | True Moving Bed |

# Chapter 1

# Motivation and Outline

Chiral separation is an important issue in various areas and particularly in the health-related field. It is well known that the two enantiomers can have different therapeutical value and there is pressure of regulatory agencies to the separation of chiral drugs.

In view of these demands, Simulated Moving Bed (SMB) technology has been recently applied in the areas of biotechnology, pharmaceuticals and fine chemistry. Particularly, in the pharmaceutical industry, the two pure enantiomers are required for comparative biological testing. Nevertheless, the use of the SMB technology in the pharmaceutical world is not limited to laboratory tests. Its use at production scale has been considered as an alternative to up to now leading techniques such as enantioselective synthesis or diastereoisomeric crystallization.

A Simulated Moving Bed adsorber is essentially a binary separator, so particularly appropriated for chiral separations. Briefly, SMB chromatography allows the continuous injection and separation of binary mixtures. The simulated countercurrent contact between the solid and liquid phases maximizes the mass-transfer driving force, leading to a significant reduction in mobile and stationary phases consumption when compared with elution chromatography. Hence, with SMB technology, large scale separations can now be carried out under cost-effective conditions.

The selection of the SMB operating conditions is not straightforward. The main problem of the SMB operation consists in choosing the right solid (switch time interval) and liquid flow-rates. Designed for high productivity separations, SMB units usually operate at high feed concentrations leading to non-linear competitive adsorption

behaviours. Therefore, modeling and simulation tools are of crucial importance before running the system.

The aim of the thesis is to study the operation of a Simulated Moving Bed for the chromatographic separation of enantiomers.

In *Chapter 2* the Simulated Moving Bed is introduced focusing chiral separation for pharmaceutical purposes. Methods for chiral separation and chiral chromatography are reviewed. The principles of SMB technology are described and a literature survey on the applications of SMB chromatographic separation of enantiomers is presented.

*Chapter 3* introduces two modeling strategies to describe Simulated Moving Bed adsorbers. The simulated moving bed model, that considers the real shift of the injection and collection points, is compared with the true moving bed approach that considers liquid and solid flow in opposite directions. The predictions of these two models are compared in terms of steady-state performance, steady-state internal concentration profiles, and transient behaviour of the extract and raffinate purities. The influence of the degree of subdivision of the bed in the SMB model predictions is also analyzed and compared with the true moving bed performance.

In *Chapter 4*, the true moving bed model is used to carry out the simulation of a SMB unit. The effect of model parameters and operating variables on the SMB performance is studied. Both transient and steady-state behaviours are presented and the performance of the SMB operation is analyzed in terms of purity, recovery, solvent consumption, and adsorbent productivity. The separation of bi-naphthol enantiomers is used as illustrative example.

A simple optimization procedure for choosing the best SMB operating conditions is proposed. This procedure is developed addressing some behaviours found for the SMB performance and how the operating conditions influence it. Namely, an optimization procedure is proposed based on the path of equal purities.

*Chapter 5* presents the experimental operation of a SMB pilot unit. First, the SMB unit used during this work (*Licosep 12-26, Novasep, France*) is described. Then, two case studies are presented: the separation of bi-naphthol and chiral epoxide enantiomers.

For each system, a methodology for obtaining basic data (adsorption equilibrium isotherms, axial dispersion, and mass transfer coefficient) is experimentally carried out. The operation of the SMB pilot unit is described for the separation of racemic mixtures of the two systems. Experimental results are reported in terms of

process performance, steady-state internal concentration profiles and transient evolution of the concentration of both species in the extract and raffinate streams. The experimental results obtained in the SMB pilot unit are also compared with the model predictions obtained with the simulation packages developed in the previous chapters.

The main conclusions of the thesis are presented in *Chapter 6* and future work is addressed.

Chapter 2

# Simulated Moving Bed: Principles and Applications

*The importance of chirality, particularly in the health-related field, is introduced, and some examples of differences in biological activity of enantiomers are presented. Methods for chiral separation and chiral chromatography are reviewed. The main chiral stationary phases used in chiral separation are described.*

*The Simulated Moving Bed technology is introduced and a brief history of SMB applications is presented, namely the commercial Sorbex units developed by UOP and recent applications in the biotechnological and pharmaceutical fields. The principle of Simulated Moving Bed is then discussed and the different functions of a four-section SMB unit are presented. At the end of the chapter, examples of separation of enantiomers by SMB chromatography are collected, and SMB and other preparative chromatographic modes are compared in terms of process performance.*

## 2.1 Introduction

Chirality is defined as the characteristic of molecules of being mirror images of each other. Chiral molecules have, usually, a tetrahedral structure with a carbon as central atom attached to four different groups. Such molecules can occur in two mirror-image molecular forms, called enantiomers. Although they are made of the same chemical material, they are not superimposeable. Basically, chiral molecules can be thought of as a pair of hands: each one looks like the other but, when stacked upon each other, they do not coincide because the two sides of the hand (palm and back) are not identical.

Several compounds exist in nature as pure enantiomer. Human bodies are essentially asymmetrical and sensitive to chirality and its biological activity. For example, the left form of limonene tastes of lemon, while the right form tastes of orange. It is well known that the two enantiomers can have different properties in a chiral environment. Differences in the biological activity of enantiomers can be found in the flavors and fragrances fields and agrochemical, petrochemical, food or pharmaceutical industries (*Table 2.1*).

Table 2.1. Differences in the biological activity of enantiomers.
(Crosby, 1992; Sheldon, 1993)

| Name of Compound | Biological Effect of (S)-Enantiomer | Biological Effect of (R)-Enantiomer |
|---|---|---|
| Limonene | lemon odor | orange odor |
| Carvone | caraway flavor | spearmint flavor |
| Asparagine | bitter | sweet |
| Aspartame | sweet | bitter |
| Thalidomide | teratogen | sedative |
| Ethambutol | tuberculostatic | causes blindness |
| Penicillamine | antiarthritic | mutagen |
| Ketamine | anaesthetic | hallucinogen |
| Dopa | anti-Parkinson | serious side effects |
| Chloramphenicol | inactive | antibacterial |
| Propranolol | antihypertensive, antiarrhythmic | contraceptive |
| Paclobutrazol | plant growth regulator | fungicide |

In the nineties, there is an increasing interest in the separation of racemic mixtures, specially for therapeutic purposes. When chiral drugs are made without including an enantiomeric reagent or catalyst in their synthesis, the result is a fifty-fifty mixture of the two enantiomers, called racemate. These two isomers frequently have different biological activity: one enantiomer can be beneficial whereas the other may not have the same function. Instead, the second isomer may be inactive or, in the worst scenario, may even have adverse properties. Moreover, the optically pure drug may be more than twice as active as the racemate (Crosby, 1992). For example, Ibuprofen is a chiral drug used in a daily basis for pain relief, headaches and anti-inflammation. While the (S)-ibuprofen enantiomer helps the body to relief the pain, the (R)-ibuprofen is inactive. However, (S)-ibuprofen needs only 12 minutes to take effect, whereas the racemate needs 38 minutes (Stinson, 1993).

Examples of property differentiation between the two enantiomeric forms of a chiral drug are numerous and sometimes dramatic. The most sad example is the case of Thalidomide, a chiral drug prescribed in the 1960s to pregnant women who were suffering from morning sickness. In fact, this is the effect of the right form. Unfortunately, the left form proved to have tragic side effects: at the same time that Thalidomide was being prescribed to pregnant woman, there was an unusually high amount of babies born with birth defects. This problem was found to be directly correlated to the prescription of Thalidomide and its use has been discontinued since then.

Ketoprofen is an example of how opposite enantiomers can differ in pharmacological properties. While the (S)-ketoprofen is a nonsteroidal anti-inflammatory drug, the (R)-ketoprofen is being considered as a toothpaste additive to prevent periodontal disease. The same occurs with Timolol: one of its enantiomers is used to control high blood pressure; the other is prescribed to people who suffer from glaucoma, an eye disease (Stinson, 1995).

A new challenge is now being addressed to the pharmaceutical world. For many years it was common practice to market chiral drugs as racemates. However, the situation is rapidly changing and, in 1994, single enantiomers were already 20% of the best selling drugs (Stinson, 1994; *Figure 2.1*). Also according to Stinson (1997a), two-thirds of drugs in development are chiral; half are developed as single enantiomer (*Figure 2.2*). On the other hand, there is a movement to racemic switches: single enantiomers are being redeveloped from old chiral drugs originally marketed as racemates (Stinson, 1993). The production of chiral material is now a legal question in certain countries. For example, in the United States, the FDA (Food and Drug

Administration) requires toxicology data on individual enantiomers as well as the racemate (de Camp, 1989; Deutsch, 1991; U.S. FDA, 1992). FDA is considering a new rule that could change the terms of competition in the pharmaceutical industry. Specifically, FDA may rule that single enantiomers of a racemic mixture drug already approved are new chemical entities. In this way, single enantiomer forms of an old racemic mixture may be eligible for five years of marketing exclusivity (Stinson, 1997b).

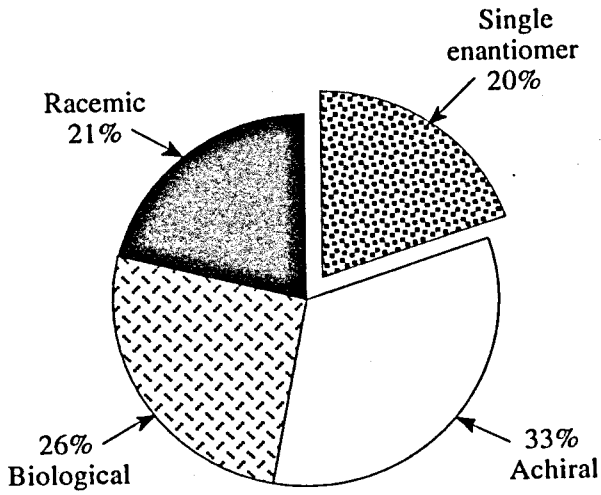


Figure 2.1. Best selling drugs.
(Stinson, 1994)

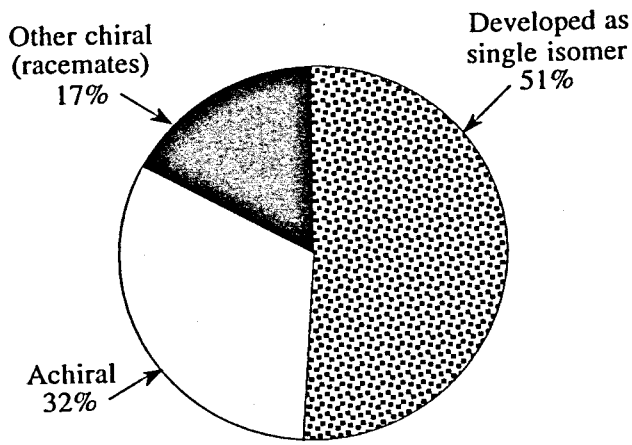


Figure 2.2. Developmental drugs worldwide.
(Stinson, 1997a)

## 2.2 Methods for Chiral Separations

As it was mentioned earlier, the two enantiomers of a racemic mixture can exhibit different properties when put into a chiral environment. These properties can be used to perform chiral discrimination. Techniques for separating enantiomers are available since the pioneering work of Louis Pasteur, who observed that the sodium-ammonium salt of racemic tartaric acid crystallized in two different forms and succeeded in separating these crystals manually (Feibush and Grinberg, 1988; Sheldon, 1993). Since then, various techniques to obtain pure enantiomers have been developed, such as selective crystallization, assymetric synthesis reactions, and chiral chromatography (Crosby, 1992; Samdani, 1993; Camilleri *et al.*, 1994; Cannarsa, 1996, Repic, 1998).

Basically, there are two approaches to obtain enantiomerically pure compounds. The first consists of preparing the racemic material which is later resolved into its two enantiomeric forms. The second method is based on a stereoselective synthesis and leads to the production of only one enantiomer. Both approaches have their advantages and disadvantages. For example, in the racemic approach (first method) the racemic material is prepared by a reaction sequence that generally is much more simpler than for the corresponding optically active forms. The racemic mixture is then separated using diastereoisomeric and enzymatic resolution methods or by chromatography in chiral stationary phases (Francotte, 1997). In the second approach, an enantiomeric reagent or catalyst is used to carry out a reaction that produces only one enantiomer. If both enantiomers are desired, two parallel steps are needed. Asymmetric synthesis has been used frequently in the past. However, this method can be economically not recommended because of the greater number of steps and the costly enantiomeric reagents needed. In fact, in 1995, 65% of the non natural enantiomeric drugs were made by resolution of racemic drugs and not by asymmetric synthesis (Stinson, 1995).

Following the interest for resolution methods, preparative chiral chromatography is getting increasing attention nowadays. Although the resolution via the formation of diastereoisomers is still often used, the direct separation of enantiomers by chromatography on chiral stationary phases has become an important alternative technique in the last years. One reason chromatography is preferred is that the process results in both high yields and purities of both enantiomers. On the other hand, this technique is applicable to a wide variety of racemic structures, since chromatographic stationary phases for enantiomer separation are now available.

## 2.3 Chiral Chromatography and Chiral Stationary Phases

The use of chromatographic techniques for the resolution of enantiomers is not new (Buss and Vermeulen, 1968). However, its use has significantly increased with the evolution of the chromatographic techniques and the design of new chiral stationary phases. Chiral chromatography is not only a method of choice to determine enantiomeric purity. The preparative potential of the method has often been recognized and the number of applications is rapidly growing (Zief and Crane, 1988; Krstulovic, 1989; Francotte and Junker-Buchheit, 1992; Perrut, 1992; Francotte, 1993; Aboul-Enein and Wainer, 1997).

Basically, there are two types of chiral stationary phases: one, which uses an enantiomeric chiral selector bound to an achiral substract such as silica; a second, which is a chiral polymer like a polysaccharide or synthetic resin made from an enantiomeric monomer or by chiral polymerization. An extensive review of preparative applications reported in literature can be found in Francotte and Junker-Buchheit (1992).

*Cellulose derivatives:*

Cellulose triacetate has received considerable attention and has been the most widely used stationary phase in preparative applications. The pioneering work was carried out by Hesse and Hagel (1973) who prepared microcrystaline cellulose triacetate for the chromatographic separation of Tröger's base enantiomers. The key of success was the heterogeneous acetylation of microcrystaline cellulose and subsequent swelling in boiling alcohol, so that the original structure of the polymer was preserved. This material in its swollen state proved to be able to the chromatographic resolution of various chiral compounds (Koller *et al.*, 1983; Rimböck *et al.*, 1985; Shibata *et al.*, 1986; Blaschke, 1986; Dingenen *et al.*, 1992). Another reason for this success is due to the easy modulation of the chiral recognition properties by simply change the derivatization group on the hydroxy functions of the glucose moieties (*Figure 2.3*).

Alternatively, Okamoto and *Daicel* researchers proposed the use of cellulose derivatives prepared under homogeneous conditions. This material, commercially known as *Chiralcel*, is dissolved, reprecipitated and coated onto the surface of a silica support. The homogeneous acetylation causes the loss of the microcrystaline structure of the cellulose, leading to a material with a lower chiral recognition ability. However, the chromatographic performance is enhanced by controlling the particle size and increasing the exchange surface. Several applications of these alternative cellulosic adsorbents can be found in the literature (Shibata *et al.*, 1986; Ichida and Shibata, 1988; Oguni *et al.*, 1995).

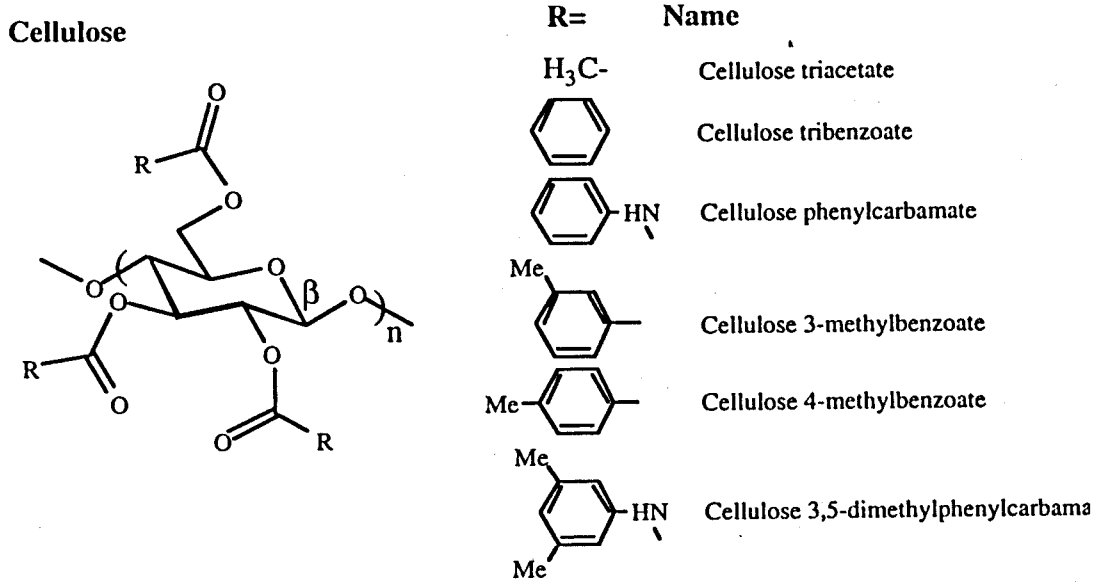


Figure 2.3. Structure of cellulose-based CSPs (Francotte, 1997).

It should be pointed out that the chiral discrimination mechanism of coated cellulose is quite different from the one for the microcrystalline structure. The last one operates by an inclusion mechanism, as it was first proposed by Hesse and Hagel (1976), and is characterized by slow sorption kinetics. For coated cellulose, this mechanism is probably a more rapid but less selective adsorption-desorption process (Francotte *et al.*, 1985; Isaksson *et al.*, 1990; Francotte and Junker-Buchheit, 1992).

More than 70% of the reported preparative separation of enantiomers have been performed using cellulose-based chiral stationary phases, since it has a recognized versatility, high loading capacity and low production costs (Francotte, 1998; *Figure 2.4*). In fact, Eric Francotte estimated that a very high percentage of the racemates prepared for biological purposes can be resolved on a limited number of polysaccharides derivatives.

*Brush-type phases:*

The best known and also the first commercially available brush-type chiral phase for HPLC was based on N-(3,5-dinitrobenzoyl)phenylglycine (DNBPG) which was immobilized on a silica support. It was synthesized by Pirkle and co-workers and its chiral recognition mechanism was extensively studied (Pirkle and Pochapsky, 1989). Other frequently used brush-type phase is derived from the leucine amino acid (DNBLeu). These chiral stationary phases are commercially available for both analytical and preparative separations, since they are stable at high pressures and exhibit

good chromatographic performances (Zief, 1988). This fact may justify its second position on the list of the most used chiral stationary phases for preparative chromatographic enantioseparations.

*Polyacrylamides and polymethacrylamides phases:*

Polyacrylamides and polymethacrylamides are polymeric chiral stationary phases, first proposed by Blaschke (1986). Some preparative applications were since then reported. However, the original gel structure confined its use to low pressure applications. Fortunately, improvements on the mechanical structure of this material were achieved by polymerization of the acrylic monomer on the surface of a silica gel support.

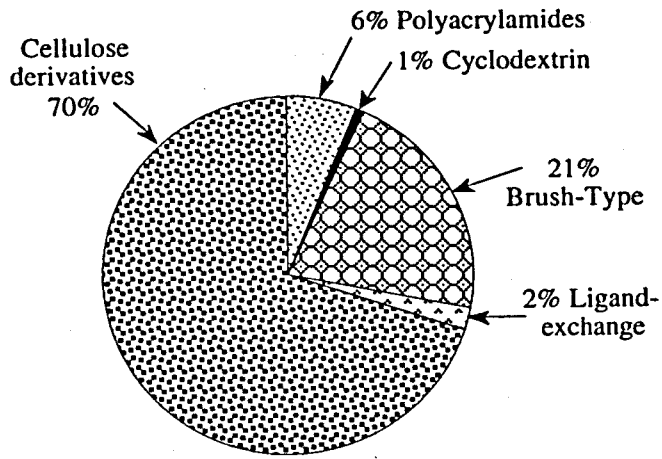


Figure 2.4. Most used CSPs for chromatographic enantioseparation (Francotte, 1998).

*Ligand-exchange phases:*

Ligand-exchange chromatographic phases for the separation of chiral compounds were first developed by Davankov and co-workers (1971; 1973). These chiral stationary phases are based on the reversible formation of complexes between metal ions (usually $Cu^{2+}$ and $Ni^{2+}$) and a chiral complexing agent like α-amino acid. Gübitz and co-workers (1981) extended this principle to silica-based stationary phases. This type of chiral phases is commercially available for preparative enantioseparations.

*Cyclodextrins :*

Cyclodextrins are a family of cyclic D-gluco-oligossacharides produced from starch by enzymatic action. Cyclodextrins with six to twelve D-glucose units can be produced, but only those containing six, seven or eight (α, β or γ-cyclodextrins) units

are commercially available. Cyclodextrins can form stable inclusion complexes in their cavities with a wide variety of molecules. The size of the cavity and the nature of the substituent play the decisive role for chiral discrimination. Initially the cyclodextrins were cross-linked to give a gel structure, but higher efficiency can be obtained by immobilization in silica gel. The optimization of the enantioseparation can be achieved by controling several factors, such as pH, temperature and buffer concentration, or the concentration and nature of the organic modifier (Armstrong and Han, 1988; White, 1991).

The design and development of chiral stationary phases are far away to be completed. Some reviews of the commercially available chiral stationary phases for enantioseparation can be found in literature (Däppen *et al.*, 1986; Francotte and Junker-Buchheit, 1992; Francotte, 1997; Stalcup, 1997). The need for more sophisticated production processes enhanced the scale up from analytical to preparative scale. The goal is to produce selective and stable chiral stationary phases. Kinkel and co-workers (1991) proposed a guideline for the optimization of preparative chromatographic separations of enantiomers. The criterion for choosing a chiral stationary phase is not only confined to chiral selectivity. When dealing with preparative chromatography, other parameters are equally important, such as loading capacity of the adsorbent, solubility of the solute in the mobile phase, and mechanical and chemical stability of the chiral stationary phase (Francotte, 1996).

## 2.4 Simulated Moving Bed Technology: An Introduction

Adsorption and chromatographic processes are widely used in chemical industry for separation, purification, or recovery purposes. Extensive reviews about adsorption techniques with applications in the field of preparative and production scale chromatography can be found in literature (Giddings, 1965, 1990; Rodrigues and Tondeur, 1981; Ruthven, 1984; Rodrigues *et al.*, 1989; Suzuki, 1990; Dondi and Guiochon, 1992; Ganetsos and Barker, 1993; Guiochon *et al.*, 1994).

Adsorption processes are generally more complex than the more conventional separation methods such as fractional distillation, solvent-aided separations, or crystallization. However, separation by adsorption can be achieved for some systems which are either difficult or impossible to obtain by other simple methods (Broughton, 1977, 1984).

Simulated Moving Bed (SMB) is one of the most powerful and promising

techniques for preparative scale chromatography. Briefly, the SMB technology allows the continuous injection and separation of binary mixtures. The simulated countercurrent contact between the solid and liquid phases maximizes the mass-transfer driving force, leading to a significant reduction in mobile and stationary phases consumption when compared with elution chromatography.

In the Chemical Engineering field, the concept of the Simulated Moving Bed has been known since 1961 when the first patent by *UOP* (*Universal Oil Products, Des Plaines, Illinois, USA*) appeared (Broughton and Gerhold, 1961). This technology was originally developed in the areas of petroleum refining and petrochemicals, and become known generally as the *Sorbex* process (Broughton, 1968, 1984; Broughton *et al.*, 1970; de Rosset *et al.*, 1981; Johnson, 1989; Johnson and Kabza, 1993; Gembicki *et al.*, 1997). More than 100 *Sorbex* units have been licensed until now, leading to a production of more than 10 millions tons per year of desired products (*Table 2.2*, Gattuso *et al.*, 1994). An alternative process for the production of p-xylene using the SMB technology was also developed in 1973 by the *Toray Industries* (*Tokyo, Japan*) (Otani, 1973; Otani *et al.*, 1973).

Table 2.2. Commercial *Sorbex* units.
(Gattuso *et al.*, 1994).

| Process | Separation | Units licensed |
|---|---|---|
| *Parex* | p-Xylene from C8 aromatics | 53 |
| *Molex* | n-Paraffins from branched and cyclic hydrocarbons | 33 |
| *Olex* | Olefins from paraffins | 6 |
| *Cymex* | p- or m-Cymene from cymene isomers | 1 |
| *Cresex* | p- or m-Cresol from cresol isomers | 1 |
| *Sarex* | Fructose from corn syrup | 5 |
| *Citrex* | Citric acid purification | 1 |

Other successful SMB processes in the carbohydrate industry are the production of high-fructose corn syrup (HFCS) and the recovery of sucrose from molasses. This technology was also originally developed by *UOP* in 1977, known as the *Sarex* process (de Rosset *et al.*, 1981; Gembicki *et al.*, 1997). With the expiration of the *UOP* patents,

other companies developed alternative processes for the fructose-glucose separation, such as *Illinois Water Treatment* (*Rockford, Illinois, USA*), *Mitsubishi* (*Tokyo, Japan*), *Finnish Sugar* (*Kantvik, Finland*), and *Amalgamated Sugar Co.* (*Twin Falls, Idaho, USA*) (Heikkilä, 1983; Nicoud, 1992; Rearick *et al.*, 1997).

Developed for large-scale hydrocarbon and carbohydrate separations, the SMB technology has found new applications in the areas of biotechnology, pharmaceuticals and fine chemistry. Recently, *UOP* has announced that SMB *Sorbex* technology can be adapted to process small scale separations, including those typically found in the pharmaceutical and biotechnology industries (Keller II, 1995; Gattuso *et al.*, 1994, 1995, 1996). Following the increasing interest in preparative chromatographic separations, other companies developed alternative SMB schemes. For example, *Separex* (now *Novasep, Vandœuvre-lès-Nancy, France*) and the *Institut Français du Pétrole* (*Rueil-Malmaison, France*) developed a commercial SMB plant where the unique rotary valve, used in the *Sorbex* technology, was replaced by a combination of commonly used chromatography columns and commercial valves (Nicoud, 1992). *Novasep* offers now the *Licosep* SMB systems for a full range of production rates: from the *Licosep Lab 12/26*, which is capable to separate 10 to 1000 grams per day, to the *Industrial Licosep 6/450*, which can perform industrial enantioseparations with a productivity of 5 to 50 tons per year. Other suppliers of semi-preparative and preparative SMB equipments are *Prochrom* (*Champigneulles, France*), *Mitsubishi* (*Tokyo, Japan*), *Advanced Separation Technologies Inc.* (*Lakeland, Florida, USA*), or *Knauer* (*Berlin, Germany*).

Small scale SMB units constitute a useful tool for the pharmaceutical industry. For preliminary biological tests, only a few grams of the chiral drug are needed. Furthermore, SMB can provide the two pure enantiomers, which are required for comparative biological testing (Francotte, 1998). On the other hand, pharmaceutical companies work with short drug development times. SMB technology, combined with proper chromatographic chiral stationary phases now available, can be a quick system, easily to set up, enhancing at the same time a high throughput of drug material (Guest, 1997). *Table 2.3* presents some recent patents on SMB chromatography, showing the increasing interest on this technology for the separation of optical isomers and for continuous chromatographic separation of sugars.

However, the use of SMB technology in the pharmaceutical industry is not limited to laboratory tests. Its use at production scale is been considered as an alternative to up to now leading techniques such as enantioselective synthesis or diastereoisomeric crystallization. Large scale chromatographic separations were in the

past limited mainly due to the high cost of the adsorbent, the high dilution of products, and the large amounts of mobile phase needed. With the introduction of the Simulated Moving Bed technology, large scale separations can now be carried out under cost-effective conditions. Moreover, in large scale chiral separation processes, new trends are being developed like coupling SMB with other techniques such as racemization and enantioselective crystallization (Blehaut, 1997; Canvat *et al.*, 1997).

Simulated Moving Bed technology found new preparative and industrial applications. Because it is basically a binary separation system, it is specially suitable for pharmaceutical process development. Furthermore, it offers many advantages over conventional preparative chromatography, leading to cleaner, smaller, safer, and faster processes (Nicoud, 1997).

Table 2.3. Recent U.S. Patents on Simulated Moving Bed.

| Title | Inventors | Assignee | Patent Number and Date |
|---|---|---|---|
| Process for Separating Optical Isomers | Yamashita and Shoji | Daicel Chemical Industries, Ltd. (Osaka, Japan) | 5,126,055 (1992) |
| Process for Recovering Optical Isomers and Solvent, Process for Using Solvent by Circulation and Process for Reusing Optical Isomers in Optical Resolution | Negawa and Shoji | | 5,434,298 5,434,299 5,498,752 5,763,645 (1995a, b; 1996; 1998) |
| Simulated Moving Bed Separation System | | | 5,456,825 (1995c) |
| Simulated Moving Bed Chromatographic Separation Process | Ikeda *et al.* | | 5,770,088 (1998) |
| Chromatographic Simulated Mobile Bed Separation Process with Dead Volume Correction Using Period Desynchronization | Hotier and Nicoud | Institut Français du Pétrole (Rueil-Malmaison, France) and Separex (Champigneulles, France) | 5,578,215 (1996a) |
| Chromatographic Simulated Mobile Bed Separation Process with Dead Volume Correction Using Length Reduction | | | 5,578,216 (1996b) |
| Chromatographic Simulated Mobile Bed Separation Process with Dead Volume Correction Using an Increase in Flow Rate | Hotier *et al.* | Institut Français du Pétrole (Rueil-Malmaison, France) | 5,582,736 (1996) |

Table 2.3. (continued) Recent U.S. Patents on Simulated Moving Bed.

| Title | Inventors | Assignee | Patent Number and Date |
|---|---|---|---|
| Process for Regulating at Least One Fluid Flow Circulating in a Simulated Moving Bed Chromatographic Separation Loop | Cohen *et al.* | Institut Français du Pétrole (Rueil-Malmaison, France) | 5,685,992 (1997) |
| Process for Simulated Moving Bed Separation with a Constant Recycle Rate | Hotier | | 5,762,806 (1998) |
| Small Scale Simulated Moving Bed Separation Apparatus and Process | Priegnitz | UOP (Des Plaines, Illinois, USA) | 5,470,464 (1995) |
| Small Scale Simulated Moving Bed Separation Process | | | 5,565,104 (1996) |
| Chiral Separation by Simulated Moving Bed Chromatography Operating at Low k' Values | Priegnitz and McCulloch | | 5,518,625 (1996) |
| Separation by Simulated Moving Bed Chromatography Operating at Low k' Values Using Weakly Interating Adsorbents as the Stationary Phase | | | 5,626,762 5,645,729 (1997a,b) |
| Simulated Moving Bed Adsorptive Separation Process | Moran | | 5,635,072 (1997) |
| Simulated Moving Bed Adsorptive Separation Apparatus | | | 5,705,061 (1998) |
| Chromatographic Separator Sorbent Bed Preparation | Kearney and Mumm | The Amalgamated Sugar Company (Ogden, Utah, USA) | 4,990,259 (1991) |
| Time Variable Simulated Moving Bed Process | Kearney and Hieb | | 5,102,553 (1992) |
| Process and a Device for Continuous Chromatography | Reuter | Reuter Chemischer Apparatebau GmbH (Freiburg, Germany) | 5,578,111 (1996) |
| Continuous Chromatography | | | 5,770,087 (1998) |
| Method for Fractionating a Solution | Heikkila *et al.* | Xyrofin Oy (Finland) | 5,730,877 (1998) |
| Fractionation Method of Sucrose-Containing Solutions | Hyoky, *et al.* | Cultor Ltd. (Helsinki, Finland) | 5,795,398 (1998) |

## 2.5 The Principle of Simulated Moving Bed Technology

The principle of Simulated Moving Bed operation can be best understood by reference to the equivalent True Moving Bed (TMB) process. In the ideal TMB operation, liquid and solid flow in opposite directions (*Figure 2.5*). Furthermore, liquid and adsorbent streams are continuously recycled: the liquid flowing out of section IV is recycled to section I, while the solid coming out of section I is recycled to section IV. The feed is continuously injected in the middle of the system and two product lines can be collected: the extract, rich in the compounds that are more retained and so preferentially carried with the solid phase, and the raffinate, rich in the less retained species that move upwards with the liquid phase. Pure eluent is continuously injected at the beginning of section I, with the liquid recycled from the end of section IV.

Because of the addition and withdrawal of the four streams (eluent, extract, feed, and raffinate), the TMB unit is divided into four sections:

Section I, begins with the eluent inlet, and ends in the extract withdraw point;
Section II, begins after the extract withdraw point, ends before the feed inlet;
Section III, which begins with the feed inlet, ends in the raffinate withdraw point;
Section IV, begins after the raffinate withdraw point, ends before the eluent inlet.

In the TMB operation, the solid flow-rate is constant all over the unit. However, due to the injection and withdrawal points, the liquid flow-rates differ from section to section. This fact, able the four sections of the unit to perform different functions.

To simplify the description of the function of each section, let us consider a feed mixture containing only two components: component A, the less adsorbed species and preferentially recovered in the raffinate, and species B, the more retained component and desirably recovered in the extract.

In sections II and III the two components must move in opposite directions. The less retained component A must be desorbed and carried with the liquid phase, while the more retained species B must be adsorbed and carried with the solid phase. Considering that in these zones the objective is to prevent the contamination of the extract and raffinate streams by the undesired component, we can summarize saying that section II is the zone of desorption of the less retained species A, while section III is the zone of adsorption of the more retained component B.

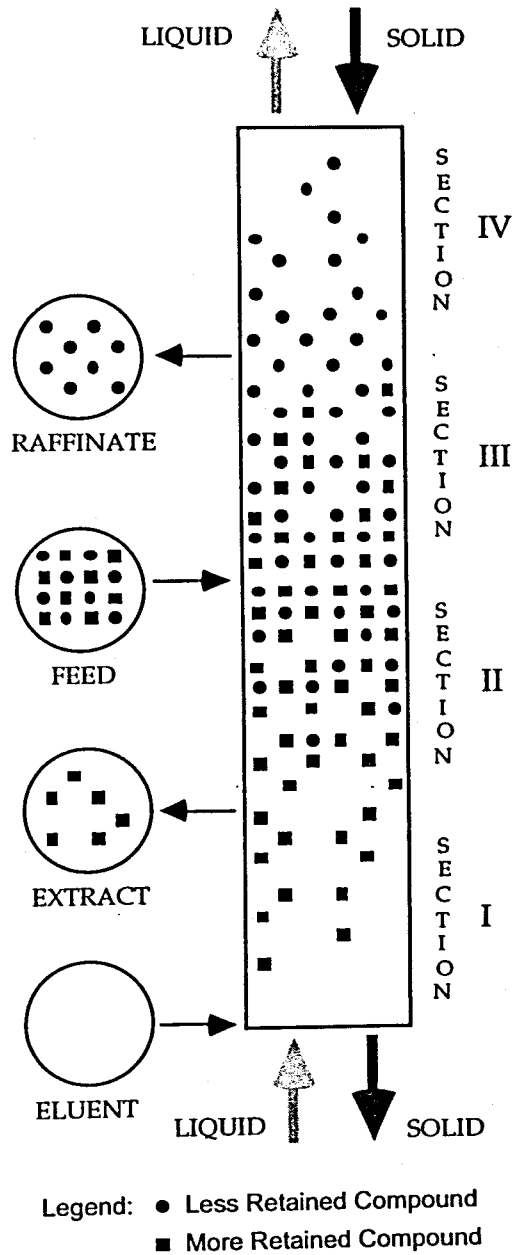


Figure 2.5. Schematic diagram of a True Moving Bed.

In section IV both components must be adsorbed in order to regenerate the eluent that will be recycled to the first zone. Since the component A is the less retained species, the conditions for adsorption of this component will allow also the adsorption of the more retained species.

On the other hand, section I is the zone of solid regeneration. In this section, both components must be desorbed in order to obtain a solid phase free from both components at the beginning of this zone. Since the component B is the more retained species, the conditions for desorption of this component will allow also the desorption of the less retained component.

Summarizing, each section plays a different function regarding its critical component (*Figure 2.6*). *Figure 2.7* presents typical concentration profiles in the liquid phase of a true moving bed, and *Table 2.4* summarizes the different roles of each section in the TMB operation.

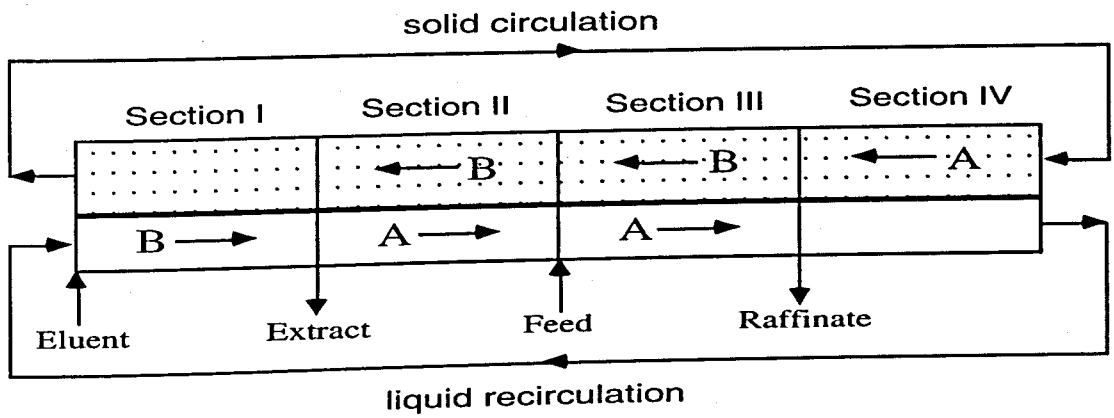


Figure 2.6. Schematic diagram of a True Moving Bed with the desired net fluxes of the two components in each section.

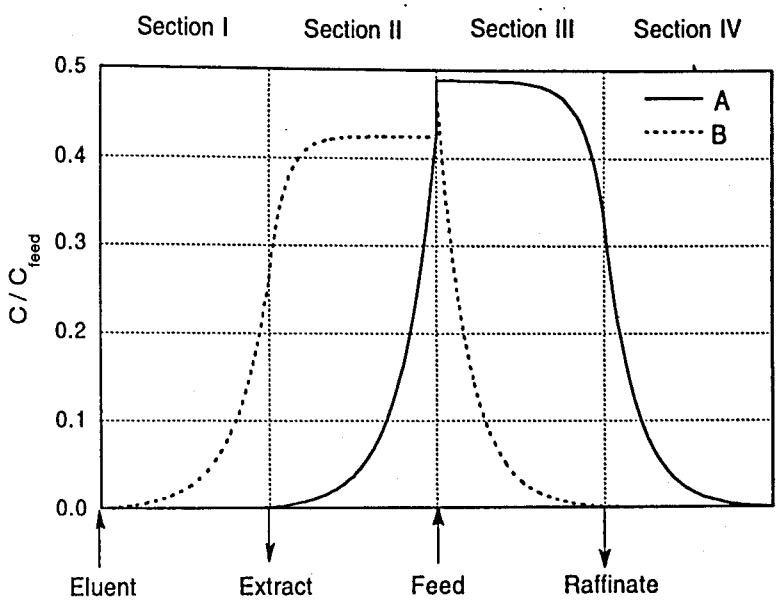


Figure 2.7. Typical internal concentration profiles in a True Moving Bed.
(A - Less retained component; B - More retained component)

Table 2.4. Functions of the four different sections of a True Moving Bed.

| Section | Role | Goal |
|---|---|---|
| I | Desorption of B | Ensure that the solid that reaches the beginning of this section is completely free from the two species and can be recycled to zone IV, using it as clean adsorbent. |
| II | Desorption of A | Prevent that the less retained component A reaches the beginning of this section and contaminates the extract. |
| III | Adsorption of B | Prevent that the more retained component B reaches the end of this section and contaminates the raffinate. |
| IV | Adsorption of A | Ensure that the liquid that reaches the end of this section is completely free from the two species and can be recycled to zone I, using it as pure eluent. |

The operation of a true moving bed introduces problems concerning the movement of the solid phase. A uniform flow of both solid and liquid is difficult to obtain and also mechanical erosion of the adsorbent phase will occur. In view of these difficulties, a simulated moving bed technique was developed in order to retain the process advantages of continuous and countercurrent flow without introducing the problems associated with the actual movement of the solid phase (*Figure 2.8*).

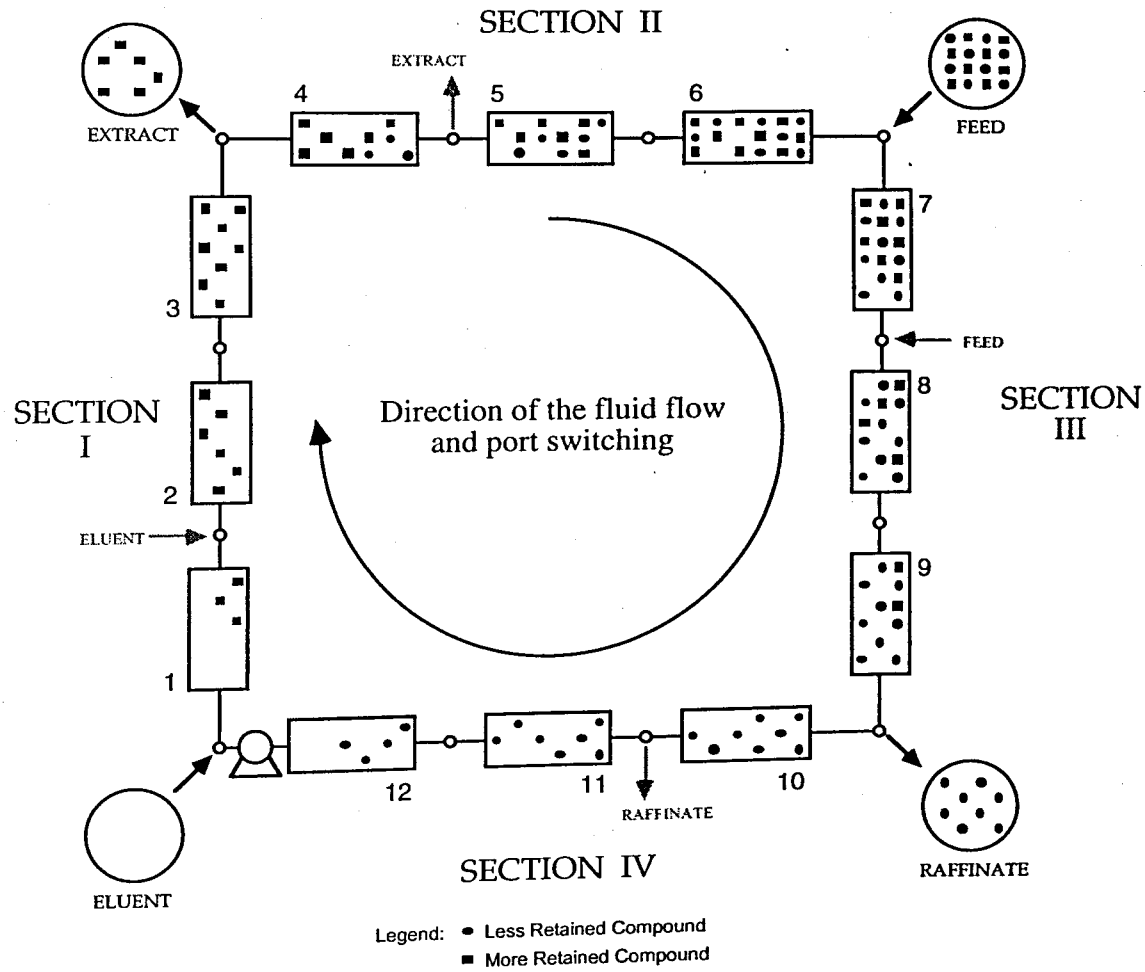


Figure 2.8. Schematic diagram of a Simulated Moving Bed.

In the simulated moving bed system the solid phase is fixed and the positions of the inlet and outlet streams move periodically. This shift, carried out in the same direction of the liquid phase, simulates the movement of the solid phase in the opposite direction.

However, it is impractical to move the liquid inlet and withdrawal positions continuously. Nevertheless, approximately the same effect can be obtained by dividing the adsorbent bed into a number of fixed-bed columns and providing multiple access lines for the liquid streams between each column. Thereby, the four liquid access lines between each column can be used to perform a discreet movement of the inlet and outlet streams in the same direction of the liquid phase.

In the *Sorbex* SMB technology developed by *UOP* a complex rotary valve is used to periodically change the position of the eluent, extract, feed, and raffinate lines along the adsorbent bed (Broughton and Gerhold, 1961). At any particular moment, only four lines between the rotary valve and the adsorbent bed are active. However, there are alternative techniques to perform the port switching. As a general rule, scaling down of the *Sorbex* flowsheet becomes less economical than using a set of individual on-off valves connecting the inlet and outlet streams to each node between columns (Keller II, 1995; Humphrey and Keller II, 1997).

## 2.6 Applications of Simulated Moving Bed Technology in the Separation of Enantiomers

Since the sixties, SMB technology has been applied to industrial scale separations, mainly in the petrochemical field for the production of p-xylene and n-paraffins and in carbohydrate industry for the production of fructose.

Recently, this technology has been applied in the pharmaceutical industry for the separation of chiral drugs. Generally, for pharmaceutical applications, small size SMB units are preferable and a special emphasis is addressed to the versatility of this type of units to perform different chiral separations without major design modifications (Hotier, 1992; Nicoud, 1993).

Following the increasing interest in the SMB technology for chiral separations, recent examples of resolution of enantiomers by SMB liquid chromatography from laboratory to industrial scale have been published and are summarized in *Table 2.5*.

Table 2.5. Recent examples of resolution of enantiomers by SMB chromatography.

| Racemic mixture | Stationary phase | Mobile phase | Selectivity factor (linear) | Stationary phase inven tory (ml) | Purity (%) | Productivity (g feed / day lbed) | Absolute Productivity (g feed/day) | Solvent Consump. (l / g feed) | References |
|---|---|---|---|---|---|---|---|---|---|
| 1-phenylethanol | Chiralcel OD (20 µm) | hexane-iso propanol (9:1) | | 377 | 98 | 49.2 | 18.5 | 2.54 | Negawa and Shoji (1992) |
| D-L Threonine | Chirosolve L (200 µm) | buffer acetic acid cupric acetate | 1.67 | 6080 | 100 | 5.0 | 30.2 | 0.50 | Fuchs *et al.* (1992) |
| Sandoz epoxide | MCTA (25-40 µm) | methanol | 1.26 | 701 | 98 | 31.2 | 21.9 | 0.40 | Nicoud *et al.* (1992, 1993a) |
| Praziquantel | MCTA (25-40 µm) | methanol | 1.76 | 218 | 92 | 98.9 | 21.6 | 0.29 | Ching *et al.* (1993) |
| Sandoz epoxide | Chiralcel OD (20 µm) | hexane-isopropanol (7:3) | 1.44 | 241 | 97 | 47.7 | 11.5 | 0.25 | Küsters *et al.* (1995) |
| EMD 53986 | Cellusphere (20-45 µm) | methanol | 1.80 | 361 | 97 | 162 | 58.3 | 0.74 | Charton and Nicoud (1995) |
| Praziquantel | MCTA (25-40 µm) | methanol | 1.76 | 353 | 97 | 32.6 | 11.5 | 0.43 | Lim and Ching (1996) |
| 3-chloro-1-phenyl-propanol | Chiracel OD (50 µm) | hexane-isopropyl alcohol (80:20) | 1.30 | 314 | 99 | 31.2 | 9.8 | 0.85 | Dandekar *et al.* (1996) |

Table 2.5. (continued) Recent examples of resolution of enantiomers by SMB chromatography.

| Racemic mixture | Stationary phase | Mobile phase | Selectivity factor (linear) | Stationary phase inven tory (ml) | Purity (%) | Productivity (g feed / day lbed) | Absolute Productivity (g feed/day) | Solvent Consump. (l / g feed) | References |
|---|---|---|---|---|---|---|---|---|---|
| EMD 53986 | Chiralpak AD (20 µm) | ethanol | 3.10 | 212 | 99 | 407 | 86.4 | 1.3 | Schulte *et al.* (1997) |
| Tramadol | Chiralpak AD (20 µm) | benzine-2-propanol (95:5) | 2.13 | 424 | 99.9 | 680 | 288 | 0.14 | Cavoy *et al.* (1997) |
| Guaifenesine | Chiracel OD (20 µm) | heptane-ethanol (65:35) | 2.19 | 193 | 99.5 | 168 | 32.4 | 0.38 | Francotte and Richert (1997) |
| Binaphthol | DNBPG-Silica (25-40 µm) | heptane-iso propanol (72:28) | 1.44 | 446 | 97 | 68.2 | 30.4 | 1.19 | Pais *et al.* (1997a,b) |
| Racemic drug | Chiralpak AD (20 µm) | hexane-2-propanol (95:5) | 1.8 | 446 | 99 | 280 | 125 | 0.32 | Guest (1997) |
| "DOLE" | Chiralcel OF (20 µm) | hexane-isopropyl alcohol (1:1) | | 6283 | 98.5 | 19.6 | 123 | 0.22 | Nagamatsu *et al.* (1998) |
| Sandoz epoxide | MCTA (45 µm) | methanol | 1.28 | 420 | 91 | 52.1 | 21.9 | 0.40 | Pais *et al.* (1998) |

Productivity is defined as the amount of racemic mixture treated per volume of adsorbent bed and per unit of time.

Absolute productivity is defined as the amount of racemic mixture treated per unit of time.

Solvent consumption is defined as the total amount of solvent used (in eluent and feed) per unit of racemic amount treated.

Both SMB productivity and solvent consumption depend on the selectivity factor of the separation system. *Figure 2.9* presents some experimental productivities obtained for the separation of enantiomers by SMB chromatography published in literature. Experimental data, presented in *Table 2.5*, represents systems which use an inventory of stationary phase between 200 and 700 ml, and purities obtained are, at least, 97%. In this way, *Figure 2.9* shows the range of productivities that can be expected in a SMB pilot unit for the separation of enantiomers.

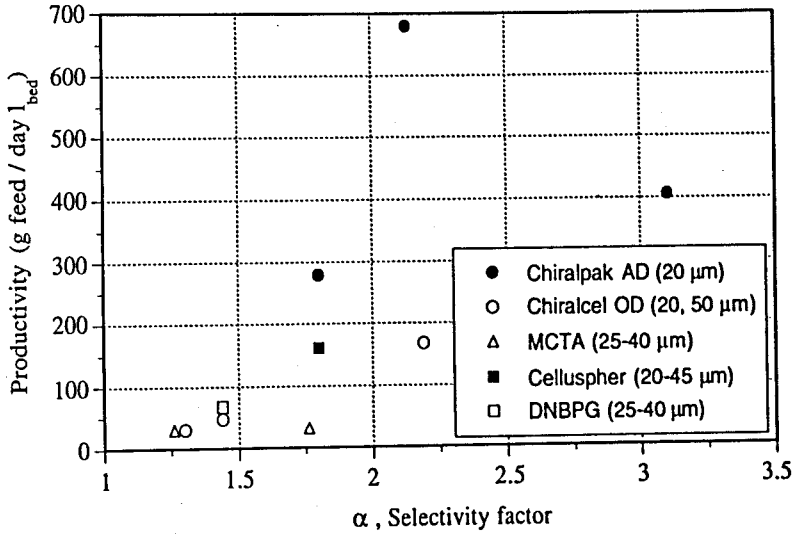


Figure 2.9. Influence of the selectivity factor on SMB productivity (experimental results reported in literature: purities at least 97%, stationary phase inventory between 200 and 700 ml, particle diameter between 20 and 50 µm).

## 2.7 Comparison between Simulated Moving Bed Technology and Other Preparative Chromatographic Modes

The Simulated Moving Bed concept was developed in order to overcome the limitations of conventional batch chromatography, mainly the discontinuous character of the process and its high cost due to the large eluent and adsorbent requirements.

*Table 2.6* presents some comparative results between SMB and other preparative chromatographic modes. This comparison is often difficult to establish essentially for two main reasons: first, different batch chromatographic modes are available, from the classical elution chromatography to more complex techniques such as recycling and displacement chromatography. Of course, the performance will depend on which chromatographic mode is used. On the other hand, comparisons are often

Table 2.6. Comparison between SMB and other chromatographic modes. Experimental results reported in literature.

| Racemic mixture | Selectivity factor (linear) | Batch chromatographic mode | Productivity SMB/Batch | Solvent Consumption Batch/SMB | References |
|---|---|---|---|---|---|
| 1-phenylethanol | | Elution | 16 | 87 | Negawa and Shoji (1992) |
| Sandoz epoxide | 1.26 | Elution | | 100 | Nicoud *et al.* (1992, 1993a) |
| | | Elution (overloaded) | 0.6 | 8 | |
| WEB 2170 | 1.77 | Elution | 45 | 2.3 | Nicoud *et al.* (1993b) |
| | | Recycling | 23 | 1.0 | |
| Sandoz epoxide | 1.44 | Elution | 0.6 | 5.4 | Küsters *et al.* (1995) |
| Tramadol | 2.13 | Elution | 3.1 | 3.5 | Cavoy *et al.* (1997) |
| Guaifenesine | 2.19 | Elution | 2.7 | 6.3 | Francotte and Richert (1997) |
| Formoterol | 1.31 | Elution | 6.3 | 5.2 | Francotte and Richert (1997) |
| Hypolipidaemic | 1.83 | Elution | 25.9 | 33.8 | Francotte (1998) |
| "DOLE" | | Elution | 22 | 22 | Nagamatsu *et al.* (1998) |
| Rolipram | 1.66 | Elution | 2.8 | | Möller (1998) |
| | | Recycling | 1.5 | | |
| Propylrolipram | 1.20 | Recycling | 0.8 | 1.4 | Möller (1998) |

carried out without optimization of the operating conditions.

Nevertheless, some general conclusions can be established. The solvent consumption and the dilution of products are always lower for SMB operation. For batch chromatography, maximizing productivity and minimizing solvent consumption are two non compatible tasks. Since the solvent consumption is often the largest expense in a preparative operation, this fact can justify the use of SMB systems over batch chromatographic methods (Nicoud *et al.*, 1998; Nicoud and Ludemann-Hombourger, 1998).

The interest for SMB operation increases for low selectivity separations. At high selectivity, the column can be highly loaded and there is little differences between the performances of SMB and other discontinuous techniques (Hashimoto *et al.*, 1993; Nicoud *et al.*, 1998; Cox *et al.*, 1998).

Generally, batch processes are more economic at very small scale if we take into account the lower cost of equipment. At larger scales, however, the savings in both solvent and chiral stationary phases make SMB technology the right choice (Nicoud, 1997; Schulte, 1997; Cox, 1998; Cox *et al.*, 1998).

In view of these generic properties, SMB technology is particularly appropriate for chiral separations. The resolution of enantiomers is usually a binary separation problem characterized by low selectivities and high costs of eluent and chiral stationary phases.

## 2.8 References

Aboul-Enein, H.Y., and Wainer, I.W., *The Impact of Stereochemistry on Drug Development and Use*, Chemical Analysis Series, Volume 42, John Wiley & Sons, England (1997).

Armstrong, D.W., and Han, S.M., "Enantiomeric Separation in Chromatography," *CRC Crit. Rev. Anal. Chem.* **19**, 175-224 (1988).

Blaschke, G., "Chromatographic Resolution of Chiral Drugs on Polyamides and Cellulose Triacetate," *J. Liq. Chromatogr.* **9**, 341-368 (1986).

Blehaut, J., "Large Scale Separation of Optical Isomers," *Recent Advances in Industrial Chromatographic Processes*, R.-M. Nicoud, ed., Nancy, France, p. 8-9 (1997).

Broughton, D.B., and Gerhold, C.G., "Continuous Sorption Process Employing Fixed Bed of Sorbent and Moving Inlets and Outlets," U.S. Patent No. 2,985,589 (1961).

Broughton, D.B., "Molex: Case History of a Process," *Chem. Engng Prog.* **64**, 60-65 (1968).

Broughton, D.B., Neuzil, R.W., Pharis, J.M., and Brearley, C.S., "The Parex Process for Recovering Paraxylene," *Chem. Engng Prog.* **66**, 70-75 (1970).

Broughton, D.B., "Bulk Separations via Adsorption," *Chem. Engng Prog.* **73**, 49-51 (1977).

Broughton, D.B., "Production-Scale Adsorptive Separations of Liquid Mixtures by Simulated Moving-Bed Technology," *Sep. Sci. Tech.* **19**, 723-736 (1984).

Buss, D.R., and Vermeulen, T., "Optical Isomer Separation. Quest for a New Biochemical Technology," *Ind. Engng Chem.* **60**, 12-28 (1968).

Camilleri, P., Biasi, V., and Hutt, A., "Resolving the Problem," *Chem. Britain*, January, 43-46 (1994).

Cannarsa, M.J., "Single Enantiomer drugs: New Strategies and Directions," *Chem. Ind.*, May 20, 374-378 (1996).

Canvat, J.P., Deleers, M., Duchêne, G., Hamende, M., Cavoy, E., and Zimmermann, V., "Methodology and Problems to Be Solved to Implement an Industrial GMP production using a SMB System, *Recent Advances in Industrial Chromatographic Processes*, R.-M. Nicoud, ed., Nancy, France, p. 14-17 (1997).

Cavoy, E., Deltent, M.-F., Lehoucq, S., and Miggiano, D., "Laboratory-Developed Simulated Moving Bed for Chiral Drug Separations. Design of the System and Separation of Tramadol Enantiomers," *J. Chromatogr. A* **769**, 49-57 (1997).

Charton, F., and Nicoud, R.-M., "Complete Design of a Simulated Moving Bed," *J. Chromatogr. A* **702**, 97-112 (1995).

Ching, C.B., Lim, B.G., Lee, E., Ng, S.C., "Preparative Resolution of Praziquantel Enantiomers by Simulated Counter-Current Chromatography," *J. Chromatogr.* **634**, 215-219 (1993).

Cohen, C., Jacob, R., Colombier, G., and Hotier, G., "Process for Regulating at Least One Fluid Flow Circulating in a Simulated Moving Bed Chromatographic Separation Loop," U.S. Patent No. 5,685,992 (1997).

Cox, G., "Preparative Enantioselective Chromatography," *Proceedings of the EUROTECH'98 Preparative and Process Scale Separations*, G. Subramanian, ed., Cambridge, England (1998).

Cox, G., Dapremont, O., Suteu, C., Murakami, T., and Briand, V., "Development of Enantioselective Large Scale Preparative Separations," poster presented at *ISCD'98 10th Int. Symp. on Chiral Discrimination*, Vienna, Austria (1998).

Crosby, J., "Chirality in Industry - An Overview," *Chirality in Industry. The Commercial Manufacture and Applications of Optically Active Compounds*, A.N. Collins, G.N. Sheldrake, and J. Crosby, eds., John Wiley & Sons, West Sussex, England, p. 1-66 (1992).

Dandekar, H.W., Chandhok, A.K., and Priegnitz, J.W., "Modeling and Simulation of SMB Technology for Pharmaceutical and Fine Chemical Applications," *Fundamentals of Adsorption*, M.D. LeVan, ed., Kluwer Academic Publishers, Boston, Massachusetts, p. 243-250 (1996).

Däppen, R., Arm, H., and Meyer, V.R., "Applications and Limitations of Commercially Available Chiral Stationary Phases for High-Performance Liquid Chromatography," *J. Chromatogr.* **373**, 1-20 (1986).

Davankov, V.A., and Rogozhin, S.V., "Ligand Chromatography as a Novel Method for the Investigation of Mixed Complexes: Stereoselective Effects in α-Amino Acid Copper (II) Complexes, *J. Chromatogr.* **60**, 280-283 (1971).

Davankov, V.A., Rogozhin, S.V., Semechkin, A.V., and Sachkova, T.P., "Ligand-Exchange Chromatography of Racemates. Influence of the Degree of Saturation of the Asymmetric Resin by Metal Ions on Ligand Exchange," *J. Chromatogr.* **82**, 359-365 (1973).

de Camp, W., "The FDA Perspective on the Development of Stereoisomers," *Chirality* **1**, 2-6 (1989).

de Rosset, A.J., Neuzil, R.W., and Broughton, "Industrial Applications of Preparative Chromatography," *Percolation Processes, Theory and Applications*, A.E. Rodrigues and D. Tondeur, eds., NATO ASI Series, Vol. 33, Sijthoff & Noordhoff, The Netherlands, p. 249-281 (1981).

Deutsch, D.H., "Chiral Drugs: The Coming Revolution," *Chemtech*, March, 157-159 (1991).

Dingenen, J., Somers, I., Pauwels, F., and Van Loon, A., "Enantiomer Separations: Limitations and Possibilities of Preparative Chromatography," *Proceedings of the 9th International Symposium on Preparative and Industrial Chromatography*, M. Perrut, ed., Société Française de Chemie, Nancy, France, p. 359-373 (1992).

Dondi, F., and Guiochon, G., eds., *Theoretical Advancement in Chromatography and Related Separation Techniques*, NATO ASI Series, Vol. 383, Kluwer Academic Publishers, The Netherlands (1992).

Feibush, B., and Grinberg, N., "The History of Enantiomeric Resolution," *Chromatographic Chiral Separations*, M. Zief, and L.J. Crane, eds., Chromatographic Science Series, Volume 40, Marcel Dekker, New York, USA, p. 1-14 (1988).

Francotte, E., Wolf, R.M., Lohmann, D., and Mueller, R., "Chromatographic Resolution of Racemates on Chiral Stationary Phases. I. Influence of the Supramolecular Structure of Cellulose Triacetate," *J. Chromatogr.* **347**, 24-36 (1985).

Francotte, E. and Junker-Buchheit, A., "Preparative Chromatographic Separation of Enantiomers," *J. Chromatogr.* **576**, 1-45 (1992).

Francotte, E., "Preparative Chromatographic Resolution of Racemates," *Simulated Moving Bed: Basics and Applications*, R.-M. Nicoud, ed., Institut National Polytechnique de Lorraine, Nancy, France, p. 35-53 (1993).

Francotte, E., "Chromatography as a Separation Tool for the Preparative Resolution of Racemic Compounds," *Chiral Separations. Applications and Technology*, S. Ahuja, ed., American Chemical Society, p. 271-308 (1996).

Francotte, E., and Richert P., "Applications of Simulated Moving-Bed Chromatography to the Separation of the Enantiomers of Chiral Drugs," *J. Chromatogr. A* **769**, 101-107 (1997).

Francotte, E., "Preparation of Drug Enantiomers by Chromatographic Resolution on Chiral Stationary Phases," *The Impact of Stereochemistry on Drug Development and Use*, H.Y. Aboul-Enein, and I.W. Wainer, eds., Chemical Analysis Series, Volume 42, John Wiley & Sons, England, p. 633-683 (1997).

Francotte, E., "Enantioselective Chromatography: A Real Alternative to Enantioselective Synthesis?," *Proceedings of the EUROTECH'98 Preparative and Process Scale Separations*, G. Subramanian, ed., Cambridge, England (1998).

Fuchs, G., Nicoud, R.-M., and Bailly, M. "Optical Isomers Purification with the Simulated Moving Bed Technology: Experimental and Theoretical Approaches," *Proceedings of the 9th International Symposium on Preparative and Industrial Chromatography*, M. Perrut, ed., Société Française de Chemie, Nancy, France, p. 395-402 (1992).

Ganetsos, G., and Barker, P.E., eds., *Preparative and Production Scale Chromatography*, Chromatographic Science Series, Vol. 61, Marcel Dekker, New York, USA (1993).

Gattuso, M.J., McCulloch, B., and Priegnitz, J.W., "UOP Sorbex Simulated Moving Bed Technology. A Cost Effective Route to Chiral Products," *Proceedings of Chiral Europe'94*, Nice, France (1994).

Gattuso, M.J., McCulloch, B., House, D.W., and Baumann, W.M., "UOP Simulated Moving Bed Technology - The Preparation of Single Enantiomer Drugs," *Proceedings of Chiral USA'95*, Boston, Massachusetts, USA, p. 51-53 (1995).

Gattuso, M.J., McCulloch, B., House, D.W., Baumann, W.M., and Gottschall, K., "Simulated Moving Bed Technology - The Preparation of Single Enantiomer Drugs," *Pharm. Tech. Europe* **8**, 20-25 (1996).

Gembicki, S.A., Oroskar, A.R., and Johnson, J.A., "Adsorption, Liquid Chromatography," *Encyclopedia of Separation Technology*, D. M. Ruthven, ed., John Wiley & Sons, New York, USA, p. 172-199 (1997).

Giddings, J.C., *Dynamics of Chromatography. Part I - Principles and Theory*, Marcel Dekker, New York, USA (1965).

Giddings, J.C., *Unified Separation Science*, John Wiley & Sons, New York, USA (1990).

Gübitz, G., Jellenz, W., and Santi, W., *J. Chromatogr.* **203**, 377 (1981).

Guest, D.W., "Evaluation of Simulated Moving Bed Chromatography for Pharmaceutical Process Development," *J. Chromatogr. A* **760**, 159-162 (1997).

Guiochon, G., Shirazi, S.G., and Katti, A.M., *Fundamentals of Preparative and Nonlinear Chromatography*, Academic Press, Boston, USA (1994).

Hashimoto, K., Kawase, M., Adachi, S., and Shirai, Y., "Comparison of Efficiency in the Separation of Binary Components between a Conventional Batch Chromatographic System and a Simulated Moving Bed Adsorber," *Proceedings of APCChE & CHEMECA 93*, 307-312 (1993).

Heikkilä, H., "Separating Sugars and Amino Acids with Chromatography," *Chem. Engng*, January 24, 50-52 (1983).

Heikkilä, H., Kuisma, J., and Paananen, H., Method for Fractionating a Solution," U.S. Patent No. 5,730,877 (1998).

Hesse, G., and Hagel, R., "Eine Vollständige Racemattrennung durch Elutions-Chromatographie an Cellulose-tri-acetat," *Chromatographia* **6**, 277-280 (1973).

Hesse, G., and Hagel, R., "Über Inclusions-Chromatographie und ein neues Retentionsprinzip für Benzolderivate," *Chromatographia* **9**, 62-68 (1976).

Hotier, G., "Simulated Moving Bed Separation: Actual and Future Applications," *Proceedings of the 9th International Symposium on Preparative and Industrial Chromatography*, M. Perrut, ed., Société Française de Chemie, Nancy, France, p. 235-240 (1992).

Hotier, G., and Nicoud, R.-M., "Chromatographic Simulated Mobile Bed Separation Process with Dead Volume Correction Using Period Desynchronization," U.S. Patent No. 5,578,215 (1996a).

Hotier, G., and Nicoud, R.-M., "Chromatographic Simulated Mobile Bed Separation Process with Dead Volume Correction Using Length Reduction," U.S. Patent No. 5,578,216 (1996b).

Hotier, G., Cohen, C., Couenne, N., and Toussaint, J.-M., "Chromatographic Simulated Moving Bed Separation Process with Dead Volume Correction Using an Increase in Flow Rate," U.S. Patent No. 5,582,736 (1996).

Hotier, G., "Process for Simulated Moving Bed Separation with a Constant Recycle Rate," U.S. Patent No. 5,762,806 (1998).

Humphrey, J.L., and Keller II, G.E., Separation Process Technology, McGraw-Hill, New York, USA (1997).

Hyoky, G., Paananen, H., Monten, K., Heikkilä, H., and Kuisma, J., "Fractionation Method of Sucrose-Containing Solutions," U.S. Patent No. 5,795,398 (1998).

Isaksson, R., Erlandsson, P., Hanson, L., Holmberg, A., and Berner, S., "Triacetylcellulose as a Chiral Stationary Phase for High-Performance Liquid Chromatography," *J. Chromatogr.* **498**, 257-280 (1990).

Ichida, A., and Shibata, T, "Cellulose Derivatives as Stationary Chiral Phases," *Chromatographic Chiral Separations*, M. Zief, and L.J. Crane, eds., Chromatographic Science Series, Volume 40, Marcel Dekker, New York, USA, p. 219-243 (1988).

Ikeda, H., Negawa, M., and Shoji, F., "Simulated Moving Bed Chromatographic Separation Process," U.S. Patent No. 5,770,088 (1998).

Johnson, J.A., "Sorbex: Continuing Innovation in Liquid Adsorption," *Adsorption: Science and Technology*, A.E. Rodrigues, M.D. LeVan, and D. Tondeur, eds., NATO ASI Series, Vol. 158, Kluwer Academic Publishers, The Netherlands, p. 383-395 (1989).

Johnson, J.A., and Kabza, R.G., "Sorbex: Industrial-Scale Adsorptive Separation," *Preparative and Production Scale Chromatography*, G. Ganetsos, and P.E. Barker, Marcel Dekker Inc., New York, p. 257-271 (1993).

Kearney, M., and Mumm, M., "Chromatographic Separator Sorbent Bed Preparation," U.S. Patent No. 4,990,259 (1991).

Kearney, M., and Hieb, K., "Time Variable Simulated Moving Bed Process," U.S. Patent No. 5,102,553 (1992).

Keller II, G.E., "Adsorption: Building Upon a Solid Foundation," *Chem. Engng Prog.*, October, 56-67 (1995).

Kinkel, J.N., Cabrera, K., and Eisenbeiss, F., "Preparative Direct Chromatographic Separation of Enantiomers on Chiral Stationary Phases," *Preparative and Process-Scale Liquid Chromatography*, G. Subramanian, ed., Ellis Horwood, Chichester, England, p. 265-283 (1991).

Koller, H., Rimböck, K.-H., and Mannschreck, A., "High-Pressure Liquid Chromatography on Triacetylcelulose. Characterization of a Sorbent for the Separation of Enantiomers," *J. Chromatogr.* **282**, 89-94 (1983).

Krstulovic, A.M., *Chiral Separations by HPLC*, Ellis Horwood, Chichester, England (1989).

Küsters, E., Gerber, G., and Antia, F.D., "Enantioseparation of a Chiral Epoxide by Simulated Moving Bed Chromatography using Chiralcel-OD," *Chromatographia* **40**, 387-393 (1995).

Lim, B.G., and Ching, C.B., "Preliminary Design of a Simulated Counter-Current Chromatographic System for the Separation of Praziquantel Enantiomers," *J. Chromatogr. A* **734**, 247-258 (1996).

Möller, P., "High Performance Silica for Preparative Chromatography: Important Characteristics and Some New Applications," *Proceedings of the EUROTECH'98 Preparative and Process Scale Separations*, G. Subramanian, ed., Cambridge, England (1998).

Moran, M.G., "Simulated Moving Bed Adsorptive Separation Process," U.S. Patent No. 5,635,072 (1997).

Moran, M.G., "Simulated Moving Bed Adsorptive Separation Apparatus," U.S. Patent No. 5,705,061 (1998).

Nagamatsu, S., Murazumi, K., and Makino, S., "Chiral Separation of a Pharmaceutical Intermediate by SMB Process," poster presented at *PREP'98 Int. Symp. on Preparative Chromatography*, Washington, DC, USA (1998).

Negawa, M., and Shoji, F., "Optical Resolution by Simulated Moving-Bed Adsorption Technology," *J. Chromatogr.* **590**, 113-117 (1992).

Negawa, M., and Shoji, F., "Process for Recovering Optical Isomers and Solvent, Process for Using Solvent by Circulation and Process for Reusing Optical Isomers in Optical Resolution," U.S. Patent No. 5,434,298 (1995a).

Negawa, M., and Shoji, F., "Process for Recovering Optical Isomers and Solvent, Process for Using Solvent by Circulation and Process for Reusing Optical Isomers in Optical Resolution," U.S. Patent No. 5,434,299 (1995b).

Negawa, M., and Shoji, F., "Simulated Moving Bed Separation System," U.S. Patent No. 5,456,825 (1995c).

Negawa, M., and Shoji, F., "Process for Recovering Optical Isomers and Solvent, Process for Using Solvent by Circulation and Process for Reusing Optical Isomers in Optical Resolution," U.S. Patent No. 5,498,752 (1996).

Negawa, M., and Shoji, F., "Process for Recovering Optical Isomers and Solvent, Process for Using Solvent by Circulation and Process for Reusing Optical Isomers in Optical Resolution," U.S. Patent No. 5,763,645 (1998).

Nicoud, R.-M., "The Simulated Moving Bed: A Powerful Chromatographic Process," *LC-GC Intl.* **5**, 43-47 (1992).

Nicoud, R.-M., Fuchs, G., Küsters, E., Antia, F., Reuille, R., and Schmid, E., "Preparative Scale Enantioseparation of a Chiral Epoxide - A Comparison of Liquid Chromatography and Simulated Moving-Bed Adsorption Technology," Proceedings of the 3rd International Symposium on Chiral Discrimination, Tübigen, Germany (1992).

Nicoud, R.-M., Fuchs, G., Adam, P., Bailly, M., Küsters, E., Antia, F., Reuille, R., and Schmid, E., "Preparative Scale Enantioseparation of a Chiral Epoxide: Comparison of Liquid Chromatography and Simulated Moving Bed Adsorption Technology," *Chirality* **5**, 267-271 (1993a).

Nicoud, R.-M., "Simulated Moving Bed (SMB) in Preparative Chromatography: Basics, Limitations and Use," *Simulated Moving Bed: Basics and Applications*, R.-M. Nicoud, ed., Institut National Polytechnique de Lorraine, Nancy, France, p. 54-64 (1993).

Nicoud, R.-M., Bailly, M., Kinkel, J.N., Devant, R.M., Hampe, Th.R., and Küsters, E., "Simulated Moving Bed (SMB): Applications for Enantiomer Separations on Chiral Stationary Phases," *Simulated Moving Bed: Basics and Applications*, R.-M. Nicoud, ed., Institut National Polytechnique de Lorraine, Nancy, France, p. 65-88 (1993b).

Nicoud, R.-M., "Recent Advances in Industrial Chromatographic Processes," *Recent Advances in Industrial Chromatographic Processes*, R.-M. Nicoud, ed., Nancy, France, p. 4-5 (1997).

Nicoud, R.-M., and Ludemann-Hombourger, O., "Preparative Chromatographic Techniques for Performing Chiral Separations," poster presented at *PREP'98 Int. Symp. on Preparative Chromatography*, Washington, DC, USA (1998).

Nicoud, R.-M., Hauck, W., and Ludemann-Hombourger, O., "Binary Separation: Batch or Continuous?," poster presented at *PREP'98 Int. Symp. on Preparative Chromatography*, Washington, DC, USA (1998).

Oguni, K., Oda, H., and Ichida, A., "Development of Chiral Stationary Phases Consisting of Polysaccharide Derivatives," *J. Chromatogr.* **694**, 91-100 (1995).

Otani, S., "Adsorption Separates Xylenes," *Chem. Engng*, September 17, 106-107 (1973).

Otani, S., Iwamura, T., Sando, K., Kanaoka, M., Matsumura, K., Akita, S., Yamamoto, T., Takeushi, I., Tsuchiya, T., Noguchi, Y., Mori, T., "Separation Process of Components of Feed Mixture Utilizing Solid Sorbent," U.S. Patent No. 3,761,533 (1973).

Pais, L.S., Loureiro, J.M., and Rodrigues, A.E., "Separation of 1,1'-bi-2-naphthol Enantiomers by Continuous Chromatography in Simulated Moving Bed," *Chem. Engng Sci.* **52**, 245-257 (1997a).

Pais, L.S., Loureiro, J.M., and Rodrigues, A.E., "Modeling, Simulation and Operation of a Simulated Moving Bed for Continuous Chromatographic Separation of 1,1'-bi-2-naphthol Enantiomers," *J. Chromatogr. A* **769**, 25-35 (1997b).

Pais, L.S., Loureiro, J.M., and Rodrigues, A.E., "Separation of Enantiomers of a Chiral Epoxide by Simulated Moving Bed Chromatography," *J. Chromatogr. A* **827**, 215-233 (1998).

Perrut, M., *Proceedings of the 9th International Symposium on Preparative and Industrial Chromatography*, Société Française de Chemie, Nancy, France (1992).

Pirkle, W.H., and Pochapsky, T.C., "Considerations of Chiral Recognition Relevant to the Liquid Chromatographic Separation of Enantiomers," *Chem. Rev.* **89**, 347-362 (1989).

Priegnitz, J.W., "Small Scale Simulated Moving Bed Separation Apparatus and Process," U.S. Patent No. 5,470,464 (1995).

Priegnitz, J.W., "Small Scale Simulated Moving Bed Separation Process," U.S. Patent No. 5,565,104 (1996).

Priegnitz, J.W., and McCulloch, B., "Chiral Separations by Simulated Moving Bed Chromatography Operating at Low k' Values," U.S. Patent No. 5,518,625 (1996).

Priegnitz, J.W., and McCulloch, B., "Separations by Simulated Moving Bed Chromatography Operating at Low k' Values Using Weakly Interating Adsorbents as the Stationary Phase," U.S. Patent No. 5,626,762 (1997a).

Priegnitz, J.W., and McCulloch, B., "Separations by Simulated Moving Bed Chromatography Operating at Low k' Values Using Weakly Interating Adsorbents as the Stationary Phase," U.S. Patent No. 5,645,729 (1997b).

Rearick, D.E., Kearney, M., and Costesso, D.D., "Simulated Moving-Bed Technology in the Sweetener Industry," *Chemtech*, September, 36-40 (1997).

Repic, O., *Principles of Process Research and Chemical Development in the Pharmaceutical Industry*, John Wiley & Sons, New York, USA (1998).

Reuter, K.A., "Process and a Device for Continuous Chromatography," U.S. Patent No. 5,578,111 (1996).

Reuter, K.A., "Continuous Chromatography," U.S. Patent No. 5,770,087 (1998).

Rimböck, K.-H., Kastner, F., and Mannschreck, A., "Liquid Chromatography on Triacetylcelulose. Preparative Separation of Enantiomers on an Axially Compressed Column," *J. Chromatogr.* **329**, 307-310 (1985).

Rodrigues, A.E., and Tondeur, D., eds., *Percolation Processes: Theory and Applications*, NATO ASI Series, Vol. 33, Sijthoff & Noordhoff, The Netherlands (1981).

Rodrigues, A.E., LeVan, M.D., and Tondeur, D., eds., *Adsorption: Science and Technology*, NATO ASI Series, Vol. 158, Kluwer Academic Publishers, The Netherlands (1989).

Ruthven, D.M., *Principles of Adsorption and Adsorption Processes*, John Wiley & Sons, New York, USA (1984).

Samdani, G., "Chiral Engineering Breaks Through the Looking Glass," *Chem. Engng*, October, 35-39 (1993).

Schulte, M., "Strategies for Economical Preparative Enantioseparation," *Proceedings of the Simp. on Chiral Technologies and Enantioseparation*, G. Subramanian, ed., Cambridge, England (1997).

Schulte, M., Ditz, R., Devant, R.M., Kinkel, J.N., and Charton, F., "Comparison of the Specific Productivity of Different Chiral Stationary Phases Used for Simulated Moving-Bed Chromatography," *J. Chromatogr. A* **769**, 93-100 (1997).

Sheldon, R.A., *Chirotechnology. Industrial Synthesis of Optically Active Compounds*, Marcel Dekker, New York, USA (1993).

Shibata, T., Okamoto, I., and Ishii, K., "Chromatographic Optical Resolution on Polysaccharides and their Derivatives," *J. Liq. Chromatogr.* **9**, 313-340 (1986).

Stalcup, A.M., "Chromatography, Chiral Separations," *Encyclopedia of Separation Technology*, D. M. Ruthven, ed., John Wiley & Sons, New York, USA, p. 320-355 (1997).

Stinson, S.C., "Chiral Drugs," *C&EN*, September 27, 38-65 (1993).

Stinson, S.C., "Chiral Drugs," *C&EN*, September 19, 38-72 (1994).

Stinson, S.C., "Chiral Drugs," *C&EN*, October 9, 44-74 (1995).

Stinson, S.C., "Chiral Drug Market Shows Signs of Maturity," *C&EN*, October 20, 38-70 (1997a).

Stinson, S.C., "FDA May Confer New Status On Enantiomers" *C&EN*, July 2, 28-29 (1997b).

Suzuki, M., *Adsorption Engineering*, Chemical Engineering Monographs, Vol. 25, Elsevier, Tokyo, Japan (1990).

U.S. Food and Drug Administration, "FDA's Policy Statement for the Development of New Stereoisomeric Drugs," *Chirality* **4**, 338-340 (1992).

White, C.A., "An Introduction to Large-Scale Enantioseparation," *Preparative and Process-Scale Liquid Chromatography*, G. Subramanian, ed., Ellis Horwood, Chichester, England, p. 250-264 (1991).

Yamashita, A., and Shoji, F., "Process for Separating Optical Isomers," U.S. Patent No. 5,126,055 (1992).

Zief, M., "Preparative Enantiomeric Separation," *Chromatographic Chiral Separations*, M. Zief, and L.J. Crane, eds., Chromatographic Science Series, Volume 40, Marcel Dekker, New York, USA, p.337-353 (1988).

Zief, M., and Crane, L.J., *Chromatographic Chiral Separations*, Chromatographic Science Series, Volume 40, Marcel Dekker, New York, USA (1988).

Chapter 3

# Simulated Moving Bed Strategies of Modeling

*A comparative study of modeling strategies of simulated moving bed adsorbers is presented. Two models are compared: the simulated moving bed model (SMB), that takes into account the real shift of the injection and collection points, and the true moving bed approach (TMB), that considers liquid and solid flow in opposite directions. The predictions of these two models are compared in terms of steady-state performance, steady-state internal concentration profiles, and transient behaviour of the extract and raffinate concentrations. The influence of the degree of subdivision of the bed in the SMB model predictions is also analyzed and compared with the TMB performance.*

## 3.1 Introduction

Modeling and simulation of a chemical engineering process always attracted a special attention since it could lead to significant savings in time and materials.

The problem of modeling a simulated moving bed separation process can be analyzed by two different strategies: one, by simulating the system directly, taking into account its intermittent behaviour, other by representing its operation in terms of a true countercurrent system. The first model represents the real SMB and considers the periodic switch of the injection and collection points. The second is developed by assuming the equivalence with the true moving bed, where solid and fluid phases flow in opposite directions.

Several authors have developed models to predict the performance of a SMB separation process, with reasonable agreement with experimental results. These models can be classified according to the description of the fluid flow as continuous flow models (plug or axial dispersed plug flow) or as mixing cell models. Otherwise, some authors considered mass transfer resistances by including an appropriate rate expression, usually by using the linear driving force (LDF) model (Glueckauf, 1955; Ruthven, 1984). Others used the equilibrium theory and neglected mass transfer resistances and axial mixing. Some references about the SMB modeling assuming the TMB equivalence or directly through the SMB intermittent model can be found in Ruthven and Ching (1989) or, for more recent studies, in Pais *et al.* (1998). *Table 3.1* presents a literature survey on these modeling strategies.

Several authors carried out the modeling of the SMB operation considering linear equilibrium isotherms, namely for the glucose-fructose separation (Hashimoto *et al.*, 1983; Ching, 1983; Ching and Ruthven, 1985a). Nevertheless, SMB units usually operate at high feed concentrations leading, for the majority of the separation mixtures, to non-linear competitive adsorption behaviours. A constant selectivity factor model, like the multicomponent Langmuir isotherm, usually is used to described this behaviour. However, this type of isotherms is not suitable for many separation systems, such as chiral separations. It is well known that the selectivity factor decreases with the increase of the concentration of chiral species. To overcome this lack of information, a concentration-dependent selectivity factor model is needed, such as the linear + Langmuir or the bi-Langmuir competitive isotherm (Jacobson *et al.*, 1991; Nicoud and Seidel-Morgenstern, 1993; Bellot and Condoret, 1993; Lim *et al.*, 1995).

Table 3.1. Literature survey on the modeling strategies for SMB separation processes.

| Modeling Strategy | Description of the Fluid Flow | Mass Transfer Resistance | References |
|---|---|---|---|
| True Moving Bed | Continuous Flow model | No<br>Equilibrium Theory | Storti *et al.* (1989a, b, 1993a, b, 1995)<br>Mazzotti *et al.* (1994, 1996a, b, 1997a, b)<br>Chiang (1998) |
| | | Yes<br>Linear Driving Force model | Hashimoto *et al.* (1983, 1987, 1993)<br>Ching and Ruthven (1985a)<br>Ching *et al.* (1985, 1991, 1992)<br>Kubota *et al.* (1989)<br>Storti *et al.* (1989a, b, 1993a)<br>Hidajat and Ching (1990)<br>Ruthven and Ching (1993)<br>Hassan *et al.* (1994)<br>Shamsur Rahman *et al.* (1994)<br>Chu and Hashim (1995)<br>Rodrigues *et al.* (1996)<br>Dandekar *et al.* (1996)<br>Hotier (1996)<br>Zhong and Guiochon (1996)<br>Schmidt-Traub and Strube (1996)<br>Pais *et al.* (1997a, b, 1998a, b)<br>Strube *et al.* (1997)<br>Ma and Wang (1997)<br>Navarro *et al.* (1997) |
| | Mixing Cell model | No<br>Equilibrium Stage model | Ching and Ruthven (1985a, b)<br>Ching *et al.* (1985)<br>Ernst and Hsu (1989, 1992)<br>Charton and Nicoud (1995)<br>Navarro *et al.* (1997) |

Table 3.1. (continued) Literature survey on the modeling strategies for SMB separation processes.

| Modeling Strategy | Description of the Fluid Flow | Mass Transfer Resistance | References |
|---|---|---|---|
| Simulated Moving Bed | Continuous Flow model | No<br>Ideal and Equilibrium-Dispersive model | Zhong and Guiochon (1996, 1998)<br>Zhong *et al.* (1997)<br>Yun *et al.* (1997a, b, c) |
| | | Yes<br>Linear Driving Force model | Hashimoto *et al.* (1983, 1987, 1993)<br>Carta and Pigford (1986)<br>Storti *et al.* (1988, 1989a)<br>Lameloise and Viard (1993)<br>Chu and Hashim (1995)<br>Hassan *et al.* (1995)<br>Lim and Ching(1996)<br>Hotier (1996)<br>Schmidt-Traub and Strube (1996)<br>Strube *et al.* (1997)<br>Zhong and Guiochon (1997a, b)<br>Ma and Wang (1997)<br>Pais *et al.* (1998a)<br>Azevêdo *et al.* (1998) |
| | Mixing Cell model | No<br>Equilibrium Stage model | Barker *et al.* (1983)<br>Ching (1983)<br>Hidajat *et al.* (1986a, b)<br>Ching *et al.* (1987, 1988, 1993)<br>Ruthven and Ching (1993)<br>Charton and Nicoud (1995) |

This chapter addresses some questions concerning the equivalence between SMB and TMB strategies of modeling, namely:

i. What is the *degree of equivalence* between SMB and TMB approaches? This question will be answered by looking at:

a. Transient evolution of extract and raffinate concentrations predicted by the SMB and TMB models;

b. Steady-state extract and raffinate concentrations and purities predicted by the SMB and TMB models;

c. Steady-state internal concentration profiles for TMB and SMB operation;

d. Influence of subdivision of the bed in the SMB operation, and which degree of subdivision is equivalent to the TMB approach.

ii. Are both strategies equivalent in terms of process optimization, i.e., the better choice of liquid and solid (switch time interval) flow-rates?

Three cases are analyzed for the SMB system: SMB4, constituted by four columns, one in each section; SMB8, with 8 columns, two per section; and SMB12, with three columns per section.

The mathematical models developed to carried out this comparative study are based in the following assumptions:

1. An axially dispersed plug flow model is used to describe the fluid phase flow;

2. A plug flow model is used to represent the countercurrent solid flow in the TMB approach;

3. The adsorbent particles are considered as homogeneous material and mass transfer between fluid and solid is described by the linear driving force (LDF) model;

4. The model can handle any kind of adsorption equilibrium isotherm.

## 3.2 The Simulated Moving Bed Model

The concept of the simulated moving bed was described in the previous chapter and illustrated by *Figure 2.8*. In the SMB operation, the countercurrent motion of fluid and solid is simulated with a discrete jump of injection and collection points in the same direction of the fluid phase. The SMB system is then constituted by a set of identical fixed-bed columns, connected in series.

The model equations for the SMB model result from the mass balances over a volume element of the bed and at a particle level. The transient SMB model equations are summarized below, with initial and boundary conditions, as well as with the necessary mass balances at the nodes between each column.

***Model equations for the transient SMB***

*Mass balance in a volume element of the bed k:*

$$\frac{\partial c_{ik}}{\partial t} = D_{L_k} \frac{\partial^2 c_{ik}}{\partial z^2} - v_k^* \frac{\partial c_{ik}}{\partial z} - \frac{(1-\varepsilon)}{\varepsilon} k(q_{ik}^* - q_{ik}) \tag{3.1}$$

where the subscripts $i$ *(i = A, B)* refers to the species in the mixture, and $k$ *(k= 1,2, ..., NCOL)* is the column number, $c_{ik}$ and $q_{ik}$ are the fluid phase and average adsorbed phase concentrations of species $i$ in column $k$ of the SMB unit, respectively, $z$ is the axial coordinate, $t$ is the time variable, $\varepsilon$ is the bed porosity, $v_k^*$ is the interstitial fluid velocity in the $k^{th}$ SMB column, $D_{L_k}$ is the axial dispersion coefficient, and $k$ is the intraparticle mass transfer coefficient.

*Mass balance in the particle:*

$$\frac{\partial q_{ik}}{\partial t} = k(q_{ik}^* - q_{ik}) \tag{3.2}$$

where $q_{ik}^*$ is the adsorbed phase concentration in equilibrium with $c_{ik}$.

*Initial conditions:*

$$t = 0: \qquad c_{ik} = q_{ik} = 0 \tag{3.3}$$

*Boundary conditions for column k:*

$$z = 0: \qquad c_{ik} - \frac{D_{L_k}}{v_k^*}\frac{dc_{ik}}{dz} = c_{ik,0} \tag{3.4}$$

where $c_{ik,0}$ is the inlet concentration of species $i$ in column $k$.

$z = L_k$ :

For a column inside a section and for extract and raffinate nodes

$$c_{ik} = c_{ik+1,0} \tag{3.5a}$$

For the eluent node $$c_{ik} = \frac{v_I^*}{v_{IV}^*} c_{ik+1,0} \tag{3.5b}$$

For the feed node $$c_{ik} = \frac{v_{III}^*}{v_{II}^*} c_{ik+1,0} - \frac{v_F}{v_{II}^*} c_i^F \tag{3.5c}$$

*Global balances:*

Eluent node $$v_I^* = v_{IV}^* + v_E \tag{3.6a}$$

Extract node $$v_{II}^* = v_I^* - v_X \tag{3.6b}$$

Feed node $$v_{III}^* = v_{II}^* + v_F \tag{3.6c}$$

Raffinate node $$v_{IV}^* = v_{III}^* - v_R \tag{3.6d}$$

*Multicomponent adsorption equilibrium isotherm:*

$$q_{Ak}^* = f_A(c_{Ak}, c_{Bk}) \quad \text{and} \quad q_{Bk}^* = f_B(c_{Ak}, c_{Bk}) \tag{3.7}$$

Introducing the dimensionless variables $x = z / L_k$ and $\theta = t / t^*$, where $t^*$ is the switch time interval, and $L_k$ is the length of one SMB column, the model equations *3.1* and *3.2* become:

$$\frac{\partial c_{ik}}{\partial \theta} = \gamma_k^* \left\{ \frac{1}{Pe_k}\frac{\partial^2 c_{ik}}{\partial x^2} - \frac{\partial c_{ik}}{\partial x} \right\} - \frac{(1-\varepsilon)}{\varepsilon} \alpha_k (q_{ik}^* - q_{ik}) \tag{3.8}$$

and

$$\frac{\partial q_{ik}}{\partial \theta} = \alpha_k (q_{ik}^* - q_{ik}) \tag{3.9}$$

The initial and boundary conditions are the same presented before (*Equations 3.3* to *3.5*) and, for $x = 0$ ($z = 0$), *Equation 3.4* becomes:

$$c_{ik} - \frac{1}{Pe_k}\frac{dc_{ik}}{dx} = c_{ik,0} \tag{3.10}$$

The resulting model parameters are:

the ratio between solid and fluid volumes, $\frac{1-\varepsilon}{\varepsilon}$ (3.11)

the ratio between fluid and solid interstitial velocities, $\gamma_k^* = \frac{v_k^*}{u_s} = \frac{v_k^*}{L_k / t^*}$ (3.12)

the Peclet number, $Pe_k = \frac{v_k^* L_k}{D_{Lk}}$ (3.13)

the number of mass transfer units, $\alpha_k = \frac{k\, L_k}{u_s} = k\, t^*$ (3.14)

where $u_s$ is the interstitial solid velocity in the equivalent TMB model. To complete the list of model parameters, the adsorption equilibrium parameters have to be added.

Due to the switch of inlet and outlet lines, each column plays different functions during a whole cycle, depending on its location (section). As a consequence, we shall notice that the boundary conditions for each column change after the end of each switch time interval. This time-dependence of the boundary conditions leads to a cyclic steady-state for this system, instead of a real steady-state present in the TMB model. This means that, after cyclic steady-state is reached, the internal concentration profiles vary during a given cycle, but they are identical at the same time for two successive cycles.

## 3.3 The True Moving Bed Model

The TMB concept can be used as an alternative strategy to predict the SMB operation. In the TMB model, the solid phase is assumed to move in plug flow in the opposite direction of the fluid phase, while the inlet and outlet lines remain fixed. As a consequence, each column plays the same function, depending of its location (*Chapter 2, Figure 2.5*).

An equivalence between the TMB and the SMB models can be made by keeping constant the liquid velocity relative to the solid velocity, i.e., the liquid velocity in the TMB is

$$v_j = v_j^* - u_s \tag{3.15}$$

where $v_j^*$ and $v_j$ are the interstitial liquid velocities in the SMB and TMB, respectively, and $u_s$ is the interstitial solid velocity. Also, the solid velocity in the TMB model $u_s$ must be evaluated from the value of the switch time interval $t^*$ of the SMB model, as

$$u_s = L_c / t^* \tag{3.16}$$

where $L_c$ is the length of one SMB column.

Alternatively, the equivalence can be made in terms of flow-rates:

$$Q_j = Q_j^* - \frac{\varepsilon}{1-\varepsilon} Q_s \tag{3.17}$$

with

$$Q_s = \frac{(1-\varepsilon)V_c}{t^*} \tag{3.18}$$

where $Q_j^*$ and $Q_j$ are the volumetric liquid flow-rates in section $j$ of a SMB and TMB, respectively, $Q_s$ is the solid flow-rate in the equivalent TMB model, and $V_c$ is the volume of one SMB column.

The resulting model equations for the transient TMB are shown below.

***Model equations for the transient TMB***

*Mass balance in a volume element of the bed j:*

$$\frac{\partial c_{ij}}{\partial t} = D_{L_j}\frac{\partial^2 c_{ij}}{\partial z^2} - v_j\frac{\partial c_{ij}}{\partial z} - \frac{(1-\varepsilon)}{\varepsilon}k(q_{ij}^{*} - q_{ij}) \tag{3.19}$$

*Mass balance in the particle:*

$$\frac{\partial q_{ij}}{\partial t} = u_s\frac{\partial q_{ij}}{\partial z} + k(q_{ij}^{*} - q_{ij}) \tag{3.20}$$

*Initial conditions:*

$$t = 0: \qquad c_{ij} = q_{ij} = 0 \tag{3.21}$$

*Boundary conditions for section j:*

$$z = 0: \qquad c_{ij} - \frac{D_{L_j}}{v_j}\frac{dc_{ij}}{dz} = c_{ij,0} \tag{3.22}$$

where $c_{ij,0}$ is the inlet concentration of species $i$ in section $j$.

$z = L_j$ :

For the eluent node $$c_{iIV} = \frac{v_I}{v_{IV}}c_{iI,0} \tag{3.23a}$$

For the extract node $$c_{iI} = c_{iIII,0} \tag{3.23b}$$

For the feed node $$c_{iII} = \frac{v_{III}}{v_{II}}c_{iIII,0} - \frac{v_F}{v_{II}}c_i^F \tag{3.23c}$$

For the raffinate node $$c_{iIII} = c_{iIV,0} \tag{3.23d}$$

And $$q_{iIV} = q_{iI,0}\ ,\ q_{iI} = q_{iII,0}\ ,\ q_{iII} = q_{iIII,0}\ ,\ q_{iIII} = q_{iIV,0} \tag{3.24}$$

*Global balances:*

Eluent node $$v_I = v_{IV} + v_E \tag{3.25a}$$

Extract node $$v_{II} = v_I - v_X \tag{3.25b}$$

Feed node $$v_{III} = v_{II} + v_F \tag{3.25c}$$

Raffinate node $$v_{IV} = v_{III} - v_R \tag{3.25d}$$

*Multicomponent adsorption equilibrium isotherm:*

$$q_{Aj}^* = f_A(c_{Aj}, c_{Bj}) \quad \text{and} \quad q_{Bj}^* = f_B(c_{Aj}, c_{Bj}) \tag{3.26}$$

Introducing the dimensionless variables $x = z / L_j$ and $\theta = t / \tau_s$, with $\tau_s = L_j / u_s = N_s t^*$, where $\tau_s$ is the solid space time in a section of a TMB unit, $L_j$ is the length of a TMB section, and $N_s$ is the number of columns per section in a SMB unit, the model *Equations 3.19* and *3.20* become:

$$\frac{\partial c_{ij}}{\partial \theta} = \gamma_j \left\{ \frac{1}{Pe_j} \frac{\partial^2 c_{ij}}{\partial x^2} - \frac{\partial c_{ij}}{\partial x} \right\} - \frac{(1-\varepsilon)}{\varepsilon} \alpha_j (q_{ij}^* - q_{ij}) \tag{3.27}$$

and

$$\frac{\partial q_{ij}}{\partial \theta} = \frac{\partial q_{ij}}{\partial x} + \alpha_j (q_{ij}^* - q_{ij}) \tag{3.28}$$

The initial and boundary conditions are the same presented before (*Equations 3.21* to *3.24*) and, for $x = 0$ ($z = 0$), *Equation 3.22* becomes:

$$c_{ij} - \frac{1}{Pe_j} \frac{dc_{ij}}{dx} = c_{ij,0} \tag{3.29}$$

The resulting model parameters are similar to the ones presented for the SMB model, except that they are expressed in terms of the length of the TMB sections:

the ratio between solid and fluid volumes, $$\frac{1-\varepsilon}{\varepsilon} \tag{3.30}$$

the ratio between fluid and solid intertitial velocities, $$\gamma_j = \frac{v_j}{u_s} \tag{3.31}$$

the Peclet number, $$Pe_j = \frac{v_j L_j}{D_{Lj}} \tag{3.32}$$

the number of mass transfer units, $$\alpha_j = \frac{k\, L_j}{u_s} \tag{3.33}$$

Adsorption equilibrium parameters have to be added to the list above.

## 3.4 Numerical Aspects

The SMB and TMB models, defined by a set of partial differential equations, were numerically solved by using the *PDECOL* software (Madsen and Sincovec, 1979) based on the method of orthogonal collocation in finite elements (OCFE).

For the TMB model, there are four PDEs for each section: for each component there is a PDE resulting from the mass balance in a volume element of the bed, and other resulting from the mass balance in the particle. Since the TMB unit is composed by four sections, and considering a binary separation, the TMB system is defined by a set of 16 PDEs.

In the SMB model, four equivalent PDEs must be written but now for each column. The four-section SMB system for a binary separation is then defined by a set of $4N_c$ PDEs, where $N_c$ is the total number of columns used in the SMB unit.

The *PDECOL* software is based on the method of lines and uses a finite element collocation procedure for the discretization of the spatial variable. The collocation procedure reduces the PDE system to an initial-value ODE system, which then depends only on the time variable. The time integration is then accomplished by using the ODE solver *STIFIB*, which is a modified version of the *GEARIB* ODE package developed by Hindmarsh (1976).

The user must specify the piecewise polynomial which is to be used to compute the approximate solution. In selecting this space, the order, *KORD*, of the polynomials to be used must first be specified (*KORD* = polynomial degree + 1). Next, the number of intervals, *NINT*, into which the spacial domain is to be divided, is chosen. The approximate solution at any time will be a polynomial of order (*KORD* - 1) in each $i$ subinterval ($i = 1, 2, ..., NINT$). The common value $KORD = 4$ was used and an equal number of intervals, $NINT = 20$, was used to divide the spatial domain of each section or column in the TMB and SMB models, respectively. The number of continuity conditions, *NCC*, to be imposed on the polynomial pieces across all of the interior breakpoints is then chosen to complete the definition of the piecewise polynomial space. The common value $NCC = 2$ was used, which requires that the approximate solution and its first spatial derivative are continuous at the breakpoints and hence on the entire spatial domain.

The dimension of this linear space is known and finite and is $NCPTS = KORD*NINT - NCC*(NINT - 1)$, where *NCPTS* means the number of collocation points used for each equation. Summarizing, *PDECOL* software reduces a set of *NPDE* partial differential equations to a set of $N = NPDE*NCPTS$ time dependent ordinary differential equations.

The model equations for the transient SMB or TMB operation are solved, from an initial condition where no feed components are present (columns are filled with the eluent) until steady-state is reached. In the TMB and SMB packages developed, the steady-state is considered to be achieved when:

i. The relative errors between the average concentrations (evaluated during a full cycle, for the SMB cases, and during a solid space time interval, for the TMB model) of each component in the extract and raffinate streams for two successive iterations are less than a maximum error defined by the user, and;

ii. The relative errors between the total amount of each component that enters (in the feed stream) and leaves (in the extract and raffinate streams) the system (evaluated during a full cycle, for the SMB cases, and during a solid space time interval, for the TMB model) are less than a maximum error defined by the user.

In fact, an unique global error is defined as

$$e = e_X + e_R + e_A + e_B \tag{3.34}$$

where:

$e_X$ is the relative error of the average concentrations of the two components in the extract for two successive iterations

$$e_X = \frac{\left|\overline{C}^A_{X[i]} - \overline{C}^A_{X[i-1]}\right|}{\overline{C}^A_{X[i]}} + \frac{\left|\overline{C}^B_{X[i]} - \overline{C}^B_{X[i-1]}\right|}{\overline{C}^B_{X[i]}} \tag{3.35}$$

$e_R$ is the relative error of the average concentrations of the two components in the raffinate in two successive iterations

$$e_R = \frac{\left|\overline{C}^A_{R[i]} - \overline{C}^A_{R[i-1]}\right|}{\overline{C}^A_{R[i]}} + \frac{\left|\overline{C}^B_{R[i]} - \overline{C}^B_{R[i-1]}\right|}{\overline{C}^B_{R[i]}} \tag{3.36}$$

$e_A$ is the relative error between the amount of the less retained component that enters (in the feed stream) and leaves (in the extract and raffinate streams) the system

$$e_A = \frac{\left| Q_F C_F^A - \left( Q_X \overline{C}_X^A + Q_R \overline{C}_R^A \right) \right|}{Q_F C_F^A} \tag{3.37}$$

$e_B$ is the relative error between the amount of the more retained component that enters (in the feed stream) and leaves (in the extract and raffinate streams) the system

$$e_B = \frac{\left| Q_F C_F^B - \left( Q_X \overline{C}_X^B + Q_R \overline{C}_R^B \right) \right|}{Q_F C_F^B} \tag{3.38}$$

The steady-state is considered to be achieved when the global error $e$, defined by *Equation 3.34*, is less than a maximum error defined by the user, $\delta$. For both modeling strategies, TMB and SMB, it was used a value of $\delta = 0.01$.

As it was pointed out in *Chapter 2*, the countercurrent motion of fluid and solid phases in the SMB operation is achieved with a discrete jump of the injection (feed and eluent) and collection (extract and raffinate) points. Due to this switch of the inlet and outlet points, the boundary conditions for each column vary with time, changing with the end of each switch time interval. Hence, the SMB model must take into account this time-dependence of the boundary conditions.

Some difficulties appeared in reaching the cyclic steady-state for the SMB model, namely in what concerns the global balance for the more retained component B (*Equation 3.38*). These difficulties increased for the SMB cases with a higher number of columns per section, i.e., with the increase of the number of equations to solve. Increasing the *NINT* or *KORD* values did not solve the problem. For an efficient integration, a small value for the relative time error bound, *EPS*, used by the *STIFIB* integrator, was needed. *Table 3.2* presents the results obtained with the SMB package for the SMB4 case (1 column per section). For a maximum error $\delta$ of *0.01*, the *EPS* value must be of the order of $10^{-10}$.

Table 3.2. Influence of the *EPS* value (SMB4 case, 12 full cycles).
(Personal Computer Duo Pentium Pro 200 MHz, 512 Kb Cache, 64 Mb RAM)
(*PDECOL* parameters: *KORD* = 4, *NINT* = 20, *NCC* = 2).

| *EPS* | Error *e* | Running Time (min) | Extract Purity (%) | Raffinate Purity (%) |
|---|---|---|---|---|
| $10^{-10}$ | 0.01 | 330 | 89.5 | 95.2 |
| $10^{-8}$ | 0.02 | 95 | 89.5 | 95.2 |
| $10^{-6}$ | 0.1 | 45 | 92.3 | 95.0 |

The values of the *PDECOL* parameters (*NPDE*, *KORD*, and *NINT*) and the *STIFIB* parameter (*EPS*) used influence directly the running time. The numerical evolution of the SMB operation is very time consuming. Generally, 12 full cycles were needed to achieve the cyclic steady-state operation, from an initial condition characterized by clean columns (only eluent). *Table 3.3* compares the running times for the TMB problem and SMB cases. A strong dependency between the number of PDEs and the resulting running time was found.

Table 3.3. Running times for the TMB and SMB cases (12 full cycles).
(Personal Computer Duo Pentium Pro 200 MHz, 512 Kb Cache, 64 Mb RAM)
(*PDECOL* parameters: *KORD* = 4, *NINT* = 20, *NCC* = 2, *EPS* = $10^{-10}$).

| Model | Number of Columns per Section | Number of PDEs | Number of ODEs | Running Time |
|---|---|---|---|---|
| TMB | ------ | 16 | 672 | 5.5 hours |
| SMB4 | 1 | 16 | 672 | 5.5 hours |
| SMB8 | 2 | 32 | 1344 | 3.5 days |
| SMB12 | 3 | 48 | 2016 | 1 month |

## 3.5 Simulation Results

The chromatographic resolution of bi-naphthol enantiomers (*Figure 3.1*) was considered for simulation purposes. The chiral stationary phase used in this system is 3,5-dinitrobenzoyl phenylglycine bonded to silica gel and a mixture of 72/28 (v/v) heptane/isopropanol was used as eluent. The limit of solubility in this eluent is 3 g/l of each enantiomer.

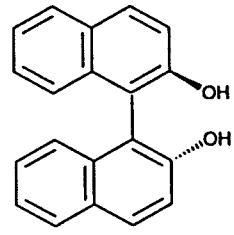


Figure 3.1. Bi-naphthol enantiomers.

The adsorption equilibrium isotherms, measured at 25 C, are of bi-Langmuir type and were proposed by the *Separex* group (personal communication):

$$q_A^* = \frac{2.69 c_A}{1+0.0336 c_A + 0.0466 c_B} + \frac{0.10 c_A}{1+c_A+3c_B} \qquad (3.39a)$$

$$q_B^* = \frac{3.73 c_B}{1+0.0336 c_A + 0.0466 c_B} + \frac{0.30 c_B}{1+c_A+3c_B} \qquad (3.39b)$$

The operating conditions and model parameters used in simulation for the TMB approach are presented in *Table 3.4*. *Tables 3.5* and *3.6* present the equivalencies in terms of flow-rates and model parameters that have to be made for the SMB systems with different subdivisions of the bed. Note that for SMB systems, the internal flow-rates in the four different sections are independent of the degree of subdivision of the bed and they are related to the TMB flow-rates by the equivalencies presented before (*Equations 3.17* and *3.18*). Three cases are analyzed for SMB system: SMB4, constituted by four columns, one in each section; SMB8, with 8 columns, two per section; and SMB12, with three columns per section. The length of each fixed-bed column in these cases was chosen by keeping constant the total length of each section. The value for switch time interval was then evaluated keeping constant the ratio $L_c / t^*$, the simulated solid velocity. Also, the number of mass transfer units per section is the same for TMB and SMB cases and is evaluated for $k$=0.1 $s^{-1}$ (*Table 3.6*). Summarizing, all the SMB cases present the same operating conditions and model parameters at a section scale (equivalent to the TMB case), except for the degree of subdivision of the bed.

Table 3.4. Operating conditions and model parameters for the TMB approach.

| **TMB operation conditions:** | | **Model parameters:** |
|---|---|---|
| Feed concentration: | 2.9 g/l each | Solid/fluid volumes, $(1-\varepsilon)/\varepsilon = 1.5$ |
| Solid flow-rate: | 11.15 ml/min | Ratio between fluid and solid velocities: |
| Recycling flow-rate: | 27.95 ml/min | $\gamma_I = 6.65$ ; $\gamma_{II} = 4.23$ |
| Eluent flow-rate: | 21.45 ml/min | $\gamma_{III} = 4.72$ ; $\gamma_{IV} = 3.76$ |
| Extract flow-rate: | 17.98 ml/min | Number of mass transfer units, |
| Feed flow-rate: | 3.64 ml/min | $\alpha = 36.0$ ($k = 0.1$ s$^{-1}$) |
| Raffinate flow-rate: | 7.11 ml/min | Peclet number, $Pe = 2000$ |
| **Columns:** | | |
| Diameter: | 2.6 cm | Section Length: 21.0 cm |

Table 3.5. Equivalence between TMB and SMB flow-rates.

| | **TMB** | | **SMB** | |
|---|---|---|---|---|
| Section | $Q_j$ | $\gamma_j$ | $Q_j^*$ | $\gamma_j^*$ |
| I | 49.40 | 6.65 | 56.83 | 7.65 |
| II | 31.42 | 4.23 | 38.85 | 5.23 |
| III | 35.06 | 4.72 | 42.49 | 5.72 |
| IV | 27.95 | 3.76 | 35.38 | 4.76 |

Table 3.6. Equivalence between TMB and SMB approaches with different subdivision of the bed.

| Case | $N_s$ | $L_c$ (cm) | $L_j$ (cm) | $t^*$ (min) | $u_s = L_c / t^*$ (cm/min) | $\alpha$ | $N_s\,\alpha$ | $Pe$ |
|---|---|---|---|---|---|---|---|---|
| TMB | ------ | ------ | 21 | ------ | 3.5 | 36 | 36 | 2000 |
| SMB4 | 1 | 21 | 21 | 6 | 3.5 | 36 | 36 | 2000 |
| SMB8 | 2 | 10.5 | 21 | 3 | 3.5 | 18 | 36 | 1000 |
| SMB12 | 3 | 7 | 21 | 2 | 3.5 | 12 | 36 | 667 |

The cyclic steady-state behaviour, characteristic of a SMB operation, is shown in *Figures 3.2* and *3.3* for the case of 8-columns configuration (2 columns per section). *Figure 3.2* presents the concentration of the two enantiomers in extract (*Figure 3.2a*) and raffinate (*Figure 3.2b*) after cyclic steady-state is reached (in this case, after 10 full cycles). Extract and raffinate exhibit concentration profiles that are reproduced in the same way fraction after fraction.

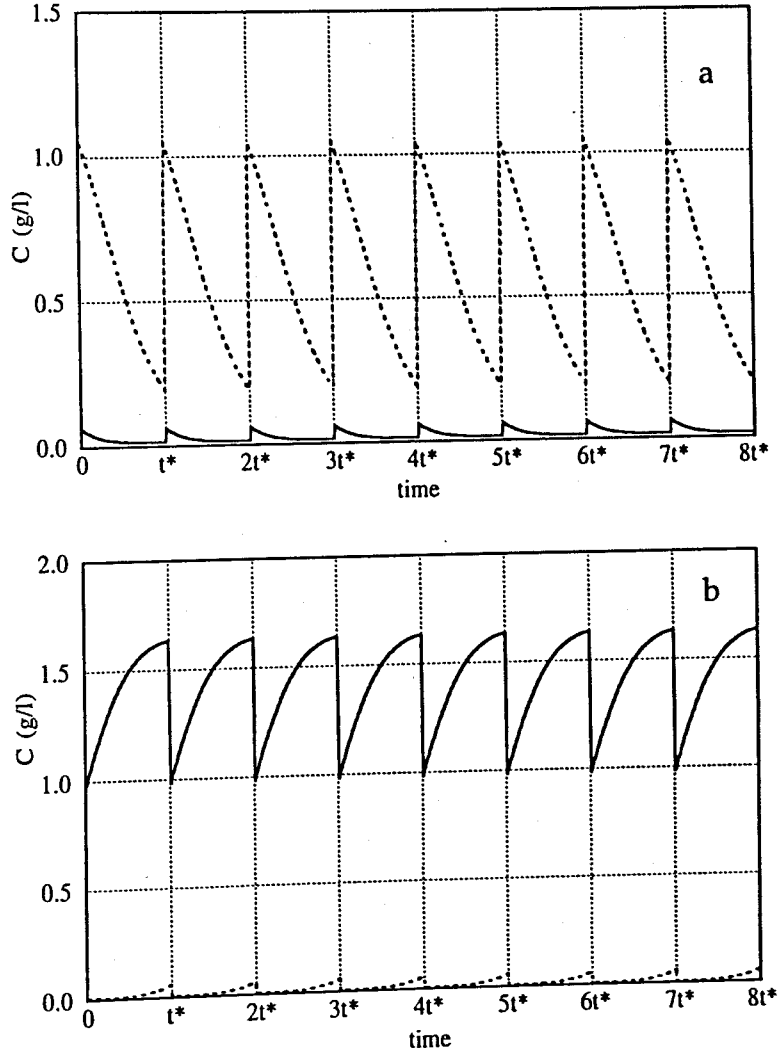


Figure 3.2. Concentration profiles in (a) the extract and (b) raffinate for SMB8 at cyclic steady-state and during a full cycle.
Dotted lines is for the more retained component;
solid line is for the less retained component.

For the same case (SMB8), *Figure 3.3* shows the evolution of the internal concentration profiles after cyclic steady-state is reached, during a switch time interval. Note that, since steady-state is achieved, the concentration profiles at the end of a switch time interval are the same at the beginning of this interval, but that they are advanced one column. Again, these profiles will be reproduced in the same way fraction after fraction and column after column.

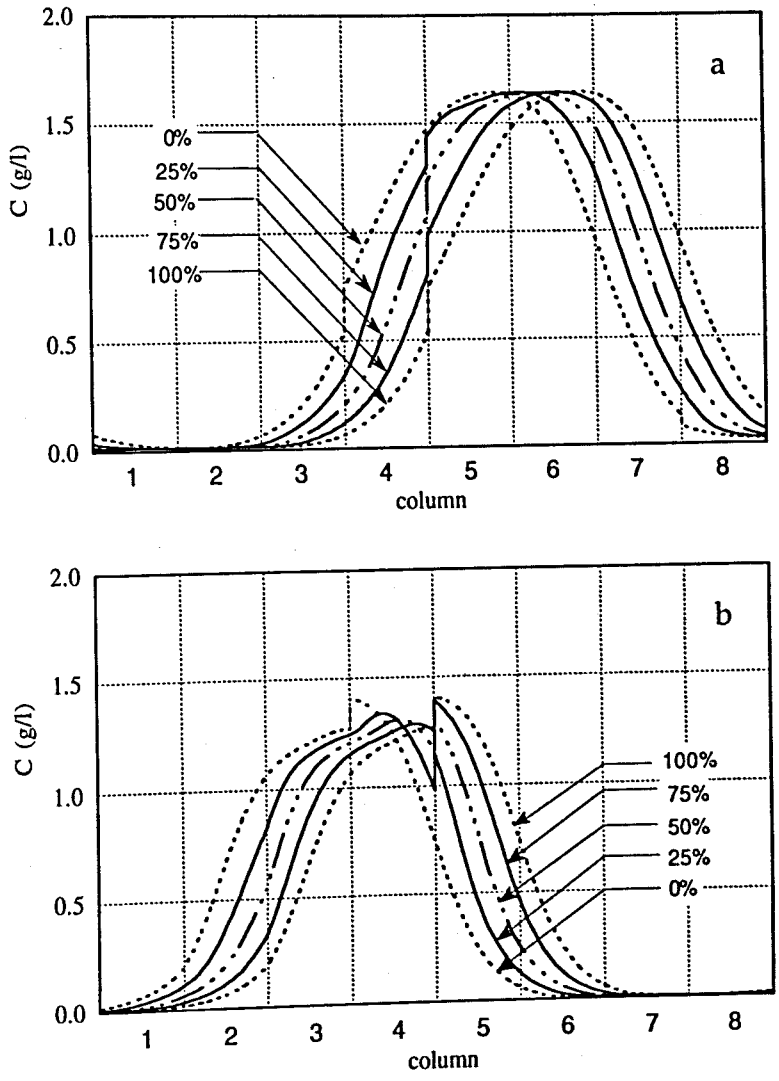


Figure 3.3. Cyclic steady-state internal concentration profiles during a switch time interval (fraction) for SMB8.
Profiles for the less retained component (a) and for the more retained component (b) at the beginning, 25%, 50%, 75%, and at the end of a switch time interval (eluent at the beginning of column 1; extract between columns 2 and 3; feed between columns 4 and 5; raffinate between columns 6 and 7).

*Figures 3.4* and *3.5* show the influence of the degree of subdivision of the bed in the transient concentration of extract and raffinate, and make the comparison with the TMB approach. The behaviour of the SMB is predicted in three ways: the exact transient evolution of concentration profiles, the average concentration evaluated at each switch time interval, and the instantaneous concentration evaluated at half time between two successive switchings. These figures show the transient evolution during the first five cycles. Although the switch time interval depends on the degree of subdivision of the bed, the duration of a full cycle will be 24 minutes for all SMB cases.

From these figures it is clear that there are differences between SMB and TMB predictions, and that they are attenuated with the increase of the number of subdivisions. In fact, the similarity would be perfect if the adsorbent bed were divided into an infinite number of fixed-bed columns and using an infinitesimal switch time interval. This can be corroborated by noticing that the amplitude of variation of exact concentration is decreasing and approaching the TMB behaviour, with the increase of the number of subsections.

The influence of the degree of subdivision of the SMB system and its comparison with the TMB approach at steady-state operation is analyzed through *Figures 3.6* to *3.9*. *Figures 3.6* to *3.8* show the cyclic steady-state behaviour for SMB operation in terms of the extract and raffinate concentrations and purities. The steady-state behaviour of the TMB operation is also shown in these figures.

We can conclude that there are differences in the extract and raffinate concentrations between the TMB and the SMB approaches. If the simulation objective is to obtain the dynamic behaviour of extract and raffinate concentrations, the SMB approach is needed, even for SMB cases with many columns per section (for instance, the SMB12 case with 3 columns per section). However, these differences are attenuated in terms of purities (*Figure 3.8*) because the concentrations of both species show similar dynamic behaviours in the extract and raffinate streams. In fact, the SMB extract concentration of both species decrease during a switch time interval (*Figure 3.6a,b*), while the SMB raffinate concentrations of the two components increase during the same interval (*Figure 3.7a,b*).

*Figure 3.9* compares the steady-state internal concentration profiles, evaluated at half time between switchings, for TMB and SMB cases. The major difference appears for the SMB4 case, while small deviations occur between SMB8 and SMB12 behaviours.

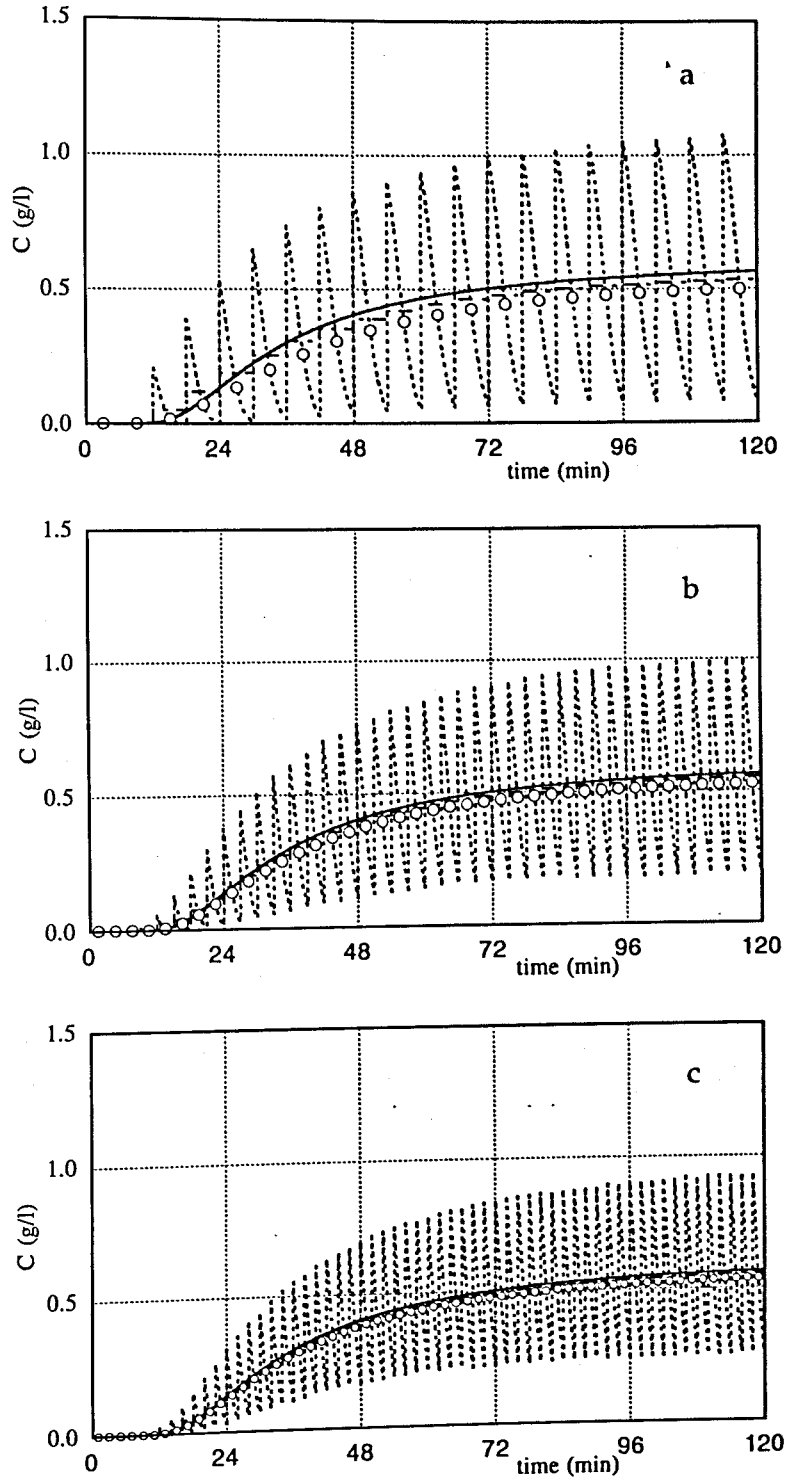


Figure 3.4. Transient evolution (first 5 cycles) of the concentration of the more retained component in the extract for (a) SMB4, (b) SMB8, and (c) SMB12. The full line is the TMB approach; the dotted line is the SMB approach; the step dotted line is the SMB approach with average concentration over a switch time interval; o o o is the SMB instantaneous concentration evaluated between switchings.

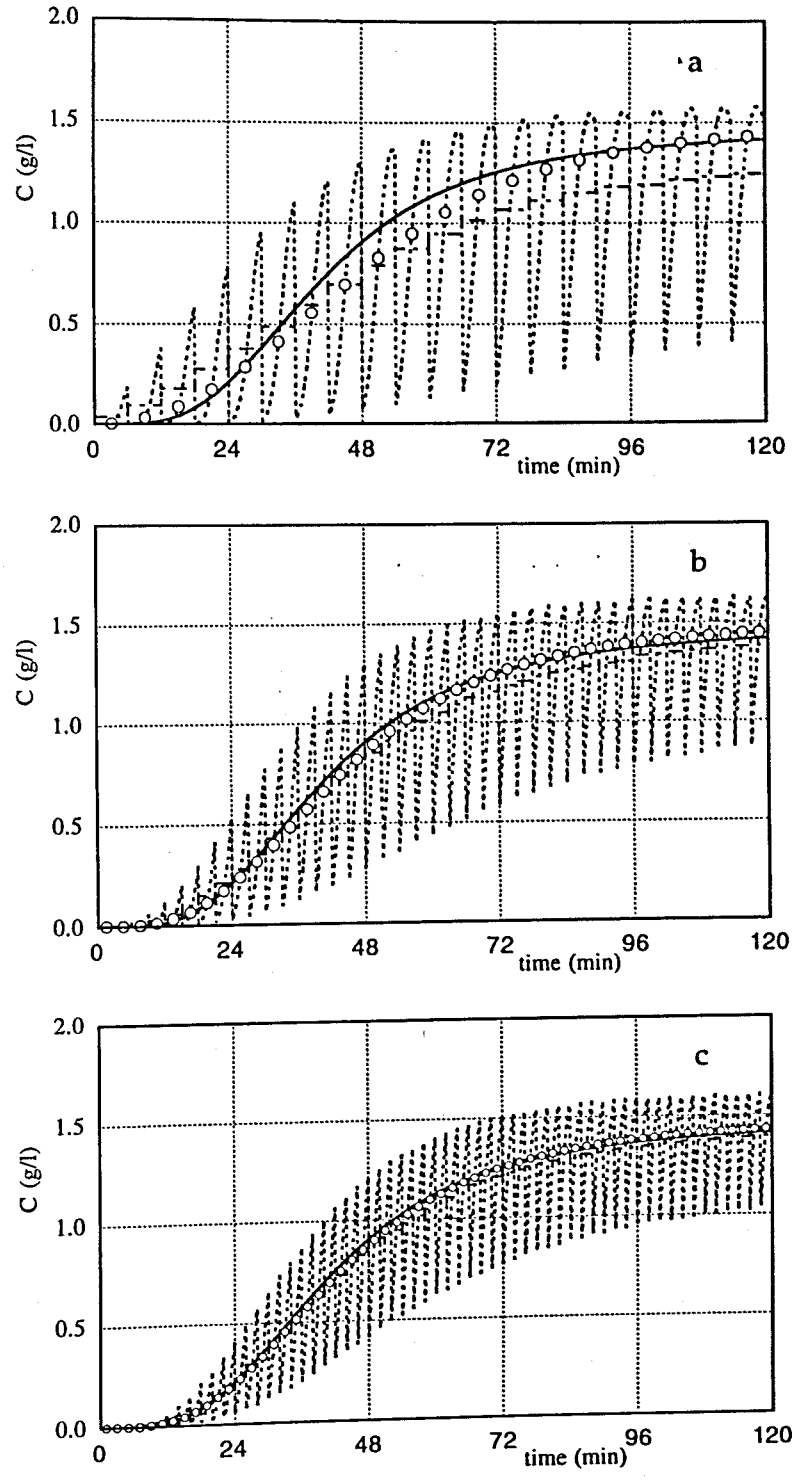


Figure 3.5. Transient evolution (first 5 cycles) of the concentration of the less retained component in the raffinate for (a) SMB4, (b) SMB8, and (c) SMB12. The full line is the TMB approach; the dotted line is the SMB approach; the step dotted line is the SMB approach with average concentration over a switch time interval; o o o is the SMB instantaneous concentration evaluated between switchings.

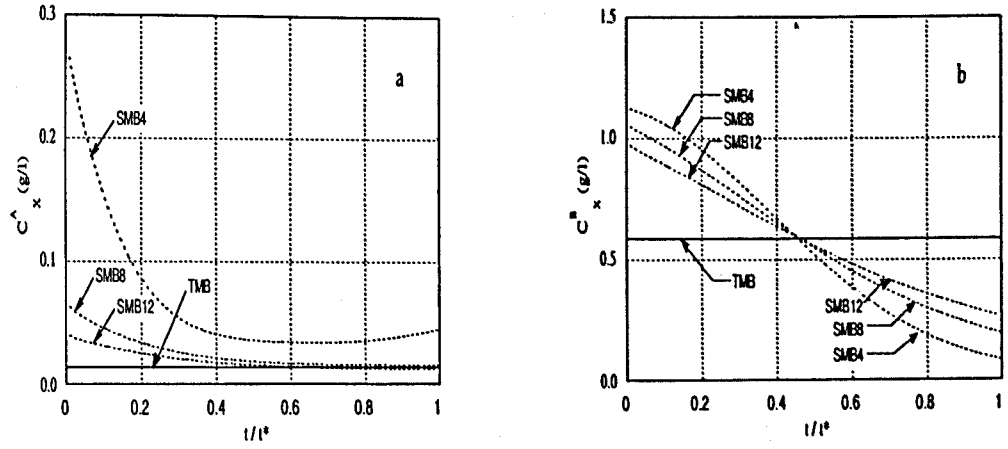


Figure 3.6. Extract concentrations at steady-state in the TMB approach and SMB cases. Concentration of the less (a) and more (b) retained components.

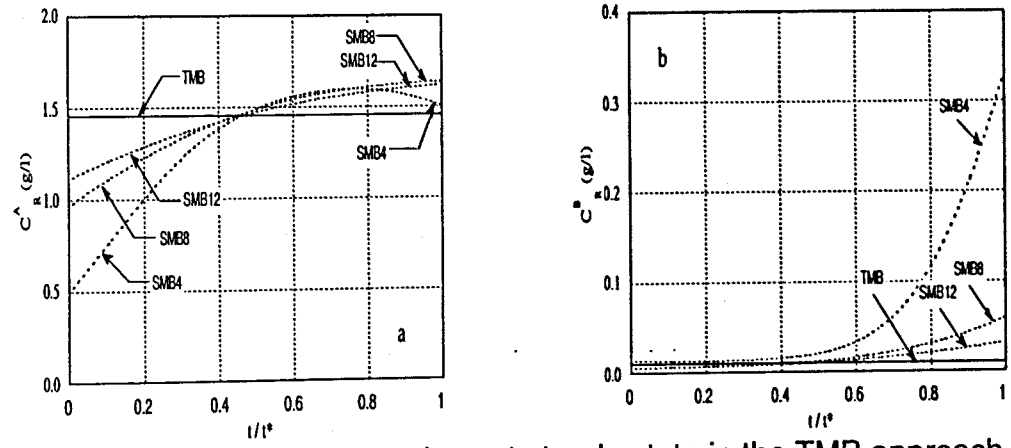


Figure 3.7. Raffinate concentrations at steady-state in the TMB approach and SMB cases. Concentration of the less (a) and more (b) retained components.

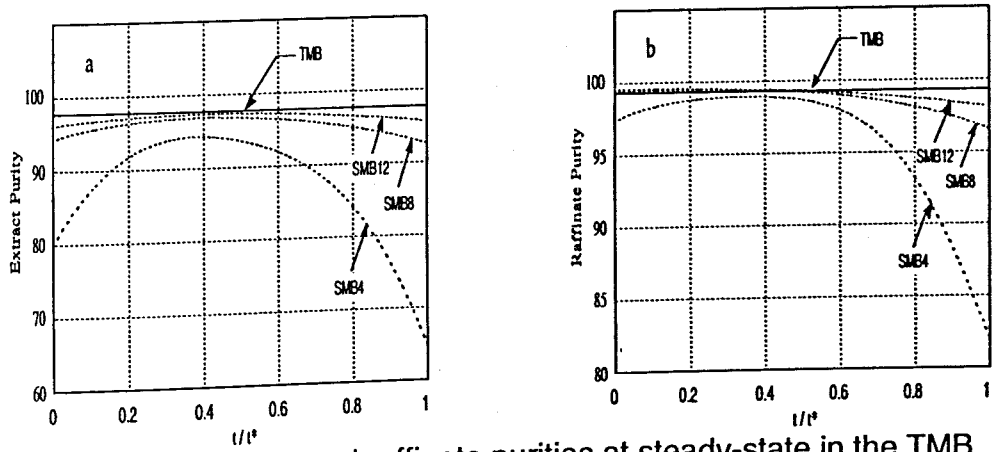


Figure 3.8. Extract and raffinate purities at steady-state in the TMB approach and SMB cases. (a) Extract purity; (b) Raffinate purity.

Nevertheless, near the feed point, there is a permanent difference between TMB and all SMB cases. This is due to the fact that the internal flow-rates in the TMB are smaller than in the SMB, leading to a small dilution of the feed stream (see *Table 3.5* and mass balances for the feed node, *Equations 3.5c* and *3.23c*). As a consequence, near the feed inlet, TMB concentrations will be higher than in the SMB operation. The opposite will occur near the eluent point, although the differences will be insignificant if concentrations are near zero, as it usually arises when flow-rates are well estimated.

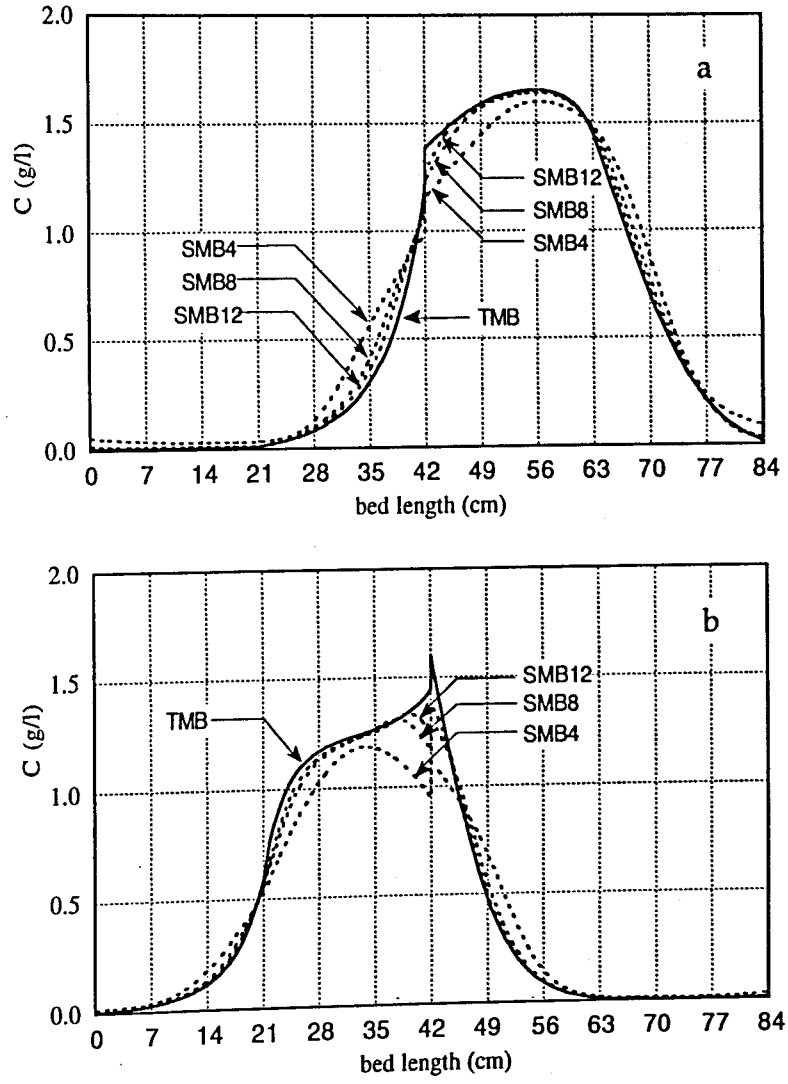


Figure 3.9. Steady-state internal concentration profiles in the TMB approach and SMB cases at half-time between switchings: (a) less retained component; (b) more retained component. The full line is for TMB approach; the dotted line is for SMB cases (eluent inlet = 0 cm; extract outlet = 21 cm; feed inlet = 42 cm; raffinate inlet = 63 cm).

For practical aims, the more important question may be what is the difference between TMB and SMB performances and what is the influence of the degree of subdivision of the adsorbent bed. *Table 3.7* shows the predictions obtained for extract and raffinate purities after steady-state is reached. The raffinate and extract purities in SMB units with 4, 8, and 12 columns are increasing towards the one obtained in the equivalent TMB unit.

Table 3.7. Comparison between extract and raffinate purities in the TMB approach and SMB cases.

| Case | Extract Purity (%) | Raffinate Purity (%) |
|---|---|---|
| SMB4 | 89.5 | 95.2 |
| SMB8 | 95.9 | 98.7 |
| SMB12 | 96.8 | 99.1 |
| TMB | 97.7 | 99.3 |

An uncommon difference appears for the SMB4 case. This can be easily explained, noticing that only in this case, the jump of one inlet or outlet line is done to a column that did not already perform the same function of the previous column (because they do not belong to the same section). In fact, the extract outlet will jump at the beginning of each switch time interval to the previous feed inlet, and the same will occur between raffinate and eluent. For the other SMB cases, the differences are not so significant, and a practical question remains: from an economic point of view, what is the optimum degree of subdivision of a SMB system?

It is obvious that a system with more columns per section will be more expensive, mainly due to the need of a more complex arrangement of valves to control the discrete jump of inlet and outlet lines. On the other hand, a system constituted by a higher number of columns will be able to perform separations with higher purities and/or higher productivities. The optimum degree of subdivision of the SMB unit will depend of the difficulty of the separation and the product purity requirements, as it was noticed by Hidajat *et al.* (1986b) and, more recently, by Tondeur and Bailly (1993) and Bauer *et al.* (1996). Typically, systems sold into the pharmaceutical industry have among 8 and 16 columns.

## 3.6 Conclusions

It is clear from this study that the prediction of the performance of a SMB operation, and so the flow-rate optimization, can be done using the TMB approach, although small differences will appear between these two strategies of modeling. These differences will be more significant if a low degree of subdivision of the adsorbent bed is used, specially in the case of a SMB with only one column per section.

For practical aims, the optimum degree of subdivision will depend on both the difficulty of the separation and the product purity requirements. Nevertheless, the SMB model will be always useful to characterize the dynamic cyclic behaviour of the concentration profiles.

To predict the steady-state performance of a simulated moving bed separation process, one can use the TMB model with obvious advantages in computing time savings. Moreover, if we are interested in characterize only the steady-state operation, we can develop a steady-state TMB model which is simpler to implement. In fact, the original problem represented by a set of partial differential equations will be simplified to a set of ordinary differential equations. In the next chapter, this strategy will be followed to study the influence of the various operating variables and model parameters on the SMB performance.

## 3.7 References

Azevedo, D.C.S., Neves, S.B., Ravagnani, S.P., Cavalcante Jr., C.L., and Rodrigues, A.E., "The Influence of Dead Zones on Simulated Moving Bed Units," *Proceedings of the 6th International Conference on Fundamentals of Adsorption*, Presqu'île de Giens, France (1998).

Barker, P.E., England, K., and Vlachogiannis, G., "Mathematical Model for the Fractionation of Dextran on a Semi-Continuous Counter-Current Simulated Moving Bed Chromatograph," *Chem. Eng. Res. Des.* **61**, 241-247 (1983).

Bauer, J., Priegnitz, A., Chandhok, A., and Wilcher, S., "UOP Sorbex Simulated Moving Bed Technology: The Effect of Bed Number on Simulated Moving Bed Performance," Poster presented at *PREP'96 Int. Symp. on Preparative and Industrial Chromatography and Related Techniques*, Basel, Switzerland (1996).

Bellot, J., and Condoret, J., "Modelling of Liquid Chromatography Equilibria," *Proc. Biochemistry* **28**, 365-376 (1993).

Carta, G., and Pigford, R.L., "Periodic Countercurrent Operation of Sorption Processes Applied to Water Desalination with Thermally Regenerable Ion-Exchange Resins," *Ind. Eng. Chem. Fundam.* **25**, 677-685 (1986).

Charton, F., and Nicoud, R.-M., "Complete Design of a Simulated Moving Bed," *J. Chromatogr. A* **702**, 97-112 (1995).

Chiang, A., "Complete Separation Conditions for a Local Equilibrium TCC Adsorption Unit," *AIChE J.* **44**, 332-340 (1998).

Ching, C.B., "A Theoretical Model for the Simulation of the Operation of the Semi-Continuous Chromatographic Refiner for Separating Glucose and Fructose," *J. Chem. Engng Japan* **16**, 49-53 (1983).

Ching, C.B., and Ruthven, D.M., "An Experimental Study of a Simulated Counter-Current Adsorption System - I. Isothermal Steady State Operation," *Chem. Engng Sci.* **40**, 877-885 (1985a).

Ching, C.B., and Ruthven, D.M., "An Experimental Study of a Simulated Counter-Current Adsorption System - II. Transient Response," *Chem. Engng Sci.* **40**, 887-891 (1985b).

Ching, C.B., Ruthven, D.M., and Hidajat, K., "Experimental Study of a Simulated Counter-Current Adsorption System - III. Sorbex Operation," *Chem. Engng Sci.* **40**, 1411-1417 (1985).

Ching, C.B., Hidajat, K., and Ruthven, D.M., "Experimental Study of a Simulated Counter-Current Adsorption System - V. Comparison of Resin and Zeolite Adsorbents for Fructose-Glucose Separation at High Concentration," *Chem. Engng Sci.* **42**, 2547-2555 (1987).

Ching, C.B., Ho, C., and Ruthven, D.M., "Experimental Study of a Simulated Counter-Current Adsorption System - VI. Non-Linear Systems," *Chem. Engng Sci.* **43**, 703-711 (1988).

Ching, C.B., Chu, K.H., Hidajat, K., and Uddin, M.S., "Experimental and Modeling Studies of the Transient Behavior of a Simulated Countercurrent Adsorber," *J. Chem. Engng Japan* **24**, 614-621 (1991).

Ching, C.B., Chu, K.H., Hidajat, K., and Uddin, M.S., "Comparative Study of Flow Schemes for a Simulated Countercurrent Adsorption Separation Process," *AIChE J.* **38**, 1744-1750 (1992).

Ching, C.B., Chu, K.H., Hidajat, K., and Ruthven, D.M., "Experimental Study of a Simulated Counter-Current Adsorption System - VII. Effects of Non-Linear and Interacting Isotherms," *Chem. Engng Sci.* **48**, 1343-1351 (1993).

Chu, K.H., and Hashim, M.A., "Simulated Countercurrent Adsorption Processes: A Comparison of Modelling Strategies," *Chem. Engng J.* **56**, 59-65 (1995).

Dandekar, H.W., Chandhok, A.K., and Priegnitz, J.W., "Modeling and Simulation of SMB Technology for Pharmaceutical and Fine Chemical Applications," *Proceedings of the 5th International Conference on Fundamentals of Adsorption*, M.D. LeVan, ed., Kluwer Academic Publishers, Boston, Massachusetts, p. 243-250 (1996).

Ernst, U., and Hsu, J., "Study of Simulated Moving-Bed Separation Processes Using a Staged Model," *Ind. Eng. Chem. Res.* **28**, 1211-1221 (1989).

Ernst, U., and Hsu, J., "Theoretic Study of Backmixing in Simulated Moving-Bed Adsorption Process with Multiple Equilibrium Stages Between Ports," *Sep. Technol.* **2**, 197-207 (1992).

Glueckauf, E., "Theory of Chromatography Part 10 - Formulæ for Diffusion into Spheres and Their Application to Chromatography," *Trans. Faraday Soc.* **51**, 1540-1551 (1955).

Hashimoto, K., Adachi, S., Noujima, H., and Maruyama, H., "Models for the Separation of Glucose/Fructose Mixture Using a Simulated Moving-Bed Adsorber," *J. Chem. Engng Japan* **16**, 400-406 (1983).

Hashimoto, K., Yamada, M., Shirai, Y., and Adachi, S., "Continuous Separation of Glucose-Salts Mixture with Nonlinear and Linear Adsorption Isotherms by Using a Simulated Moving-Bed Adsorber," *J. Chem. Engng Japan* **20**, 405-410 (1987).

Hashimoto, K., Adachi, S., Shirai, Y., and Morishita, M., "Operation and Design of Simulated Moving-Bed Adsorbers," *Preparative and Production Scale Chromatography*, G. Ganetsos and P.E. Barker, eds., Marcel Dekker, New York, p. 273-300 (1993).

Hassan, M.M., Shamsur Rahman, A., and Loughlin, K.F., "Numerical Simulation of Unsteady Continuous Countercurrent Adsorption System with Nonlinear Adsorption Isotherm," *Sep. Technol.* **4**, 15-26 (1994).

Hassan, M.M., Shamsur Rahman, A., and Loughlin, K.F., "Modelling of Simulated Moving Bed Adsorption System: A More Precise Approach," *Sep. Technol.* **5**, 77-89 (1995).

Hidajat, K., Ching, C.B., and Ruthven, D.M., "Numerical Simulation of a Semi-Continuous Counter-Current Adsorption Unit for Fructose-Glucose Separation," *Chem. Engng J.* **33**, B55-B61 (1986a).

Hidajat, K., Ching, C.B., and Ruthven, D.M., "Simulated Counter-Current Adsorption Processes: A Theoretical Analysis of the Effect of Subdividing the Adsorbent Bed," *Chem. Engng Sci.* **41**, 2953-2956 (1986b).

Hidajat, K., and Ching, C.B., "Simulation of the Performance of a Continuous Counter-Current Adsorption System by the Method of Orthogonal Collocation with Non-Linear and Interacting Adsorption Isotherms," *Trans. Int. Chem. Engng* **68**, 104-108 (1990).

Hindmarsh, A.C., "Preliminary Documentation of GEARIB. Solution of Implicit Systems of Ordinary Differential Equations with Banded Jacobians," *Rep. UCID - 30130*, Lawrence Livermore Laboratory, Livermore (1976).

Hotier, G., "Physically Meaningful Modeling of the 3-Zone and 4-Zone Simulated Moving Bed Processes," *AIChE J.* **42**, 154-160 (1996).

Jacobson, S., Golshan-Shirazi, S., and Guiochon, G., "Isotherm Selection for Band Profile Simulations in Preparative Chromatography," *AIChE J.* **37**, 836-844 (1991).

Kubota, K., Hata, C., and Hayashi, S., "A Study of a Simulated Moving Bed Adsorber Based on the Axial Dispersion Model," *Can. J. Chem. Engng* **67**, 1025-1029 (1989).

Lameloise, M.L., and Viard, V., "Modelling and Simulation of a Glucose-Fructose Simulated Moving Bed Adsorber," *Trans. Int. Chem. Engng* **71**, 27-32 (1993).

Lim, B.G., Ching, C.B., and Tan, R., "Determination of Competitive Adsorption Isotherms of Enantiomers on a Dual-site Adsorbent," *Sep. Technol.* **5**, 213-228 (1995).

Lim, B.G., and Ching, C.B., "Modelling Studies on the Transient and Steady State Behaviour of a Simulated Counter-Current Chromatographic System," *Sep. Technol.* **6**, 29-41 (1996).

Ma, Z., and Wang, L., "Standing Wave Analysis of SMB Chromatography: Linear Systems," *AIChE J.* **43**, 2488-2508 (1997).

Madsen, N.K., and Sincovec, R.F., "PDECOL: General Collocation Software for Partial Differential Equations," *ACM Trans. Math.* **5**, 326-351 (1979).

Mazzotti, M., Storti, G., and Morbidelli, M., "Robust Design of Countercurrent Adsorption Separation Processes: 2. Multicomponent Systems," *AIChE J.* **40**, 1825-1842 (1994).

Mazzotti, M., Storti, G., and Morbidelli, M., "Robust Design of Countercurrent Adsorption Separation : 3. Nonstoichiometric Systems," *AIChE J.* **42**, 2784-2796 (1996a).

Mazzotti, M., Pedeferri, M., and Morbidelli, M., "Design of Optimal and Robust Operating Conditions for Chiral Separations Using Simulated Moving Beds," *Proceedings of the Chiral Europe'96 Symposium*, Spring Innovations Limited, Stockport, UK (1996b).

Mazzotti, M., Storti, G., and Morbidelli, M., "Robust Design of Countercurrent Adsorption Separation Processes: 4. Desorbent in the Feed," *AIChE J.* **43**, 64-72 (1997a).

Mazzotti, M., Storti, G., and Morbidelli, M., "Optimal Operation of Simulated Moving Bed Units for Nonlinear Chromatographic Separations," *J. Chromatogr. A* **769**, 3-24 (1997b).

Navarro, A., Caruel, H., Rigal, L., and Phemius, P., "Continuous Chromatographic Separation Process: Simulated Moving Bed Allowing Simultaneous Withdrawal of Three Fractions," *J. Chromatogr. A* **770**, 39-50 (1997).

Nicoud, R.-M., and Seidel-Morgenstern, A., "Adsorption Isotherms: Experimental Determination and Application to Preparative Chromatography," *Simulated Moving Bed: Basics and Applications*, R.-M. Nicoud, ed., Institut National Polytechnique de Lorraine, Nancy, France, p. 4-34 (1993).

Pais, L.S., Loureiro, J.M., and Rodrigues, A.E., "Separation of 1,1'-bi-2-naphthol Enantiomers by Continuous Chromatography in Simulated Moving Bed," *Chem. Engng Sci.* **52**, 245-257 (1997a).

Pais, L.S., Loureiro, J.M., and Rodrigues, A.E., "Modeling, Simulation and Operation of a Simulated Moving Bed for Continuous Chromatographic Separation of 1,1'-bi-2-naphthol Enantiomers," *J. Chromatogr. A* **769**, 25-35 (1997b).

Pais, L.S., Loureiro, J.M., and Rodrigues, A.E., "Modeling Strategies for Enantiomers Separation by SMB Chromatography," *AIChE J.* **44**, 561-569 (1998a).

Pais, L.S., Loureiro, J.M., and Rodrigues, A.E., "Separation of Enantiomers of a Chiral Epoxide by Simulated Moving Bed Chromatography," *J. Chromatogr. A* **827**, 215-233 (1998b).

Rodrigues, A.E., Loureiro, J.M., Lu, Z.P., and Pais, L.S., "Modeling and Operation of a Simulated Moving Bed for the Separation of Optical Isomers," *Proceedings of the 5th International Conference on Fundamentals of Adsorption*, M.D. LeVan, ed., Kluwer Academic Publishers, Boston, Massachusetts, p. 765-772 (1996).

Ruthven, D.M., *Principles of Adsorption and Adsorption Processes*, John Wiley & Sons, New York, USA (1984).

Ruthven, D.M., and Ching, C.B., "Counter-Current and Simulated Counter-Current Adsorption Separation Processes," *Chem. Engng Sci.* **44**, 1011-1038 (1989).

Ruthven, D.M., and Ching, C.B., "Modeling of Chromatographic Processes," *Preparative and Production Scale Chromatography*, G. Ganetsos and P.E. Barker, eds., Marcel Dekker, New York, p. 629-672 (1993).

Schmidt-Traub, H., and Strube, J., "Dynamic Simulation of Simulated-Moving Bed Chromatographic Processes," *Comput. Chem. Engng* **20**, S641-S646 (1996).

Shamsur Rahman, A., Hassan, M.M., and Loughlin, K.F., "Unsteady State Simulation of Sorbex System with Nonlinear Adsorption Isotherm," *Sep. Technol.* **4**, 27-37 (1994).

Storti, G., Masi, M., Paludetto, R., Morbidelli, M., and Carrà, S., "Adsorption Separation Processes: Countercurrent and Simulated Countercurrent Operations," *Comput. Chem. Engng* **12**, 475-482 (1988).

Storti, G., Masi, M., and Morbidelli, M., "On Countercurrent Adsorption Separation Processes," *Adsorption: Science and Technology*, A.E. Rodrigues *et al.*, eds., NATO ASI Series, Kluwer Academic Publishers, Dordrecht, The Netherlands, p. 357-381 (1989a).

Storti, G., Masi, M., Carrà, S., and Morbidelli, M., "Optimal Design of Multicomponent Countercurrent Adsorption Separation Processes Involving Nonlinear Equilibria," *Chem. Engng Sci.* **44**, 1329-1345 (1989b).

Storti, G., Masi, M., and Morbidelli, M., "Modeling of Countercurrent Adsorption Processes," *Preparative and Production Scale Chromatography*, G. Ganetsos and P.E. Barker, eds., Marcel Dekker, New York, p. 673-700 (1993a).

Storti, G., Mazzotti, M., Morbidelli, M., and Carrà, S., "Robust Design of Binary Countercurrent Adsorption Separation Processes," *AIChE J.* **39**, 471-492 (1993b).

Storti, G., Baciocchi, R., Mazzotti, M., and Morbidelli, M., "Design of Optimal Operating Conditions of Simulated Moving Bed Adsorptive Units," *Ind. Eng. Chem. Res.* **34**, 288-301 (1995).

Strube, J., Altenhöner, U., Meurer, M., Schmidt-Traub, H., and Schulte, M., "Dynamic Simulation of Simulated Moving-Bed Chromatographic Processes for the Optimization of Chiral Separations," *J. Chromatogr. A* **769**, 81-92 (1997).

Tondeur, D., and Bailly, M. "Simulated Countercurrent, Fixed-Bed and Column Switching Schemes," *Simulated Moving Bed: Basics and Applications*, R.-M. Nicoud, ed., Institut National Polytechnique de Lorraine, Nancy, France, p. 97-117 (1993).

Yun, T., Bensetiti, Z., Zhong, G., and Guiochon, G., "Effect of the Column Efficiency on the Internal Concentration Profiles and the Performance of a Simulated Moving-Bed Unit in the Case of a Linear Isotherm," *J. Chromatogr. A* **758**, 175-190 (1997a).

Yun, T., Zhong, G., and Guiochon, G., "Simulated Moving Bed Under Linear Conditions: Experimental vs. Calculated Results," *AIChE J.* **43**, 935-945 (1997b).

Yun, T., Zhong, G., and Guiochon, G., "Experimental Study of the Influence of the Flow Rates in SMB Chromatography," *AIChE J.* **43**, 2970-2983 (1997c).

Zhong, G., and Guiochon, G., "Analytical Solution for the Linear Ideal Model of Simulated Moving Bed Chromatography," *Chem. Engng Sci.* **51**, 4307-4319 (1996).

Zhong, G., Smith, M.S., and Guiochon, G., "Effect of the Flow Rates in Linear, Ideal, Simulated Moving-Bed Chromatography," *AIChE J.* **43**, 2960-2969 (1997).

Zhong, G., and Guiochon, G., "Simulated Moving Bed Chromatography. Effects of Axial Dispersion and Mass Transfer Under Linear Conditions," *Chem. Engng Sci.* **52**, 3117-3132 (1997a).

Zhong, G., and Guiochon, G., "Simulated Moving Bed Chromatography. Comparison Between the Behaviors Under Linear and Nonlinear Conditions," *Chem. Engng Sci.* **52**, 4403-4418 (1997b).

Zhong, G., and Guiochon, G., "Steady-State Analysis of Simulated Moving Bed Chromatography Using the Linear, Ideal Model," *Chem. Engng Sci.* **53**, 1121-1130 (1998).

Chapter 4

# Simulation and Optimization of a Simulated Moving Bed

*A steady-state model, based on the analogy with the true moving bed, is developed to carry out the simulation and optimization of the SMB operation.*

*The effect of the model parameters and operating variables on the SMB performance is studied and analyzed in terms of purity, recovery, solvent consumption, and adsorbent productivity. Namely, this chapter presents the influence of the switch time interval, recycling flow-rate, and extract and feed flow-rates. Also studied is the influence of axial dispersion and mass transfer resistance on the SMB performance and on the region of separation of both enantiomers.*

*A simple optimization procedure for choosing the best SMB operating conditions is proposed. Namely, an optimization procedure is proposed based on the path of equal purities, i.e., the evaluation of the operating conditions that lead to equal extract and raffinate purities.*

*At the end of this chapter, this optimization procedure is extended to other values of feed concentrations to study its influence on the system performance and to find the optimum feed concentration.*

## 4.1 Introduction

As it was shown in the previous chapter, the prediction of the simulated moving bed operation can be carried out through the equivalent true moving bed approach. For SMB units with more than one column per section, the steady-state performance as well as the concentration internal profiles can be properly evaluated by using the TMB model.

In this chapter we are interested in studying the influence of the operating variables and model parameters on the steady-state performance of a SMB unit. Using the equivalence with the true moving bed operation, we can develop a steady-state TMB model which is characterized by a set of ordinary differential equations and is simpler to implement.

The design problem of a TMB consists on setting the flow-rates in each section to obtain the desired separation. Some constraints have to be met if one wants to recover the less adsorbed component A in the raffinate and the more retained component B in the extract. These constraints are expressed in terms of the net fluxes of components in each section. As it was pointed out in *Chapter 2* (*Figure 4.1*), in section I both species must move upwards, in sections II and III the light species must move upwards, while the net flux of the more retained component must be downwards, and in section IV the net flux of both species have to be downwards, i.e.,

$$\frac{Q_I\, c_{BI}}{Q_S\, q_{BI}} > 1 \quad ; \quad \frac{Q_{II}\, c_{AII}}{Q_S\, q_{AII}} > 1 \quad \text{and} \quad \frac{Q_{II}\, c_{BII}}{Q_S\, q_{BII}} < 1 \quad ;$$

$$\frac{Q_{III}\, c_{AIII}}{Q_S\, q_{AIII}} > 1 \quad \text{and} \quad \frac{Q_{III}\, c_{BIII}}{Q_S\, q_{BIII}} < 1 \quad ; \quad \frac{Q_{IV}\, c_{AIV}}{Q_S\, q_{AIV}} < 1 \tag{4.1}$$

where $Q_I$, $Q_{II}$, $Q_{III}$, $Q_{IV}$ are the volumetric liquid flow-rates in the various sections of the TMB, $Q_S$ is the solid flow-rate, $c_{Aj}$, $c_{Bj}$ are the concentrations of species A and B in the liquid phase and $q_{Aj}$, $q_{Bj}$ are the adsorbed concentrations of components A and B, in section $j$.

The same constraints can be expressed alternatively in terms of fluid and solid interstitial velocities. Defining the dimensionless parameter:

$$\Gamma_{ij} = \frac{\varepsilon}{(1-\varepsilon)} \frac{c_{ij}}{q_{ij}} \gamma_j \tag{4.2}$$

where $\gamma_j = v_j / u_s$ is the ratio between fluid and solid interstitial velocities in zone $j$ and $\varepsilon / (1-\varepsilon)$ is the ratio between fluid and solid volumes, the constraints defined by *Equations 4.1* become:

$$\Gamma_{BI} > 1;\ \Gamma_{A\,II} > 1 \text{ and } \Gamma_{B\,II} < 1;\ \Gamma_{A\,III} > 1 \text{ and } \Gamma_{B\,III} < 1;\ \Gamma_{A\,IV} < 1 \tag{4.3}$$

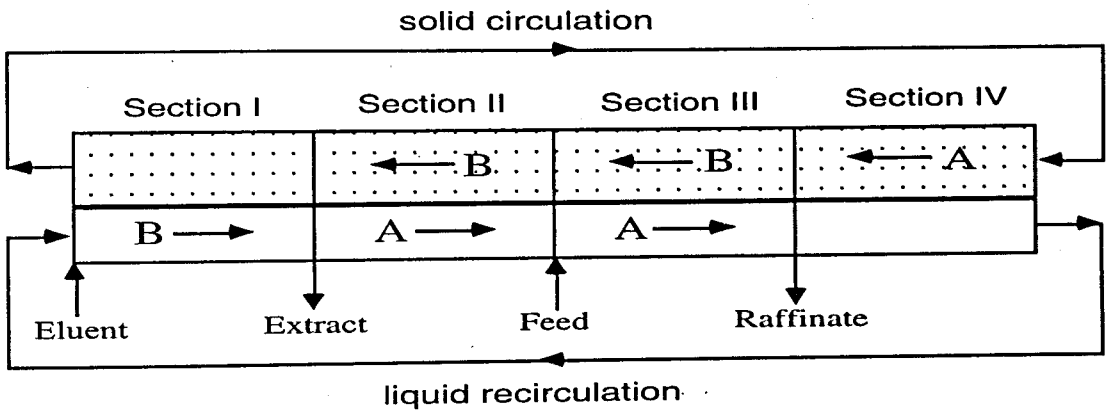


Figure 4.1. Schematic diagram of a True Moving Bed with the desired net fluxes of the two components in each section.

For the case of a binary system with linear adsorption isotherms, very simple formulas can be derived to evaluate the better TMB flow-rates (Ching *et al.*, 1985; Ruthven and Ching, 1989). For the linear case, the net fluxes constraints presented in *Equations 4.1* are reduced to only four, which are

$$\frac{Q_I}{Q_S K_B} > 1 \quad ; \quad \frac{Q_{II}}{Q_S K_A} > 1 \quad ; \quad \frac{Q_{III}}{Q_S K_B} < 1 \quad ; \quad \frac{Q_{IV}}{Q_S K_A} < 1 \tag{4.4}$$

where $K_A$ and $K_B$ are the coefficients of the linear isotherms for the less and more retained species, respectively.

If all these inequalities are assumed to be satisfied by the same margin $\beta$ ($\beta > 1$), *Equations 4.4* can be rewritten as:

$$\frac{Q_I}{Q_S K_B} = \beta \quad ; \quad \frac{Q_{II}}{Q_S K_A} = \beta \quad ; \quad \frac{Q_{III}}{Q_S K_B} = \frac{1}{\beta} \quad ; \quad \frac{Q_{IV}}{Q_S K_A} = \frac{1}{\beta} \tag{4.5}$$

Noticing that

$$Q_E = Q_I - Q_{IV} \;;\; Q_X = Q_I - Q_{II} \;;\; Q_F = Q_{III} - Q_{II} \;;\; Q_R = Q_{III} - Q_{IV} \quad (4.6)$$

where $Q_E$, $Q_X$, $Q_F$, and $Q_R$ are the eluent, extract, feed, and raffinate volumetric flow-rates, respectively, and considering that the volumetric flow-rate in the fourth section represents the recycling flow-rate, $Q_{RF} = Q_{IV}$, the flow-rates for TMB operation can be evaluated by:

$$Q_E = (\alpha\beta^2 - 1)Q_{RF} \quad (4.7a)$$

$$Q_X = (\alpha - 1)\beta^2 Q_{RF} \quad (4.7b)$$

$$Q_F = (\alpha - \beta^2)Q_{RF} \quad (4.7c)$$

$$Q_R = (\alpha - 1)Q_{RF} \quad (4.7d)$$

with

$$Q_{RF} = \frac{K_A Q_S}{\beta} \quad (4.7e)$$

where $\alpha = K_B / K_A$ is the selectivity factor of the binary linear system.

The total inlet or outlet volumetric flow-rates is given by

$$Q_E + Q_F = Q_X + Q_R = (\alpha - 1)(1 + \beta^2)Q_{RF} \quad (4.8)$$

Hence, the specification of the $\beta$ parameter and the solid flow-rate (or, alternatively, one of the liquid flow-rates) defines all the flow-rates throughout the TMB system.

It should be pointed out that the $\beta$ parameter has also a higher limit. In fact, since the feed flow-rate must be higher than zero, *Equation 4.7c* gives

$$\beta < \sqrt{\alpha} \quad (4.9)$$

and, so

$$1 < \beta < \sqrt{\alpha} \quad (4.10)$$

is the interval of possible values for the $\beta$ parameter. The limiting case of $\beta = 1$ corresponds to the situation where dilution of species is minimal, and the extract and

raffinate product concentrations approach the feed concentrations. In fact, from *Equations 4.7* and for $\beta = 1$, results that $Q_E = Q_X = Q_F = Q_R = (\alpha - 1)Q_{RF} = (K_B - K_A)Q_S$. However, under these conditions, an infinite number of stages would be required in each section (Ruthven and Ching, 1989, Nicoud, 1992). In order to improve system stability, it is better to work with higher values, typically $1.02 < \beta < 1.05$ (Nicoud, 1993). For $\beta > 1$ results, from *Equations 4.5*, that

$$Q_I > Q_{III} > Q_{II} > Q_{IV} \tag{4.11}$$

or, from *Equations 4.6*,

$$Q_E > Q_X > Q_R > Q_F \tag{4.12}$$

Considering a situation of complete separation, it follows that the concentrations of the less retained component in the raffinate and of the more retained component in the extract are, respectively

$$C_A^R = \frac{Q_F}{Q_R} C_A^F = \frac{\alpha - \beta^2}{\alpha - 1} C_A^F \tag{4.13}$$

and

$$C_B^X = \frac{Q_F}{Q_X} C_B^F = \frac{\alpha - \beta^2}{(\alpha - 1)\beta^2} C_B^F \tag{4.14}$$

From *Equations 4.13* and *4.14*, we conclude that the raffinate and extract concentrations in the TMB operation under linear conditions will never exceed the feed concentrations (Ruthven and Ching, 1989; Zhong and Guiochon, 1996).

The evaluation of the corresponding flow-rates for the equivalent SMB operation is straightforward. As it was presented in the previous chapter, the equivalence between the internal flow-rates in the two operating modes is given by

$$Q_j^* = Q_j + \frac{\varepsilon}{1 - \varepsilon} Q_s \tag{4.15}$$

with

$$Q_s = \frac{(1 - \varepsilon)V_c}{t^*} \tag{4.16}$$

where $Q_j^*$ and $Q_j$ are the volumetric liquid flow-rates in section $j$ of a SMB and TMB,

respectively, $V_c$ is the volume of one SMB column, and $t^*$ is the switch time period in the SMB operation.

Hence, following the equivalence of internal flow-rates presented by *Equation 4.15*, results that the inlet and outlet flow-rates are the same for the two operating modes (*Equations 4.7a-d*), and

$$Q_{RF}^* = Q_{RF} + \frac{\varepsilon}{(1-\varepsilon)} Q_S = \left[\frac{K_A}{\beta} + \frac{\varepsilon}{(1-\varepsilon)}\right] Q_S = \left[1 + \frac{(1-\varepsilon)}{\varepsilon}\frac{K_A}{\beta}\right] \frac{\varepsilon V_c}{t^*} \qquad (4.17)$$

where $Q_{RF}^*$ is the recycling flow-rate in the SMB operation.

For non-linear systems, however, the evaluation of the better flow-rates is not straightforward. It is well known that, for the majority of the binary systems (chiral mixtures included), the adsorption behaviour must be described with more complex models, such as, the non-linear competitive adsorption isotherm. For this kind of systems, the adsorbed concentration of a component in equilibrium with its concentration in the liquid phase depends not only on its own but also on all other species concentrations. It means that the ratio between the adsorbed-phase and fluid-phase concentrations that influences the net fluxes of both components in the TMB operation (*Equations 4.1*) are no longer constant but concentration-dependent.

Morbidelli and co-workers developed a complete design of the binary countercurrent separation processes by SMB chromatography in the frame of Equilibrium Theory. They assumed that mass transfer resistances and axial dispersion are negligible, and the adsorption equilibria were described through different models: the constant selectivity stoichiometric model (Storti *et al.*, 1993, 1995; Mazzotti *et al.*, 1994), the constant selectivity Langmuir adsorption isotherm (Mazzotti *et al.*, 1996a,b, 1997), the variable selectivity modified Langmuir isotherm (Mazzotti *et al.*, 1997b), and the bi-Langmuir isotherm (Gentilini *et al.*, 1998).

The conditions to achieve complete separation were evaluated considering the equivalent true moving bed operation. Following the assumptions of the Equilibrium Theory, they provided explicit criteria for the choice of the SMB operating conditions that lead to complete separation of a binary mixture. The region for complete separation was defined in terms of the flow-rate ratios in the four sections of the equivalent true moving bed unit:

$$m_j = \frac{Q_j^* t^* - \varepsilon V_c}{(1-\varepsilon)V_c} \tag{4.18}$$

which are related to the $\gamma_j$ ratios used in this work (*Equation 3.31*) by:

$$\gamma_j = \frac{1-\varepsilon}{\varepsilon} m_j \tag{4.19}$$

*Table 4.1* presents the necessary and sufficient conditions for complete separation considering linear isotherms:

$$q_i^* = K_i C_i \quad , \quad (i = A,B) \tag{4.20}$$

*Table 4.2* presents the necessary and sufficient conditions for complete separation considering Langmuir isotherms:

$$q_i^* = \frac{Qb_i C_i}{1 + b_A C_A + b_B C_B} \quad , \quad (i = A,B) \tag{4.21}$$

The equations presented in *Table 4.2* can also be used when a modified Langmuir isotherm (linear+Langmuir) is considered:

$$q_i^* = mC_i + \frac{Qb_i C_i}{1 + b_A C_A + b_B C_B} \quad , \quad (i = A,B) \tag{4.22}$$

In this case, the complete separation region provided by the equations presented in *Table 4.2* must be shift by using the relation

$$m_j^M = m_j^L + m \tag{4.23}$$

where $m_j^L$ is the value obtained considering only the Langmuir term (by using equations in *Table 4.2*) and $m$ is the linear coefficient of the linear+Langmuir isotherm (*Equation 4.22*).

Chiang (1998) extended this study to multicomponent systems, using the constant selectivity stoichiometric isotherm. However, if mass transfer resistance is important, this region for complete separation is reduced, as it was pointed out by Pais *et al.* (1997b, 1998a,b).

Table 4.1. Operating conditions for complete separation under Equilibrium Theory. Linear adsorption isotherms (Mazzotti *et al.*, 1997b).

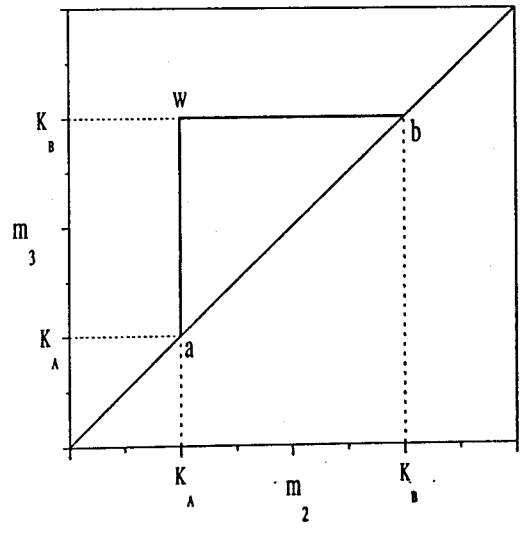


$$K_B < m_1 < \infty \tag{4.24}$$

$$K_A < m_2 < m_3 < K_B \tag{4.25}$$

$$0 < m_4 < K_A \tag{4.26}$$

Table 4.2. Operating conditions for complete separation under Equilibrium Theory. Langmuir adsorption isotherms (Mazzotti *et al.*, 1997b).

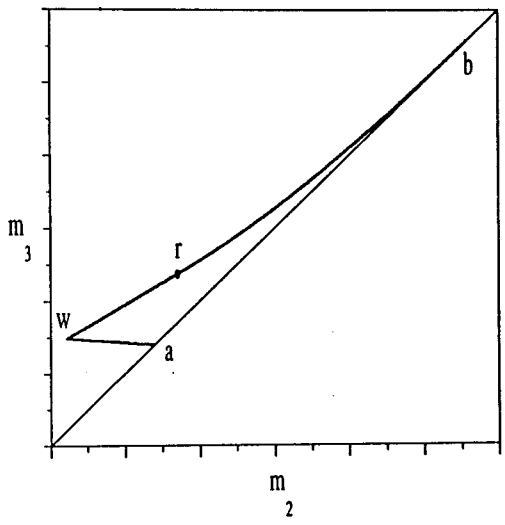


$$\lambda_B = m_{1,min} < m_1 < \infty \tag{4.27}$$

$$m_{2,min}(m_2,m_3) < m_2 < m_3 < m_{3,max}(m_2,m_3) \tag{4.28}$$

$$0 < m_4 < m_{4,max}(m_2,m_3) = \frac{1}{2}\left\{\lambda_A + m_3 + b_A C_A^F (m_3 - m_2) - \sqrt{\left[\lambda_A + m_3 + b_A C_A^F (m_3 - m_2)\right]^2 - 4\lambda_A m_3}\right\} \tag{4.29}$$

Boundaries of the complete separation region in the $(m_2,m_3)$ plane:

Straight line wr:

$$\left[\lambda_B - \omega_G\left(1 + b_B C_B^F\right)\right] m_2 + b_B C_B^F \omega_G m_3 = \omega_G\left(\lambda_B - \omega_G\right) \tag{4.30}$$

Straight line wa:

$$\left[\lambda_B - \lambda_A\left(1 + b_B C_B^F\right)\right] m_2 + b_B C_B^F \lambda_A m_3 = \lambda_A\left(\lambda_B - \lambda_A\right) \tag{4.31}$$

Table 4.2. (continued) Operating conditions for complete separation under Equilibrium Theory. Langmuir adsorption isotherms (Mazzotti *et al.*, 1997b).

Curve rb:

$$m_3 = m_2 + \frac{\left(\sqrt{\lambda_B} - \sqrt{m_2}\right)^2}{b_B C_B^F} \tag{4.32}$$

Straight line ab:

$$m_3 = m_2 \tag{4.33}$$

The coordinates of the intersection points are given by:

point a: $\left(\lambda_A, \lambda_A\right)$ (4.34)

point b: $\left(\lambda_B, \lambda_B\right)$ (4.35)

point r: $$\left(\frac{\omega_G^2}{\lambda_B}, \frac{\omega_G\left[\omega_F\left(\lambda_B - \omega_G\right)\left(\lambda_B - \lambda_A\right) + \lambda_A \omega_G\left(\lambda_B - \omega_F\right)\right]}{\lambda_A \lambda_B\left(\lambda_B - \omega_F\right)}\right) \tag{4.36}$$

point w: $$\left(\frac{\lambda_A \omega_G}{\lambda_B}, \frac{\omega_G\left[\omega_F\left(\lambda_B - \lambda_A\right) + \lambda_A\left(\lambda_A - \omega_F\right)\right]}{\lambda_A\left(\lambda_B - \omega_F\right)}\right) \tag{4.37}$$

with $\omega_G > \omega_F > 0$, which are given by the roots of the following quadratic equation:

$$\left(1 + b_A C_A^F + b_B C_B^F\right)\omega^2 - \left[\lambda_A\left(1 + b_B C_B^F\right) + \lambda_B\left(1 + b_A C_A^F\right)\right]\omega + \lambda_A \lambda_B = 0 \tag{4.38}$$

In the above equations, $C_A^F$ and $C_B^F$ are the feed concentrations of species $A$ and $B$, respectively, and

$$\lambda_i = Q b_i \quad , \quad (i = A, B) \tag{4.39}$$

The objective of this chapter is to study the influence of the operating variables and model parameters on the steady-state performance of a SMB unit. Namely, the influence of mass transfer resistance on the SMB performance and on the region of flow-rate ratios that lead to the separation of the two enantiomers of a racemic mixture will be addressed. At the end of this chapter, a simple optimization procedure for choosing the best SMB operating conditions is proposed. This procedure is developed addressing some behaviours found for the SMB performance and how the operating conditions influence it. Namely, an optimization procedure is proposed based on the path of equal purities.

## 4.2 The Steady-State True Moving Bed Model

The model equations result from the mass balances over a volume element of the bed and at a particle level. Axial dispersion flow for the bulk fluid phase is included and the linear driving force approximation is used to describe the intraparticle mass transfer rate. The steady-state TMB model equations are summarized below, with boundary conditions, as well as with the necessary mass balances at the nodes between each section.

***Model equations for the steady-state TMB***

*Mass balance in a volume element of the bed j:*

$$D_{L_j}\frac{d^2c_{ij}}{dz^2}-v_j\frac{dc_{ij}}{dz}-\frac{(1-\varepsilon)}{\varepsilon}k(q_{ij}^{*}-q_{ij})=0 \tag{4.40}$$

*Mass balance in the particle:*

$$u_s\frac{dq_{ij}}{dz}+k(q_{ij}^{*}-q_{ij})=0 \tag{4.41}$$

*Boundary conditions for section j:*

$$z=0: \qquad c_{ij}-\frac{D_{L_j}}{v_j}\frac{dc_{ij}}{dz}=c_{ij,0} \tag{4.42}$$

where $c_{ij,0}$ is the inlet concentration of species $i$ in section $j$.

$z = L_j$ :

For the eluent node $$c_{iIV} = \frac{v_I}{v_{IV}} c_{iI,0} \quad (4.43a)$$

For the extract node $$c_{iI} = c_{iII,0} \quad (4.43b)$$

For the feed node $$c_{iII} = \frac{v_{III}}{v_{II}} c_{iIII,0} - \frac{v_F}{v_{II}} c_i^F \quad (4.43c)$$

For the raffinate node $$c_{iIII} = c_{iIV,0} \quad (4.43d)$$

And $$q_{iIV} = q_{iI,0} \; , \; q_{iI} = q_{iII,0} \; , \; q_{iII} = q_{iIII,0} \; , \; q_{iIII} = q_{iIV,0} \quad (4.44)$$

*Global balances:*

Eluent node $$v_I = v_{IV} + v_E \quad (4.45a)$$

Extract node $$v_{II} = v_I - v_X \quad (4.45b)$$

Feed node $$v_{III} = v_{II} + v_F \quad (4.45c)$$

Raffinate node $$v_{IV} = v_{III} - v_R \quad (4.45d)$$

*Multicomponent adsorption equilibrium isotherm:*

$$q_{Aj}^* = f_A(c_{Aj}, c_{Bj}) \quad \text{and} \quad q_{Bj}^* = f_B(c_{Aj}, c_{Bj}) \quad (4.46)$$

Introducing the dimensionless variable $x = z / L_j$, the model *Equations 4.40* and *4.41* become:

$$\gamma_j \left\{ \frac{1}{Pe_j} \frac{d^2 c_{ij}}{dx^2} - \frac{dc_{ij}}{dx} \right\} - \frac{(1-\varepsilon)}{\varepsilon} \alpha_j (q_{ij}^* - q_{ij}) = 0 \quad (4.47)$$

and

$$\frac{dq_{ij}}{dx} + \alpha_j (q_{ij}^* - q_{ij}) = 0 \quad (4.48)$$

The boundary conditions for $x = 1$ $(z = L_j)$ are the same presented before (*Equations 4.43* and *4.44*) and, for $x = 0$ $(z = 0)$, *Equation 4.42* becomes:

$$c_{ij} - \frac{1}{Pe_j}\frac{dc_{ij}}{dx} = c_{ij,0} \tag{4.49}$$

The resulting model parameters are the same for the transient TMB model presented in the previous chapter:

the ratio between solid and fluid volumes, $\frac{1-\varepsilon}{\varepsilon}$ (4.50)

the ratio between fluid and solid interstitial velocities, $\gamma_j = \frac{v_j}{u_s}$ (4.51)

the Peclet number, $Pe_j = \frac{v_j L_j}{D_{Lj}}$ (4.52)

the number of mass transfer units, $\alpha_j = \frac{k\, L_j}{u_s}$ (4.53)

Adsorption equilibrium parameters have to be added to the list above.

## 4.3 Numerical Aspects

The steady-state true moving bed model presented in the previous section was numerically solved by using the COLNEW software (Bader and Ascher, 1987). This package solves a general class of mixed-order systems of boundary value ordinary differential equations and is a modification of the COLSYS package developed by Ascher *et al.* (1979, 1981).

Each section of the TMB unit is defined by four ODEs: for each component there is an ODE resulting from the mass balance in a volume element of the bed, and other resulting from the mass balance in the particle. Since the TMB unit is composed by four sections, and considering a binary separation, the steady-state TMB model is defined by a set of 16 ODEs.

The COLNEW software incorporates a new basis representation replacing

B-splines, and improvements for the linear and non-linear algebraic equation solvers.

The numerical approximation of mixed order systems of multipoint value ordinary differential equations by collocation requires appropriate representation of the piecewise polynomial solutions. B-splines were originally implemented in the general purpose code COLSYS, whereas a Runge-Kutta monomial basis is used for the COLNEW software. Turner and Mills (1990) applied these packages to chemical engineering systems and conclude that the COLSYS software requires more CPU time and is less stable than the newer version of COLNEW.

*Table 4.3* presents a list of parameters that must be specified to implement the COLNEW software. No initial guess to the solution is provided and we let the COLNEW software to generate the initial mesh and control it during the numerical resolution. An unique global error, similar to the one presented before in section 3.4, was used. The convergence of the method is considered to be achieved when the global error, as defined by *Equation 3.34*, is less than *0.01*.

Table 4.3. List of COLNEW parameters.

| COLNEW parameter | Description | Value used |
|---|---|---|
| IPAR(1) | Type of problem: linear (0) or non-linear (1) | 1 |
| IPAR(2) | Number of collocation points per interval | 5 |
| IPAR(3) | Number of subintervals in the initial mesh | 20 |
| TOL | Error tolerance | $10^{-5}$ |

The COLNEW software proved to be very efficient in the numerical resolution of the steady-state TMB model. For the same case studied in the previous chapter, and using the parameters presented in *Table 4.3*, the solution of the steady-state TMB model took only 35 seconds (Personal Computer Duo Pentium Pro 200 MHz, 512 Kb Cache, 64 Mb RAM). Comparing it with the running times for the transient models studied in the previous chapter, we easily conclude about the obvious advantages of using the COLNEW software if we want to characterize only the steady-state TMB operation.

## 4.4 Performance Parameters

To characterize the steady-state SMB performance, four process parameters are used: purity, recovery, solvent consumption and adsorbent productivity. These parameters are defined for the case of a binary separation (racemic mixture) in which the less retained species A is recovered in the raffinate and the more retained component B is recovered in the extract.

The purity and recovery parameters are defined for both product lines, extract and raffinate. Extract purity is defined as the ratio between the concentration of the more retained component and the total concentration of the two species in the extract. Raffinate purity is defined as the ratio between the concentration of the less retained component and the total concentration of the two species in the raffinate. The recovery is defined as the amount of the target species obtained in the desired product line per total amount of the same species fed into the system. In the extract line the target species is the more retained component, while in the raffinate line the target species is the less retained component.

The solvent consumption and productivity parameters are defined in terms of the total amount of the racemic mixture introduced into the system. Solvent consumption is defined as the total amount of solvent used (in eluent and feed) per unit of racemic amount treated. Productivity is defined as the amount of racemic mixture treated per volume of adsorbent bed and per unit of time. *Table 4.4* summarizes and defines the performance parameters used. It should be pointed out that the solvent consumption and productivity parameters are independent of the separation achieved, depending only on the eluent and feed flow-rates used. Of course, they must be analyzed together with the purities obtained.

Table 4.4. SMB performance criteria.

| Performance Parameter | Extract | Raffinate |
|---|---|---|
| Purity (%) | $PUX = 100C_B^X / (C_A^X + C_B^X)$ | $PUR = 100C_A^R / (C_A^R + C_B^R)$ |
| Recovery (%) | $RCX = 100Q_X C_B^X / Q_F C_B^F$ | $RCR = 100Q_R C_A^R / Q_F C_A^F$ |
| Solvent Consumption (ℓ/g) | $SC = (Q_E + Q_F) / [Q_F (C_A^F + C_B^F)]$ | |
| Productivity (g/day ℓ of bed) | $PR = Q_F (C_A^F + C_B^F) / V_T$ | |

## 4.5 Effect of the Operating Conditions on the SMB Performance

In this section, the effect of the operating conditions on the SMB performance is analyzed by simulation, using the steady-state TMB model presented in Section 4.2.

The resolution of the bi-naphthol enantiomers, presented in the previous chapter, was used for simulation purposes. The adsorption equilibrium isotherms are the ones presented also in the previous chapter:

$$q_A^* = \frac{2.69 c_A}{1 + 0.0336 c_A + 0.0466 c_B} + \frac{0.10 c_A}{1 + c_A + 3 c_B} \tag{4.54a}$$

$$q_B^* = \frac{3.73 c_B}{1 + 0.0336 c_A + 0.0466 c_B} + \frac{0.30 c_B}{1 + c_A + 3 c_B} \tag{4.54b}$$

A reference case relative to an eight-column configuration of the SMB, based on the values of operating variables and model parameters shown in *Table 4.5* was chosen. The reference flow-rates were provided by the *Novasep* group (personal communication) and checked by using the TMB model. *Table 4.6* presents the equivalent TMB operating conditions and model parameters for the reference case and *Figure 4.2* presents the corresponding steady-state internal concentration profiles obtained with the simulation package. *Table 4.7* shows the performance parameters obtained for this reference case.

Table 4.5. SMB operating conditions and model parameters for the reference case.

| **SMB operating conditions:** | | **Model parameters:** | |
|---|---|---|---|
| Feed concentration: | 2.9 g/l each | Solid/fluid volumes, $(1-\varepsilon)/\varepsilon = 1.5$ | |
| Switch time interval: | 3 min | Ratio between fluid and solid velocities: | |
| Recycling flow-rate: | 35.38 ml/min | $\gamma_I^* = 7.65$ ; $\gamma_{II}^* = 5.23$ | |
| Eluent flow-rate: | 21.45 ml/min | $\gamma_{III}^* = 5.72$ ; $\gamma_{IV}^* = 4.76$ | |
| Extract flow-rate: | 17.98 ml/min | Number of mass transfer units, | |
| Feed flow-rate: | 3.64 ml/min | $\alpha_k = 18.0$ ($k = 0.1$ s$^{-1}$) | |
| Raffinate flow-rate: | 7.11 ml/min | Peclet number, $Pe_k = 1000$ | |
| **Columns:** | | Column Diameter: | 2.6 cm |
| Configuration: 2 columns per section | | Column Length: | 10.5 cm |

Table 4.6. Equivalent TMB operating conditions and model parameters for the reference case.

| **TMB operating conditions:** | | **Model parameters:** |
|---|---|---|
| Feed concentration: | 2.9 g/l each | Solid/fluid volumes, $(1-\varepsilon)/\varepsilon = 1.5$ |
| Solid flow-rate: | 11.15 ml/min | Ratio between fluid and solid velocities: |
| Recycling flow-rate: | 27.95 ml/min | $\gamma_I = 6.65$ ; $\gamma_{II} = 4.23$ |
| Eluent flow-rate: | 21.45 ml/min | $\gamma_{III} = 4.72$ ; $\gamma_{IV} = 3.76$ |
| Extract flow-rate: | 17.98 ml/min | Number of mass transfer units, |
| Feed flow-rate: | 3.64 ml/min | $\alpha = 36.0$ ($k = 0.1$ s$^{-1}$) |
| Raffinate flow-rate: | 7.11 ml/min | Peclet number, $Pe = 2000$ |
| **Columns:** | | |
| Diameter: | 2.6 cm | Section Length: 21.0 cm |

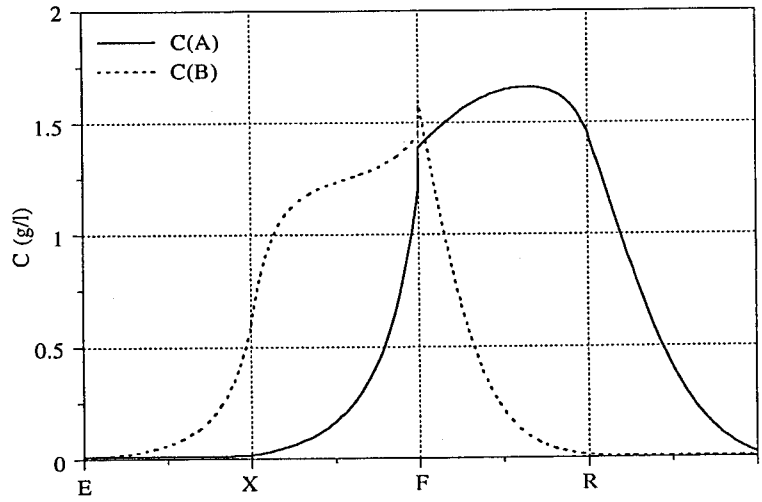


Figure 4.2. Steady-state internal concentration profiles for the reference case.

Table 4.7. Performance parameters for the reference case.

| Performance Parameter | Extract | Raffinate |
|---|---|---|
| Purity (%) | 97.6 | 99.3 |
| Recovery (%) | 99.3 | 97.6 |
| Solvent Consumption (ℓ/g) | 1.19 | |
| Productivity (g/day ℓ of bed) | 68.2 | |

*Effect of the Switch Time Interval:*

The influence of the switch time interval on the system performance is shown in *Figure 4.3*. A change on the switch time interval will lead to a change on the equivalent solid flow-rate throughout the system. In all runs the inlet and outlet flow-rates, as well as the internal liquid flow-rates in all the four sections of the SMB unit are kept constant.

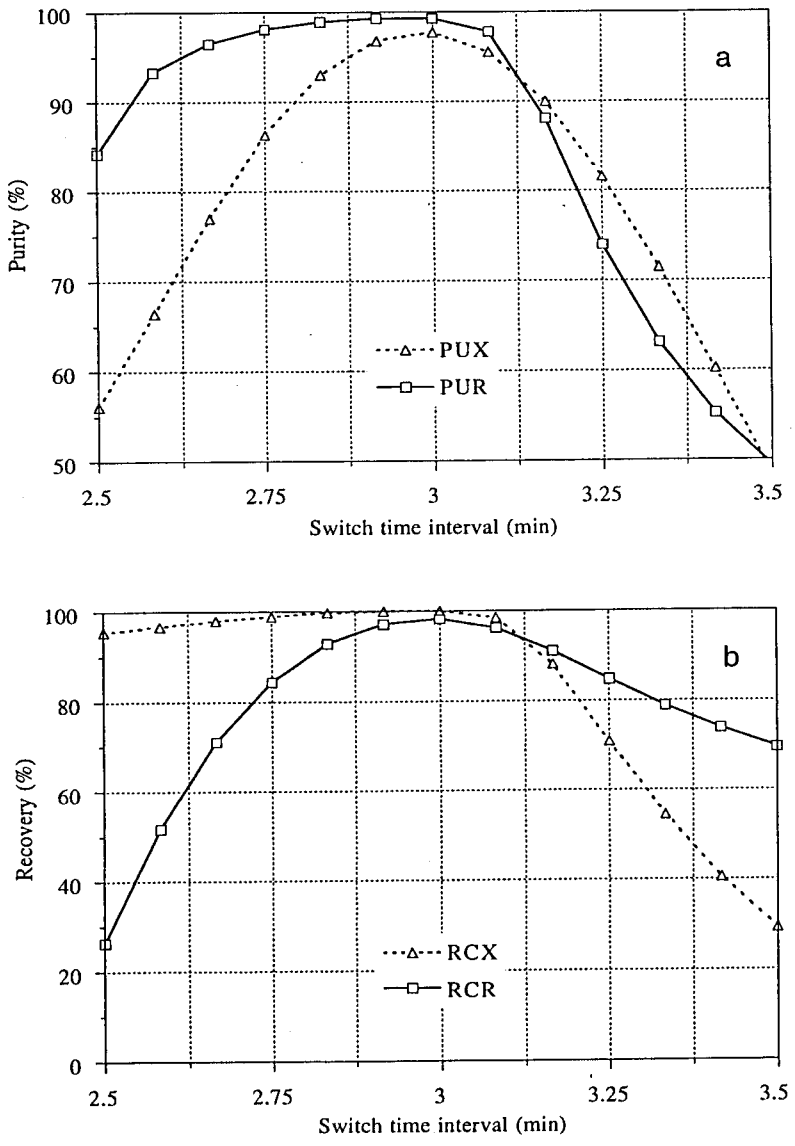


Figure 4.3. Effect of the switch time interval on the performance parameters: (a) purity; (b) recovery.

Increasing the switch time interval is equivalent to decrease the solid flow-rate and the net fluxes of components in all the four sections of the TMB unit will be pushed in the same direction of the liquid phase. This implies that, first, the more retained component will move upwards in section III and will contaminate the raffinate stream; and the less retained species will move upwards in section IV, will be recycled to section I, and will contaminate also the extract stream.

The decrease of the switch time interval will have similar consequences. The equivalent solid flow-rate will increase and the net fluxes of component in all four sections of the TMB unit will be pushed in the opposite direction of the liquid phase. This implies that, first, the less retained species will move downwards in section II and will contaminate the extract stream; and the more retained component will also move downwards in section I, will be recycled with the solid phase to the section IV, and will contaminate the raffinate stream.

Looking for *Figure 4.3*, we can conclude that high purities and recoveries can be obtained only in a narrow window of switch time interval values. *Figure 4.4* emphasis this idea in a purity versus recovery plot. It is clear from this figure that it is possible to obtain simultaneously high purities and recoveries in a simulated moving bed system but the tuning has to be carefully done.

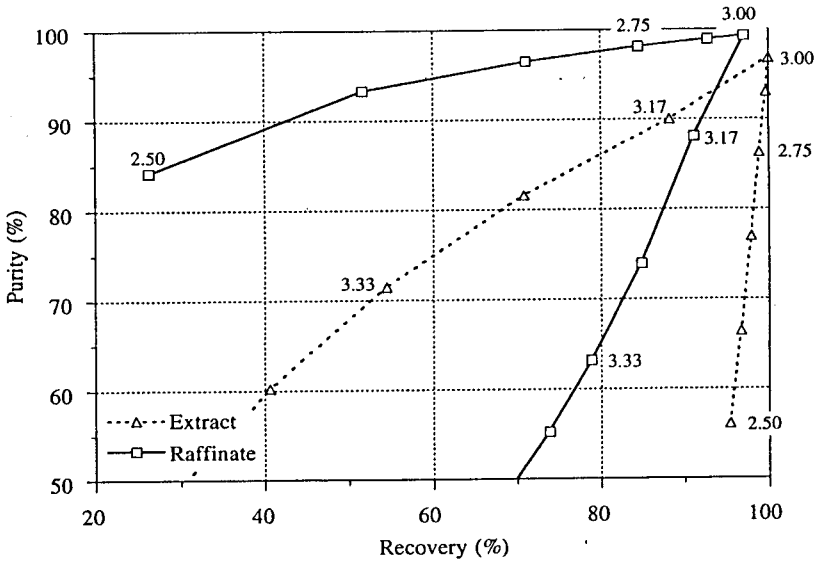


Figure 4.4. Purity versus recovery plot for extract and raffinate for different values of the switch time interval.

*Effect of the recycling flow-rate:*

A similar behaviour to the one shown before, by changing the switch time interval, can be obtained by changing the value of the liquid recycling flow-rate. The recycling flow-rate used will also influence the net fluxes in all the four sections of the SMB unit. In all runs the inlet and outlet flow-rates, as well as the switch time interval are kept constant, changing only the internal liquid flow-rates in the four sections of the SMB unit.

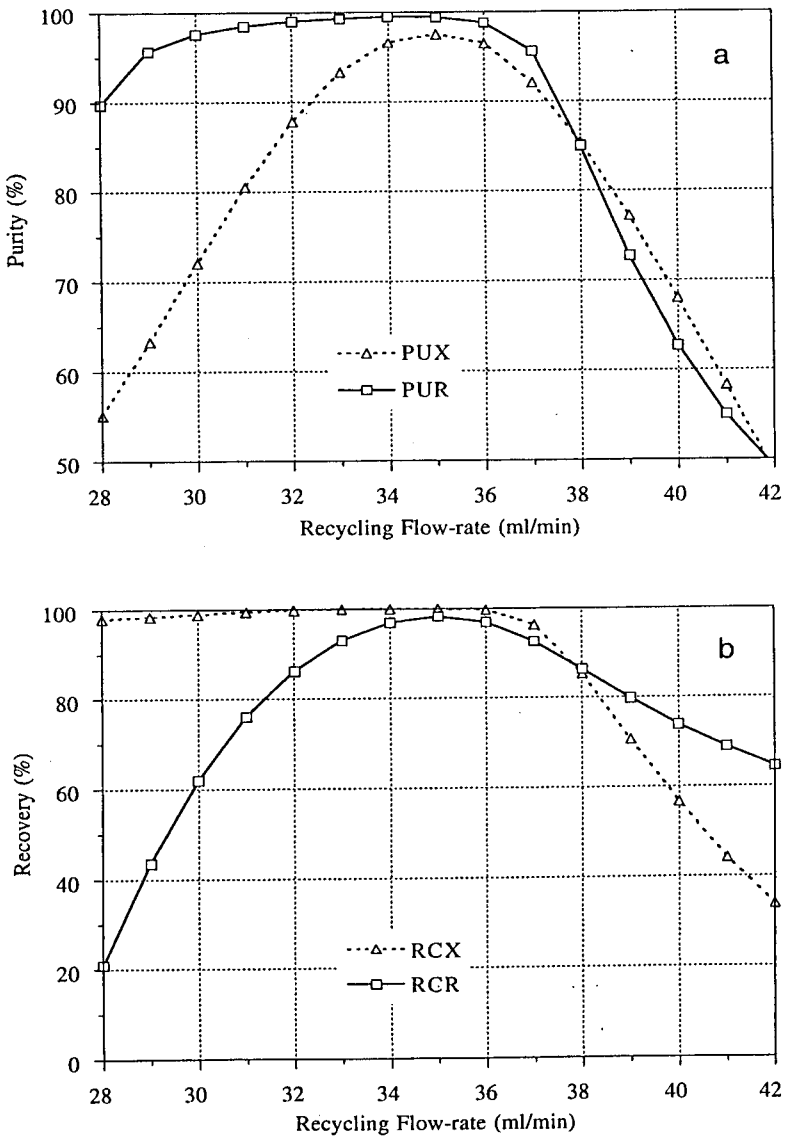


Figure 4.5. Effect of the recycling flow-rate (SMB) on the performance parameters: (a) purity; (b) recovery.

The switch time interval is inversely proportional to the solid flow-rate, as it is shown by *Equation 4.16*. Hence, the roles of increasing the recycling liquid flow-rate and decreasing the solid flow-rate (increasing $t^*$) are similar with regard to the calculation of the net flux of a species through *Equations 4.1*. The similarity can be observed by comparing the behaviour of the purity and recovery performances presented in *Figures 4.3a-4.5a* and *4.3b-4.5b*, respectively.

It should be pointed out, however, that this equivalence is not perfect. To obtain two equivalent operations, an increase by a certain percentage of the switch time interval will be equivalent to an increase of all the internal liquid flow-rates by the same percentage, and not only to an increase of the recycling liquid flow-rate. This will lead, however, to a change in the inlet and outlet flow-rates, which is not the objective of the study by now.

Besides, it must be noticed that changing the switch time interval will also change the number of mass transfer units as it was defined by *Equation 4.53*. In fact, the number of mass transfer units is given by

$$\alpha_j = \frac{k\, L_j}{u_s} = N_j\, k\, t^* \tag{4.55}$$

where $N_j$ is the number of fixed bed columns used in section $j$ of the SMB unit. Consequently, decreasing the switch time interval will lead to a decrease of the time of contact between the solid and the liquid phases within a section, expressed by a decreasing of the number of mass transfer units.

*Effect of the extract flow-rate:*

The effect of the extract flow-rate on the SMB performance is shown in *Figure 4.6*. In this figure, the eluent and feed flow-rates remain constant, while a change in the extract flow-rate is followed by a change of opposite signal in the raffinate flow-rate. For all runs, the total inlet or outlet flow-rates remains constant and equal to 25.09 ml/min. Both the switch time interval and the liquid recycling flow-rate are kept constant. In terms of the internal liquid flow-rates, a change in the extract and raffinate, keeping constant the eluent and feed flow-rates, will lead to a change in the internal liquid flow-rates in sections II and III, while the internal liquid flow-rates in sections I

and IV remain constant.

Looking for *Figure 4.6*, we can conclude that a deviation of the extract flow-rate from its optimum value drastically affects the performance of one or the other enantiomer, depending on which direction the extract flow-rate is changed.

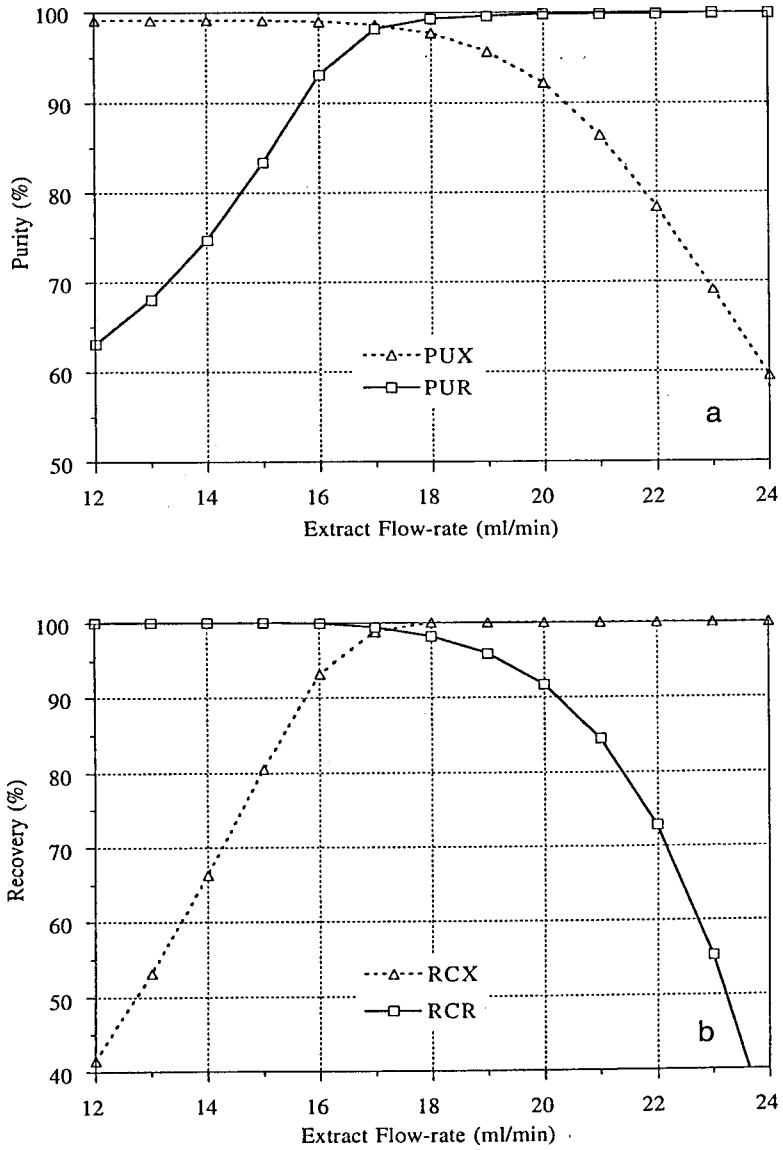


Figure 4.6. Effect of the extract flow-rate on the performance parameters: (a) purity; (b) recovery.

In fact, increasing the extract flow-rate will lead to a lower liquid flow-rate in section II and the constraint in this section is eventually not obeyed; therefore species A will have a net flux downwards and will contaminate the extract with decrease of purity in that stream. The decrease of the liquid flow-rate in section III will not affect the raffinate purity because the more retained species will also move downwards. This explains why the raffinate purity maintains its high values for high extract flow-rates. Nevertheless, because the less retained component is contaminating the extract, the recovery of this species in the raffinate stream will be lower and lower with the increase of the extract flow-rate.

On the other hand, decreasing the extract flow-rate will lead to a higher liquid flow-rate in section III and the constraint in this section is eventually not obeyed; therefore species B will have a net flux upwards and will contaminate the raffinate with decrease of purity in that stream. The increase of the liquid flow-rate in section II will not affect the extract purity because the less retained species will also move upwards. This explains why the extract purity maintains its high values for low extract flow-rates. However, because the more retained component is contaminating the raffinate, the recovery of this species in the extract stream will be lower and lower with the decrease of the extract flow-rate.

Again, simultaneous high purities for both enantiomers can only be obtained in a narrow window of values of the extract flow-rate.

*Effect of the feed flow-rate:*

The effect of the feed flow-rate on the SMB performance is shown in *Figure 4.7*. In this figure, the extract and raffinate flow-rates remain constant, while a change in the feed flow-rate is followed by a change of opposite signal in the eluent flow-rate. For all runs, the total inlet or outlet flow-rates remains constant and equal to 25.09 ml/min. Both the switch time interval and the liquid recycling flow-rate are kept constant. Since the feed flow-rate is changing, both the solvent consumption and the adsorbent productivity performance parameters will also change.

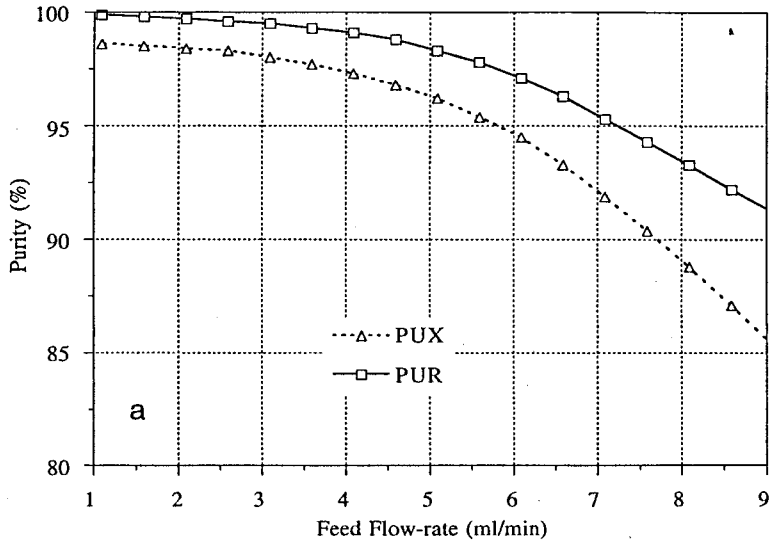
100
95
90
85
80
Purity (%)
PUX
PUR
a
1
2
3
4
5
6
7
8
9
Feed Flow-rate (ml/min)

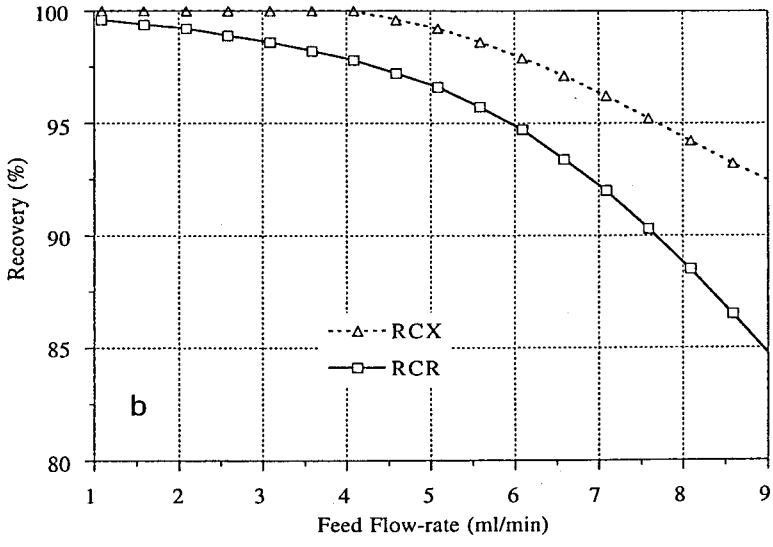
100
95
90
85
80
Recovery (%)
RCX
RCR
b
1
2
3
4
5
6
7
8
9
Feed Flow-rate (ml/min)

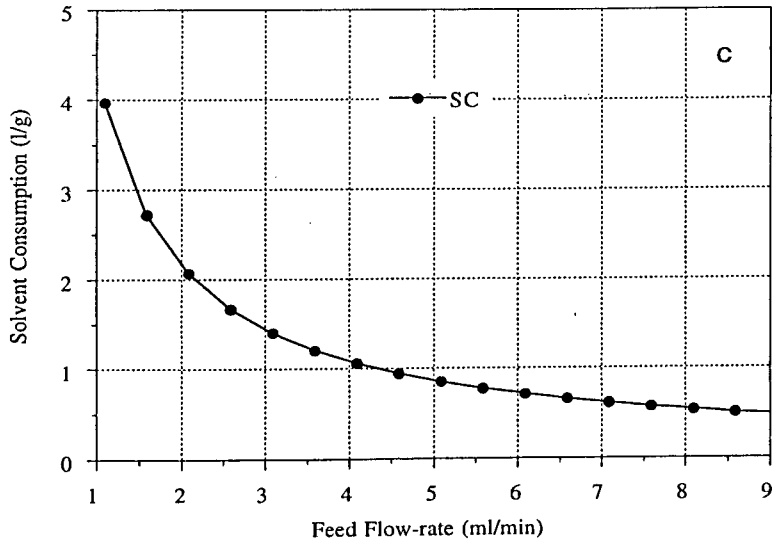
5
4
3
2
1
0
Solvent Consumption (l/g)
SC
c
1
2
3
4
5
6
7
8
9
Feed Flow-rate (ml/min)

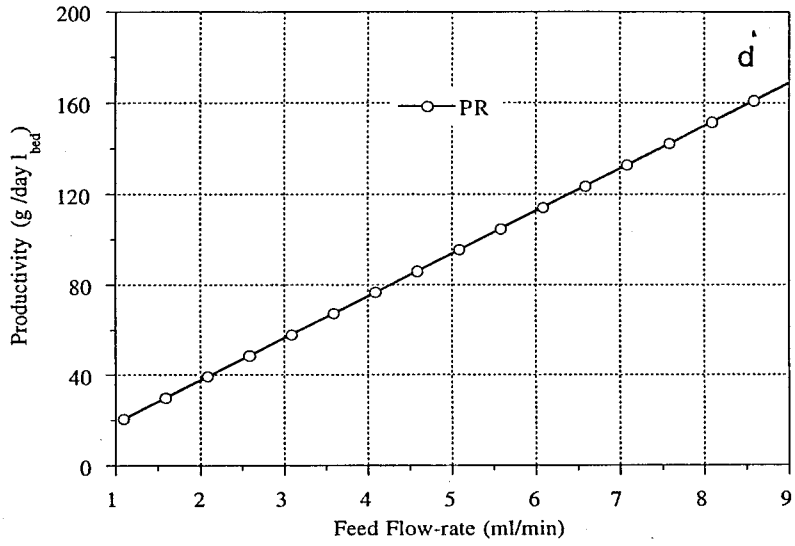


Figure 4.7. Effect of the feed flow-rate on the performance parameters: (a) purity; (b) recovery; (c) solvent consumption; (d) productivity.

In terms of the internal liquid flow-rates, a change in the feed and eluent, keeping constant the extract and raffinate as well as the recycling flow-rates, will lead to a change in the internal liquid flow-rates in sections I and II, while the internal liquid flow-rates in the two last sections remain constant.

As a general conclusion we can say that increasing the feed flow-rate improves productivity and solvent consumption but reduces both purity and recovery. In fact, increasing the feed keeping constant the recycling flow-rate, means that the internal liquid flow-rate in section II decreases and the less retained species A will move downwards and contaminate the extract stream. Also, the internal flow-rate in the first section decreases and species B eventually moves downwards, is recycled with the solid phase to section IV, and will contaminate the raffinate stream.

The decrease of the feed, keeping constant the recycling flow-rate will lead to an increase of the internal liquid flow-rates in the two first sections, while in the two last ones they remain constant. These changes will improve the separation because the net fluxes of components A and B upwards in sections II and I, respectively, will be intensified, while the net fluxes in the two last sections are not significantly affected.

It must be pointed out that, the increase of the feed flow-rate followed by the corresponding decrease of the eluent flow-rate, will lead to a more difficult separation, where the non-linear competitive behaviour (expressed by the adsorption isotherms presented by *Equations 4.54*) is more pronounced.

## 4.6 Effect of the Axial Dispersion on the SMB Performance

The influence of the axial dispersion on the performance of a simulated moving bed adsorber is shown in *Figure 4.8*. The Peclet number, defined by *Equation 4.52*, refers to a whole section of the equivalent true moving bed system.

Looking for *Figure 4.8*, we can conclude that the influence of the axial dispersion on the SMB performance is negligible for Peclet numbers higher than 500.

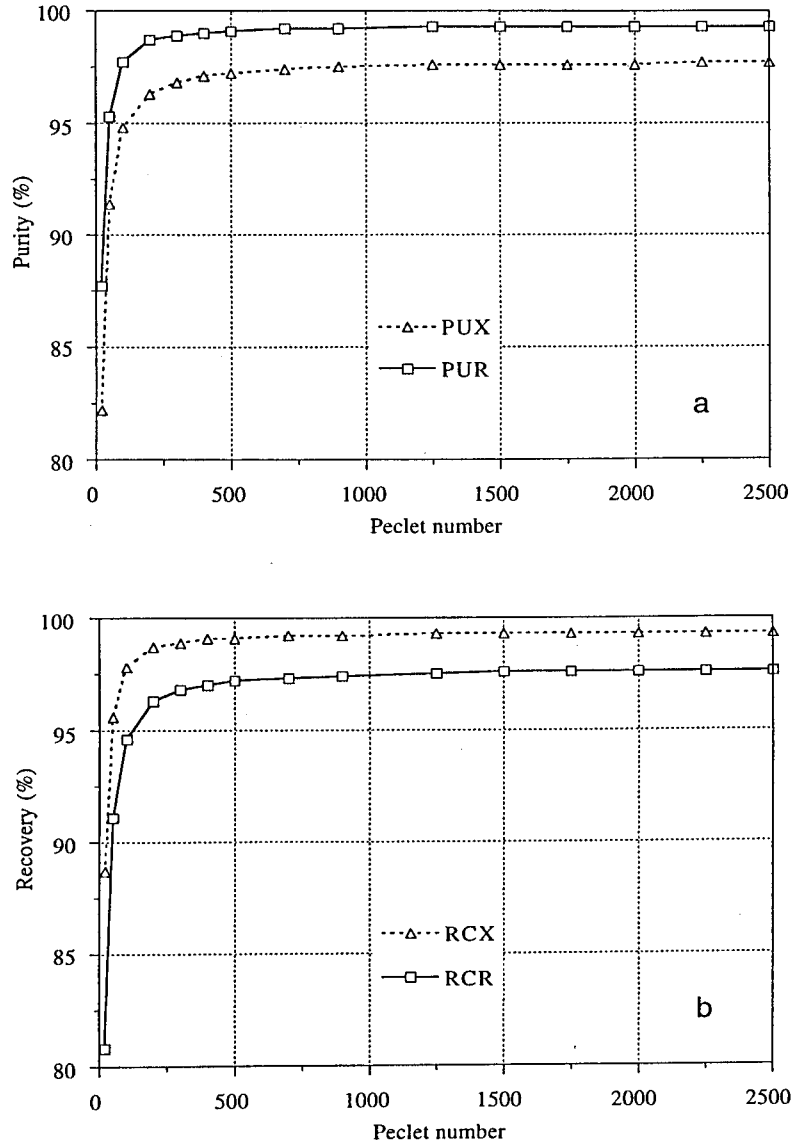


Figure 4.8. Effect of the axial dispersion on the performance parameters: (a) purity; (b) recovery.

## 4.7 Effect of the Mass Transfer Resistance on the SMB Performance

The influence of the mass transfer resistance on the performance of a simulated moving bed adsorber is shown in *Figure 4.9*. *Figure 4.10* shows its influence on the steady-state internal concentration profiles.

A higher value for the mass transfer coefficient corresponds to a situation where mass transfer resistance is less important. Obviously, the performance of the SMB

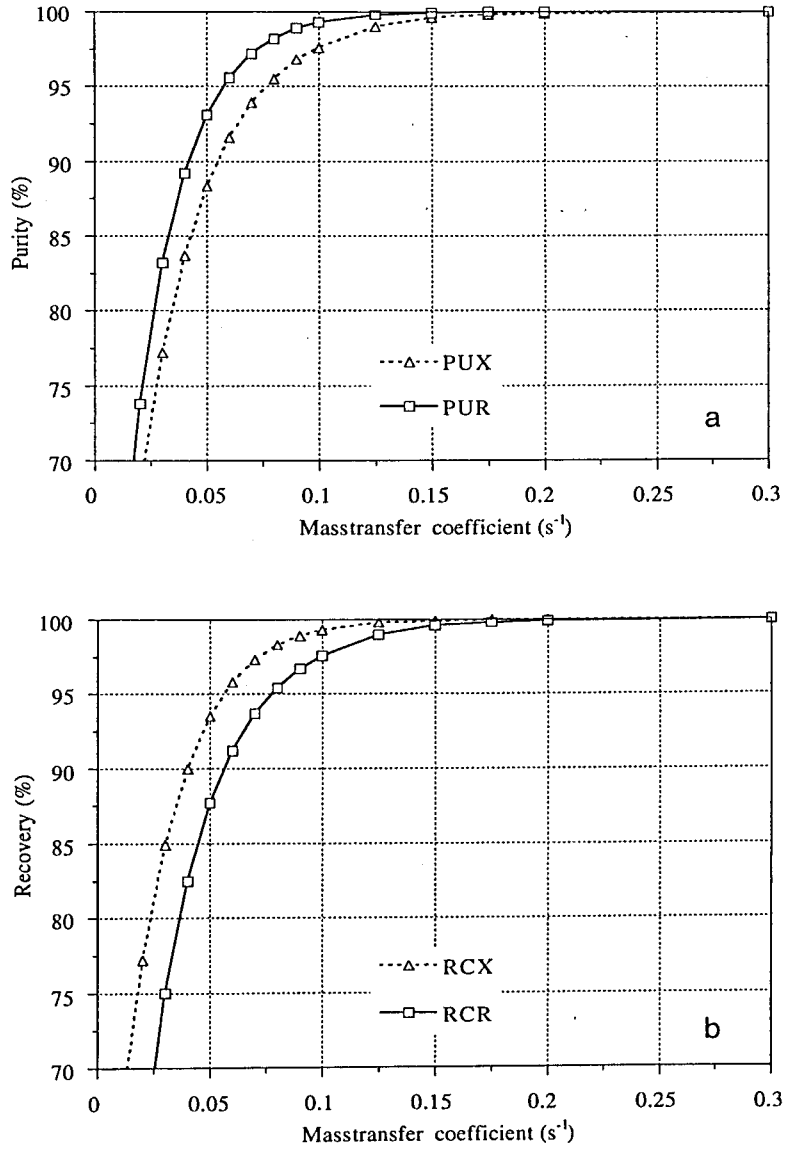


Figure 4.9. Effect of the mass transfer resistance on the performance parameters: (a) purity; (b) recovery.

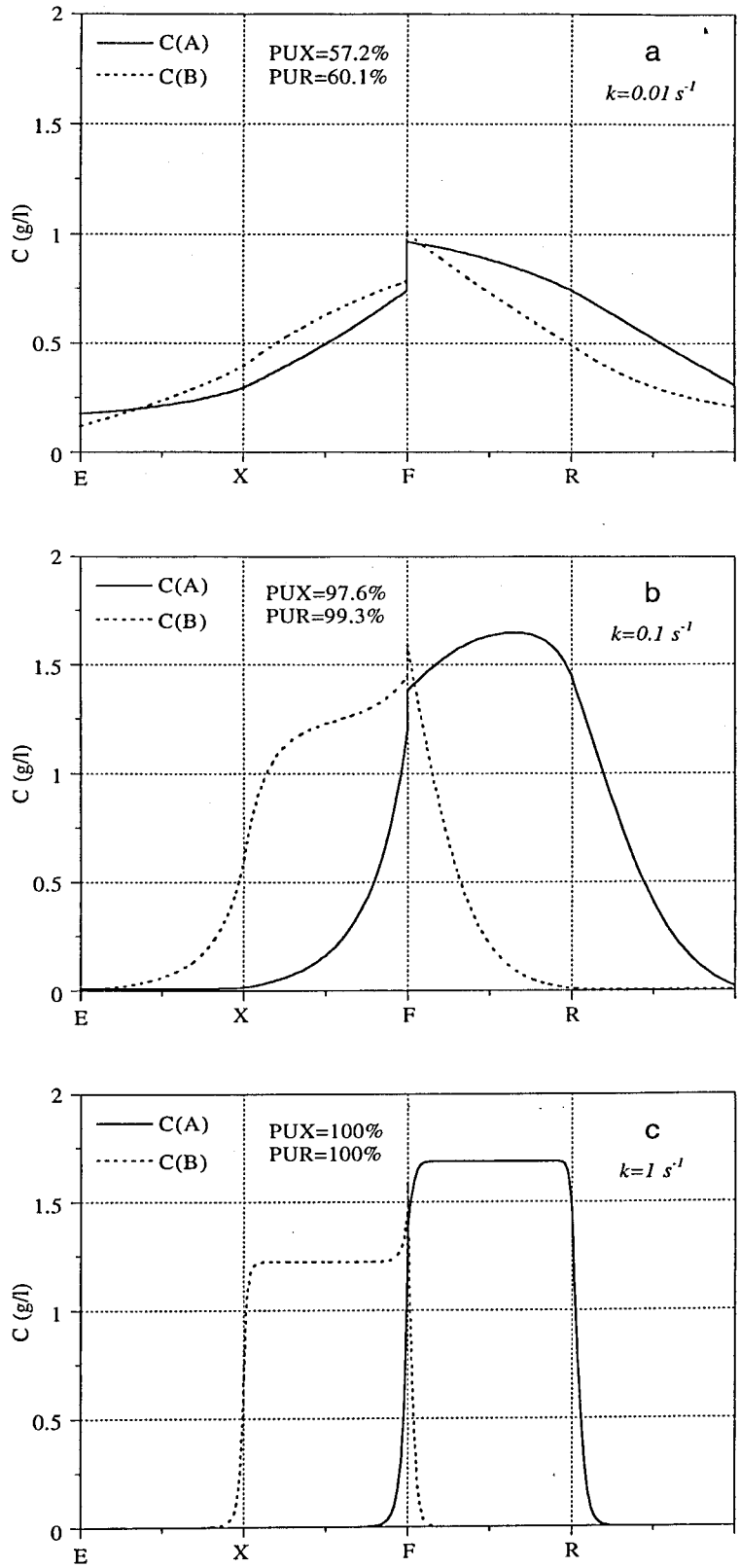


Figure 4.10. Effect of the mass transfer resistance on the internal concentration profiles: (a) $k$=0.01 $s^{-1}$; (b) $k$=0.1 $s^{-1}$; (c) $k$=1 $s^{-1}$;

system will be better for higher values of the mass transfer coefficient.

As it was proposed by Glueckauf (1955), the mass transfer coefficient used in the linear driving force approximation depends only on the intraparticle diffusivity of species and particle size. Therefore, increasing $k$ (or the corresponding dimensionless number, $\alpha$) by decreasing the particle size improves the performance of the SMB, provided the constraint of acceptable pressure drop is met. Some applications, namely in the area of protein processing, will eventually use large-pore permeable particles in which intraparticle mass transport by convective flow is important, leading to an enhancement of the mass transfer rate. The LDF models presented can still be used in that case if the mass transfer coefficient $k$ is replaced by an augmented mass transfer coefficient (Leitão e Rodrigues, 1995, 1996).

The performance of the SMB system can also be improved by increasing the section length. In fact, looking for the definition of the dimensionless parameter $\alpha$ (*Equation 4.53*), an equivalent system is obtained by incrementing the mass transfer coefficient $k$ or, alternatively, $L_j$, the length of the TMB section (Rodrigues *et al.*, 1996; Pais *et al.*, 1997a).

In *Figure 4.10* we can observe the influence of the mass transfer coefficient on the steady-state internal concentration profiles. Following the enhancement of the SMB performance, a higher mass transfer coefficient will lead to sharper internal concentration profiles.



## 4.8 Prediction of the Separation Regions

The conditions for a complete separation of a binary mixture can be defined in terms of the $\gamma_j$ model parameters (*Equation 4.51*), which are directly related with the TMB (SMB) operating variables (fluid and solid velocities in the four sections of the TMB unit).

From the four constraints presented in *Equations 4.1* or *4.3* those related to sections II and III play the crucial role on the separation performance of the TMB (Storti *et al.*, 1993). As it was mentioned before, is in these central zones that the separation between the two species takes place. The role of the adjacent sections (I and IV) is to prevent cross contamination and to allow the improvement of the continuous

operation of the system by regenerating the solid and liquid phases. Taking into account these considerations, a region of complete separation in a $\gamma_{III}$ - $\gamma_{II}$ plane can be defined. Considering that the constraints concerning sections I and IV are fulfilled, the $\gamma_{III}$ - $\gamma_{II}$ plot is an important tool in the choice of best operating conditions.

The first case studied concerns the situation where axial dispersion and mass transfer resistances are slightly important. The value for mass transfer coefficient used in this case was $k = 0.5$ s$^{-1}$ ($\alpha = 180$). Following the same methodology used to study the effect of the operating conditions and model parameters on the SMB performance, the $\gamma_{III}$ - $\gamma_{II}$ plot was built keeping constant the recycling (flow-rate in section IV) and solid flow-rates, and so $\gamma_{IV}$. The total inlet or outlet flow-rates were also kept constant in all simulations and equal to 25.09 ml/min. Other operating conditions and model parameters are summarized in *Table 4.8*. A TMB solid flow-rate of 11.15 ml/min corresponds to a switch time interval of 3 minutes in the equivalent SMB unit; a recycling flow-rate of 27.95 ml/min in the TMB corresponds to a recycling flow-rate of 35.38 ml/min in the SMB.

Table 4.8. TMB operating conditions and model parameters for the $\gamma_{III}$ - $\gamma_{II}$ plot.

| **TMB operating conditions:** | | **Model parameters:** | |
|---|---|---|---|
| Feed concentration: | 2.9 g/l each | Solid/fluid volumes: $(1-\varepsilon)/\varepsilon = 1.5$ | |
| Solid flow-rate: | 11.15 ml/min | Peclet number: $Pe = 2000$ | |
| Recycling flow-rate: | 27.95 ml/min | Ratio between fluid and solid velocities | |
| $Q_E + Q_F = Q_X + Q_R$ = | 25.09 ml/min | in section *IV*: $\gamma_{IV} = 3.76$ | |
| **Columns:** | | | |
| Diameter: | 2.6 cm | Section Length: | 21.0 cm |

*Figure 4.11* shows the $\gamma_{III}$ - $\gamma_{II}$ plot obtained for the first case where four regions are defined: a region of complete separation, two regions where only one outlet stream is 100% pure and a last region where neither of them is 100% pure. The closed circles are numerical results based on the equivalence between the TMB and the SMB; the thick lines connect those results. The thin line in *Figure 4.11* has two branches. The diagonal $\gamma_{III} = \gamma_{II}$ corresponds to zero feed flow-rate; therefore, $\gamma_{III}$ must be higher than $\gamma_{II}$. The horizontal branch $\gamma_{III} \approx 3.760$ corresponds to zero raffinate flow-rate; in this case, the extract flow-rate is 25.09 ml/min.

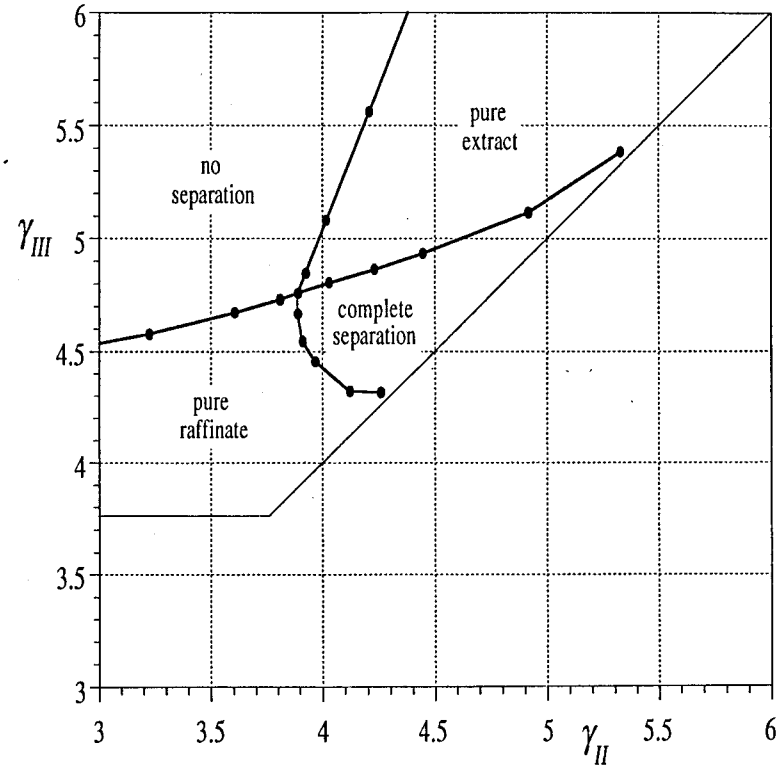


Figure 4.11. Regions of operation of the TMB in a $\gamma_{III}$ - $\gamma_{II}$ plot.
The closed circles represent numerical simulation results.
Mass transfer coefficient: $k = 0.5$ s$^{-1}$; other conditions are shown in *Table 4.8.*

In order to simplify the understanding of these plots, the relations between the TMB or SMB flow-rates and the $\gamma_j$ model parameters can be developed. The relation between the internal liquid flow-rates in the TMB unit, $Q_j$, and the $\gamma_j$ model parameters is given by

$$Q_j = \frac{\varepsilon}{1-\varepsilon} \gamma_j Q_s \tag{4.56}$$

where $Q_s$ is the volumetric solid flow-rate in the TMB system.

The inlet and outlet flow-rates can also be expressed in terms of the $\gamma_j$ model parameters:

$$Q_E = Q_I - Q_{IV} = \frac{\varepsilon}{1-\varepsilon}(\gamma_I - \gamma_{IV})Q_s \tag{4.57a}$$

$$Q_X = Q_I - Q_{II} = \frac{\varepsilon}{1-\varepsilon}(\gamma_I - \gamma_{II})Q_s \tag{4.57b}$$

$$Q_F = Q_{III} - Q_{II} = \frac{\varepsilon}{1-\varepsilon}(\gamma_{III} - \gamma_{II})Q_s \tag{4.57c}$$

$$Q_R = Q_{III} - Q_{IV} = \frac{\varepsilon}{1-\varepsilon}(\gamma_{III} - \gamma_{IV})Q_s \tag{4.57d}$$

Since these plots are built by keeping constant the total inlet or outlet flow-rates, $Q_T$, we conclude that

$$Q_T = Q_E + Q_F = Q_X + Q_R = \frac{\varepsilon}{1-\varepsilon}(\gamma_I - \gamma_{II} + \gamma_{III} - \gamma_{IV})Q_s \tag{4.58}$$

In addition, both the recycling and the solid flow-rates are also kept constant. Hence, $\gamma_{IV}$ is also constant and equal to

$$\gamma_{IV} = \frac{1-\varepsilon}{\varepsilon}\frac{Q_{RF}}{Q_s} \tag{4.59}$$

From *Equations 4.58* and *4.59*, we conclude that $\gamma_I$ is a linear function of $\gamma_{II}$ and $\gamma_{III}$:

$$\gamma_I = \frac{1-\varepsilon}{\varepsilon}\frac{(Q_{RF} + Q_T)}{Q_s} + \gamma_{II} - \gamma_{III} \tag{4.60}$$

A similar relation can be obtained in terms of the SMB operating conditions:

$$\gamma_I = \frac{(Q_{RF}^* + Q_T)t^*}{\varepsilon V_c} - 1 + \gamma_{II} - \gamma_{III} \tag{4.61}$$

where $V_c$ is the volume of one SMB column, $Q_{RF}^*$ is the SMB recycling flow-rate, and $t^*$ the switch time interval in the SMB operation.

From the relations presented before and looking for *Figure 4.12*, we can conclude that:

*1. Feed flow-rate changes:* the feed flow-rate is changed and it is followed by a change of opposite signal in the eluent flow-rate. The extract and raffinate flow-rates

remain constant. The total inlet or outlet flow-rates remain constant and equal to 25.09 ml/min. Also, both the recycling and the solid flow-rates remain constant.

Since the recycling and the raffinate flow-rates are constants, we conclude that $\gamma_{III}$ is also constant. Hence, the arrow 1 in *Figure 4.12* (parallel to the $\gamma_{II}$ axis) represents a change (increment) in the feed flow-rate, with effects on the SMB performance similar to the ones presented before in *Figure 4.7*.

*2. Extract flow-rate changes:* the extract flow-rate is changed and it is followed by a change of opposite signal in the raffinate flow-rate. The eluent and feed flow-rates remain constant. The total inlet or outlet flow-rates remain constant and equal to 25.09 ml/min. Also, both the recycling and the solid flow-rates remain constant.

Since the recycling and the eluent flow-rates are constant, we conclude that $\gamma_I$ is also constant. Moreover, since the solid and feed flow-rates are constants, from

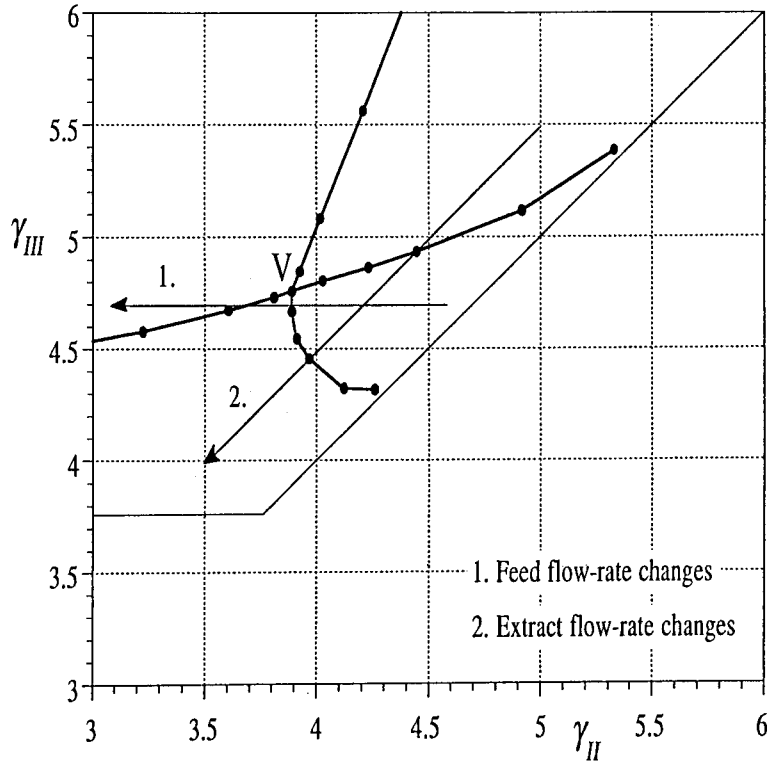


Figure 4.12. Effect of feed and extract flow-rate changes on the region of operation of a TMB system. Data as in *Figure 4.11*.

*Equation 4.57c*, we conclude that $(\gamma_{III} - \gamma_{II})$ is also constant. Hence, the arrow 2 in *Figure 4.12* (parallel to the diagonal $\gamma_{III} = \gamma_{II}$) represents a change (increment) in the extract flow-rate with effects on the SMB performance similar to the ones presented before in *Figure 4.6*.

The $\gamma_{III}$ - $\gamma_{II}$ plots provide possible operating conditions that allow the separation of a binary mixture. The separation regions drawn in this type of graphics are built imposing that the constrains concerning sections I and IV are fulfilled. Since $\gamma_I$ is a linear function of $\gamma_{II}$ and $\gamma_{III}$ (*Equations 4.60* or *4.61*), we must ensure that the region of complete separation of both species is not affected by the value of $\gamma_I$.

In fact, in section I (between the eluent and extract nodes) the objective is to ensure that the more retained species B move upwards, in the same direction of the liquid phase,

$$\frac{\varepsilon}{1-\varepsilon}\frac{c_{BI}}{q_{BI}}\gamma_I > 1 \tag{4.62}$$

The worst situation that can occur in this section is when we are dealing with low concentrations, i.e., linear conditions. Hence, if mass transfer resistance is negligible,

$$\gamma_I > \frac{1-\varepsilon}{\varepsilon} K_B \tag{4.63}$$

where $K_B$ is the initial slope of the adsorption isotherm for the more retained species.

Applying to our case (see *Table 4.8*) comes, from *Equation 4.60* or *4.61*, that

$$\gamma_I = 7.135 + \gamma_{II} - \gamma_{III} \tag{4.64}$$

From *Equation 4.63*, and since $K_B = 4.03$, the critical value for $\gamma_I$ is

$$\gamma_I > \gamma_I^c = 6.045 \tag{4.65}$$

As we concluded before, $\gamma_I$ is constant along a straight line parallel to the diagonal $\gamma_{III} = \gamma_{II}$. Furthermore, looking for *Figures 4.11* or *4.12*, we conclude that $\gamma_I$ diminishes as this straight line moves away from the diagonal $\gamma_{III} = \gamma_{II}$. Also, the

vertex of the complete separation region (point V in *Figure 4.12*) is the furthest point from the diagonal and corresponds to the optimal conditions, because both solvent consumption and adsorbent productivity are optimized. This vertex point corresponds also to the lower value for $\gamma_I$ in all the complete separation region.

The vertex of the complete separation region, evaluated for $k = 0.5$ s$^{-1}$ and under the operating conditions presented in *Table 4.8*, is characterized by $\gamma_{II} = 3.86$ and $\gamma_{III} = 4.75$. The corresponding minimum value of $\gamma_I$ is, from *Equation 4.64*, $\gamma_I = 7.135 + 3.86 - 4.75 = 6.245$, which is still higher than the critical value $\gamma_I^c = 6.045$. We conclude that, considering negligible mass transfer, within the whole separation region built under these conditions, the $\gamma_I$ value does not affect the SMB performance. It should be pointed out that the presence of mass transfer resistance can influence the critical value for $\gamma_I$ and the form of the separation region, as it was shown by Azevêdo and Rodrigues (1999).

The $\gamma_{III}$ - $\gamma_{II}$ plot provides, in this way, a tool for the choice of the SMB operating conditions, although it is built for particular values of recycling and solid flow-rates. Also, the feed concentration was kept constant in all simulations. The construction of the $\gamma_{III}$ - $\gamma_{II}$ plot for other values of the feed concentration will enable the study of its influence on the form of the separation region and on the SMB performance.

If mass transfer resistance is important, we may not obtain a region of 100% purity for both species. This case is illustrated using the same operating conditions and model parameters of the previous one, except that the mass transfer coefficient is now $k$ = 0.1 s$^{-1}$ ($\alpha = 36$). *Figure 4.13* shows the $\gamma_{III}$ - $\gamma_{II}$ plot obtained for this case where the four regions (A, B, C and D) described before are defined in terms of 99%, 95% and 90% purity criteria.

In region A, there is no separation; in region B, the raffinate purity is at least 90% when the dashed line (open circles) is used as border and at least 95% when the full line (closed circles) is used instead, whereas the extract purity is lower than those values; in region C, both the raffinate and the extract have at least 99%, 95% or 90% according to the lines used as borders (identified by closed triangles, closed circles and open circles, respectively); in region D, the extract purity is at least 90% or 95% accordingly with the line used as border (dashed or full, respectively), whereas the raffinate purity is inferior to those values.

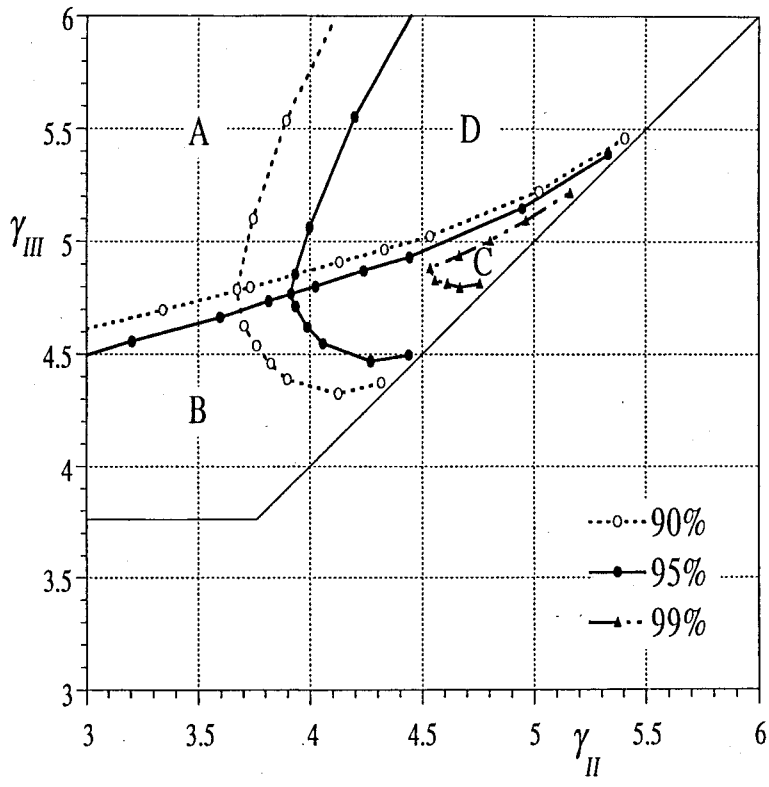


Figure 4.13. Regions of operation of the TMB in a $\gamma_{III}$ - $\gamma_{II}$ plot.
Mass transfer coefficient: $k = 0.1$ s$^{-1}$; other conditions are shown in *Table 4.8.*
(A) no separation; (B) raffinate purity of at least 90% (o), or 95% (●); (C) raffinate and extract purities of at least 90% (o), 95% (●), or 99%(▲); (D) extract purity of at least 90% (o), or 95% (●)

*Figure 4.14* emphasis the effect of the mass transfer resistances presenting the separation regions obtained for the two values of the mass transfer coefficient, $k = 0.5$ s$^{-1}$ ($\alpha = 180$) (open squares) and $k = 0.1$ s$^{-1}$ ($\alpha = 36$) (closed squares), using a 95% and 99% purity criteria. Inside the regions limited by the square points obtained numerically, both the raffinate and the extract are at least 95% (*Figure 4.14a*) or 99% (*Figure 4.14b*) pure.

It is clear from these figures that the mass transfer resistance reduces the region of separation of both species and that the region obtained for a lower mass transfer coefficient ($k = 0.1$ s$^{-1}$) lies inside the region obtained when mass transfer resistance is not so important ($k = 0.5$ s$^{-1}$).

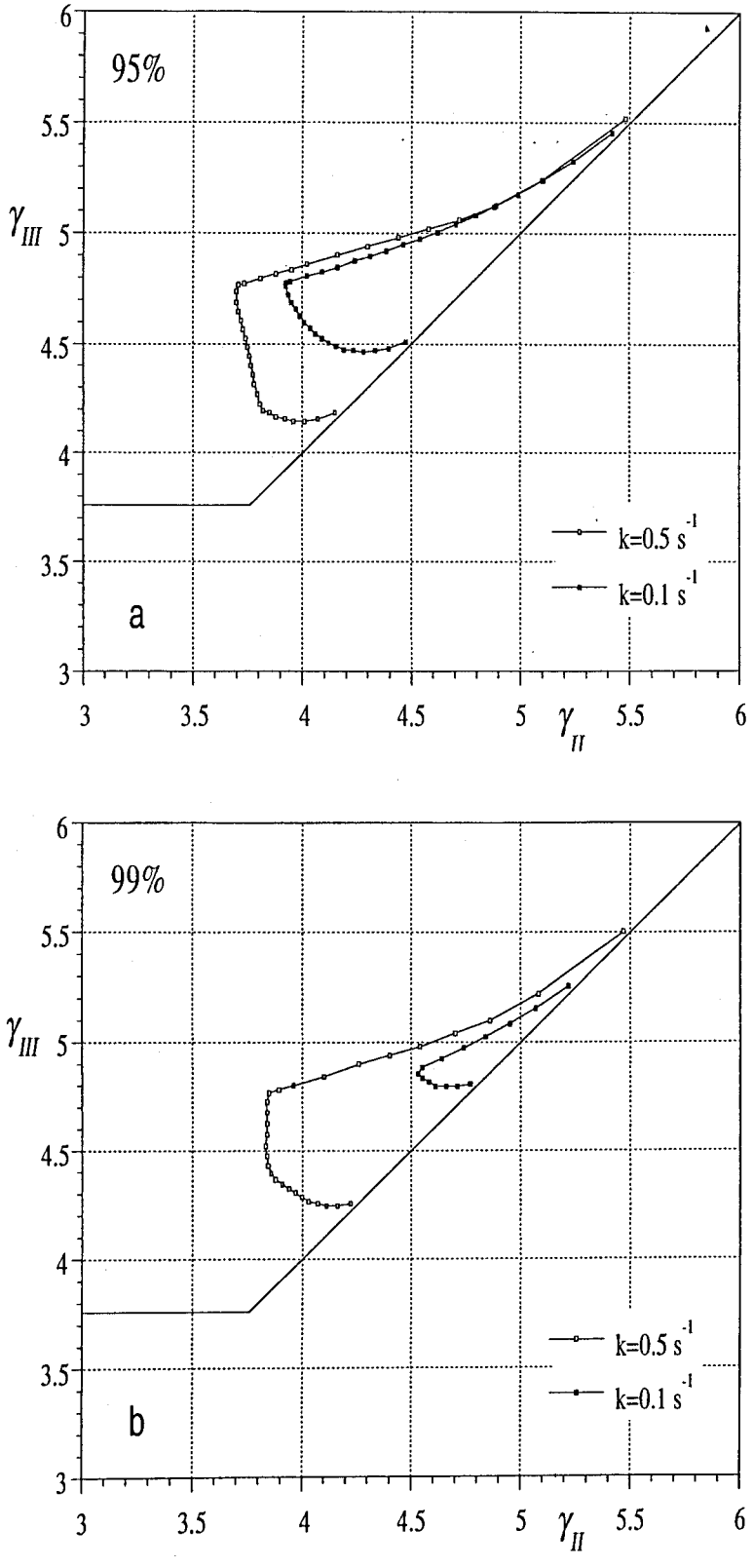


Figure 4.14. Influence of the mass transfer resistance on the separation region: $\gamma_{III}$ - $\gamma_{II}$ plot for a 95% (a) and 99% (b) purity criteria.

As it was mentioned before, the vertex of a separation region points out the better operating conditions, since it is the point where the purity criteria are fulfilled with a higher feed flow-rate (and, consequently, lower eluent flow-rate). Hence, in the operating conditions specified by the vertex point, both solvent consumption and adsorbent productivity are optimized. Comparing the vertex points obtained for the two values of mass transfer coefficient, we conclude that the mass transfer resistance influences the better SMB operating conditions. Moreover, this influence is emphasized when a higher purity requirement is desired.

*Tables 4.9* and *4.10* present the better SMB operating conditions for the two purity criteria considered. It is clear that the mass transfer resistance influences the better operating conditions, specially in what concerns the ratio between the feed and eluent flow-rates, which drastically affects the SMB performance in terms of the solvent consumption and adsorbent productivity.

Table 4.9. Influence of the mass transfer resistance on the optimum SMB operating conditions (95% vertex), solvent consumption and productivity performances.
(Other conditions as shown in *Table 4.8*)

| $k$ ($s^{-1}$) | $Q_E$ (ml/min) | $Q_X$ (ml/min) | $Q_F$ (ml/min) | $Q_R$ (ml/min) | $SC$ (ℓ/g) | $PR$ (g/day / ℓ of bed) |
|---|---|---|---|---|---|---|
| 0.5 | 17.24 | 17.62 | 7.85 | 7.47 | 0.55 | 147.0 |
| 0.1 | 18.84 | 17.57 | 6.25 | 7.52 | 0.69 | 117.0 |

Table 4.10. Influence of the mass transfer resistance on the optimum SMB operating conditions (99% vertex), solvent consumption and productivity performances.
(Other conditions as shown in *Table 4.8*)

| $k$ ($s^{-1}$) | $Q_E$ (ml/min) | $Q_X$ (ml/min) | $Q_F$ (ml/min) | $Q_R$ (ml/min) | $SC$ (ℓ/g) | $PR$ (g/day / ℓ of bed) |
|---|---|---|---|---|---|---|
| 0.5 | 18.29 | 17.62 | 6.80 | 7.47 | 0.64 | 127.3 |
| 0.1 | 22.70 | 16.90 | 2.39 | 8.19 | 1.81 | 44.8 |

## 4.9 Optimization of the Simulated Moving Bed Operation

In the last years some studies have been carried out to develop an optimization strategy for the simulated moving bed operation considering the equilibrium stage model (Charton and Nicoud, 1995; Pröll and Küsters, 1998) or taking into account mass transfer resistances by using the linear driving force approximation (Hassan *et al.*, 1996; Pais *et al.*, 1998a).

Considering that the separation system is fully characterized, i.e., adsorbent and mobile phases, column dimensions, SMB configuration and feed concentration, the optimization of the TMB operating conditions consists in setting the liquid flow-rates in each section and the solid flow-rate as well. The resulting optimization problem with five variables will be certainly tedious and difficult to implement.

Fortunately, the optimization problem can be simplified if we take into account the functions of the different sections of a TMB system. Section I, located between the eluent and extract nodes, must provide the complete regeneration of the adsorbent phase, so the solid coming out this zone is recycled to section IV completely clean of the two components. In other words, both components A and B must move upwards, following the liquid phase. Because component B is the more retained species, we have to consider only the constraint considering this component; i.e., if the constraint is fulfilled for species B, the constraint considering the less retained component A will be always met. On the other hand, the liquid flow-rate in section I is the highest flow-rate in a four-section TMB system. For practical purposes, this flow-rate will be limited by the system pressure-drop. Taking into account the maximum system pressure-drop accepted and the constraint considering the more retained component in section I, we can fix the liquid flow-rate in this zone, as well as the switch time interval for the SMB system (related to the TMB solid flow-rate). We will consider that the maximum SMB liquid flow-rate allowed is the one of the reference case presented in Section 4.5, $Q_I^* = 56.83$ ml/min.

The worst situation concerning the constraint in section I appears when dealing with low concentrations of the two species because it leads to bigger retention times. Since the function of section I is to completely regenerate the adsorbent phase, concentrations of both components at the beginning of this zone must be the lowest possible. Hence, the choice of the switch time interval must be done taking into account

the initial slope of the proposed isotherm. The linear retention time of a component *i* in section *j* is given by the following equation:

$$t_{ij} = \frac{\varepsilon V_c}{Q_j^*}\left(1 + \frac{1-\varepsilon}{\varepsilon} K_i\right) \tag{4.66}$$

where $K_i$ is the initial slope of the isotherm for component *i*. Considering that the SMB system under study is constituted by 10.5 cm (length) x 2.6 cm (diameter) columns ($V_c = 55.75$ ml), $\varepsilon = 0.4$, $K_B = 4.03$ (*Equation 4.54b*), and using the maximum flow-rate allowed in this SMB system, $Q_I^* = 56.83$ ml/min, the retention time of the more retained component in section I is $t_{BI} = 2.76$ min. Hence, the switch time interval for the SMB operation must be greater than the retention time of the more retained component in section I, if we want to fulfill the constraint previously presented for this zone. The value chosen for the switch time interval was $t^* = 3$ min, the same value used for the reference case, which is 8% higher than the critical value.

The function of section IV, located between the raffinate and eluent nodes, is to regenerate the liquid phase, so that it can be recycled to section I as pure eluent. In other words, both components A and B must move downwards, following the solid phase. Because component A is the less retained species, we have to consider only the constraint considering this component; i.e., if the constraint is fulfilled for species A, the constraint considering the more retained component B will be always met.

The evaluation of the retention times in section IV and the choice of the liquid flow-rate for this zone (the recycling flow-rate) are not straightforward as it was for section I. The worst situation, concerning the constraint in section IV, appears when dealing with non-linear behaviour because it leads to lower retention times and we must prevent that the less retained component reaches the end of this zone before the jump of the inlet/outlet lines in the SMB operation. Since the switch time interval was already chosen and, in a situation of an effective binary separation, the concentration of the more retained component along the section IV is near zero, we suggest the choice of the liquid flow-rate in section IV by using the following equation:

$$Q_{IV}^* = \frac{\varepsilon V_c}{t^*}\left(1 + \frac{1-\varepsilon}{\varepsilon}\frac{\Delta q_A^{*F}}{\Delta C_A^F}\right) \tag{4.67}$$

where $\Delta q_A^{*F} / \Delta C_A^F$ is the slope of the chord linking points $\left(C_A^F, q_A^{*F}\right)$ and $(0,0)$ with $C_B = 0$.

Considering that the feed concentration used is the same of the reference case, 2.9 g/l of each species and

$$\frac{\Delta q_A^{*F}}{\Delta C_A^F} = \frac{2.69}{1+0.0336C_A^F} + \frac{0.10}{1+C_A^F} = 2.477,$$

*Equation 4.67* gives $Q_{IV}^* = 35.05$ ml/min. The choice of the liquid flow-rate in section IV, as well as the choice of the switch time interval, will be discussed later in this chapter.

Following the procedure presented before, the $\gamma$ values for sections I and IV were fixed, in such a way that constraints concerning these zones were fulfilled: $\gamma_I = 6.646$ and $\gamma_{IV} = 3.715$. Since the liquid flow-rates in sections I and IV are constants in this study, the eluent flow-rate is also constant and equal to $Q_I^* - Q_{IV}^* = 21.78$ ml/min.

The original optimization problem with five variables was, by choosing the liquid flow-rate in section I by pressure-drop limitations and following *Equations 4.66* and *4.67* to evaluate the switch time interval and the recycling flow-rate, reduced to a two-variable optimization problem: the choice of liquid flow-rates in the two central sections. *Table 4.11* summarizes the SMB operating conditions (and equivalent TMB conditions) resulting from the application of *Equations 4.66* and *4.67*.

A region for binary separation can be defined in a $\gamma_{III}$ - $\gamma_{II}$ plane, as it was explained in the previous section and following the operating conditions and model parameters presented in *Table 4.11*. *Figure 4.15* presents the separation regions following a 95% and 99% purity criteria. In the region limited by the open squares both raffinate and extract purities are of at least 95%, while in the region limited by the closed squares, of at least 99%.

However, for practical purposes, it is desirable to work with variables directly related with the SMB unit. Instead of presenting the separation region in a $\gamma_{III}$ - $\gamma_{II}$ plot, we can report the same information in a $Q_X$ versus $Q_F$ plot. The relation between these two types of plots can be easily established using the conversion rules presented before in *Equations 4.57*. It should be pointed out, however, that in the proposed optimization procedure, both $\gamma_I$ and $\gamma_{IV}$ are constants, and so the eluent flow-rate. For a given $(Q_F, Q_X)$ point in the $Q_X$ versus $Q_F$ plot, the raffinate flow-rate can be evaluated by the global balance $Q_R = Q_E + Q_F - Q_X$.

Table 4.11. Operating conditions and model parameters.

| SMB | Equivalent TMB |
|---|---|
| Column diameter: $D_c = 2.6$ cm | Section length: $L_j = 2L_c = 19.8$ cm |
| Column length: $L_c = 10.5$ cm | Peclet number: $Pe_j = 2Pe = 2000$ |
| Configuration: 2 columns per section | |
| Bed porosity: $\varepsilon = 0.4$ | Solid flow-rate (ml/min): |
| Peclet number: $Pe = 1000$ | $Q_s = (1-\varepsilon)V_c / t^* = 11.15$ |
| Mass transfer coefficient: $k = 0.1$ s$^{-1}$ | |
| Feed concentration: $C_A^F = C_B^F = 2.9$ g/l | Flow-rates (ml/min): |
| Switch time interval: $t^* = 3$ min | Section I: |
| Flow-rates (ml/min): | $Q_I = Q_I^* - Q_s\varepsilon / (1-\varepsilon) = 49.40$ |
| Section I: $Q_I^* = 56.83$ | Section IV: |
| Section IV: $Q_{IV}^* = 35.05$ | $Q_{IV} = Q_{IV}^* - Q_s\varepsilon / (1-\varepsilon) = 27.62$ |

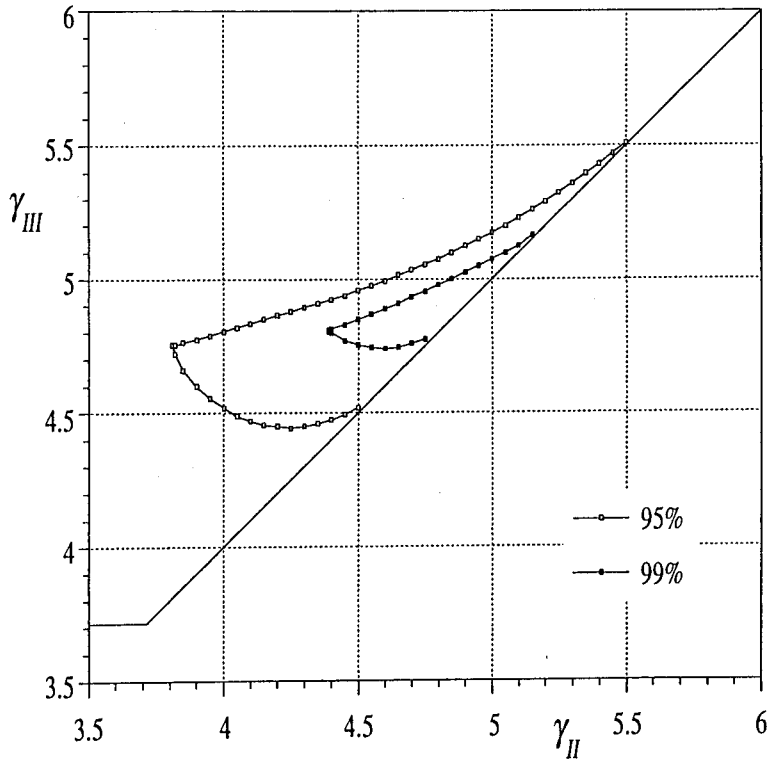


Figure 4.15. Regions of operation of the TMB in a $\gamma_{III}$ - $\gamma_{II}$ plot.
Operating conditions and model parameters are shown in *Table 4.11.*

*Figure 4.16* presents the same separation regions in a $Q_X$ versus $Q_F$ plot following a 95% and 99% purity criteria. In the region limited by the open squares both raffinate and extract purities are of at least 95%, while in the region limited by the closed squares, of at least 99%.

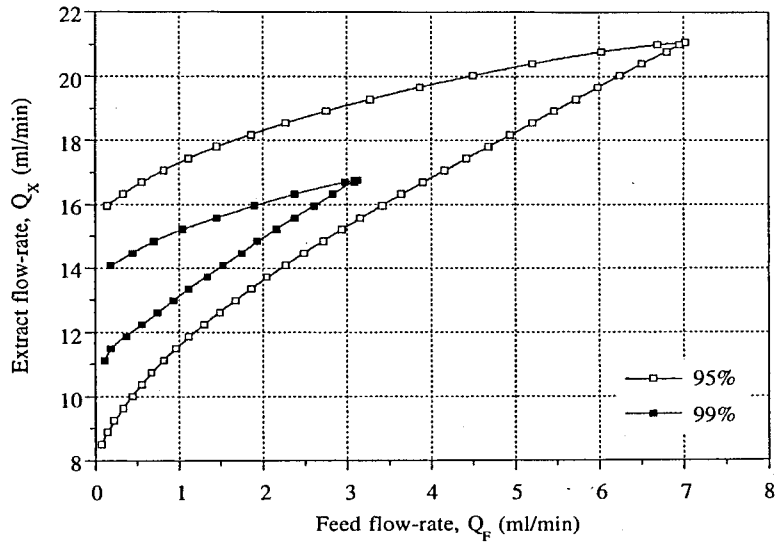


Figure 4.16. Separation region in a $Q_X$ versus $Q_F$ plot for a 95% (open squares) and 99% (closed squares) purity criteria.

It is interesting to observe what happens when we travel along a vertical line in *Figure 4.16*, i.e., for a fixed feed flow-rate, how the system behaves when extract flow-rate changes. The results are presented in *Figure 4.17*, where the purity and recovery performance parameters are evaluated as a function of the extract flow-rate variation and for a constant feed flow-rate of 2.5 ml/min.

In these figures we can observe three different regions: a central region where separation of both species is achieved with also high recoveries, and two adjacent regions where only one outlet is pure. In conclusion, the optimum extract flow-rate can be chosen so that both extract and raffinate purities are high or, alternatively, the extract purity equals the raffinate purity.

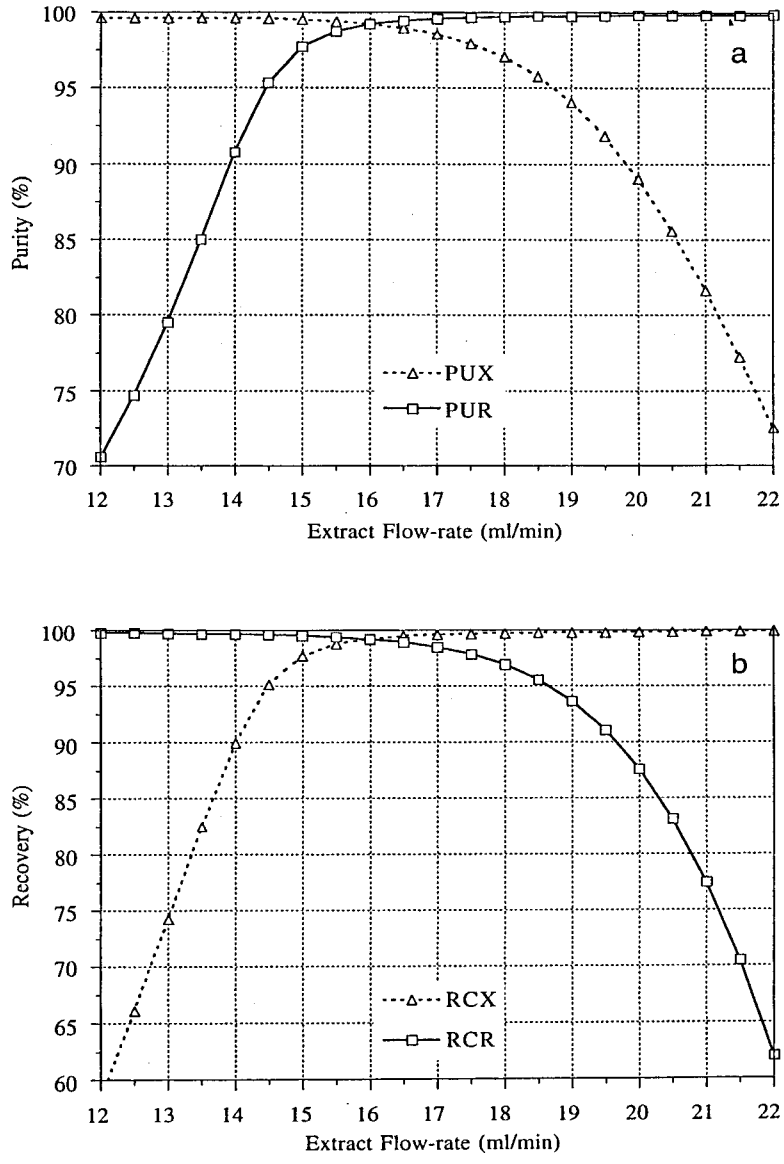


Figure 4.17. Effect of the extract flow-rate on the performance parameters: (a) purity; (b) recovery. (Same conditions as in *Table 4.11*, $Q_E = 21.78$ ml/min, $Q_F = 2.5$ ml/min, $Q_R = Q_E + Q_F - Q_X$).

If the objective of the SMB operation is to obtain the two pure components as it is, for example, the case of chiral discrimination, the path of equal purities is the optimum trajectory that must be followed. For a given feed flow-rate, the SMB optimization can be carried out by minimizing the following objective function:

$$minimize \quad \Phi = (PUX - PUR)^2 \tag{4.68}$$

The minimization was implemented by using the ZXMIN routine from IMSL (1982), which uses a quasi-Newton method to find the minimum of the $\Phi$ function. The optimization variable can be, for example, $Q_{II}^{*}$, the liquid flow-rate in section II. The liquid flow-rate in section III will be evaluated by $Q_{III}^{*} = Q_{II}^{*} + Q_F$. The results obtained are presented in *Figure 4.18*.

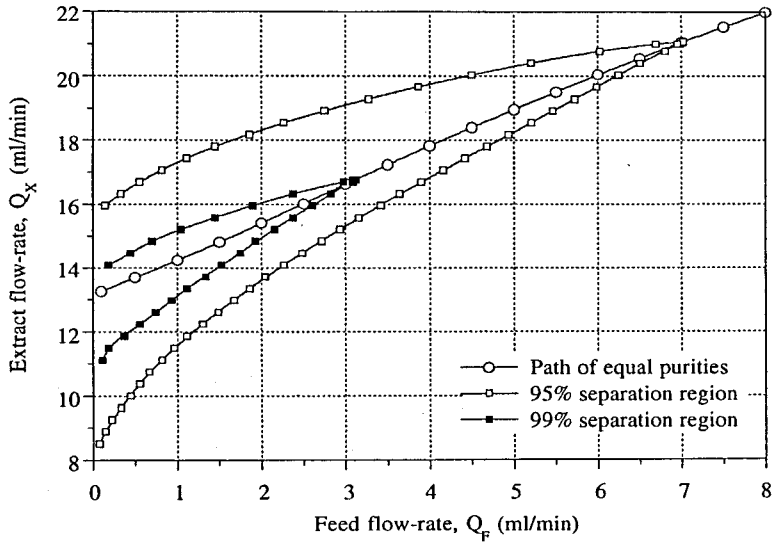


Figure 4.18. Optimum extract and feed flow-rates: path of equal raffinate and extract purities (open circles) (Same conditions as in *Table 4.11*, $Q_E = 21.78$ ml/min, $Q_R = Q_E + Q_F - Q_X$).

*Figure 4.19* presents the purities of both extract and raffinate obtained with the optimization procedure proposed in *Equation 4.68*. It should be pointed out that, when racemic mixtures are fed into a SMB unit ($C_A^F = C_B^F$), if extract and raffinate purities are equal, recoveries of both extract and raffinate are also equal and with the same value of the purity obtained. Observing *Figure 4.19*, we can conclude that, for the conditions presented in *Table 4.11*, the purity of the outlet streams is less than 99% for feed flow-rates greater than 3.3 ml/min. For higher feed flow-rates, a good separation of the two species will need a higher eluent flow-rate, which will violate the constraint for maximum liquid flow-rate in section I imposed by pressure-drop limitations.

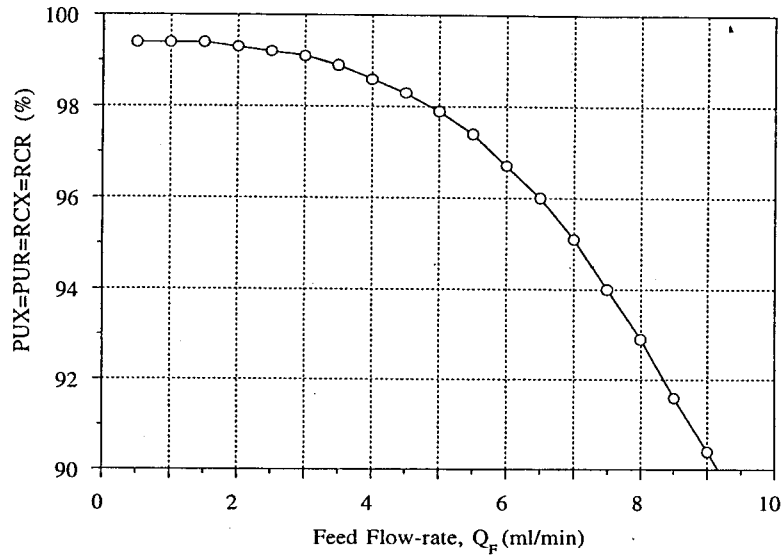


Figure 4.19. Optimum purities and recoveries as a function of the feed flow-rate. (Same conditions as in *Figure 4.18*)

*Figure 4.20* presents the solvent consumption and adsorbent productivity obtained as a function of the feed flow-rate. Of course, this figure should not be used without looking for *Figure 4.19*: the increase of the feed flow-rate leads to better solvent consumption and productivity performances, but it is followed by a decrease in both purities and recoveries of extract and raffinate.

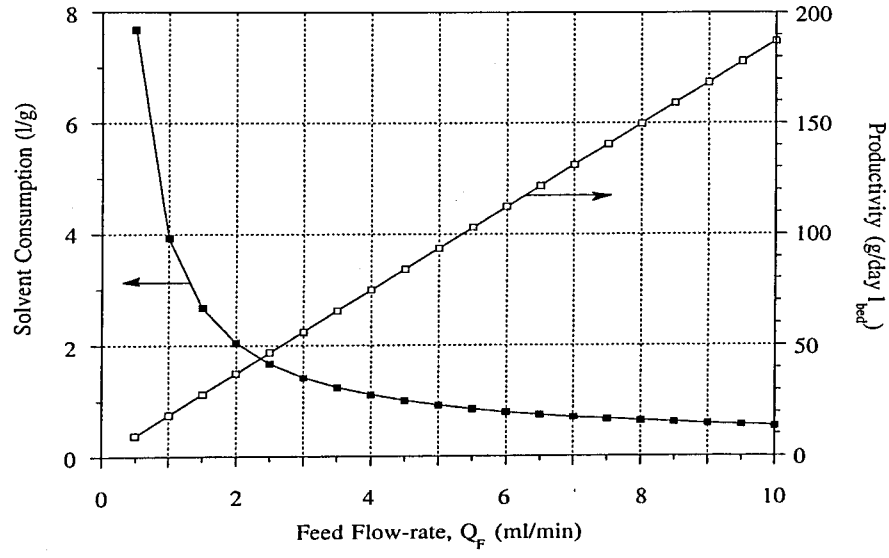


Figure 4.20. Solvent consumption (closed squares) and adsorbent productivity (open squares), obtained for the equal purities optimization procedure, as a function of the feed flow-rate (Same conditions as in *Figure 4.18*).

Furthermore, the higher the feed flow-rate, the smaller the range of extract flow-rates that leads to both enantiomers separation (see *Figure 4.16* or *4.18*). This means that the process robustness also decreases with the increase of the feed flow-rate. In conclusion, the set of *Figures 4.18* through *4.20* provide a practical tool for choosing the better SMB operating conditions as a function of the feed flow-rate. The optimum will result from a trade-off between solvent consumption and adsorbent productivity, purity and recovery requirements, and system robustness. The equal purities optimization procedure proposed by *Equations 4.66* through *4.68* provides a simple tool for choosing the best SMB operating conditions.

We will discuss now the choice of the switch time interval and the recycling flow-rate made following *Equations 4.66* and *4.67*. These equations are derived considering that there is no resistance to mass transfer. If mass transfer resistance is important the switch time interval must be higher than the one obtained through *Equation 4.66*. We did that by choosing $t^* = 3$ min, 8% higher than the value obtained through *Equation 4.66*, $t^* = 2.76$ min. On the other hand, if mass transfer resistance is important, also the recycling flow-rate might have to be lower than the one obtained through *Equation 4.67*. First, we extended the same optimization procedure defined in *Equation 4.68* to other values of recycling flow-rate, keeping the same value for the switch time interval, $t^* = 3$ min. In this way, *Equation 4.67* was used to evaluate the recycling flow-rate ($Q_{RF}^* = 35.05$ ml/min) but lower values were used to increase the safety margin. *Figure 4.21a* shows the optimum flow-rates obtained with the optimization procedure for different values of recycling flow-rate, considering a constant feed flow-rate of *3.3* ml/min. For example, a +10% safety margin means that the recycling flow-rate used was $Q_{RF}^* = 35.05 / 1.1 = 31.86$ ml/min. The 0% safety margin case corresponds to the value originally used in the optimization procedure, $Q_{RF}^* = 35.05$ ml/min. A -10% safety margin means that the recycling flow-rate used was $Q_{RF}^* = 35.05 * 1.1 = 38.56$ ml/min.

*Figure 4.21b* and *4.21c* show the purities and recoveries and the solvent consumption performance obtained with the optimization procedure for the different values of recycling flow-rate. We can conclude that no significant improvement in the purity performance is obtained by using a value lower than the one obtained through *Equation 4.67*. Moreover, using a lower value for the recycling flow-rate, means that the eluent flow-rate is higher and , consequently, the solvent consumption is also higher.

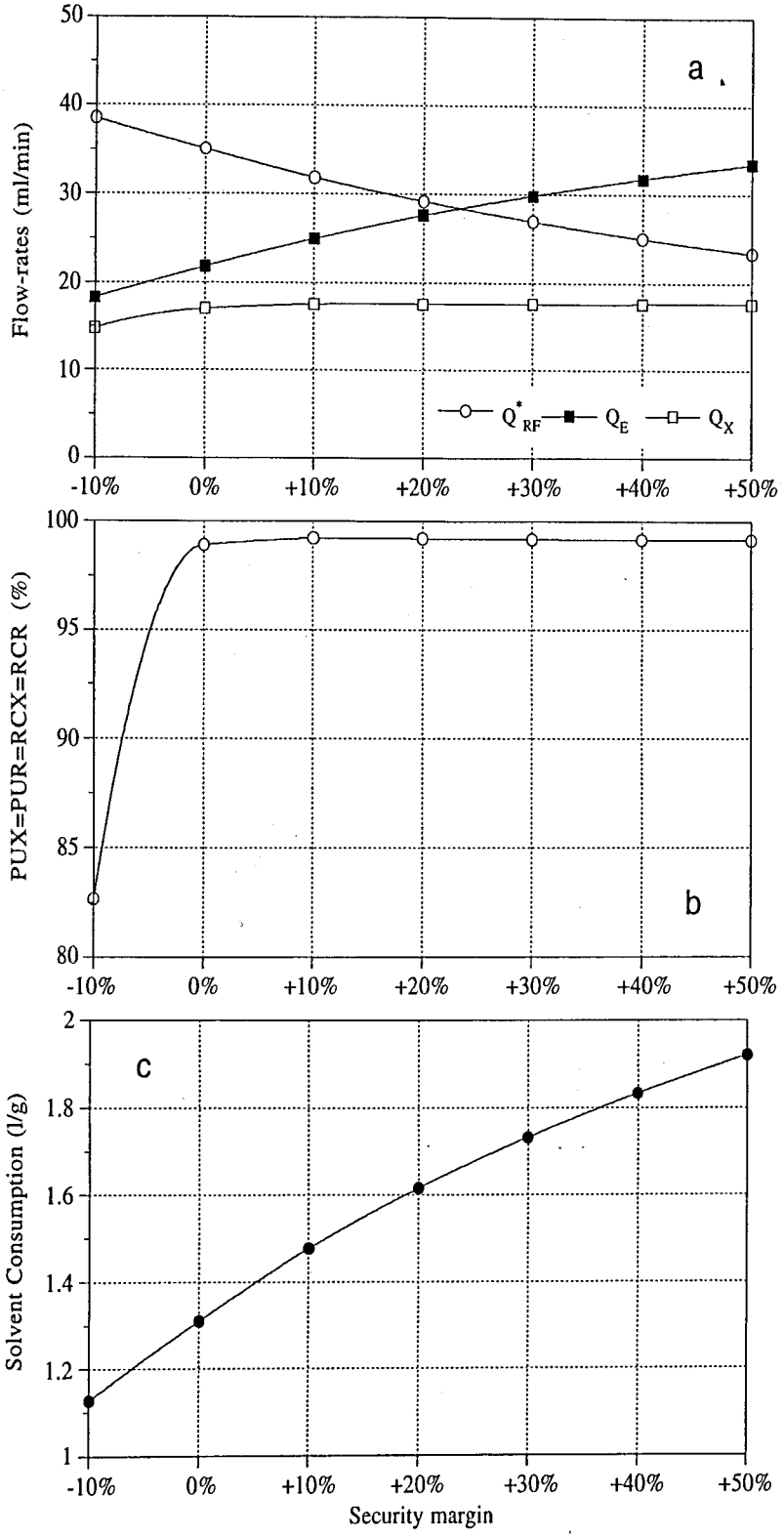


Figure 4.21. Optimization results: (a) Recycling and eluent flow-rates used and optimum extract flow-rate; (b) Optimum purities and recoveries; (c) Solvent consumption. (Operating conditions and model parameters as in *Table 4.11*, except the value of the recycling flow-rate. Feed flow-rate, $Q_F = 3.3$ ml/min.)

We decided to extend the optimization procedure not only for other values of the recycling flow-rate, but also for other values of the switch time interval. *Figure 4.22a* shows the optimum flow-rates obtained with the optimization procedure for different values of switch time interval and recycling flow-rate, and using a constant feed flow-rate of *3.3* ml/min. *Figure 4.22b* shows the values of the switch time interval used in each case. A positive safety margin means that the switch time interval is higher than the one obtained by *Equation 4.66* ($t^* = 2.76$ min). For example, for a safety margin of +10%, $t^* = 2.76 * 1.1 = 3.04$ min. The recycling flow-rate used in this case is evaluated by the *Equation 4.67* with the value of switch time interval $t^* = 3.04$ min, decreased by the factor 1.1, i.e., $Q^*_{RF} = 34.59 / 1.1 = 31.44$ ml/min. Note that the 0% safety margin case is not equal to the one used originally for the optimization procedure. In the original case the switch time interval used was $t^* = 3$ min, 8% higher than the critical value $t^* = 2.76$ min.

*Figures 4.22c* and *4.22d* show the purities and recoveries and the solvent consumption performance obtained with the optimization procedure for different values of switch time interval and recycling flow-rate. We conclude once more that no significant improvement on the purity performance is obtained by increasing the safety margin on the values of both switch time interval and recycling flow-rate. Furthermore, solvent consumption will increase with the increase of the safety margin.

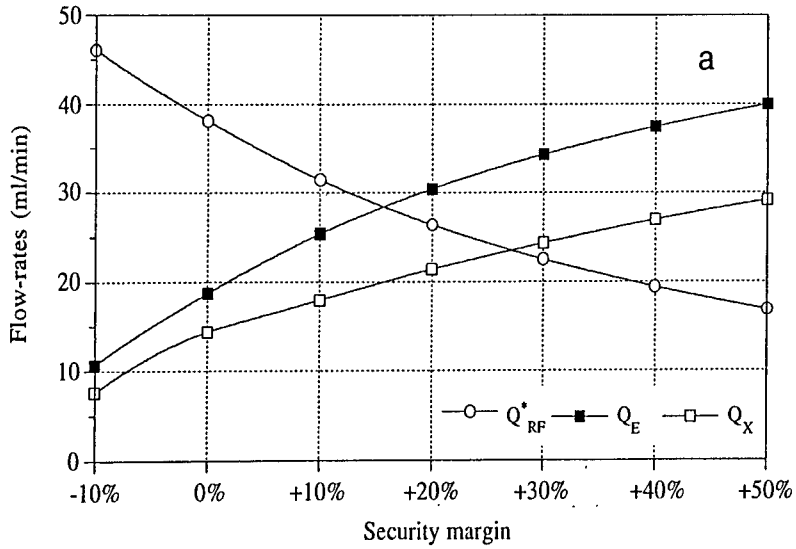

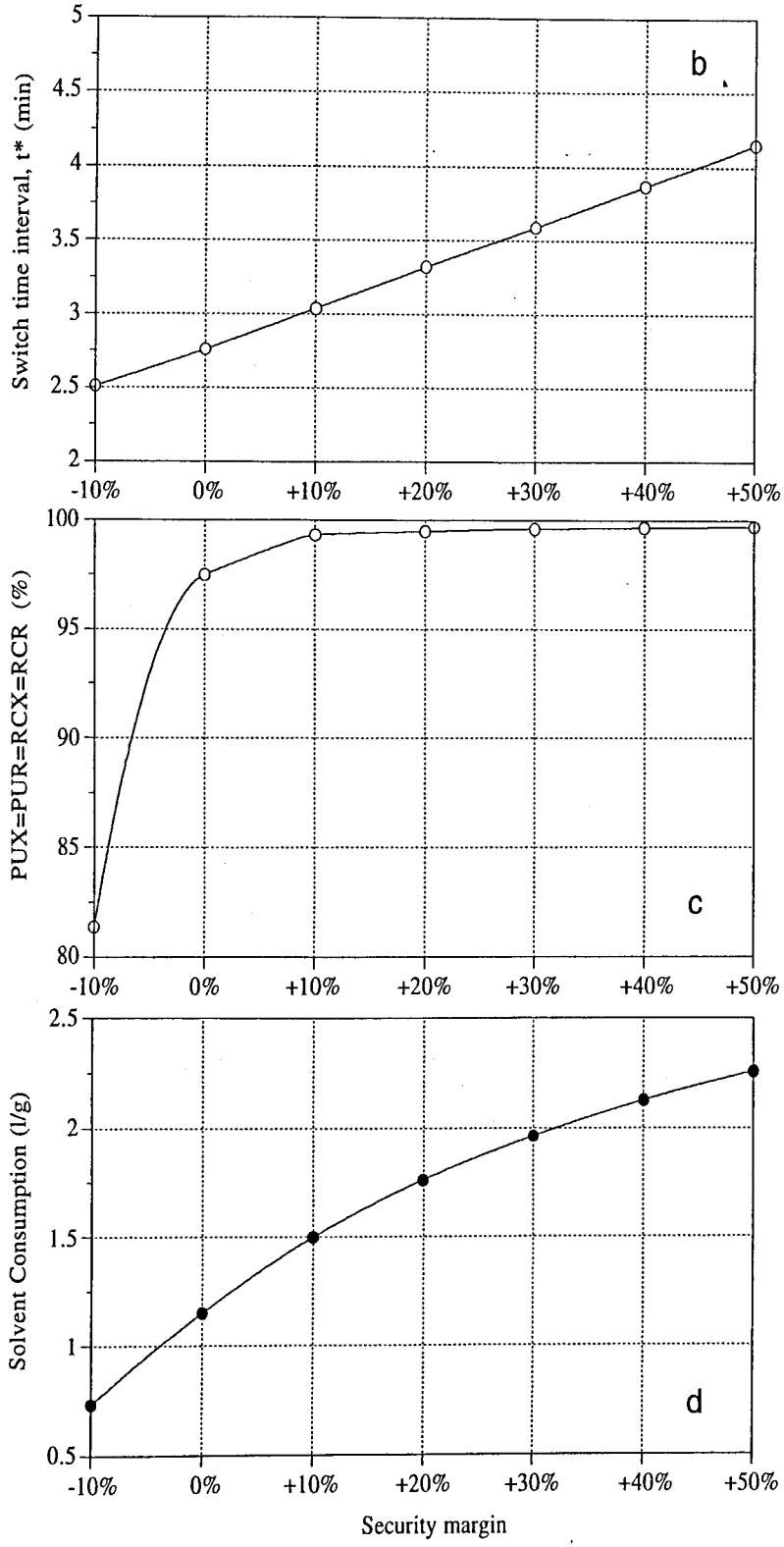


Figure 4.22. Optimization results: (a) Recycling and eluent flow-rates used and optimum extract flow-rate; (b) Values of switch time interval used; (c) Optimum purities and recoveries; (d) Solvent consumption. (Conditions as in *Table 4.11*, except the value of the switch time interval and recycling flow-rate. Feed flow-rate, $Q_F = 3.3$ ml/min.)

*Figures 4.21* and *4.22* show that the optimization procedure proposed by *Equations 4.66* through *4.68* is a simple and quick optimization tool for the choice of the SMB operating conditions. Considering that the mass transfer resistance is important, we can increase process robustness by increasing the switch time interval and decreasing the recycling flow-rate evaluated by *Equations 4.66* and *4.67*, as it was shown previously. Of course, the drawback of increase process robustness will be the increase of the solvent consumption.

## 4.10 Optimization of the Feed Concentration

In the previous section we carried out an optimization procedure to find the optimum SMB operating conditions. This procedure was developed for a constant feed concentration. However, the feed concentration is one of the most important variables on the SMB performance, as we can easily conclude from the definitions of the solvent consumption and adsorbent productivity performance parameters. Hence, the feed concentration must be also optimized. It must be mentioned that, for the illustrative example followed in this chapter, the bi-naphthol enantiomers, the limit of solubility is 3 g/l of each enantiomer (in a 72:28 heptane-isopropanol solvent). Nevertheless, we will continue to use the same isotherms presented in *Equations 4.54* to illustrate the influence of the feed concentration on the SMB performance.

The optimization procedure proposed in the previous section (*Equations 4.66* through *4.68*) was carried out for various values of feed concentration. The operating conditions and model parameters are the ones presented in *Table 4.11*, except the recycling flow-rate that is evaluated through *Equation 4.67* which depends of the feed concentration. The switch time interval is the same for all the feed concentration cases and equal to *3* minutes. *Figure 4.23* presents the recycling and eluent flow-rates as a function of the feed concentration, and result from the application of the *Equation 4.67* with $t^* = 3$ min. Note that the maximum liquid flow-rate allowed is the same of the previous section, $Q_I^* = 56.83$ ml/min. The eluent flow-rate for each feed concentration case is constant and equal to $Q_I^* - Q_{RF}^*$.

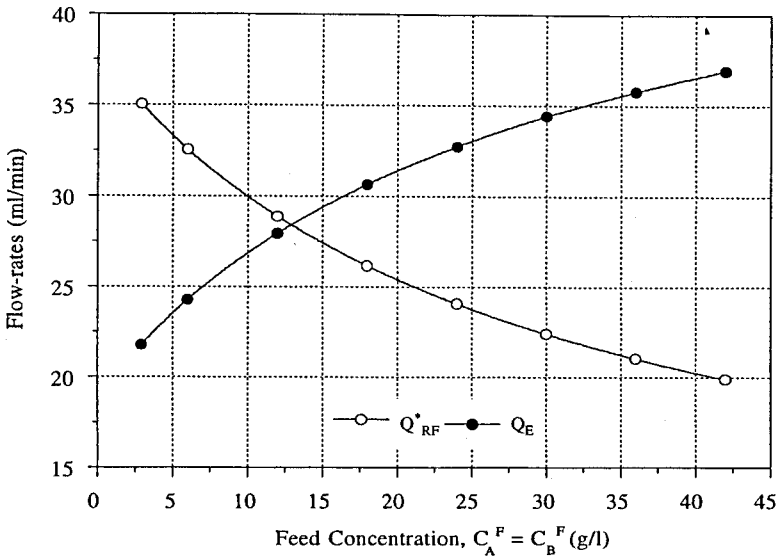


Figure 4.23. Influence of the feed concentration on the evaluation of the recycling and eluent flow-rates through *Equation 4.67.*

*Figure 4.24* presents the optimum extract and feed flow-rates, following the path of equal purities optimization procedure, obtained for different values of feed concentration. *Figure 4.25* presents the corresponding purities and recoveries of both extract and raffinate obtained. Observing this figure, we conclude that the higher the feed concentration, the lower the feed flow-rate that can be used to obtain a certain purity requirement.

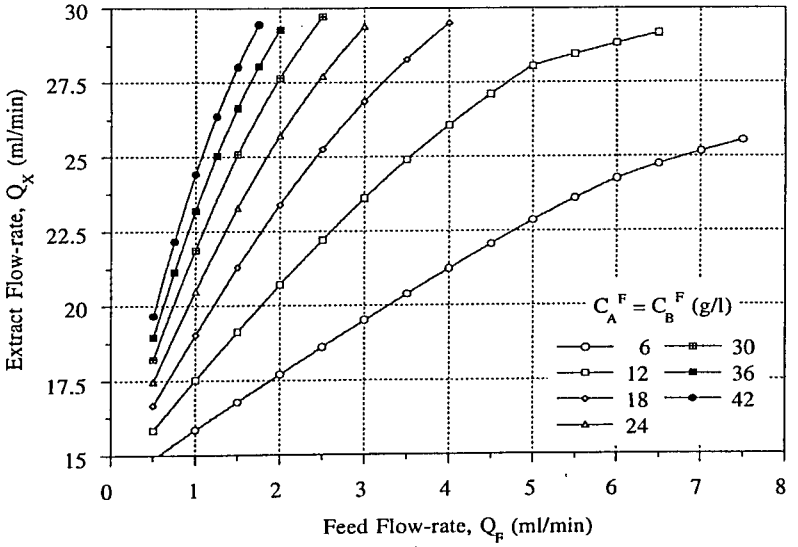


Figure 4.24. Influence of the feed concentration on the optimum extract and feed flow-rates: path of equal purities. (Eluent flow-rate given in *Figure 4.23*, $Q_R = Q_E + Q_F - Q_X$).

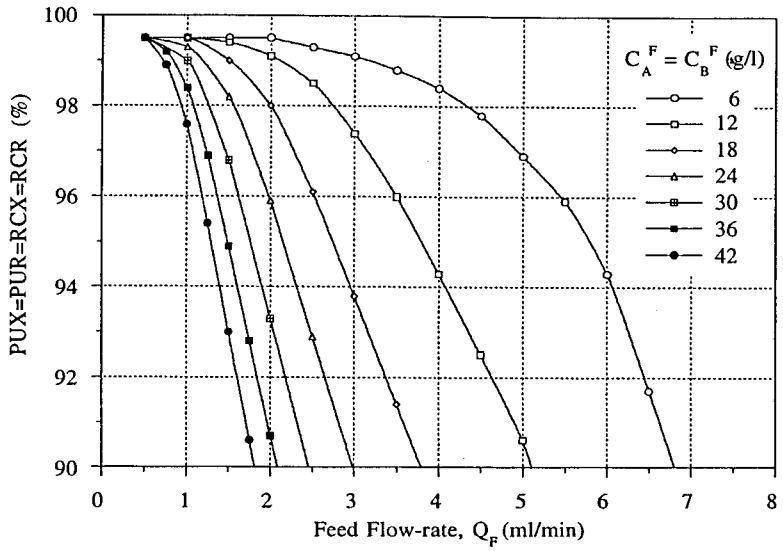


Figure 4.25. Influence of the feed concentration on the optimum purities and recoveries obtained with the optimization procedure. (Same conditions as in *Figure 4.24*).

*Figures 4.26* and *4.27* show the solvent consumption and adsorbent productivity obtained as a function of the feed flow-rate for different values of feed concentration. Once more, these figures should not be used without looking for *Figure 4.25*. The increase of the feed flow-rate leads to better solvent consumption and productivity performances, but it is followed by a decrease in both purities and recoveries of extract and raffinate. Moreover, higher feed concentrations will impose lower feed flow-rates to obtain the same purity performance.

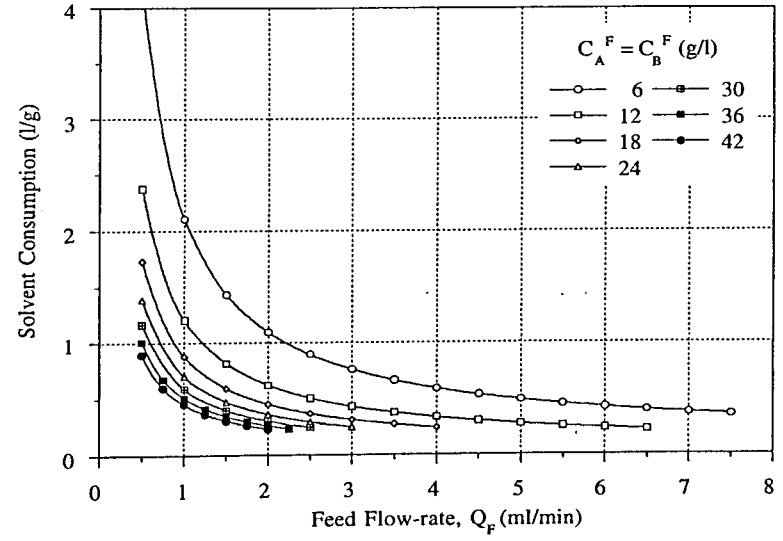


Figure 4.26. Influence of the feed concentration on the solvent consumption performance obtained with the optimization procedure. (Same conditions as in *Figure 4.24*.)

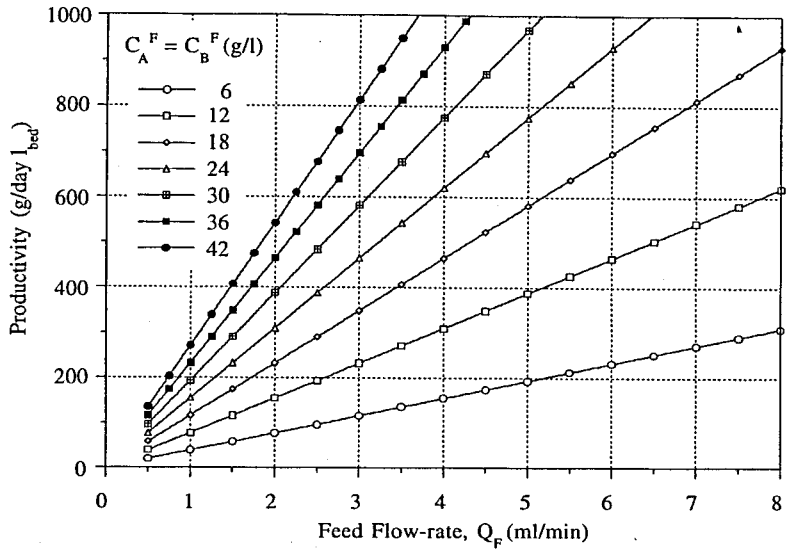


Figure 4.27. Influence of the feed concentration on the adsorbent productivity performance obtained with the optimization procedure. (Same conditions as in *Figure 4.24.*)

With the results obtained with the optimization procedure carried out before, we evaluated, for each value of feed concentration, the maximum feed flow-rate that can be used to obtain a given purity requirement. *Figure 4.28* presents the maximum feed flow-rates allowed, as well as the eluent flow-rates, for a 99% (*Figure 4.28a*) and 95% (*Figure 4.28b*) purity requirement. It should be noticed that, since the operating conditions are evaluated by *Equations 4.66* and *4.67*, the eluent flow-rate is constant for a given feed concentration, and those values are the ones presented before in *Figure 4.23*. Looking for *Figure 4.28*, we conclude that a higher feed concentration will allow a lower feed flow-rate to obtain the same purity performance. A higher purity requirement will need, naturally, a lower feed flow-rate, as we can easily conclude by comparing *Figures 4.28a* and *4.28b*.

*Figures 4.29* and *4.30* present the solvent consumption and productivity performances corresponding to the maximum feed flow-rates allowed to obtain a 99% (closed squares) and 95% (open squares) purity requirements. We conclude that the solvent consumption decreases and the productivity increases when the feed concentration increases. However, the influence of the feed concentration is more pronounced in the lower concentration range and more smooth for higher values of feed concentration, as it was noticed by Charton and Nicoud (1995). For the bi-naphthol enantiomers system, solvent consumption does not diminish significantly for feed concentrations higher than 12 g/l of each enantiomer, while the productivity performance do not increase significantly for feed concentrations higher than 20 g/l of

each enantiomer. For this system, if we did not have the limit imposed by the enantiomers solubility, the optimum feed concentration would be in the range 10-20 g/l of each enantiomer. Using higher values of feed concentration will not lead to significant improvements on the SMB performance. Furthermore, as it was noticed also by Charton and Nicoud (1995), very high feed concentrations can lead to a very low feed flow-rate, which might be difficult to control experimentally.

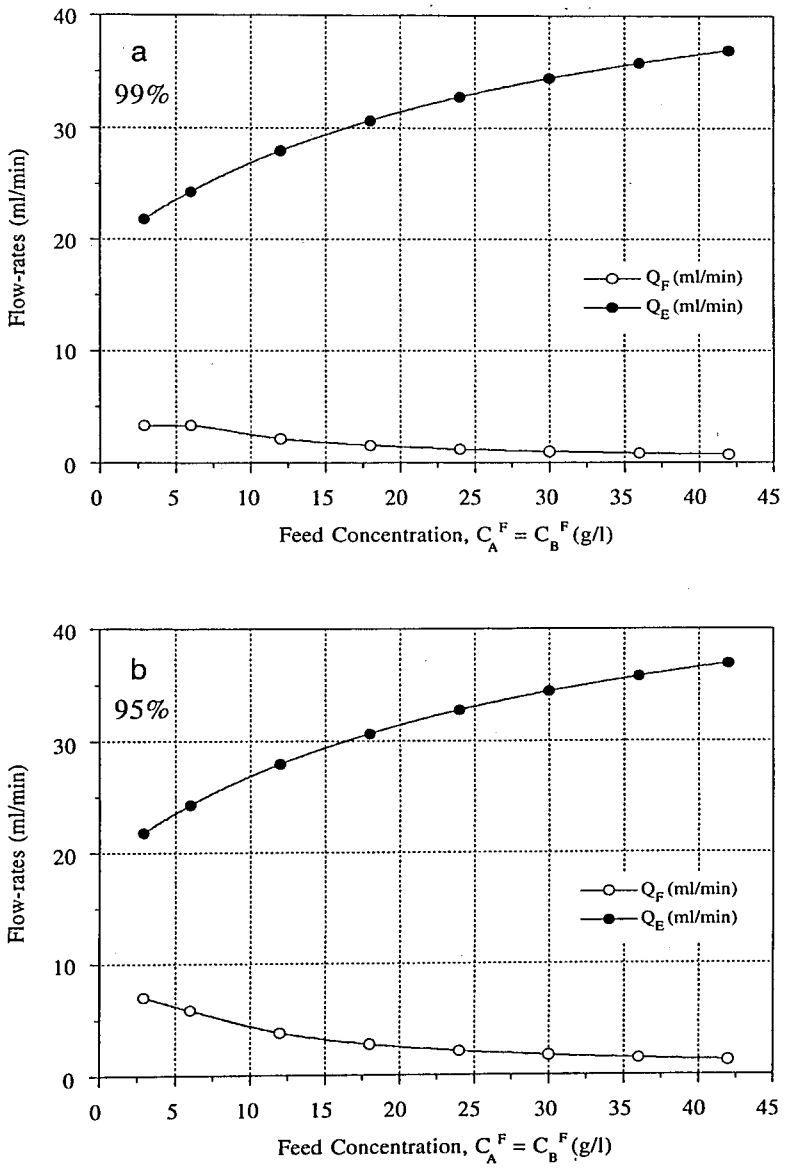


Figure 4.28. Maximum feed flow-rates allowed to obtain a given purity requirement as a function of the feed concentration: (a) 99%; (b) 95% purity requirement. (Same conditions as in *Figure 4.24.*)

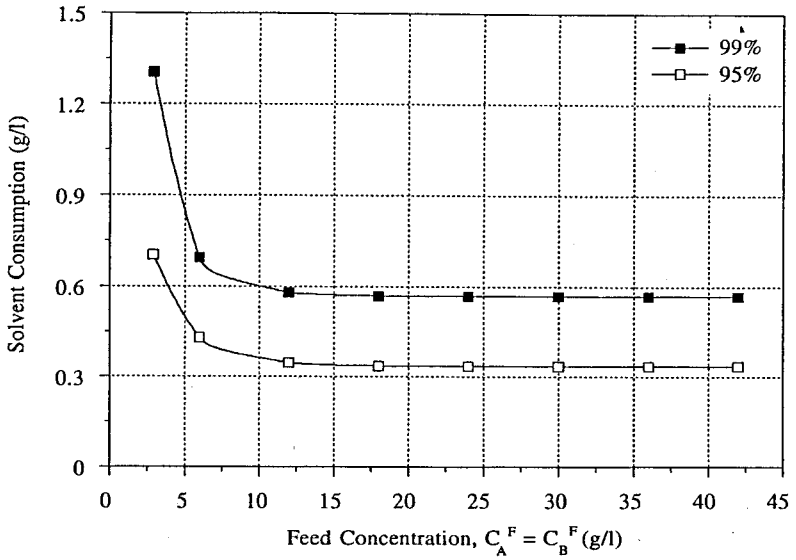


Figure 4.29. Solvent consumption performance corresponding to the maximum feed flow-rates allowed to obtain a given purity requirement as a function of the feed concentration: 99% (closed squares) and 95% (open squares) purity requirement. (Same conditions as in *Figure 4.24*.)

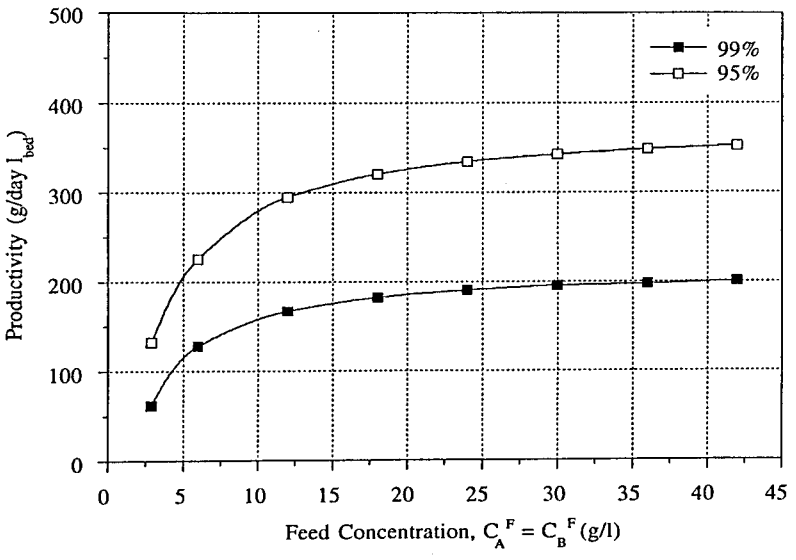


Figure 4.30. Adsorbent productivity performance corresponding to the maximum feed flow-rates allowed to obtain a given purity requirement as a function of the feed concentration: 99% (closed squares) and 95% (open squares) purity requirement. (Same conditions as in *Figure 4.24*).

## 4.11 Conclusions

The true moving bed steady-state model was used to study the influence of the operating conditions on the SMB performance, namely, the influence of the switch time interval, recycling flow-rate, and extract and feed flow-rates. This influence was explained on the basis of the net fluxes of species in the four sections of the SMB unit.

The bi-naphthol enantiomers system was used to carried out our study. For this system, the effect of the axial dispersion on the SMB performance can be considered negligible for Peclet numbers higher than 500. Later in this chapter, we shown how mass transfer resistance can influence the SMB performance, namely in what concerns the regions for separation of both enantiomers and its better operating conditions.

At the end of the chapter, a simple optimization procedure for choosing the best SMB operating conditions was suggested and tested with the bi-naphthol system. This procedure was also applied to other values of feed concentration to study its influence on the SMB performance and to optimize it.

## 4.12 References

Ascher, U., Christiansen, J., and Russell, R.D., "A Collocation Solver for Mixed Order Systems of Boundary Value Problems," *Math. Comput.* **33**, 659-679 (1979).

Ascher, U., Christiansen, J., and Russell, R.D., "Collocation Software for Boundary-Value ODEs," *ACM Trans. Math. Software* **7**, 209-222 (1981).

Azevêdo, D.C.S., and Rodrigues, A.E., "Design of a Simulated Moving Bed Separator in the Presence of Mass Transfer Resistances," *AIChE J.* **45**, 956-966 (1999).

Bader, G., and Ascher, U., "A New Basis Implementation for a Mixed Order Boundary Value ODE Solver," *SIAM J. Sci. Stat. Comput.* **8**, 483-500 (1987).

Charton, F., and Nicoud, R.-M., "Complete Design of a Simulated Moving Bed," *J. Chromatogr. A* **702**, 97-112 (1995).

Chiang, A., "Complete Separation Conditions for a Local Equilibrium TCC Adsorption Unit," *AIChE J.* **44**, 332-340 (1998).

Ching, C.B., and Ruthven, D.M., "An Experimental Study of a Simulated Counter-Current Adsorption System - I. Isothermal Steady State Operation," *Chem. Engng Sci.* **40**, 877-885 (1985a).

Gentilini, A., Migliorini, C., Mazzotti, M., and Morbidelli, M., "Optimal Operation of Simulated Moving-Bed Units for Non-Linear Chromatographic Separations. II. Bi-Langmuir Isotherm," *J. Chromatogr. A* **805**, 37-44 (1998).

Glueckauf, E., "Theory of Chromatography Part 10 - Formulæ for Diffusion into Spheres and Their Application to Chromatography," *Trans. Faraday Soc.* **51**, 1540-1551 (1955).

Hassan, M.M., Loughlin, K.F., and Biswas, M.E., "Optimization of Continuous Countercurrent Adsorption Systems," *Sep. Technol.* **6**, 19-27 (1996).

IMSL International Mathematical & Statistical Libraries, Inc., *Reference Manual*, Texas, USA (1982).

Leitão, A., and Rodrigues, A.E., "Adsorptive Processes Using Large-Pore Materials: Analysis of a Criterion for Equivalence of Diffusion-Convection, Apparent Diffusion and Extended Linear Driving Force Models," *Chem. Engng J.* **60**, 81-87 (1995).

Leitão, A., and Rodrigues, A.E., "The Performance of the Extended Linear Driving Force Model to Simulate Adsorptive Processes Using Large-Pore Materials," *Proceedings of the 5th International Conference on Fundamentals of Adsorption*, M.D. LeVan, ed., Kluwer Academic Publishers, Boston, Massachusetts, p. 505-512 (1996).

Mazzotti, M., Storti, G., and Morbidelli, M., "Robust Design of Countercurrent Adsorption Separation Processes: 2. Multicomponent Systems," *AIChE J.* **40**, 1825-1842 (1994).

Mazzotti, M., Storti, G., and Morbidelli, M., "Robust Design of Countercurrent Adsorption Separation : 3. Nonstoichiometric Systems," *AIChE J.* **42**, 2784-2796 (1996a).

Mazzotti, M., Pedeferri, M., and Morbidelli, M., "Design of Optimal and Robust Operating Conditions for Chiral Separations Using Simulated Moving Beds," *Proceedings of the Chiral Europe'96 Symposium*, Spring Innovations Limited, Stockport, UK (1996b).

Mazzotti, M., Storti, G., and Morbidelli, M., "Robust Design of Countercurrent Adsorption Separation Processes: 4. Desorbent in the Feed," *AIChE J.* **43**, 64-72 (1997a).

Mazzotti, M., Storti, G., and Morbidelli, M., "Optimal Operation of Simulated Moving Bed Units for Nonlinear Chromatographic Separations," *J. Chromatogr. A* **769**, 3-24 (1997b).

Nicoud, R.-M., "The Simulated Moving Bed: A Powerful Chromatographic Process," *LC-GC Intl.* **5**, 43-47 (1992).

Nicoud, R.-M., "Simulated Moving Bed (SMB) in Preparative Chromatography: Basics, Limitations and Use," *Simulated Moving Bed: Basics and Applications*, R.-M. Nicoud, ed., Institut National Polytechnique de Lorraine, Nancy, France, p. 54-64 (1993).

Pais, L.S., Loureiro, J.M., and Rodrigues, A.E., "Separation of 1,1'-bi-2-naphthol Enantiomers by Continuous Chromatography in Simulated Moving Bed," *Chem. Engng Sci.* **52**, 245-257 (1997a).

Pais, L.S., Loureiro, J.M., and Rodrigues, A.E., "Modeling, Simulation and Operation of a Simulated Moving Bed for Continuous Chromatographic Separation of 1,1'-bi-2-naphthol Enantiomers," *J. Chromatogr. A* **769**, 25-35 (1997b).

Pais, L.S., Loureiro, J.M., and Rodrigues, A.E., "Separation of Enantiomers of a Chiral Epoxide by Simulated Moving Bed Chromatography," *J. Chromatogr. A* **827**, 215-233 (1998a).

Pais, L.S., and Rodrigues, A.E., "Separation of Enantiomers by SMB Chromatography: Strategies of Modeling and Process Performance," *Proceedings of the 6th International Conference on Fundamentals of Adsorption*, Presqu'île de Giens, France (1998b).

Pröll, T., and Küsters, E., "Optimization Strategy for Simulated Moving Bed Systems," *J. Chromatogr. A* **800**, 135-150 (1998).

Rodrigues, A.E., Loureiro, J.M., Lu, Z.P., and Pais, L.S., "Modeling and Operation of a Simulated Moving Bed for the Separation of Optical Isomers," *Proceedings of the 5th International Conference on Fundamentals of Adsorption*, M.D. LeVan, ed., Kluwer Academic Publishers, Boston, Massachusetts, p. 765-772 (1996).

Ruthven, D.M., and Ching, C.B., "Counter-Current and Simulated Counter-Current Adsorption Separation Processes," *Chem. Engng Sci.* **44**, 1011-1038 (1989).

Storti, G., Mazzotti, M., Morbidelli, M., and Carrà, S., "Robust Design of Binary Countercurrent Adsorption Separation Processes," *AIChE J.* **39**, 471-492 (1993).

Storti, G., Baciocchi, R., Mazzotti, M., and Morbidelli, M., "Design of Optimal Operating Conditions of Simulated Moving Bed Adsorptive Units," *Ind. Eng. Chem. Res.* **34**, 288-301 (1995).

Turner, J.R., and Mills, P.L., "Evaluation of Finite-Element Collocation Techniques for Boundary-Value ODEs and Their Application to Chemical Engineering Systems," presented at the *AIChE Annual Meeting* (1990).

Zhong, G., and Guiochon, G., "Analytical Solution for the Linear Ideal Model of Simulated Moving Bed Chromatography," *Chem. Engng Sci.* **51**, 4307-4319 (1996).

Chapter 5

# Experimental Operation of a Simulated Moving Bed

*In this chapter the experimental work carried out in the SMB pilot unit is presented. First, the SMB unit used (Licosep 12-26, Novasep, France) is described. Then, two case studies are presented: the separation of bi-naphthol and chiral epoxide enantiomers.*

*For the bi-naphthol system purities and recoveries higher than 95% were obtained for both extract and raffinate. A 450 ml inventory of stationary phase was used, which corresponds to an adsorbent productivity of 68 grams of racemic mixture processed per day and per liter of bed. The solvent consumption was 1.2 liter per gram of racemic mixture processed. For the chiral epoxide system, a first set of experimental runs led to purities and recoveries higher than 90%. The inventory of stationary phase used was 420 ml, which corresponds to an adsorbent productivity of 52 grams of racemic mixture per day and per liter of bed, and a solvent consumption of 0.4 liter of mobile phase per gram of racemic mixture processed. In a second set of experimental runs, we obtained 98% pure extract and raffinate, with a productivity of 34 grams per day and per liter of bed, and a solvent consumption of 1.3 liter per gram.*

*The experimental results obtained are reported in terms of process performance and steady-state internal concentration profiles. The simulation packages developed in the previous chapters, namely the steady-state TMB model, is used to compare experimental results and model predictions. The dynamic behaviour of the internal concentration profiles under cyclic steady-state operation is also evaluated, and the SMB model is used to compare predicted and experimental profiles.*

## 5.1 The *Licosep 12-26* SMB Pilot Unit

The SMB pilot unit used in this work is the *Licosep 12-26* (*Figure 5.1*), developed by *Separex* (*Champigneulles, France*) in cooperation with the *Institut Français du Pétrole* (*Rueil-Malmaison, France*). The *Licosep* technology is now available through *Novasep, SA* (*Vandœuvre-lès-Nancy, France*).

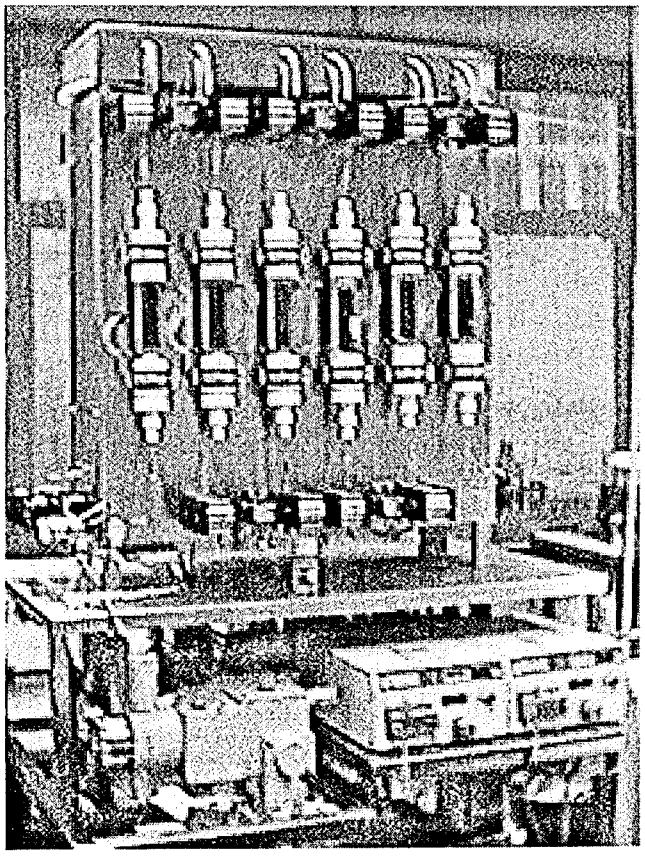

Figure 5.1. The *Licosep 12-26* Simulated Moving Bed pilot unit at the *Laboratory of Separation and Reaction Engineering* (*Porto, Portugal*).

*Figure 5.2* presents the flowsheet of a *Licosep 12-26* SMB pilot unit. It is a continuous chromatographic system constituted by 12 columns connected in series. The columns are *Superformance 300-26* (*Merck, Darmstadt, Germany*) with 26 mm internal diameter and adjustable length (5-20 cm). They have a jacket which allows operation of

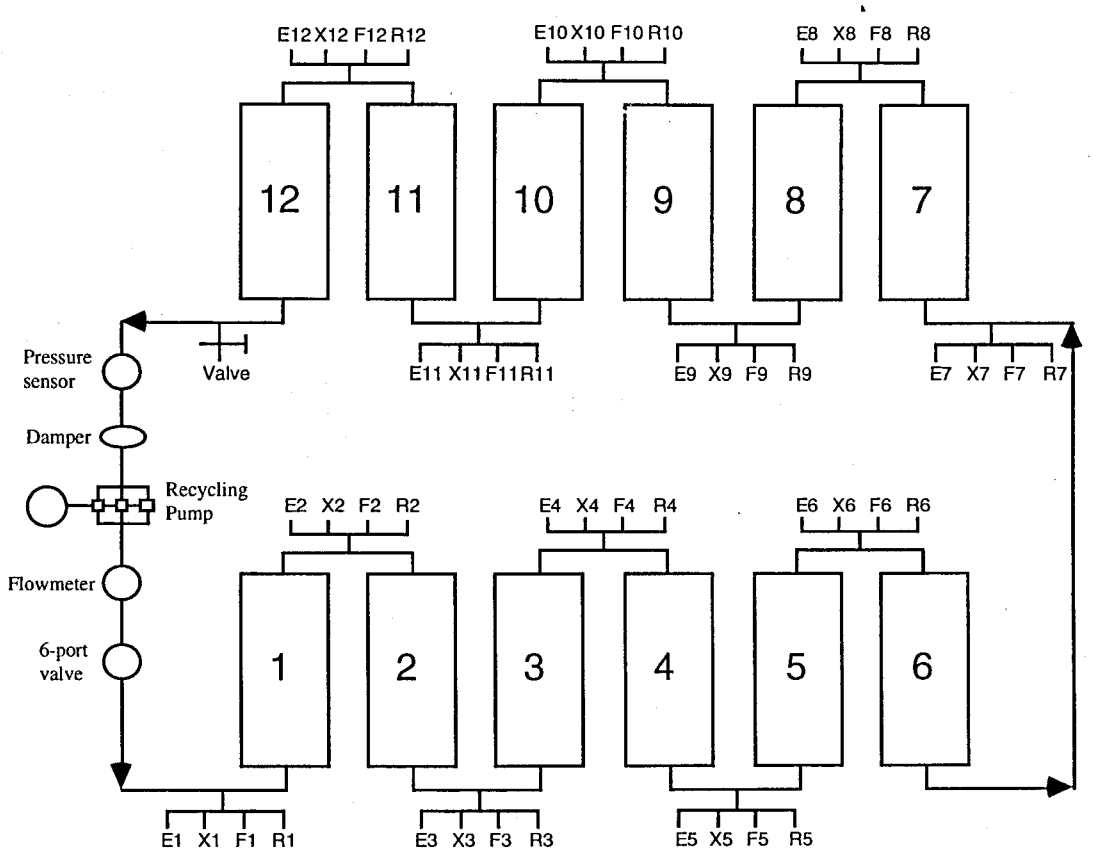


Figure 5.2. Flowsheet of the *Licosep 12-26* Simulated Moving Bed pilot unit.

the SMB up to 60 C. All tubings are stainless steel, 1/16" external diameter, 1 mm internal diameter. Each column is connected with four lines (eluent, feed, extract and raffinate lines) and 48 two-way high pressure pneumatic valves (*TOP Industrie, France*) allow the connection of the inlet-outlet lines of the columns. Consequently, there are 12 lines of each type. At a given time, only one line of each type must be opened. The valves work at a minimum air pressure of 6 bar provided by an air compressor.

Following the Simulated Moving Bed concept described in Chapter 2, the eluent, extract, feed and raffinate lines are shifted after a given time period, the switch time interval, $t^*$. For the 12-columns SMB configuration presented in *Figure 5.2*, a whole cycle is made of 12 successive periods allowing the different lines to come back to their initial positions. Depending on the injection and collection lines positions, four zones can be defined in the system:

Zone I, between the eluent and the extract lines;
Zone II, between the extract and the feed lines;
Zone III, between the feed and the raffinate lines;
Zone IV, between the raffinate and the eluent lines.

A three-head membrane pump (*Milroyal, Pont St. Pierre, France*) is used for the recycling flow. This pump is fixed in the system, between the last and the first columns. Consequently, depending also on the injection and collection lines positions, the recycling pump can be, successively, in zone IV, III, II or I, and its flow-rate must be set accordingly. Following the same notation used in the previous chapters, we define the recycling flow-rate as the flow-rate occurring in section IV. During the SMB operation, the flow-rates in sections I, II, III and IV must be kept constant, in agreement with the flow-rates sought. Consequently, the recycling pump flow-rate must vary according to its location, as it is presented in *Table 5.1.*

Table 5.1. Relation between the recycling pump location and its flow-rate.

| Recycling pump location | Zone I | Zone II | Zone III | Zone IV |
|---|---|---|---|---|
| Recycling pump flow-rate | $Q_{RF}^{*}+Q_E$ | $Q_{RF}^{*}+Q_E$ $-Q_X$ | $Q_{RF}^{*}+Q_E$ $-Q_X+Q_F$ | $Q_{RF}^{*}$ |

It should be mentioned that the recycling pump introduces a dead volume $V_d$, which delays the concentrations leaving the last and entering the first columns. To assess the possible effect of this dead volume, we can calculate an average dead time $t_d$ taking into account the successive positions of the recycling pump in sections I to IV:

$$t_d = \frac{V_d}{\frac{(Q_I^{*}+Q_{II}^{*}+Q_{III}^{*}+Q_{IV}^{*})}{4}} \tag{5.1}$$

If $t_d$ is not negligible (higher than a few percent of the switch time interval), the recycling pump dead volume can modify the performance of the *Licosep 12-26* unit (for instance, lower purities than those expected can be reached).

The *Separex* group found that this effect could be compensated thanks to an appropriate shifting of the injection and withdrawal points which are no longer translated at the same time. In this way, a dead volume correction is accomplished by using a period desynchronization: the injection or collection lines which have passed the last column, during a given cycle, are shifted with a delay equal to $t_d$ (Hotier and Nicoud, 1996a). An alternative methodology, also proposed by the *Separex* group, involves the dead volume correction by using a length reduction procedure (Hotier and Nicoud, 1996b).

The maximum flow-rate allowed in the recycling pump is 120 ml/min. The other flows (eluent, extract, feed and raffinate) are controlled by four *Merck-Hitachi* pumps (*Merck-Hitachi* models *L-6000* and *L-6200, Darmstadt, Germany*), connected to the computer via RS-232. The maximum flow-rate allowed in the eluent and extract pumps is 30 ml/min, while in the feed and raffinate pumps is 10 ml/min.

The system temperature is measured and controlled through a thermostatic bath (*Lauda* model *RM6, Germany*). The *Licosep* pilot unit can stand pressures up to 60 bar. The SMB unit is controlled by a central system using the *Licosep* control software. The central system is composed by a microcomputer (*Arche 386SX*, 25 MHz), analogical and numerical in/out cards type *Data Translation* and two output ports *RS-232*. An electronic interface allows processing of information coming from the captors and translates the orders coming from the computer.

The pressure measurements are achieved by a transmitter *JUMO* (0-60 bar, 4-20 mA) located between the last column and the recycling pump. This allows the measurement of the pressure at the recycling pump inlet that is set to 1.5 bar and is used to control the extract flow-rate. The recycling pump flow-rate is controlled through a flowmeter located at its outlet. The description of the methodology for the calibration of the recycling pump and of the flowmeter can be found in *Appendix B*. A valve, located at the end of the last column, allows the connection of the system with a detector. A 6-port valve, located before the first column, allows the withdrawal of samples from the system to evaluate the internal concentration profiles (see *Appendix C*).

A full description of the control software, *Licosep 1.1*, as well as some informations about how to start with the SMB pilot unit operation can be found in the *Licosep 12-26 Instruction Manual* (*Separex*, 1994a).

## 5.2 Separation of Bi-Naphthol Enantiomers

### 5.2.1 The Bi-Naphthol System

The first system studied experimentally in our SMB pilot unit was the separation of bi-naphthol enantiomers (*Figure 5.3*) presented in the previous chapters for simulation purposes (Pais *et al.*, 1997a,b, 1998a). These enantiomers are also known as 2,2'-dihydroxy-1,1'-binaphthyl or, more simply, 1,1'-bi-2-naphthol enantiomers. The purified bi-naphthol enantiomers are used as chiral building blocks in asymmetric synthesis and as catalysts in some chemical reactions (*Separex*, 1994b).

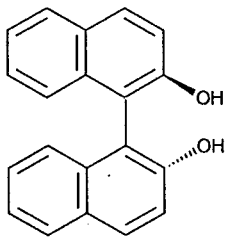


Figure 5.3. Bi-naphthol enantiomers.

The separation of bi-naphthol enantiomers can be performed using a Pirkle type stationary phase, the 3,5-dinitrobenzoyl phenylglycine covalently bonded to silica gel (3,5-DNBPG-Silica). The chiral stationary phase used in this work was provided by the *Separex* group and was synthesized at the *Merck* laboratories (*Merck, Darmstadt, Germany*). Eight *Superformance* columns (26 mm internal diameter, 105 mm length) were packed with this material with a particle diameter of 25-40 μm.

The eluent choice for this system is simple since these types of chiral stationary phases are usually used in heptane/isopropanol mixtures. However, the composition of the eluent mixture strongly affects the adsorption isotherms of the bi-naphthol enantiomers on the 3,5-DNBPG-Silica chiral stationary phase. For example, for an eluent mixture of 90/10 (v/v) of heptane/isopropanol, the slope of the adsorption equilibrium isotherm in the linear region for the less retained enantiomer (at 25 C) is $K_A = 8.39$; for a 75/25 (v/v) eluent mixture, this value is $K_A = 3.00$ (*Separex*, 1994b). *Table 5.2* describes the bi-naphthol system.

Table 5.2. The bi-naphthol system.

Bi-naphthol enantiomers:
$C_{20}H_{14}O_2$

| | |
|---|---|
| Molecular weight: | 286.33 g/mol |
| Melting point: | 215 °C |
| Solubility limit: | 7 - 8 g/l (racemic) (*Separex*, 1995) |
| (in 72/28 v/v heptane/isopropanol solvent) | |

Solvent:

72/28 (v/v) heptane/isopropanol

Heptane:
$C_7H_{16}$

| | |
|---|---|
| Molecular weight: | 100.21 g/mol |
| Melting point: | - 91 °C |
| Boiling point: | 98 °C |
| Viscosity at 25 °C: | 0.386 cP |

Isopropanol:
$C_3H_8O$

| | |
|---|---|
| Molecular weight: | 60.10 g/mol |
| Melting point: | - 89.5 °C |
| Boiling point: | 82.4 °C |
| Viscosity at 25 °C: | 1.988 cP |

*Figure 5.4* shows *SEM* microphotographs (*Scanning Electron Microscope*) of the silica particles. They have a regular pattern, although they are not perfectly spherical.

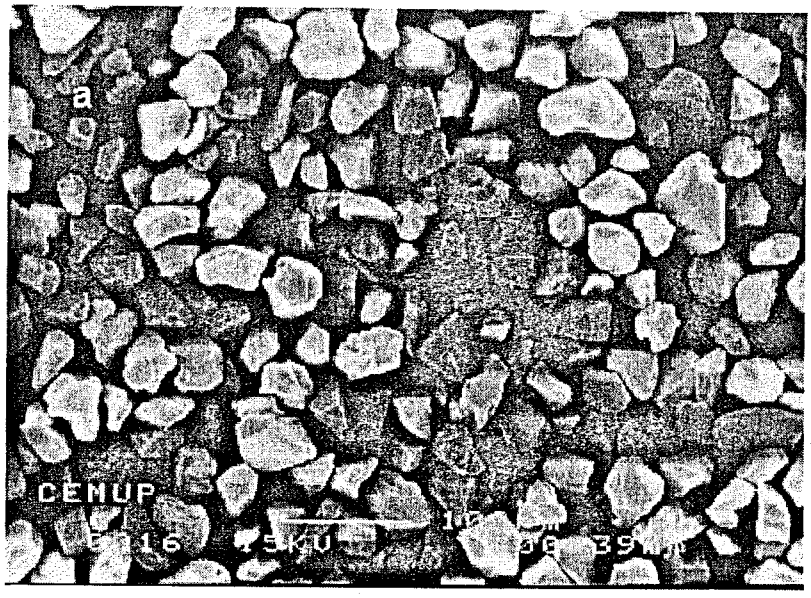
a
CEMUP

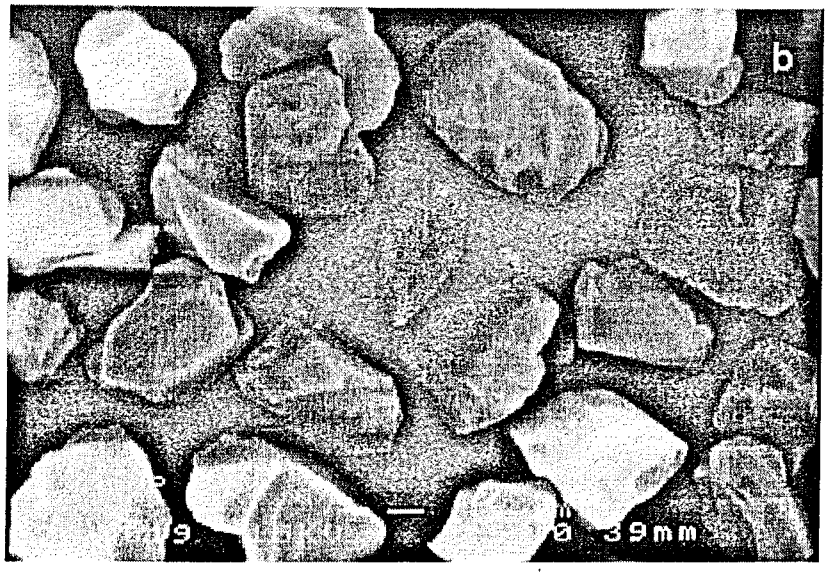
b
39mm

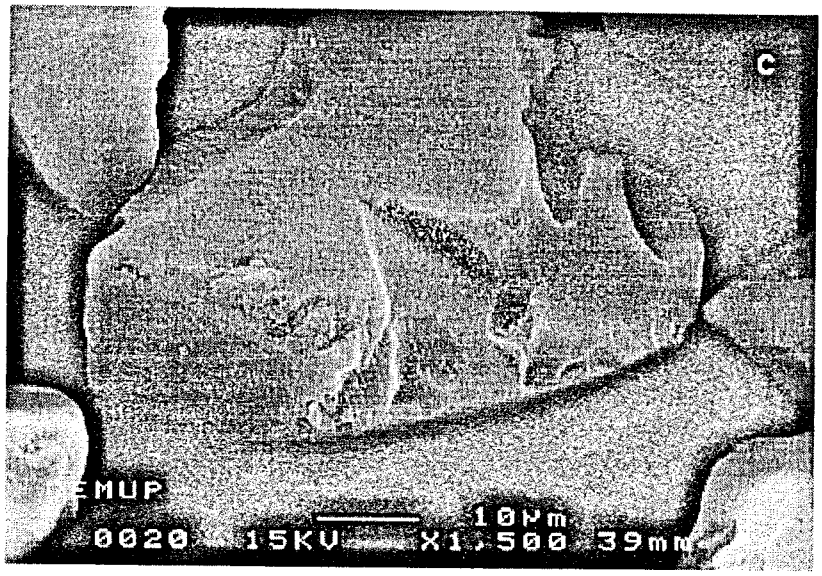


Figure 5.4. SEM microphotographs of the silica gel support:
(a) Under 200 X magnification, Scale 100 μm;
(b) Under 500 X magnification, Scale 10 μm;
(c) Under 1,500 X magnification, Scale 10 μm.

The composition of the mobile phase used in this work was 72/28 (v/v) of heptane/isopropanol. The adsorption equilibrium isotherms were determined by the *Separex* group. Frontal chromatography experiments were performed at 25 C in one of the SMB columns provided. The isotherms found, assuming $\varepsilon = 0.4$, were the ones presented in the previous chapters:

$$q_A^* = \frac{2.69 c_A}{1 + 0.0336 c_A + 0.0466 c_B} + \frac{0.10 c_A}{1 + c_A + 3 c_B} \tag{5.2a}$$

$$q_B^* = \frac{3.73 c_B}{1 + 0.0336 c_A + 0.0466 c_B} + \frac{0.30 c_B}{1 + c_A + 3 c_B} \tag{5.2b}$$

In the above equations, $q_i^*$ is the adsorbed phase concentration in equilibrium with the fluid phase concentration. In fact, $q_i^*$ includes both the adsorbed phase concentration and the concentration in the fluid inside pores. This overall retained concentration $q_i^*$ is used to be consistent with the models presented for the SMB simulations based on homogeneous particles.

The second term of the adsorption isotherms, with a very low saturation capacity, is supposed to explain the tailing which is seen on chromatograms even when injecting rather small amounts of enantiomers (*Separex*, 1995). *Figure 5.5* presents the adsorption isotherms for the bi-naphthol enantiomers considering racemic mixtures (*Figure 5.5a*) and pure enantiomers (*Figures 5.5b* and *5.5c*). *Figure 5.6* shows the influence of the enantiomers concentration on the selectivity factor.

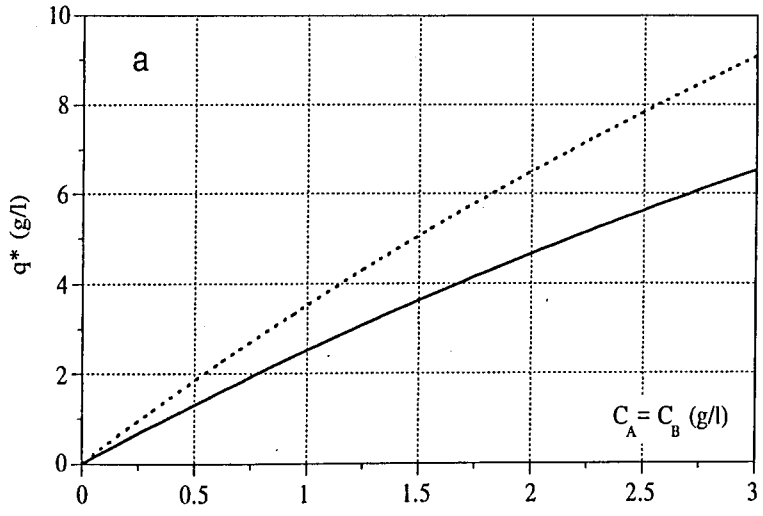

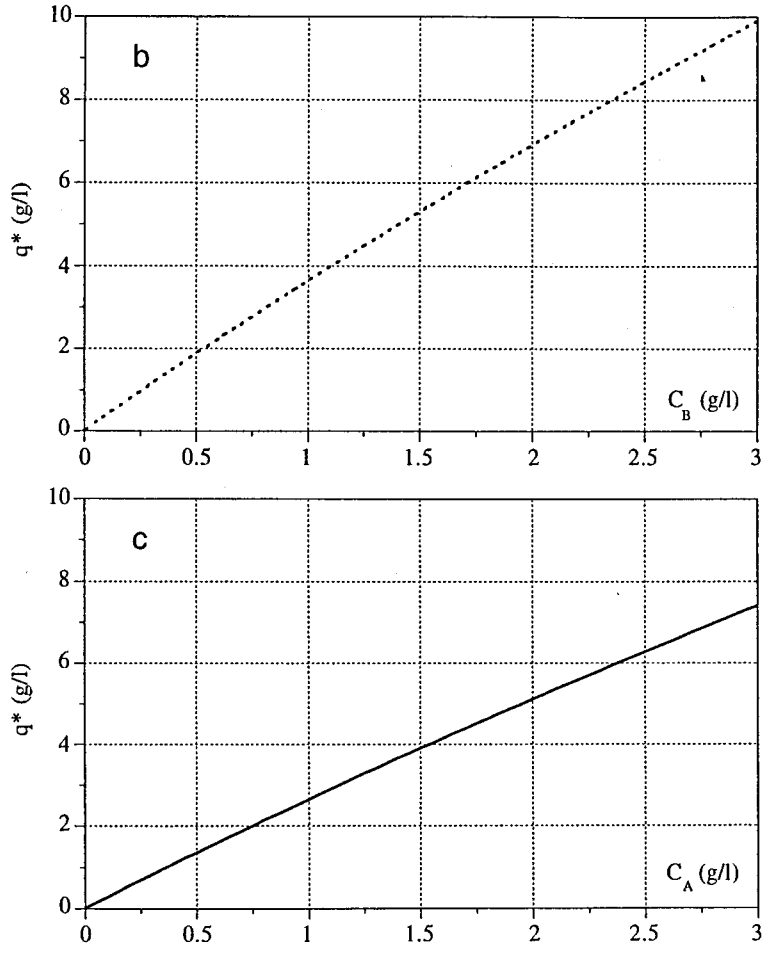


Figure 5.5. Adsorption isotherms for the bi-naphthol enantiomers:
(a) racemic mixtures; (b) pure B; (c) pure A.
Full and dashed lines for the less and more retained component, respectively.

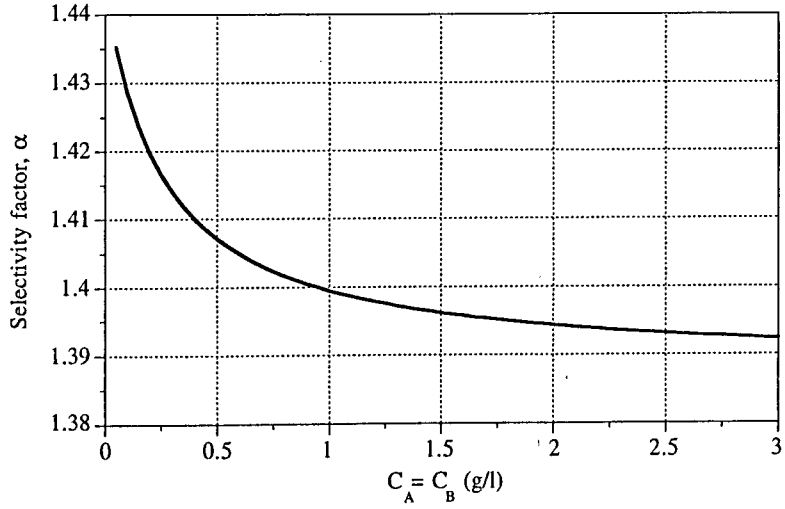


Figure 5.6. Influence of the enantiomers concentration
on the selectivity factor (racemic mixtures).

## 5.2.2 Experimental Results

The operating conditions used as first attempt for the SMB separation of the bi-naphthol enantiomers were also proposed by the *Separex* group and are presented in *Table 5.3*. The feed composition used was $C_A = C_B = 2.9$ g/l, which is close to the solubility limit in this solvent. The value for the switch time interval was chosen experimentally in order to obtain high purities.

The internal concentration profiles were measured using the 6-port valve of the *Licosep* SMB pilot to withdraw samples from the system (see *Appendix C*). The samples were collected at each half-time period and after 40 full cycles of continuous operation. The experimental performance parameters were determined by analysis of the extract and raffinate samples collected during the whole cycle 40 (cyclic steady-state).

Table 5.3. Experimental conditions for the separation of the bi-naphthol enantiomers on the SMB pilot unit.

| | | | |
|---|---|---|---|
| Columns: | | Flow-rates (ml/min): | |
| Diameter (cm) | 2.6 | Recycling | 35.38 |
| Length (cm) | 10.5 | Eluent | 21.45 |
| Number of columns | 8 | Extract | 17.98 |
| Configuration | 2-2-2-2 | Feed | 3.64 |
| | | Raffinate | 7.11 |
| Temperature (C) | 25 | Pressure drop (bar) | 20 (at 40 ml/min) |

The samples collected were analyzed in a HPLC system (*Gilson, Villiers le Bel, France*) using a 250 mm (length) x 4 mm (diameter) column filled with 5 μm poly-N-acryloyl-(S)-phenylalanine diethylamide as stationary phase. The eluent was the same mixture of heptane/isopropanol and the outlet concentration was followed by UV detection at 254 nm.

For the conditions presented before in *Table 5.3*, the better purity performance was obtained for a switch time interval of $t^* = 2.87$ min. For this value, purities as high as 94.5% in the extract and 98.9% in the raffinate were obtained with good recoveries.

The steady-state TMB model presented in Chapter 4 was used to simulate the

SMB operation by predicting its performance and its internal concentration profiles. *Table 5.4* summarizes the operating conditions and model parameters used with the simulation package. *Table 5.5* compares the experimental and the predicted SMB performance.

Table 5.4. SMB and equivalent TMB operating conditions and model parameters used with the simulation package (steady-state TMB model).

| SMB operating conditions | Equivalent TMB operating conditions | Model parameters |
|---|---|---|
| Columns:<br>Diameter: 2.6 cm<br>Length: 10.5 cm<br>Number of columns: 8<br>Configuration: 2-2-2-2 | Sections:<br>Diameter: 2.6 cm<br>Length: 21 cm<br>Number of sections: 4 | Solid/fluid volumes:<br>$(1-\varepsilon)/\varepsilon = 1.5$<br><br>Peclet number:<br>$Pe = 2000$ |
| Flow-rates (ml/min):<br>Eluent: 21.45<br>Extract: 17.98<br>Feed: 3.64<br>Raffinate: 7.11<br>Section I: 56.83<br>Section II: 38.85<br>Section III: 42.49<br>Section IV: 35.38 | Flow-rates (ml/min):<br>Eluent: 21.45<br>Extract: 17.98<br>Feed: 3.64<br>Raffinate: 7.11<br>Section I: 49.06<br>Section II: 31.08<br>Section III: 34.72<br>Section IV: 27.61 | Number of mass transfer units:<br>$\alpha = 34.44$<br>$(k = 0.1\ s^{-1})$<br><br>Ratio between fluid and solid velocities (TMB):<br>$\gamma_I = 6.31$<br>$\gamma_{II} = 4.00$<br>$\gamma_{III} = 4.47$<br>$\gamma_{IV} = 3.55$ |
| Switch time interval:<br>2.87 min | Solid flow-rate:<br>11.65 ml/min | |

Table 5.5. Comparison between the experimental and predicted performance parameters (Operating conditions as in *Table 5.4*).

| Performance Parameter | Extract Purity PUX (%) | Raffinate Purity PUR (%) | Extract Recovery RCX (%) | Raffinate Recovery RCR (%) |
|---|---|---|---|---|
| Experimental | 94.5 | 98.9 | 99.1 | 94.1 |
| Predicted | 95.2 | 99.1 | 99.2 | 95.0 |

*Figure 5.7* compares the experimental and simulated internal concentration profiles. Although there are some discrepancies, specially for the concentration of the more retained component in the second section, the agreement between model and experimental results is reasonable.

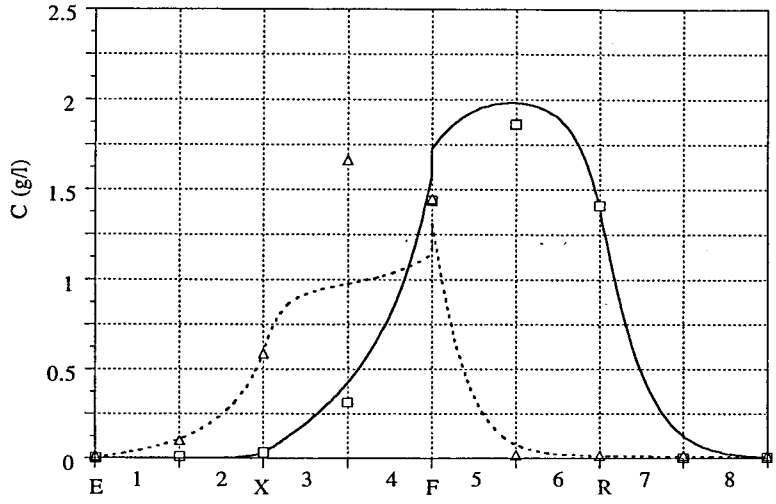


Figure 5.7. Internal concentration profiles: comparison between experimental (points) and simulated (lines) results. Solid line and squares for the less retained component, dashed line and triangles for the more retained component. Operating conditions and model parameters as in *Table 5.4*.

The second step of our SMB experiments was to diminish the extract flow-rate (and increase the raffinate flow-rate) in order to get a better extract purity, approaching the value obtained for the raffinate stream. This decision was taken looking for the simulation studies carried out in the previous chapter (see *Figure 4.6*). In fact, a high extract flow-rate can lead to a very low liquid flow-rate in section II and the less retained component can eventually move downwards, contaminating the extract stream. In this way, we decided to reduce the extract flow-rate (followed by the increase of the raffinate flow-rate in the same amount) keeping constant all the other operating conditions presented in *Table 5.4*. The new flow-rates are $Q_X = 16.00$ ml/min and $Q_R = 9.09$ ml/min.

The experimental purities obtained were 95.0% for the extract and 92.8 for the raffinate stream. Comparing these results to the ones obtained in the first run, we conclude that the extract purity is a little higher (95.0% instead of 94.5%) but the raffinate purity decreased significantly (from 98.9% to 92.8%).

Analyzing these results we conclude that the decrease of the extract flow-rate was too strong. Its decrease led to an increase of the liquid flow-rate in section III with the consequent contamination of the raffinate stream by the more retained species. However, the increment of the extract purity in this second run was not very significant. For this reason, we decided to improve the purity performance by adjusting the switch time interval and using the same conditions of the last run ($Q_X = 16.00$ ml/min, $Q_R = 9.09$ ml/min). The results obtained are presented in *Table 5.6*.

Table 5.6. Ratio between fluid and solid interstitial velocities (TMB) and experimental performances obtained in the SMB runs. ($Q_X = 16.00$ ml/min, $Q_R = 9.09$ ml/min).

| Switch Time Interval $t^*$ (min) | $\gamma_I$ | $\gamma_{II}$ | $\gamma_{III}$ | $\gamma_{IV}$ |
|---|---|---|---|---|
| 2.55 | 5.499 | 3.669 | 4.085 | 3.046 |
| 2.75 | 6.008 | 4.035 | 4.484 | 3.363 |
| 2.80 | 6.136 | 4.127 | 4.584 | 3.442 |
| 2.87 | 6.314 | 4.255 | 4.724 | 3.554 |
| 3.05 | 6.773 | 4.585 | 5.082 | 3.839 |

| Switch Time Interval $t^*$ (min) | Extract Purity PUX (%) | Raffinate Purity PUR (%) | Extract Recovery RCX (%) | Raffinate Recovery RCR (%) |
|---|---|---|---|---|
| 2.55 | 74.0 | 93.8 | 96.0 | 66.6 |
| 2.75 | 93.0 | 96.2 | 97.3 | 91.6 |
| 2.80 | 95.6 | 95.4 | 95.0 | 96.1 |
| 2.87 | 95.0 | 92.8 | 91.8 | 95.8 |
| 3.05 | 91.5 | 70.9 | 61.5 | 94.7 |

The better performance was obtained for a switch time interval between 2.75 and 2.80 min. The internal concentration profiles were evaluated for the run using $t^* = 2.75$ min. The results obtained as well as the corresponding model predictions are presented in *Figure 5.8*. Table 5.7 compares the experimental and the predicted SMB performance.

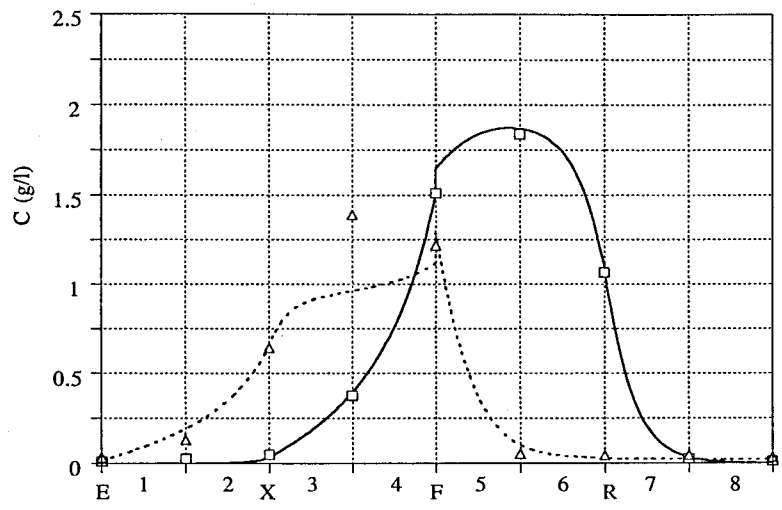


Figure 5.8. Internal concentration profiles: comparison between experimental (points) and simulated (lines) results. Solid line and squares for the less retained component, dashed line and triangles for the more retained component. ($Q_X = 16.00$ ml/min, $Q_R = 9.09$ ml/min, $t^* = 2.75$ min).

Table 5.7. Comparison between the experimental and predicted performance parameters ($Q_X = 16.00$ ml/min, $Q_R = 9.09$ ml/min, $t^* = 2.75$ min).

| Performance Parameter | Extract Purity PUX (%) | Raffinate Purity PUR (%) | Extract Recovery RCX (%) | Raffinate Recovery RCR (%) |
|---|---|---|---|---|
| Experimental | 93.0 | 96.2 | 97.3 | 91.6 |
| Predicted | 95.5 | 97.6 | 97.6 | 95.4 |

The agreement between model and experimental results is reasonable, in spite of the discrepancies in the concentration of the more retained component in the second section.

*Figures 5.9* and *5.10* show the experimental purities and recoveries obtained in the five runs carried out with different values for the switch time interval and using an extract flow-rate of $Q_X = 16.00$ ml/min ($Q_R = 9.09$ ml/min). Also shown are the model predictions for three values of the mass transfer coefficient: $k = 0.5$, $k = 0.1$ and $k = 0.05$ $s^{-1}$. Looking for these figures, we conclude that the TMB model can predict the influence of the switch time interval on the SMB performance. A reasonable agreement between model and experimental results is obtained for $k = 0.1$ $s^{-1}$.

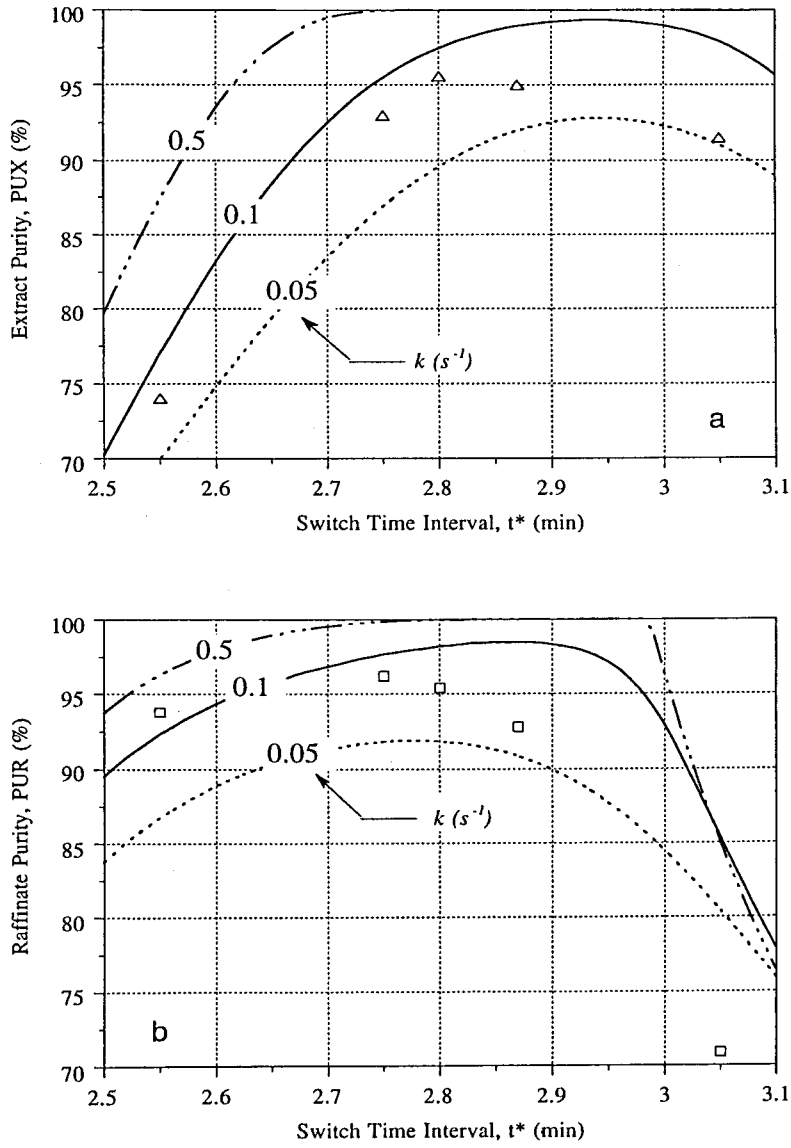


Figure 5.9. Purity performances. Comparison between experimental (points) and simulated (lines) results: (a) Extract purity; (b) Raffinate purity. ($Q_X = 16.00$ ml/min, $Q_R = 9.09$ ml/min).

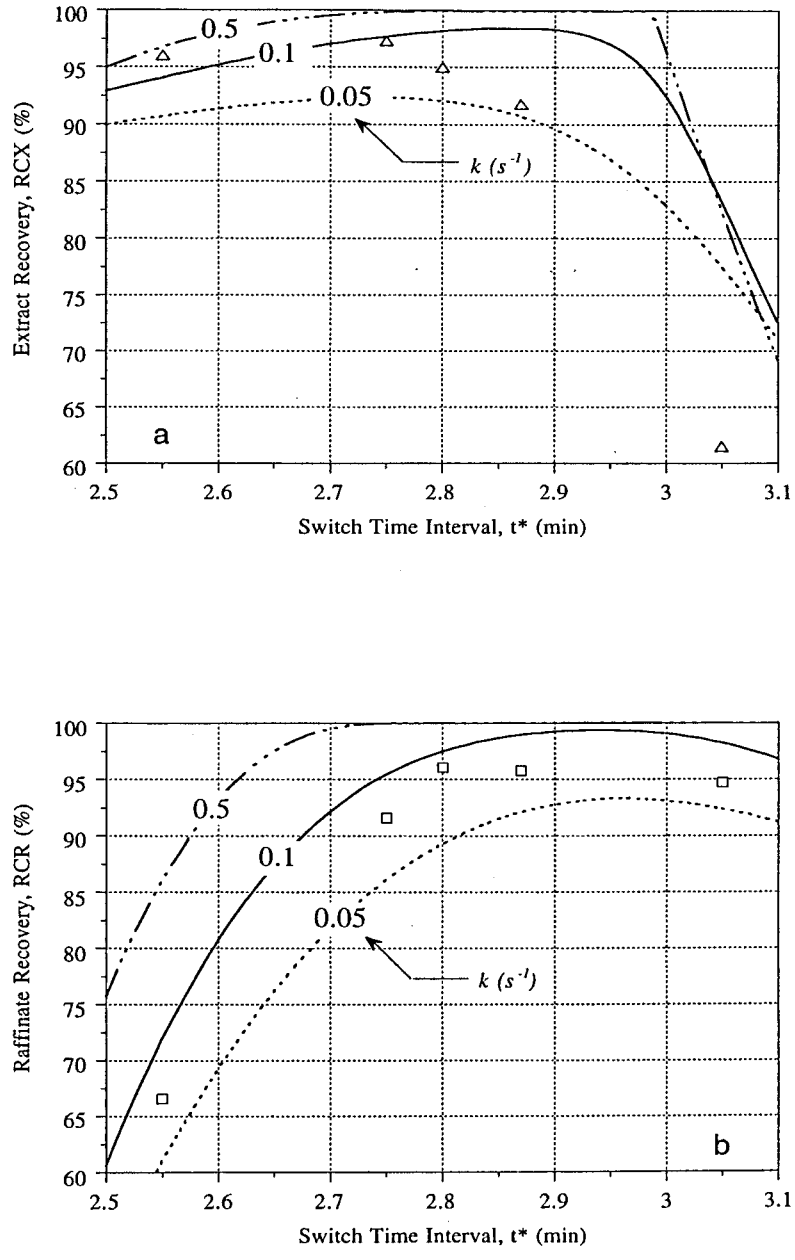


Figure 5.10. Recovery performances. Comparison between experimental (points) and simulated (lines) results: (a) Extract recovery; (b) Raffinate recovery. ($Q_X = 16.00$ ml/min, $Q_R = 9.09$ ml/min).

We can also estimate a value for the mass transfer coefficient. Establishing the equivalence between the model used in this work, the linear driving force (LDF) model for homogeneous particles, and the LDF model considering porous particles, we get

$$k = \frac{k_{pe}}{\varepsilon_p + K_p} = \frac{k_{pe}}{K} \tag{5.3}$$

where $k$ is the mass transfer coefficient used in the LDF model for homogeneous particles, $k_{pe}$ is the mass transfer coefficient used in the LDF model for porous particles, $\varepsilon_p$ is the particle porosity, $K_p$ is the initial slope of the isotherm considering only the adsorbent solid (excluding pores), and $K$ is the initial slope of the isotherm considering the adsorbent as homogeneous particles (the one used in this work).

The value for $k_{pe}$ is usually evaluated by

$$k_{pe} = \frac{\psi D_{pe}}{R_p^2} \tag{5.4}$$

being $\psi$ a coefficient between 10 and 15, $D_{pe}$ the effective diffusivity, and $R_p$ the particle radius. The effective diffusivity is evaluated through

$$D_{pe} = \frac{\varepsilon_p D_m}{\tau} \tag{5.5}$$

where $D_m$ is the molecular diffusivity, and $\tau$ is the tortuosity factor. Tortuosity is essentially a geometric factor with values between 2 and 8. At ordinary temperatures liquid phase diffusivities generally fall within the range $10^{-4}$ - $10^{-6}$ $cm^2 s^{-1}$ (Ruthven, 1984). As it was stated by Ruthven, methods of correlation and prediction of diffusion in liquid-filled pores are less accurate than for gaseous systems, since the fundamental theory of diffusion in the liquid phase is less well developed than the theory of molecular diffusion in the vapor phase. Correlations based on the Stokes-Einstein and Nernst-Einstein equations must be treated with caution. Nevertheless, we will use the Wilke-Chang estimation method, which is, in essence, an empirical modification of the Stokes-Einstein relation (Reid *et al.*, 1987):

$$D_m = \frac{7.4\,10^{-8}(\phi M)^{1/2} T}{\eta V^{0.6}} \tag{5.6}$$

where $D_m$ is the molecular diffusivity ($cm^2s^{-1}$), $M$ is the molecular weight of the solvent ($g\ mol^{-1}$), $T$ is the temperature (K), $\eta$ is the solvent viscosity (cP), $V$ is the molar volume of the solute at its normal boiling temperature ($cm^3mol^{-1}$), $\phi$ is an association factor of the solvent (dimensionless). In the previous equation, the Le Bas additive volume table can be used to estimate the molar volume of the solute at its normal boiling temperature. Wilke and Chang recommend that $\phi$ be chosen as 2.6 if the solvent is water, 1.9 if it is methanol, 1.5 if it is ethanol, and 1.0 if it is unassociated (Reid *et al.*, 1987).

Considering *Equations 5.3* to *5.5*, the mass transfer coefficient used in the LDF model for homogeneous particles can be estimated by

$$k = \frac{\psi\, \varepsilon_p\, D_m}{K\, \tau\, R_p^2} \tag{5.7}$$

Applying to the case of the bi-naphthol enantiomers separation, using a 72/28 (v/v) mixture of n-heptane/isopropanol as eluent and a temperature of 25 C, we get from *Equation 5.6*, $D_m = 8.1 \times 10^{-6}$ $cm^2s^{-1}$. Considering $\varepsilon_p = 0.45$, $\psi = 10$, $\tau = 5$, $K_A = 2.79$ and $K_B = 4.03$ (from the equilibrium adsorption isotherms presented in *Equation 5.2*), and $R_p = 1.625 \times 10^{-3}$ cm (particle diameter, $d_p = 25 - 40$ μm), we get $k_A = 0.98$ and $k_B = 0.68$ $s^{-1}$.

If we take into account the same values proposed before but considering the lower value for the liquid phase diffusivity proposed by Ruthven ($10^{-6}$ $cm^2s^{-1}$) we get $k_A = 0.12$ and $k_B = 0.08$ $s^{-1}$. The value used in our SMB simulations that led to a reasonable agreement between model and experimental results was $k_A = k_B = 0.1$ $s^{-1}$, which is closer to the value obtained using the lower value for the liquid diffusivity proposed by Ruthven.

On the other hand, the value used for the mass transfer coefficient can be supported not only by the experimental results in terms of the purity performances, but also in terms of the experimental internal concentration profiles. *Figure 5.11* compares the experimental and simulated internal concentration profiles for different values of the mass transfer coefficient. Once more, the value that shows a better agreement between experimental and simulation predictions is $k = 0.1$ $s^{-1}$.

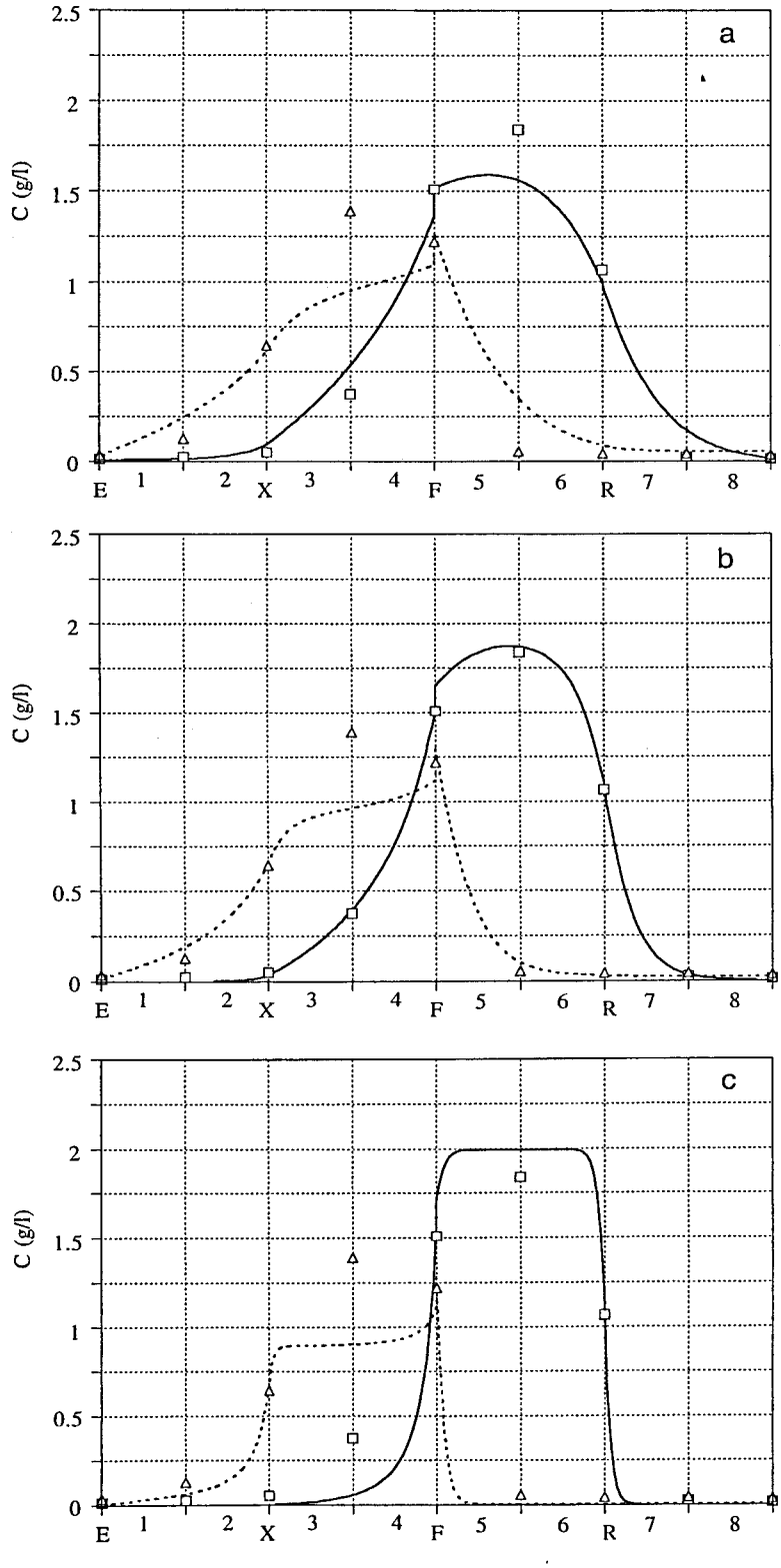


Figure 5.11. Internal concentration profiles: comparison between experimental (points) and simulated (lines) results: (a) $k = 0.05$; (b) $k = 0.1$; (c) $k = 0.5$ $s^{-1}$. Solid line and squares for the less retained component, dashed line and triangles for the more retained component. (Operating conditions as in *Figure 5.8*).

Other runs were carried out to study the effect of the configuration in the internal concentration profiles and in the SMB performance. The configurations tested were 2-2-2-2 (two columns per zone), 1-3-3-1 (three columns in the two central sections, one column in the adjacent sections), and 1-2-4-1 (four columns in section III, two columns in section II, and one column in sections I and IV). The experimental conditions were the same of the previous run ($Q_X = 16.00$ ml/min, $Q_R = 9.09$ ml/min, $t^* = 2.75$ min).

Although no specific optimization was made for each configuration, no significant differences were observed in the SMB performance among the three configurations studied. *Table 5.8* presents the results obtained as well as the predicted performances using the TMB model.

*Figure 5.12* shows the SMB experimental internal profiles for the three configurations, evaluated after the cyclic steady-state was achieved. Simulated results are also displayed using $k = 0.1$ $s^{-1}$. Once more, the agreement between model and experimental results is very reasonable except in what concerns the concentrations of the more retained species in section II.

Table 5.8. Experimental and (predicted) performances for the three configurations ($Q_X = 16.00$ ml/min, $Q_R = 9.09$ ml/min, $t^* = 2.75$ min).

| Configuration | Extract Purity PUX (%) | Raffinate Purity PUR (%) | Extract Recovery RCX (%) | Raffinate Recovery RCR (%) |
|---|---|---|---|---|
| 2-2-2-2 | 93.0 (95.5) | 96.2 (97.6) | 97.3 (97.6) | 91.6 (95.4) |
| 1-3-3-1 | 94.8 (97.0) | 95.0 (94.5) | 97.1 (95.0) | 96.8 (97.1) |
| 1-2-4-1 | 92.6 (94.6) | 95.2 (94.3) | 97.5 (94.9) | 94.5 (94.7) |

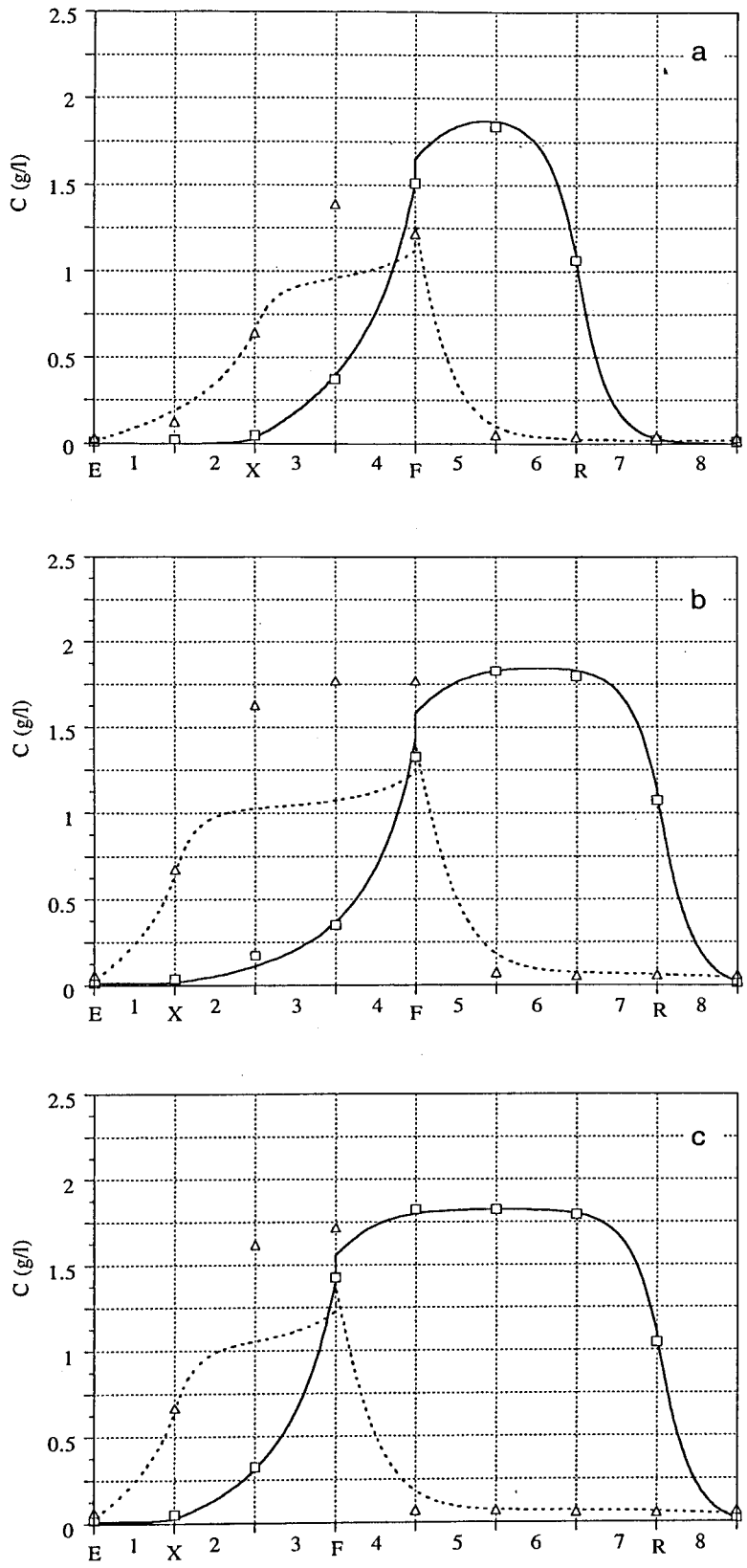


Figure 5.12. Comparison between experimental (points) and simulated (lines) internal profiles. Influence of the system configuration: (a) 2-2-2-2; (b) 1-3-3-1; (c) 1-2-4-1 ($Q_X = 16.00$ ml/min, $Q_R = 9.09$ ml/min, $t^* = 2.75$ min).

The experimental operation of the *Licosep* pilot unit was carried out for the separation of the bi-naphthol enantiomers. A global productivity of 68 grams of racemic mixture processed per day and per liter of bed was achieved. The corresponding solvent consumption, as it is defined in *Chapter 4* (*Table 4.2*), was 1.2 liter per gram of racemic mixture processed.

The better purities obtained under these conditions were 94.5% for the extract and 98.9% for the raffinate ($Q_X = 17.98$ ml/min, $Q_R = 7.11$ ml/min, $t^* = 2.87$ min). Adjusting the extract flow-rate we improved the extract purity up to 95.6%, but the raffinate purity decreased to 95.4% ($Q_X = 16.00$ ml/min, $Q_R = 9.09$ ml/min, $t^* = 2.80$ min). Keeping the same productivity and solvent consumption performance, i.e., maintaining the same eluent and feed flow-rates ($Q_E = 21.45$ ml/min, $Q_F = 3.64$ ml/min), no better purities were obtained by adjusting the other operating conditions.

To finish our experimental studies in the SMB pilot unit for the bi-naphthol system, we decided to evaluate the internal concentration profiles at different moments of a switch time interval. These internal profiles were evaluated after cyclic steady-state was achieved (after more than 25 full cycles of continuous operation). The operating conditions used were the same of those presented before in *Figure 5.8*.

Simulations with the same operating conditions were also carried out using the SMB model presented previously in this work (see *Section 3.2* of *Chapter 3*), in order to predict the dynamic behaviour of the SMB internal concentration profiles during each switch time interval.

*Table 5.9* presents the experimental and predicted purities and recoveries obtained. Two models are compared: the steady-state TMB model and the SMB model with 8-columns (2 per section). As we found in *Chapter 3* (see *Table 3.7*), the main difference between the two model predictions occurs for the extract purity. Moreover, the purities and recoveries performances predicted by the SMB model are lower than the ones predicted by the TMB package and closer to the experimental results.

*Figure 5.13* presents the internal concentration profiles at different moments of a switch time interval and after the cyclic steady-state was achieved: at 25, 50, and 75% of a switch time interval. The model predictions obtained with the SMB model are also presented. Although the discrepancies for the concentration of the more retained species in Section II remain, the SMB model predicts well the dynamic behaviour of the SMB internal concentration profiles during each switch time interval.

Nevertheless, if the objective is to simply evaluate the internal concentration profiles at half-time period (at 50% of the switch time interval), the steady-state TMB model can be safely used instead of the SMB model, with obvious time savings.

This can be concluded, looking for *Figure 5.14*, which presents the internal concentration profiles predicted by both models. It is clear that the internal concentration profiles predicted by the two models (SMB and steady-state TMB model) are very similar. The only exception concerns the concentration profiles near the feed point. This is due to the fact that the internal liquid flow-rates in the TMB operation are smaller than in the equivalent SMB operation. As a consequence, near the feed inlet, TMB concentrations will be higher than in the SMB operation, as it was already explained in *Chapter 3*.

Table 5.9. Comparison between the experimental and predicted performance parameters ($Q_X = 16.00$ ml/min, $Q_R = 9.09$ ml/min, $t^* = 2.75$ min).

| Performance Parameter | Extract Purity PUX (%) | Raffinate Purity PUR (%) | Extract Recovery RCX (%) | Raffinate Recovery RCR (%) |
|---|---|---|---|---|
| Experimental | 93.0 | 96.2 | 97.3 | 91.6 |
| Predicted SMB model | 93.8 | 96.8 | 95.9 | 92.8 |
| Predicted TMB model | 95.5 | 97.6 | 97.6 | 95.4 |

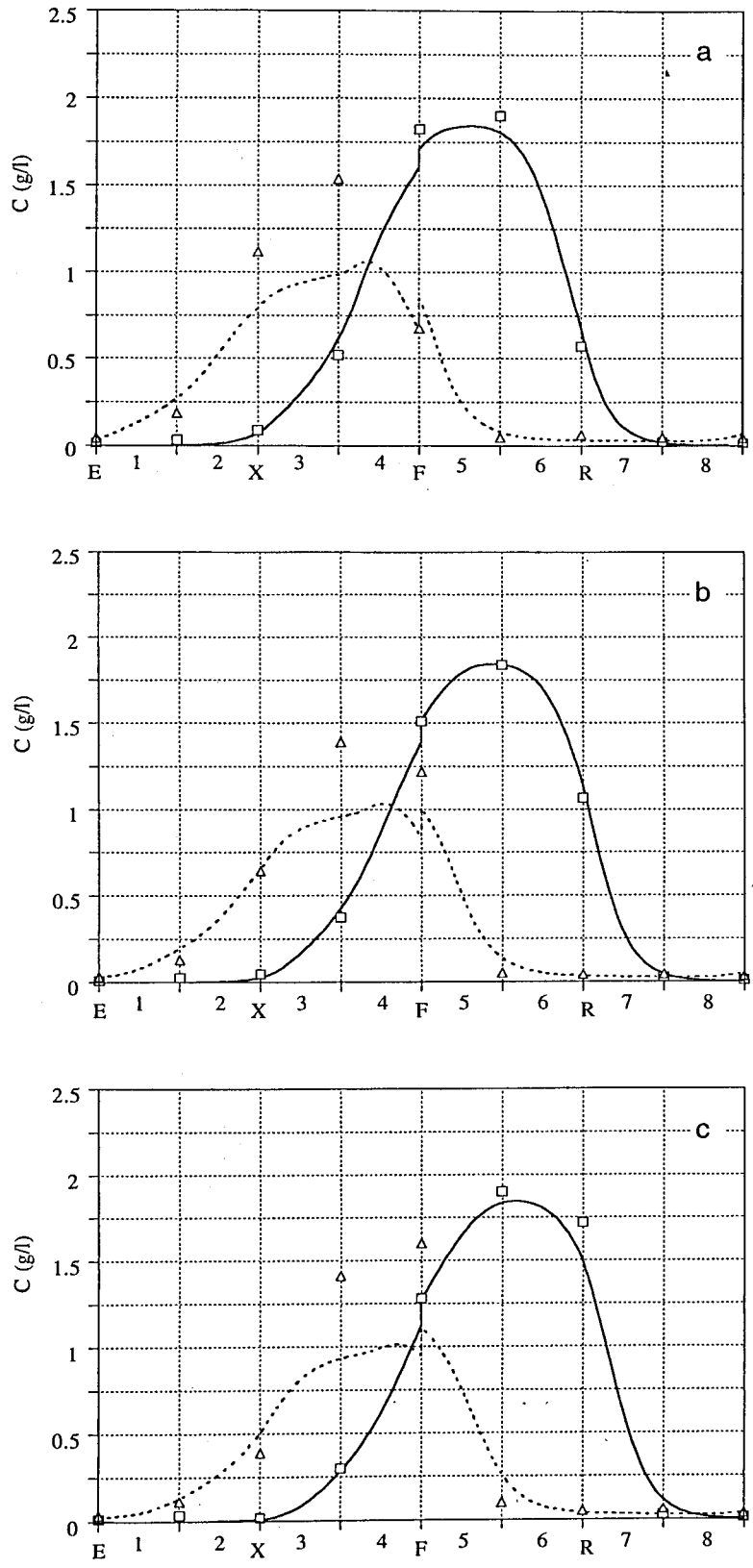


Figure 5.13. Experimental (points) vs simulated (lines) internal concentration profiles evaluated at (a) 25%, (b) 50%, (c) 75% of a switch time interval. ($Q_X = 16.00$ ml/min, $Q_R = 9.09$ ml/min, $t^* = 2.75$ min).

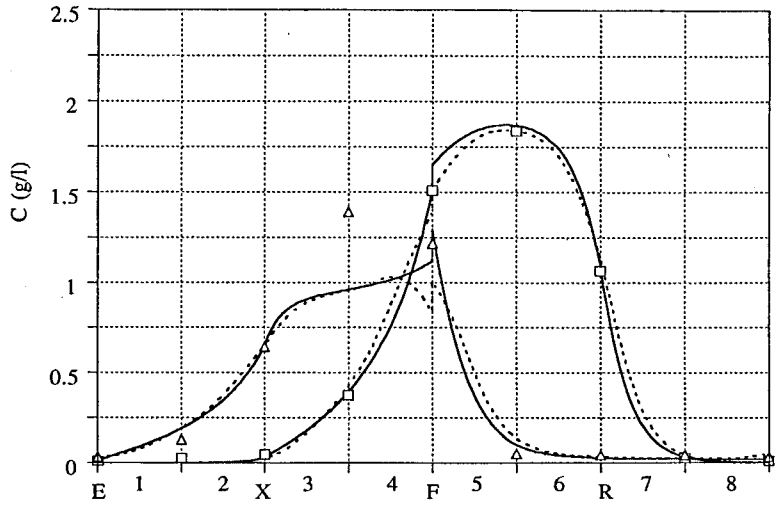


Figure 5.14. Internal concentration profiles at half-time period: comparison between the predictions obtained with the steady-state TMB model (full lines) and the SMB model (dashed lines). Points represent experimental concentrations: squares for the less retained species, triangles for the more retained species ($Q_X = 16.00$ ml/min, $Q_R = 9.09$ ml/min, $t^* = 2.75$ min).

### 5.2.3. Reasons for the Discrepancy Between the Experimental Results and Model Predictions

In the last section, experimental results and model predictions were compared in terms of process performance and internal concentration profiles. The agreement between them is reasonable although some discrepancies appear, namely in what concerns the internal concentration profile of the more retained species in Zone II. In this section we will analyze some factors that can influence the system behaviour in terms of the internal concentration profiles and purity performance.

As explained in *Appendix B*, the recycling pump and the flowmeter need to be calibrated with the eluent used. This calibration must be carried out at the SMB operating pressure. Moreover, the recycling pump flow-rate varies along the operation, depending of its position (Section) in the SMB system. For these reasons, it is possible that there are some deviations from the expected flow-rates.

*Figure 5.15* shows the influence of the recycling flow-rate (SMB recycling pump flow-rate in Section IV) on the internal concentration profiles. *Figure 5.15b* shows the predicted internal profiles obtained for the operating conditions and model parameters presented in *Table 5.4*. *Figures 5.15a* and *5.15c* show the predicted internal profiles when the recycling flow-rate is 5% lower (*Figure 5.15a*) and 5% higher (*Figure 5.15c*) than the one used in *Figure 5.15b*. These figures elucidate how a change of 5% in the recycling flow-rate can modify significantly the internal concentration profiles. *Table 5.10* presents the corresponding purity performances for the three cases mentioned.

Table 5.10. Influence of the recycling flow-rate on the purity performance.
(Operating conditions and model parameters as in *Table 5.4*).

| Recycling flow-rate $Q^*_{RF}$ (ml/min) | Extract Purity PUX (%) | Raffinate Purity PUR (%) |
|---|---|---|
| 33.61 (-5%) | 86.9 | 98.5 |
| 35.38 | 95.2 | 99.1 |
| 37.15 (+5%) | 96.7 | 99.2 |

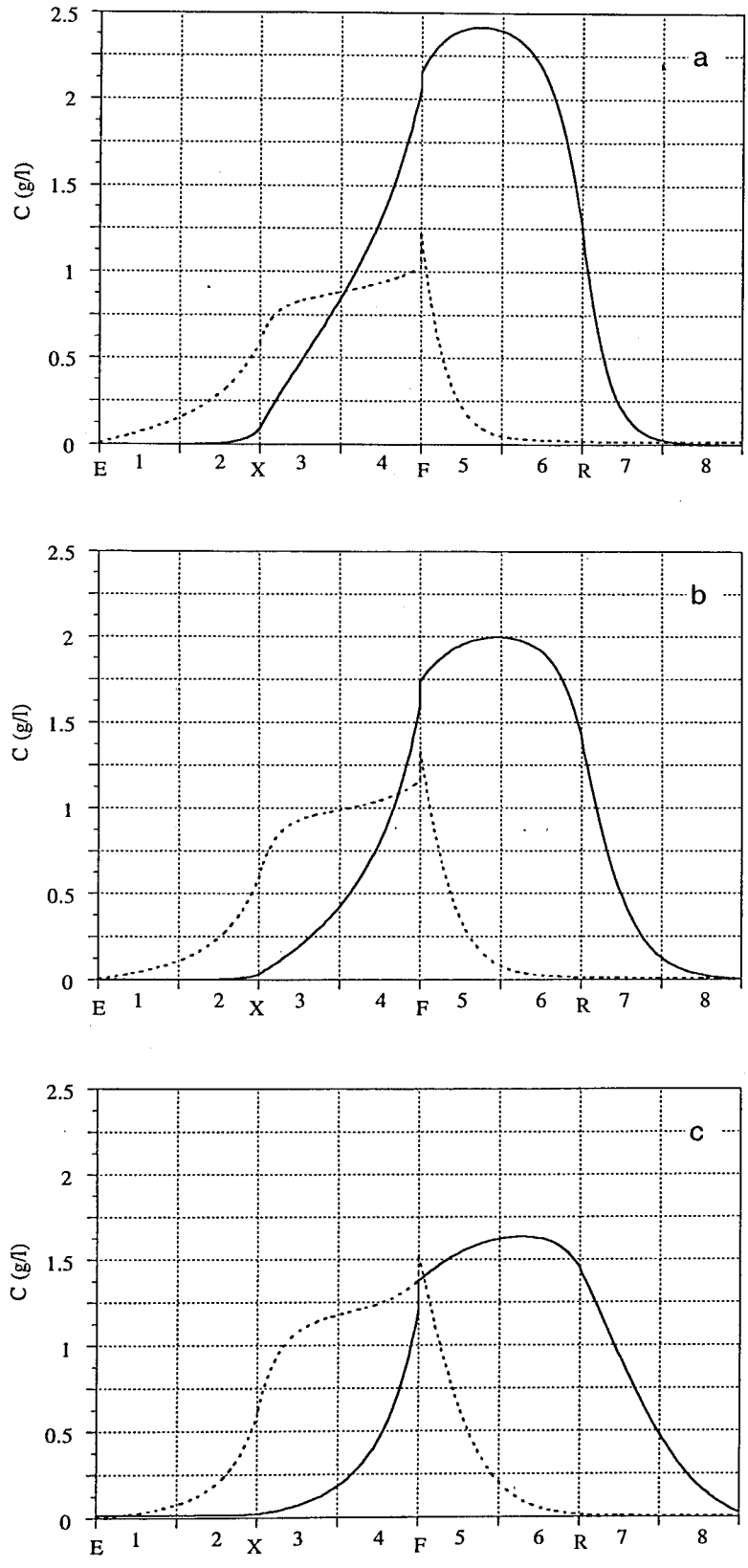


Figure 5.15. Influence of the recycling flow-rate on the internal concentration profiles: (a) $Q^*_{RF} = 33.61$ ml/min, (b) $Q^*_{RF} = 35.38$ ml/min, (c) $Q^*_{RF} = 37.15$ ml/min (solid and dashed lines for the less and more retained components, respectively).

In the operation of the SMB *Licosep* pilot unit, the eluent, feed and raffinate flow-rates are set by the user. However, the extract flow-rate is controlled around the initial value calculated by the *Licosep* software ($Q_X = Q_E + Q_F - Q_R$), according to the pressure measured at the recycling pump inlet. This pressure should be about 1.5 bar; if it is higher, the extract flow-rate is increased, otherwise it is decreased. Hence, it is admissible that the extract flow-rate also varies during the SMB operation.

*Figure 5.16* shows the influence of the extract flow-rate on the internal concentration profiles. *Figure 5.16b* corresponds to the operating conditions and model parameters presented in *Table 5.4*. *Figures 5.16a* and *5.16c* show the predicted internal profiles when the extract flow-rate is 5% lower (*Figure 5.16a*) and 5% higher (*Figure 5.16c*) than the one presented in *Table 5.4*. The raffinate flow-rate is $Q_R = Q_E + Q_F - Q_X$. Once again, a change of 5% in the extract flow-rate can modify significantly the internal concentration profiles. *Table 5.11* presents the purity performances for the three cases studied.

Table 5.11. Influence of the extract flow-rate on the purity performance.
(Operating conditions and model parameters as in *Table 5.4*).

| Extract flow-rate $Q_X$ (ml/min) | Raffinate flow-rate $Q_R$ (ml/min) | Extract Purity PUX (%) | Raffinate Purity PUR (%) |
|---|---|---|---|
| 17.08 (-5%) | 8.01 | 97.5 | 99.0 |
| 17.98 | 7.11 | 95.2 | 99.1 |
| 18.88 (+5%) | 6.21 | 91.5 | 99.3 |

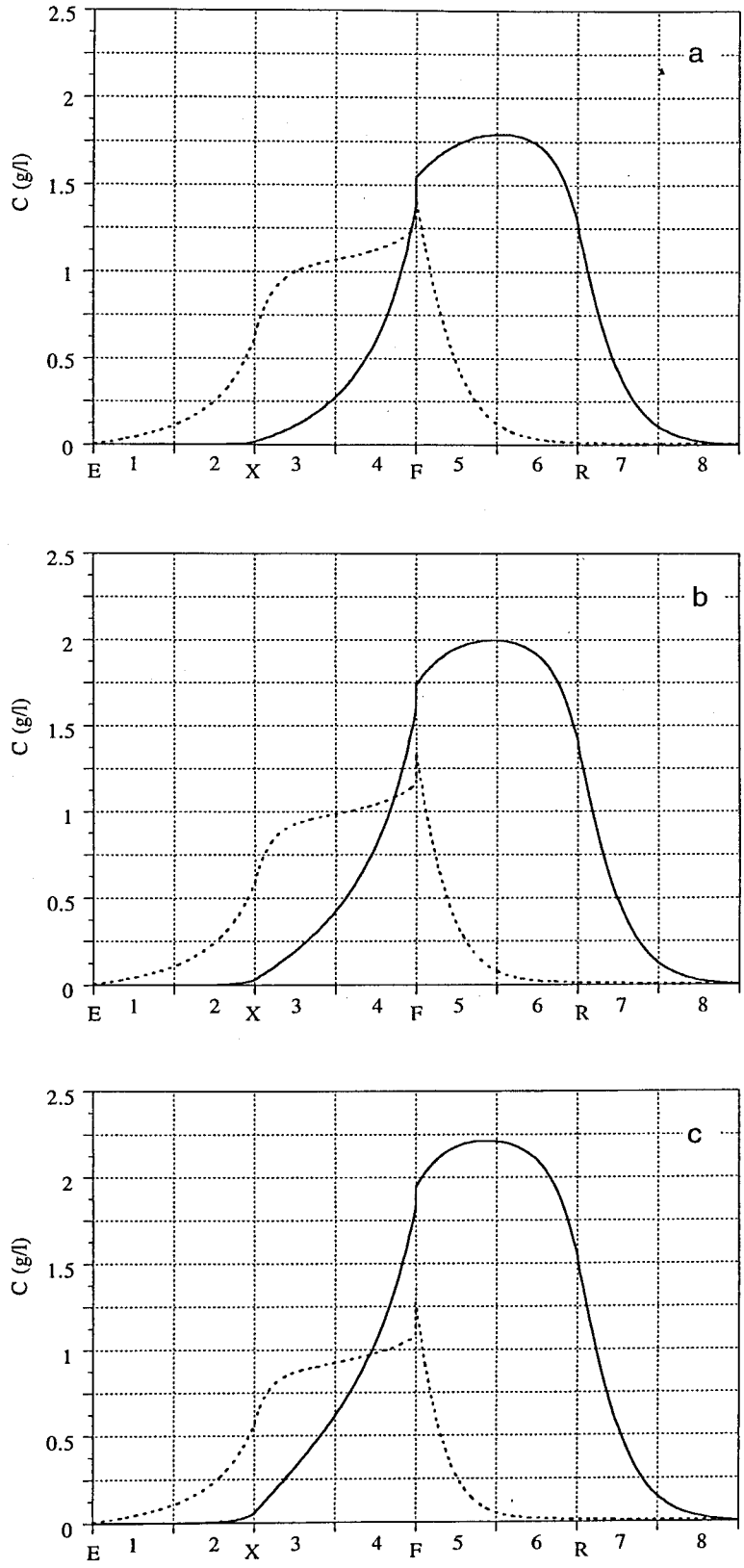


Figure 5.16. Influence of the extract flow-rate on the internal concentration profiles: (a) $Q_X = 17.08$ ml/min, (b) $Q_X = 17.98$ ml/min, (c) $Q_X = 18.88$ ml/min (solid and dashed lines for the less and more retained components, respectively).

The *Figures 5.15* and *5.16* presented before show how small variations in the flow-rates can modify significantly the internal concentration profiles as well as the purity performance of the SMB operation. However, under the operating conditions and model parameters used in our study, these variations influence particularly the internal profiles of the less retained species. None of them can explain the discrepancies between the experimental and predicted concentrations of the more retained component in Section II.

Next, we will consider that the two enantiomers can have different mass transfer coefficients. *Figure 5.17* shows its influence on the internal concentration profiles. *Figure 5.17b* corresponds to an experimental run carried out in the *Licosep* pilot unit (*Figure 5.8* and *Table 5.7*). Two other situations were considered: being the mass transfer coefficient for the less retained species higher than the one for the more retained enantiomer, *Figure 5.17a* presents the case where the mass transfer coefficient of the more retained species is half of the one used until now; in *Figure 5.17c* the mass transfer coefficient of the less retained component is double of the one used before. *Table 5.12* presents the corresponding purity performances. Looking for *Figure 5.17*, we conclude that the influence of the mass transfer coefficient under the operating conditions studied do not explain the discrepancies observed. Its variation influences mainly the internal profiles of the less retained species in Sections II and IV and the internal profiles of the more retained component in Sections I and III.

Table 5.12. Influence of the mass transfer coefficient on the purity performance. ($Q_X = 16.00$ ml/min, $Q_R = 9.09$ ml/min, $t^* = 2.75$ min).

| $k_A$ ($s^{-1}$) | $k_B$ ($s^{-1}$) | Extract Purity PUX (%) | Raffinate Purity PUR (%) |
|---|---|---|---|
| 0.1 | 0.05 | 95.1 | 92.2 |
| 0.1 | 0.1 | 95.5 | 97.6 |
| 0.2 | 0.1 | 99.0 | 97.7 |

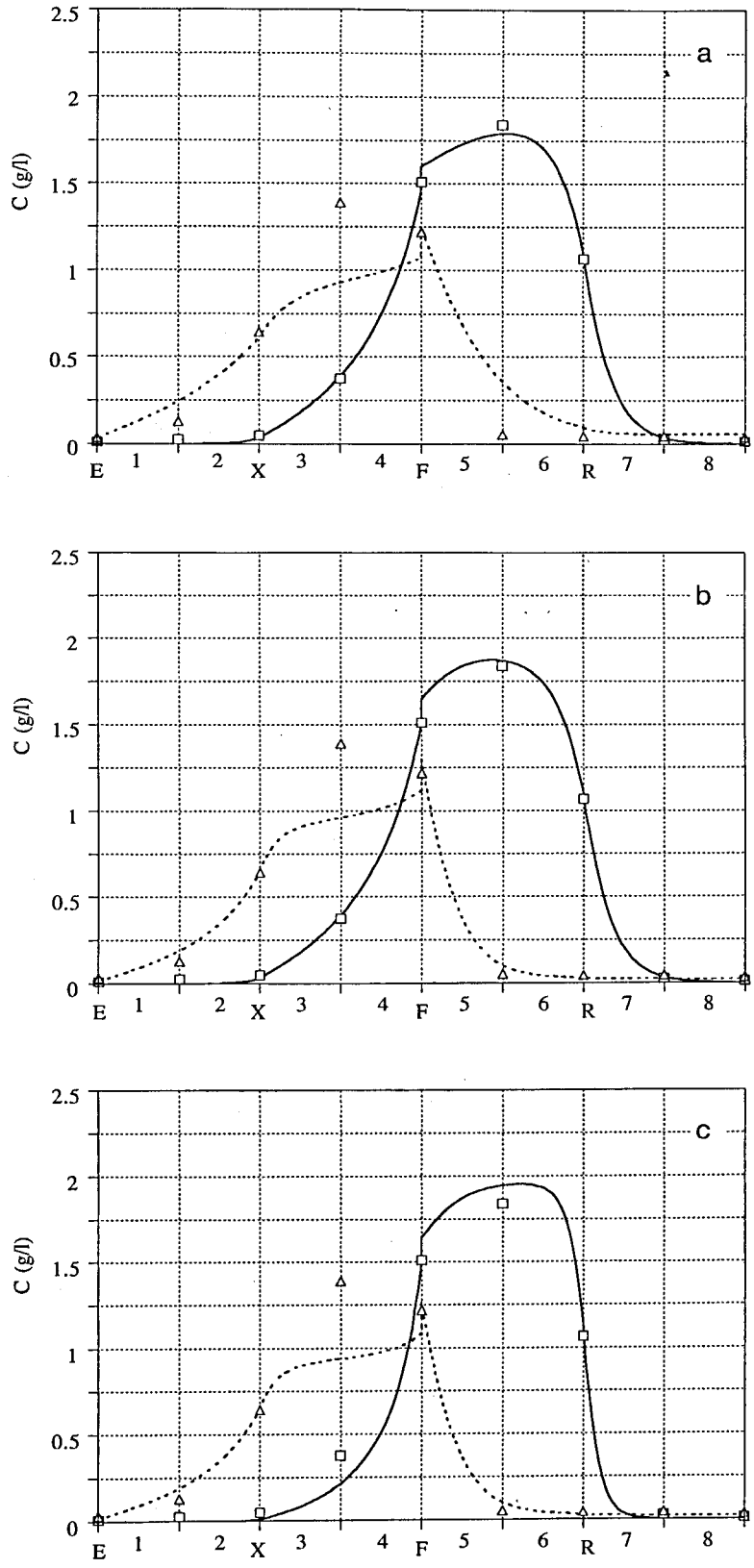


Figure 5.17. Influence of the mass transfer coefficient on the internal profiles: (a) $k_A = 0.1$, $k_B = 0.05$ s$^{-1}$; (b) $k_A = k_B = 0.1$ s$^{-1}$; (c) $k_A = 0.2$, $k_B = 0.1$ s$^{-1}$ ($Q_X = 16.00$ ml/min, $Q_R = 9.09$ ml/min, $t^* = 2.75$ min).

Probably, the discrepancies between the experimental and predicted internal concentration profiles for the more retained species in Section II are due to an inaccurate description of the binary adsorption equilibrium.

*Figure 5.18* presents the predicted internal concentration profiles, using an adsorption isotherm parameter for the more retained species of $b_B = 0.0932$ l/g, instead of $b_B = 0.0466$ l/g (two times higher). *Figure 5.19* compares the two adsorption isotherms considering racemic mixtures (*Figure 5.19a*) and a solution containing pure B, the more retained species (*Figure 5.19b*) (note that for pure A there are no differences between the two isotherms). Comparing *Figure 5.18* and *Figure 5.8*, we can see that the concentration of the more retained species in Section II approaches the experimental results. However, the concentration profiles for the less retained species in Section II and for the more retained species in Section III are not so well predicted. The knowledge of the adsorption isotherms is, certainly, the more important prerequisite to predict adequately the SMB operation.

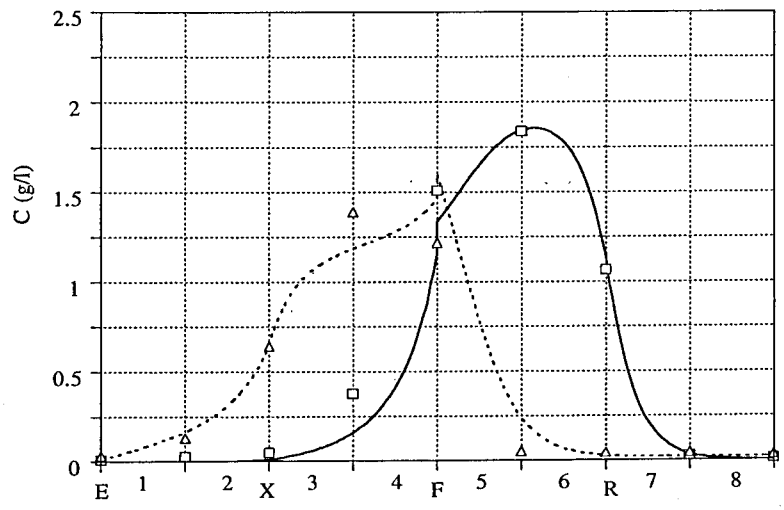


Figure 5.18. Internal concentration profiles obtained with the adsorption isotherm parameter $b_B = 0.0932$ l/g.
Other model parameters and operating conditions as in *Figure 5.8*.

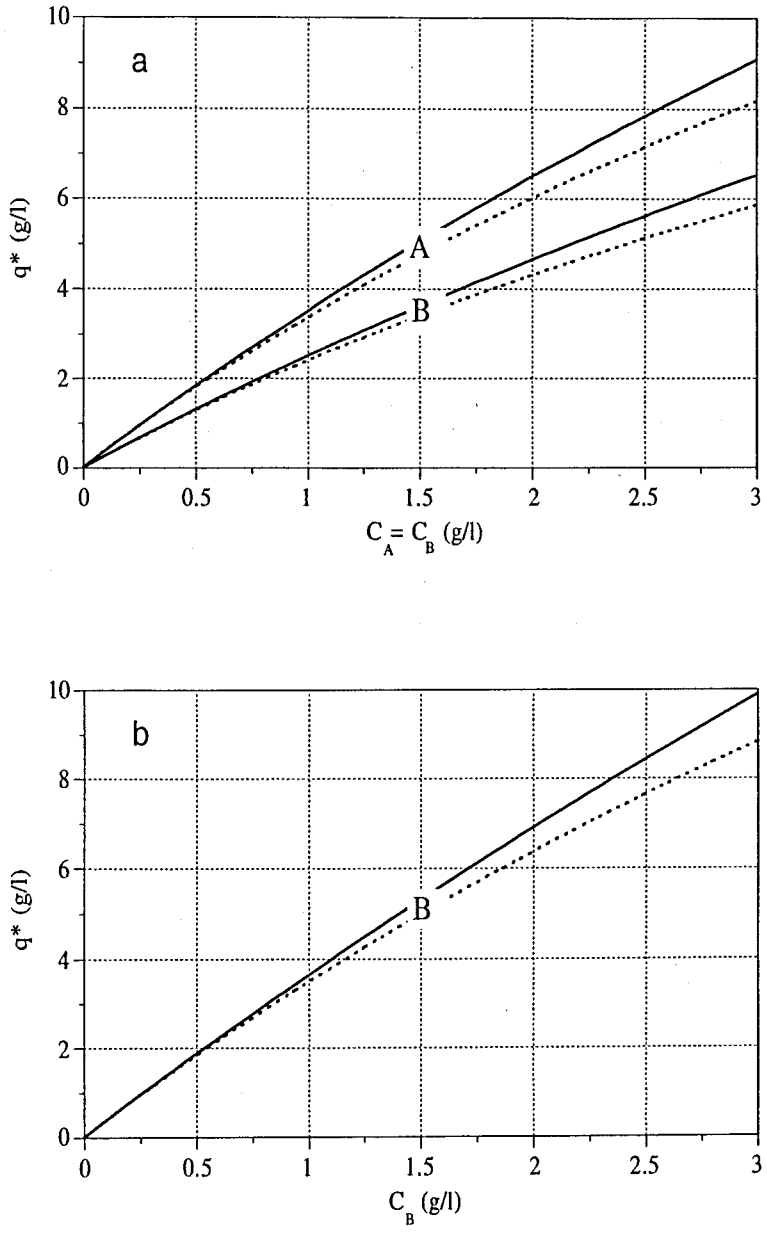


Figure 5.19. Comparison between the two adsorption isotherms: (a) racemic mixtures; (b) pure B, the more retained component. Full lines for the original adsorption isotherms, described in *Equation 5.2*; dashed lines for the modified adsorption isotherm, with $b_B = 0.0932$ l/g.

## 5.3 Separation of the Chiral Epoxide Enantiomers

### 5.3.1 The Chiral Epoxide System

The second system studied experimentally in our SMB pilot unit was the separation of the chiral epoxide enantiomers (*Figure 5.20*). These enantiomers are used as an intermediate in the enantioselective synthesis of optically active drugs where kilogram quantities of both enantiomers are required (Küsters *et al.*, 1995). Its complete name is 1a,2,7,7a-tetrahydro-3-methoxynaphth-(2,3b)-oxirane and was developed by *Sandoz Pharma* (*Basel, Switzerland*).

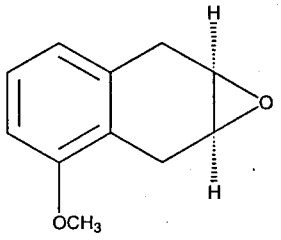


Figure 5.20. The chiral epoxide enantiomers.

The lack of a functional group which would enable a separation via formation of diastereoisomers, indicates that chromatography is the method of choice for this enantioseparation (Nicoud *et al.*, 1992). Particularly, the simulated moving bed technology as been used to carry out this chiral separation (Separex, 1992; Nicoud *et al.*, 1992, 1993a; Küsters *et al.*, 1995; Pais *et al.*, 1998b).

The separation of the chiral epoxide enantiomers can be performed using microcrystalline cellulose triacetate as stationary phase. The chiral stationary phase used in this work was gently provided by Dr. J. Kinkel (*Merck* and *Georg-Simon-Ohm Fachhochschule, Germany*). The eluent used was pure methanol. *Table 5.13* describes the chiral epoxide system.

Table 5.13. The chiral epoxide system.

Chiral epoxide enantiomers:
$C_{11}H_{12}O_2$

| | |
|---|---|
| Molecular weight: | 176.22 g/mol |
| Solubility limit: | at least 50 g/l (racemic) (Küsters *et al.*, 1995) |

Solvent:

Methanol, $CH_4O$

| | |
|---|---|
| Molecular weight: | 32.04 g/mol |
| Melting point: | - 98 °C |
| Boiling point: | 64.7 °C |
| Viscosity at 25 °C: | 0.55 cP |

## 5.3.2 The Cellulose Triacetate Stationary Phase

In 1973, Hesse and Hagel proposed for the first time the use of microcrystalline cellulose triacetate for the chromatographic separation of enantiomers. They reported the complete separation of 100 mg Tröger's base using 40 g microcrystalline cellulose triacetate and ethanol as eluent (Hesse and Hagel, 1973). The key of success was the heterogeneous acetylation of microcrystalline cellulose and subsequent swelling in boiling alcohol, so that the original structure of the polymer was preserved. This microcrystalline cellulose triacetate in its swollen state proves to be able to the chromatographic resolution of various chiral compounds (Koller *et al.*, 1983; Blaschke, 1986; Shibata *et al.*, 1986; Francotte and Junker-Buchheit, 1992).

Although the ability of microcrystalline cellulose triacetate to chiral resolution has been reported by several authors, the mechanism of the chiral recognition is still unclear. Hesse and Hagel (1976) proposed the concept of inclusion chromatography: the interaction with the chiral compounds occurs by inclusion into the asymmetric cavities of the polysaccharide network. The strength of the interaction will be determined by the fit of the chiral species to the chiral cavities of the swollen microcrystalline cellulose triacetate. On the contrary of common stationary phases, adsorption on microcrystalline cellulose triacetate seems to be more influenced by steric effects than it is by the chemical nature of the interaction between the chiral species and the stationary phase substituents. Hesse and Hagel highlighted the crucial contribution of the crystalline structure of the adsorbent. As it was mentioned by several authors, only the cellulose triacetate obtained from the heterogeneous acetylation of microcrystalline cellulose has chiral recognition properties. These properties are mostly lost if the cellulose triacetate is obtained by homogeneous acetylation because the dissolution will cause the loss of crystallinity of the adsorbent structure. The microcrystalline structure of this adsorbent will determine the geometric arrangement of the chiral environment (Hesse and Hagel, 1973, 1976; Francotte *et al.*, 1985; Isaksson *et al.*, 1990; Peterson and Lipkowitz, 1997).

The chiral recognition property is not necessarily confined to microcrystalline cellulose triacetate. Shibata *et al.* (1986) and Okamoto (1987) proposed the use of cellulose triacetate and other cellulose derivatives prepared under homogeneous conditions. This material is dissolved, reprecipitated and coated onto the surface of a silica support. The homogeneous acetylation causes the loss of the microcrystalline structure of the cellulose triacetate, leading to a material with a lower chiral recognition ability. Its chromatographic performance can, however, be enhanced, for example, by controlling the particle size. It should be pointed out that the chiral discrimination mechanism of coated cellulose triacetate is quite different from the one described for the microcrystalline form. Various applications of this alternative material can be found in literature (Shibata *et al.*, 1986; Ichida *et al.*, 1988; Oguni *et al.*, 1995).

In the last years several stationary phases have been developed for the preparative chromatographic separation of enantiomers. Since microcrystalline cellulose triacetate is a natural product and can be synthesized at low cost, it is a material of choice for preparative chromatographic applications (Dingenen, 1992). Some semi-preparative and preparative chiral separations on cellulose triacetate have been reported in literature (Rimböck *et al.*, 1985; Blaschke, 1986; Zief, 1988; Francotte and Junker-Buchheit, 1992; Francotte, 1993, 1996, 1997).

### 5.3.3 Packing Procedure of the SMB Columns

The microcrystalline cellulose triacetate used as stationary phase was swollen in boiling methanol, followed by a decanting procedure in order to remove the finest particles. The final material has an average particle diameter greater than 45 μm. *Figure 5.21* shows the *SEM* microphotographs (*Scanning Electron Microscope*) of the microcristalline cellulose triacetate particles. They have a wide range of dimensions, from 10 to more than 100 μm.

A packing procedure proposed by Nicoud (1993) was used to fill eight SMB columns. Each column was packed with the adsorbent material and the bed was compacted with methanol at a progressive flow rate up to 90 ml/min during one hour. After this step, the pressure at the column outlet was increased to 30 bar and a constant flow rate of 50 ml/min was imposed during 20 minutes. The adsorbent bed was compacted until the column reached approximately 10 cm length.

The eight columns were tested individually with a non-retained compound (1,3,5-tri-*tert.*-butylbenzene, *Sigma, St. Louis, USA*) (Koller, 1983), to compare retention times. *Table 5.14* shows test results with the non-retained compound. Retention times are very reproducible, showing deviations smaller than 2%.

Table 5.14. Test of the SMB columns with the non-retained compound (50 μg). Flow rate: 8 ml/min.

| Column | Length (cm) | Deviation (%) | Retention time (min) | Deviation (%) |
|---|---|---|---|---|
| 1 | 10.1 | 1.76 | 4.43 | 1.98 |
| 2 | 9.8 | -1.26 | 4.27 | -1.70 |
| 3 | 10.0 | 0.76 | 4.37 | 0.60 |
| 4 | 9.9 | -0.25 | 4.33 | -0.32 |
| 5 | 9.9 | -0.25 | 4.30 | -1.01 |
| 6 | 9.9 | -0.25 | 4.38 | 0.83 |
| 7 | 9.9 | -0.25 | 4.36 | 0.37 |
| 8 | 9.9 | -0.25 | 4.31 | -0.78 |
| Average: | 9.925 | | 4.34 | |

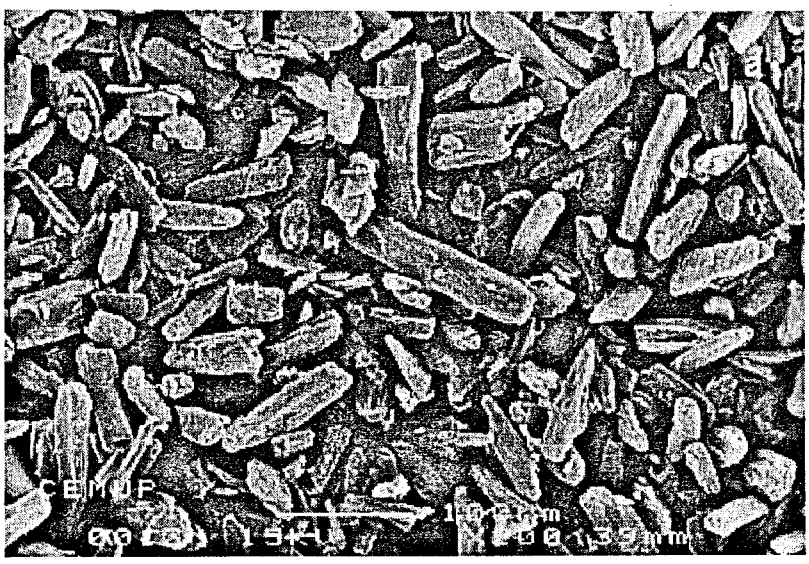

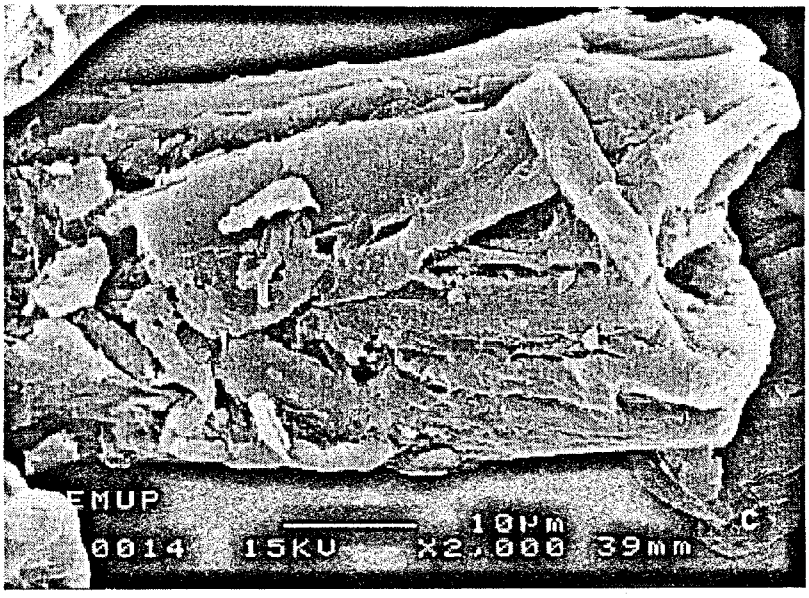


Figure 5.21. SEM microphotographs

of the microcrystalline cellulose triacetate:

(a) Under 200 X magnification, Scale 100 µm;

(b) Under 500 X magnification, Scale 10 µm;

(c) Under 2,000 X magnification, Scale 10 µm.

## 5.3.4 Hydrodynamic Study of a SMB Column

One SMB column prepared following the procedure described before was used to carry out a hydrodynamic study. The total porosity, $\varepsilon_T$, was evaluated by injecting a non-retained compound (1,3,5-tri-*tert.*-butylbenzene). A value of $\varepsilon_T = 0.67$ was found, in agreement with other published results for microcrystalline cellulose triacetate (see *Table 5.15*).

The influence of the linear velocity, $v$, upon plate height, $H$, was also examined by using the non-retained compound. The usual decreasing of $H$ upon decreasing $v$ can be found in *Figure 5.22* (see *Appendix A* for more detailed information). Unfortunately, pure enantiomers of the chiral epoxide were not available. Anyway, 90% pure enantiomers were injected and 1370 and 1550 μm plate heights were found for a flow rate of 22.8 ml/min (1.8 mm/sec) at 25 °C. Although these results could be affected by the presence of a small amount of the other enantiomer, they are qualitatively in agreement with previous work published by Koller *et al.* (1983) for the separation of various enantiomers in microcrystalline cellulose triacetate.

Table 5.15. Total porosity of columns filled with microcrystalline cellulose triacetate.

| Column dimensions L x D (mm) | Particle diameter $d_P$ (μm) | Eluent | Total porosity $\varepsilon_T$ | Reference |
|---|---|---|---|---|
| 250 x 8 | 10 - 20 | ethanol 4% water | 0.60 | Koller, 1983 |
| 243 x 40 | 20 - 30 | ethanol 4% water | 0.625 | Rimböck *et al.*, 1985 |
| 250 x 10 | 10 | methanol | 0.73 | Rizzi, 1989 |
| 250 x 5 | 15 - 25 | ethanol 5% water | 0.63 | Isaksson *et al.*, 1990 |
| 445 x 12.5 | 25 -40 | methanol | 0.70 | Lim *et al.*, 1995 |
| 99 x 26 | 45 | methanol | 0.67 | This work |

A breakthrough curve with the non-retained compound was carried out to estimate the axial dispersion in the SMB column. A Peclet number of $Pe = 1000$ was found by comparing experimental and simulated results from a model which includes

axial dispersion in the interparticle fluid phase, accumulation in both interparticle and intraparticle fluid phases and assuming that the average pore concentration is equal to the bulk fluid concentration; this assumption is justified by the fact that the ratio of time constant for pore diffusion and space time in the column is of the order of $10^{-4}$ (see *Figure 5.23*).

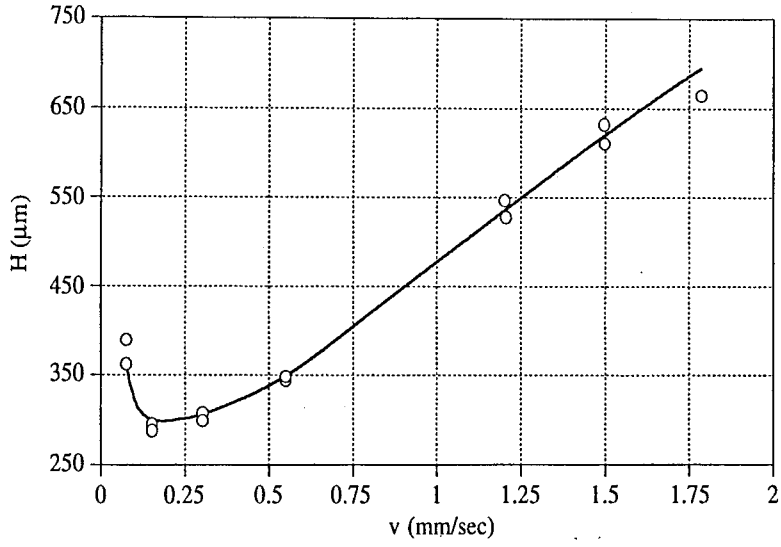


Figure 5.22. Influence of the linear velocity upon plate height for the non-retained compound (1,3,5-tri-*tert.*-butylbenzene).

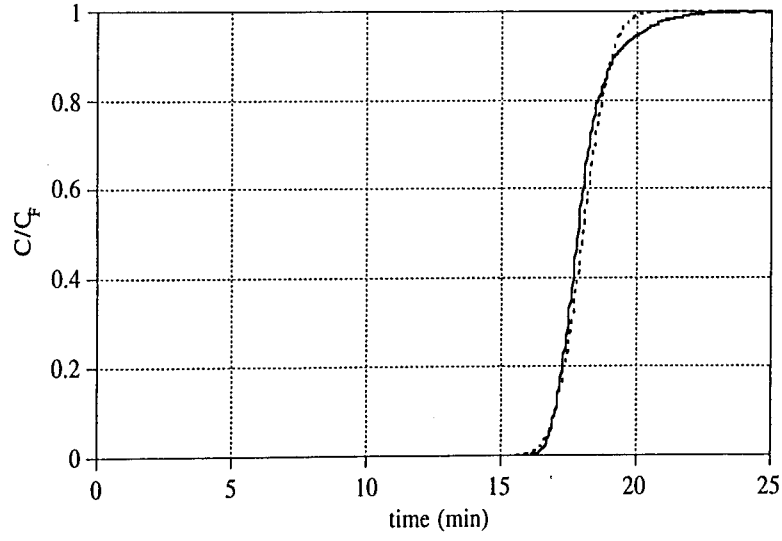


Figure 5.23. Breakthrough curve obtained for the non-retained (1,3,5-tri-*tert.*-butylbenzene) compound. Comparison between experimental (full line) and model (dashed line) results. Flow-rate: 2 ml/min.

### 5.3.5 Experimental Determination and Modeling of Competitive Adsorption Isotherms

To develop chromatographic separation processes such as simulated moving bed technology, modeling and simulation are essential issues of the design. The modeling of the chromatographic process requires the knowledge of the adsorption isotherms. When dealing with preparative scale separations it is advisable to determine experimentally the competitive adsorption isotherms, instead of predicting those from single component isotherms. Some examples of determination of competitive adsorption isotherms of enantiomers on chiral stationary phases were recently published (Nicoud *et al.*, 1993a, b; Seidel-Morgenstern and Guiochon, 1993a, b).

The competitive adsorption isotherms were experimentally determined for the separation of chiral epoxide enantiomers at 25 C. The method followed was a combination of static adsorption-desorption measurements checked with a dynamic method of frontal chromatography. In the adsorption-desorption method, a SMB column initially equilibrated with the eluent, is fed with a large amount of a solution with known concentrations $c_A^F$ and $c_B^F$, until equilibrium is reached. The column is then completely desorbed with the eluent. The eluted volume resulting from the desorption step is analyzed.

The mass balance

$$V^d c_i^d = \varepsilon V_c c_i^F + (1-\varepsilon) V_c q_i^* \tag{5.8}$$

will allow the knowledge of the concentration of each component retained in the particle, $q_i^*$, in equilibrium with the feed concentration, $c_i^F$. In fact $q_i^*$ includes both the adsorbed phase concentration and the concentration in the fluid inside pores. This overall retained concentration $q_i^*$ is used to be consistent with the models presented for the SMB simulations based on homogeneous particles. In this balance, $c_i^d$ is the concentration of each component in the eluted volume obtained in the desorption step, $V^d$ is the eluted volume, $V_c$ is the column volume, and $\varepsilon$ the bed porosity. The bed porosity was taken as $\varepsilon = 0.4$ since the total porosity was measured as $\varepsilon_T = 0.67$ and the particle porosity of microcrystalline cellulose triacetate is $\varepsilon_P = 0.45$ (Lim *et al.*, 1995).

This procedure provides one point of the adsorption isotherm for each component ($c_i^F, q_i^*$). The determination of the complete isotherm will require a set of experiments using different feed concentrations.

To support the isotherms measured by the adsorption-desorption procedure, a dynamic method of frontal chromatography is implemented. This method is based on the mathematical analysis of the response curves to a step change in feed concentration (adsorption) followed by the desorption of the column with pure eluent. A complete description of these and other methods of adsorption isotherms measurements with applications to preparative chromatography can be found in Nicoud and Seidel-Morgenstern (1993).

It should be pointed out that, when using the dynamic method to describe the chromatographic curves in a SMB column, the shape of the front is not only influenced by thermodynamics but also by dispersion and mass transfer resistance phenomena. Hence, the value for the mass transfer coefficient will be predicted simultaneously with the adsorption data.

The binary Langmuir isotherm for mixtures of species *i* and *j* (*Equation 5.9*) is one of the most popular models used to represent adsorption isotherms.

$$q_i^* = \frac{Qb_iC_i}{1 + b_iC_i + b_jC_j} \tag{5.9}$$

However, for many systems, this isotherm fails when the objective is to model chromatographic results. For instance, the multicomponent Langmuir isotherm takes into account the competition between species for the available chiral sites but does not predict the concentration dependency of the selectivity factor.

It is well known that often the selectivity factor decreases with the increase of the concentration of chiral species. To overcome this lack of information, two different models have been widely used: the linear+Langmuir (*Equation 5.10*) and the bi-Langmuir (*Equation 5.11*) competitive isotherms:

$$q_i^* = mC_i + \frac{Qb_iC_i}{1 + b_iC_i + b_jC_j} \tag{5.10}$$

$$q_i^* = \frac{Qb_iC_i}{1+b_iC_i+b_jC_j} + \frac{\Theta\beta_iC_i}{1+\beta_iC_i+\beta_jC_j} \tag{5.11}$$

As it was mentioned before, the mechanism of chiral recognition in microcrystalline cellulose triacetate involves the intercalation of the chiral solutes between the polymer chains. However, this mechanism does not exclude the occurrence of simple interaction in the surface of the adsorbent. Hence, chiral stationary phases provide two types of adsorption sites: one responsible for non-selective achiral interactions, the other for chiral selective interactions between the enantiomers and the stationary phase (Lim *et al.*, 1995; Nicoud *et al.*, 1993a; Jacobson *et al.*, 1991).

Racemic (50%) and 90% pure solutions were used for adsorption isotherm measurements within a range of 0.25-5 g/l concentrations. A pulse of a racemic mixture (5 g/l each enantiomer) was carried out to check the adsorption model and to predict the mass transfer coefficient. The other model parameters used in simulation were $\varepsilon = 0.4$ and $Pe = 1000$.

The model used to fit experimental data for the chiral epoxide system was the linear+Langmuir adsorption isotherm (*Equation 5.10*) with the following results:

$$q_A^* = 1.35C_A + \frac{7.32\times 0.087C_A}{1+0.087C_A+0.163C_B} \tag{5.12a}$$

and

$$q_B^* = 1.35C_B + \frac{7.32\times 0.163C_B}{1+0.087C_A+0.163C_B} \tag{5.12b}$$

The mass transfer coefficient used to fit experimental and model predictions in the pulse experiment was $k = 0.4$ $s^{-1}$. Model and experimental results are compared in *Figures 5.24* and *5.25*. *Figure 5.26* shows the influence of the enantiomers concentration on the selectivity factor.

*Figure 5.27* presents simulated results obtained with the linear+Langmuir adsorption isotherm described in *Equation 5.12*, but using a mass transfer coefficient of $k = 0.1$ (*Figure 5.27a*) and $k = 1$ $s^{-1}$ (*Figure 5.27b*). Although no additional optimization of the adsorption isotherm parameters was made for these two values of mass transfer coefficient, it is clear that the better agreement between the experimental and simulation results for the feed pulse experiment occurs for $k = 0.4$ $s^{-1}$.

We can also estimate a value for the mass transfer coefficient in the same way we did for the bi-naphthol system. Applying to the case of the chiral epoxide enantiomers separation, using methanol as eluent and a temperature of 25 C, we get from *Equation 5.6*, $D_m = 1.3 \times 10^{-5}$ $cm^2 s^{-1}$. From *Equation 5.7* and considering $\varepsilon_p = 0.45$, $\psi = 10$, $\tau = 5$, $K_A = 1.99$ and $K_B = 2.54$ (from the equilibrium adsorption isotherms presented in *Equation 5.12*), and $R_p = 2.25 \times 10^{-3}$ cm (particle diameter, $d_p = 45$ μm), we get $k_A = 1.16$ and $k_B = 0.91$ $s^{-1}$.

If we take into account the same values proposed before but considering the lower value for the liquid phase diffusivity proposed by Ruthven ($10^{-6}$ $cm^2 s^{-1}$) we get $k_A = 0.09$ and $k_B = 0.07$ $s^{-1}$. The value used to fit experimental and model predictions in the pulse experiment ($k_A = k_B = 0.4$ $s^{-1}$) is in the range limited by these estimations.

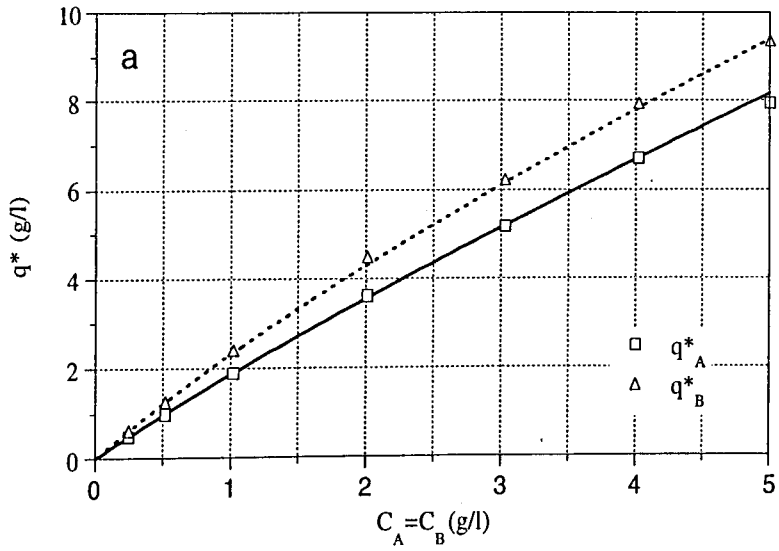

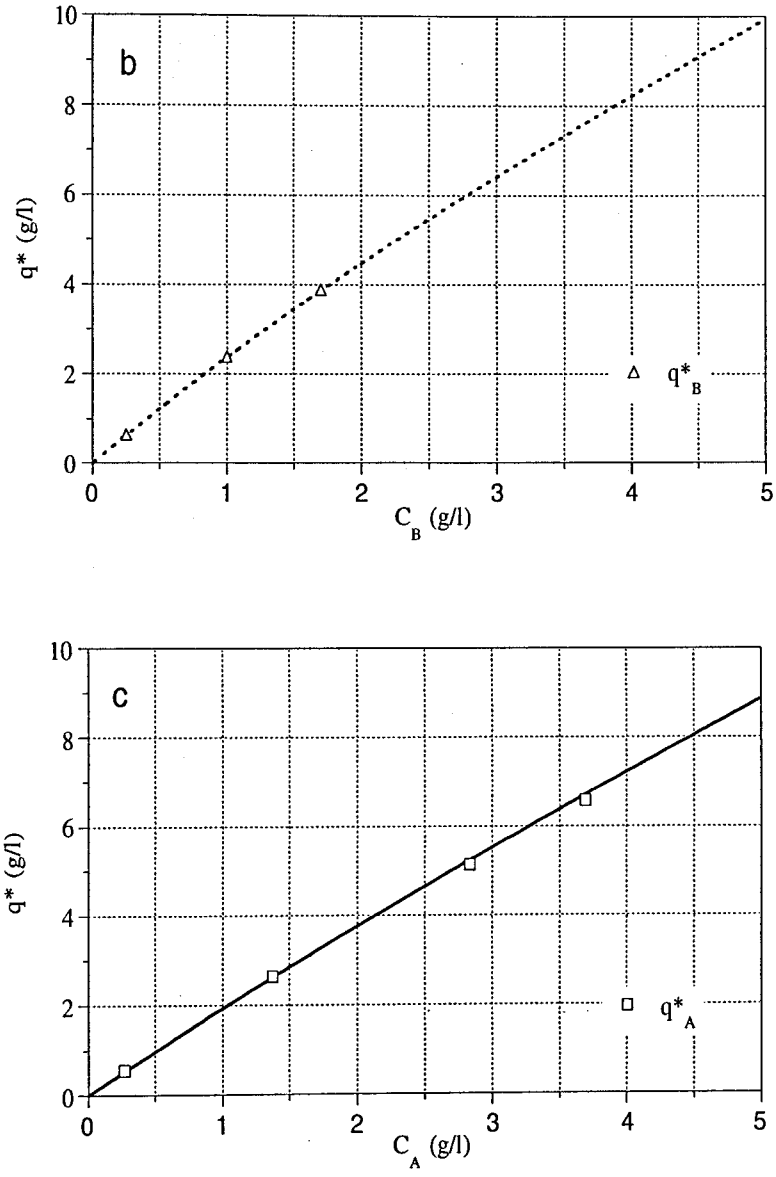


Figure 5.24. Competitive adsorption isotherms. Comparison between experimental (points) and model (lines) results: (a) racemic mixtures; (b) feed with 90% purity in the more retained species (B); (c) feed with 92% purity in the less retained species (A). Squares and full lines for the less retained component (A), triangles and dashed lines for the more retained component (B).

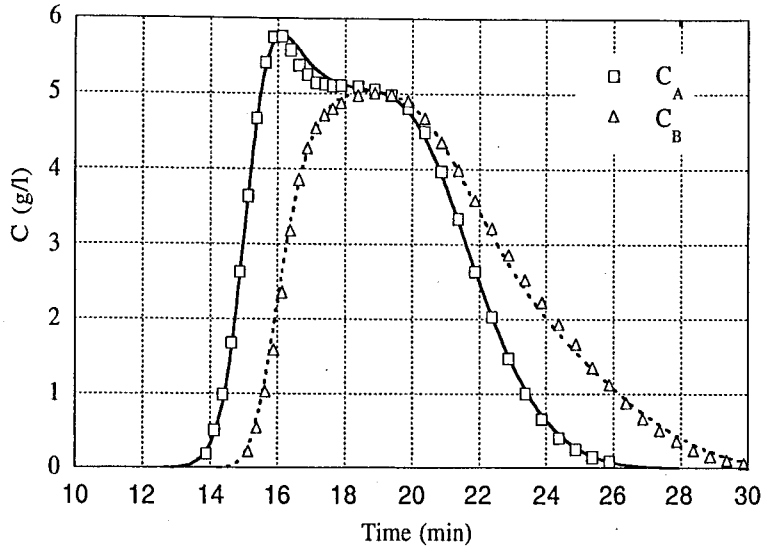


Figure 5.25. Chromatographic response to a feed pulse.
Comparison between experimental (points) and model (lines) results.
(Pulse: 5 g/l each enantiomer, during 7.5 min; flow-rate: 5 ml/min).
Squares and full lines for the less retained component (A),
triangles and dashed lines for the more retained component (B).

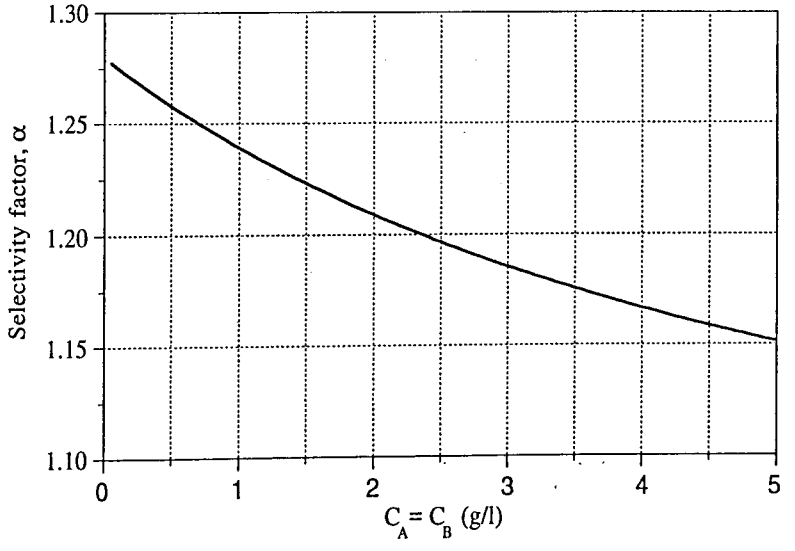


Figure 5.26. Influence of the enantiomer concentration
on the selectivity factor (racemic mixtures).

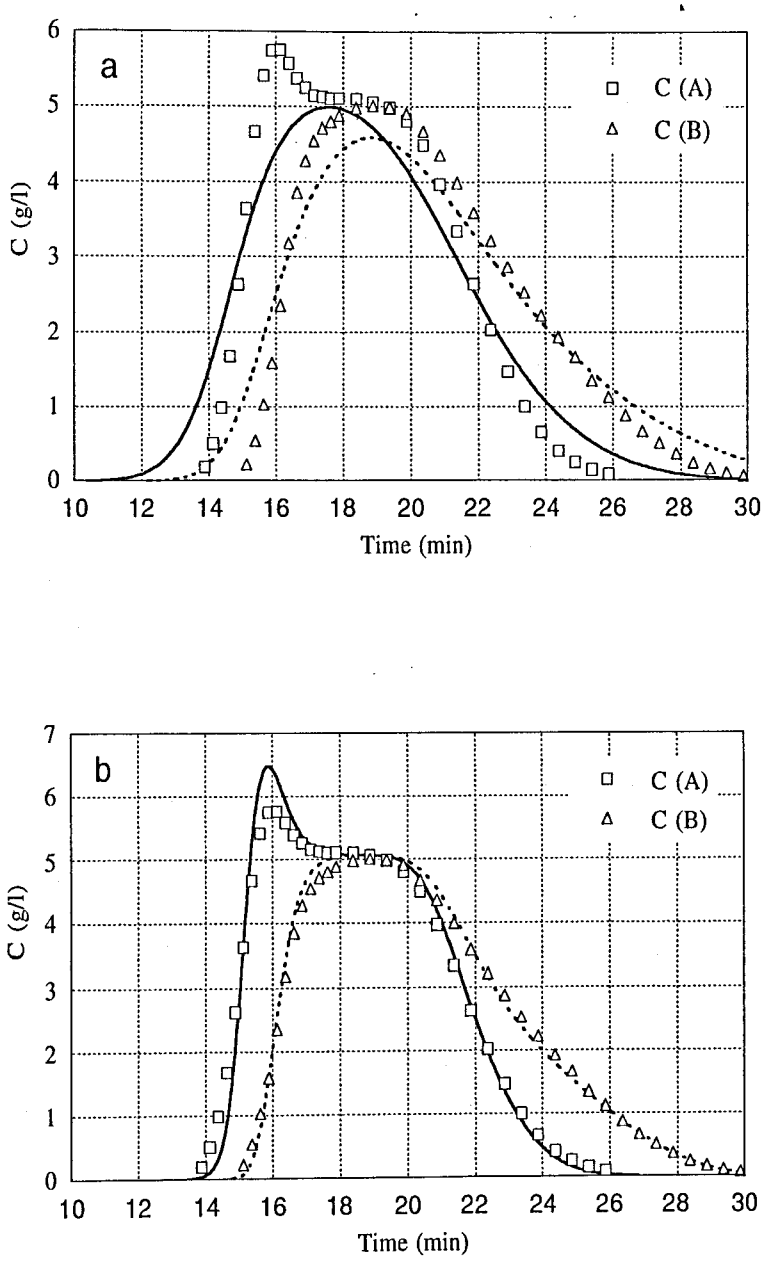


Figure 5.27. Chromatographic response to a feed pulse. Comparison between experimental (points) and model (lines) results: (a) $k = 0.1$ s$^{-1}$; (b) $k = 1$ s$^{-1}$. (Same conditions as in *Figure 5.25*).

## 5.3.6 Experimental Operation of the SMB Pilot Unit

The SMB system used to perform the separation of the chiral epoxide enantiomers is constituted by the eight columns presented in *Table 5.14* with a configuration of two columns per section. The operation temperature was fixed at 25 C and the system pressure-drop was 15 bar at a flow-rate of 25 ml/min. The feed concentration used was 5 g/l of each enantiomer. *Table 5.16* presents the experimental conditions used in the SMB operation. These are similar to the ones proposed by Nicoud and co-workers (1992, 1993a), except in what concerns the value for the recycling flow-rate. In fact, we had some difficulties to calibrate and operate the recycling pump at a range of low flow-rates (lower than 22 ml/min). We decided to choose a recycling flow-rate of $Q^*_{RF} = 23.20$ ml/min, using the same values for the eluent, extract, feed and raffinate flow-rates proposed by Nicoud and co-workers. The switch time interval was then adjusted in order to get the better SMB performance.

Table 5.16. Experimental SMB operating conditions for the chiral epoxide system.

| SMB Columns | Inlet / Outlet Flow-rates (ml/min) | Internal Liquid Flow-rates (ml/min) |
|---|---|---|
| Diameter: 2.6 cm | $Q_E = 4.53$ | $Q^*_I = 27.73$ |
| Length: 9.9 cm | $Q_X = 4.00$ | $Q^*_{II} = 23.73$ |
| Number of columns: 8 | $Q_F = 1.52$ | $Q^*_{III} = 25.25$ |
| Configuration: 2-2-2-2 | $Q_R = 2.05$ | $Q^*_{IV} = 23.20$ |

*Table 5.17* presents the experimental performances obtained as a function of the switch time interval used. According to simulation predictions, a lower switch time interval reduces first the extract purity, while a higher switch time interval will reduce the raffinate purity. This can be explained looking for the constraints of net fluxes presented in *Chapter 4* (*Equation 4.1*). Reducing the switch time interval means that the solid flow-rate is increased, which will violate the constraint for the less retained component A in section II. This means that this species will move downwards in this zone, contaminating the extract stream. On the other hand, increasing the switch time

interval means that the solid flow-rate is decreased, which will violate the constraint for the more retained component B in section III. Hence, this component will move upwards in this zone and will contaminate the raffinate stream.

Table 5.17. SMB performance parameters for the four experimental runs.

| $t^*$ (min) | *PUX* (%) | *PUR* (%) | *RCX* (%) | *RCR* (%) |
|---|---|---|---|---|
| 3.20 | 78.3 | 87.1 | 91.0 | 78.9 |
| 3.28 | 88.1 | 91.4 | 94.2 | 90.9 |
| 3.30 | 90.0 | 91.6 | 94.5 | 90.7 |
| 3.33 | 90.9 | 83.9 | 84.8 | 91.0 |

Purities and recoveries higher than 90% were obtained for a switch time interval of $t^* = 3.30$ min. The adsorbent productivity under these experimental conditions is $PR = 52$ grams of racemic mixture processed per day and per liter of bed, while the solvent consumption is $SC = 0.40$ liters of mobile phase per gram of racemic mixture processed. *Table 5.18* compares these results with the experimental performances obtained for the separation of the chiral epoxide enantiomers by SMB chromatography carried out by other authors. Although the adsorbent productivity was improved, the purities obtained in this work are significantly lower.

Table 5.18. Experimental results obtained for the separation of the chiral epoxide enantiomers by SMB chromatography.

| Stationary phase | Inventory (ml) | $C^F$ (g/l each) | Purity (%) | SC (l/g) | PR (g/day $l_{bed}$) | Reference |
|---|---|---|---|---|---|---|
| MCTA (25-40 μm) | 700 | 5 | 98 | 0.40 | 31.2 | Nicoud *et al.*, (1992, 1993a) |
| Chiralcel-OD (20 μm) | 240 | 10 | 97 | 0.25 | 47.7 | Küsters *et al.* (1995) |
| MCTA (45 μm) | 420 | 5 | 91 | 0.40 | 52.1 | This work |

The internal concentration profiles were evaluated at cyclic steady-state (after 30 full cycles of continuous operation) for the runs using a switch time interval of $t^* = 3.28$, $t^* = 3.30$ and $t^* = 3.33$ min. The samples collected were analyzed in a HPLC system (*Gilson, Villiers le Bel, France*) using a 250 mm (length) x 10 mm (diameter) column filled with 10 μm microcrystalline cellulose triacetate (*Art. 50003 Hibar, Merck, Darmstadt, Germany*). The eluent used was methanol and the outlet concentration was followed by UV detection at 220 nm.

The internal profiles obtained are presented in *Figure 5.28*. Also presented are the simulation predictions using the steady-state TMB model with the information on equilibrium and kinetic parameters obtained by the independent experiments described at the beginning of this section (see *Table 5.19*).

Table 5.19. SMB and equivalent TMB operating conditions and model parameters used with the simulation package (steady-state TMB model).

| SMB configuration | Equivalent TMB configuration | Model parameters |
|---|---|---|
| Columns:<br>Diameter: 2.6 cm<br>Length: 9.9 cm<br>Number of columns: 8<br>Configuration: 2-2-2-2 | Sections:<br>Diameter: 2.6 cm<br>Length: 19.8 cm<br>Number of sections: 4 | Solid/fluid volumes:<br>$(1-\varepsilon)/\varepsilon = 1.5$<br><br>Peclet number:<br>$Pe = 2000$ |
| Flow-rates (ml/min):<br><br>Eluent: $Q_E = 4.53$<br>Feed: $Q_F = 1.52$ | Recycling: $Q^*_{RF} = 23.20$<br>Extract: $Q_X = 4.00$<br>Raffinate: $Q_R = 2.05$ | Mass transfer coefficient:<br>$k = 0.4\ s^{-1}$ |

| Switch Time Interval $t^*$ (min) | Solid flow-rate $Q_S$ (ml/min) | Ratio between fluid and solid interstitial velocities: $\gamma_I$ | $\gamma_{II}$ | $\gamma_{III}$ | $\gamma_{IV}$ |
|---|---|---|---|---|---|
| 3.28 | 9.61 | 3.326 | 2.702 | 2.939 | 2.619 |
| 3.30 | 9.56 | 3.352 | 2.725 | 2.963 | 2.641 |
| 3.33 | 9.47 | 3.392 | 2.758 | 2.999 | 2.675 |

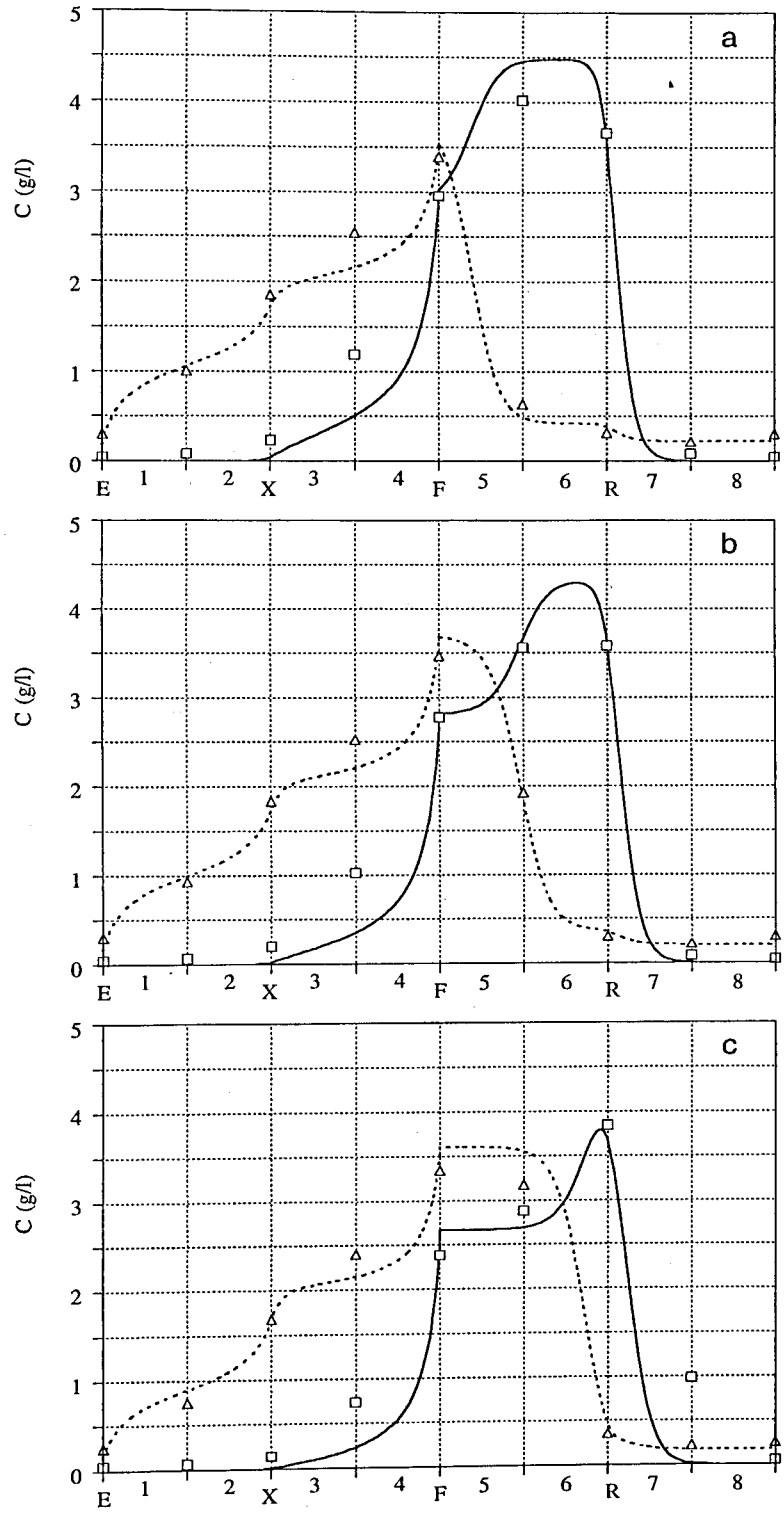


Figure 5.28. Internal concentration profiles: comparison between experimental (points) and simulated (lines) results: (a) $t^* = 3.28$ min; (b) $t^* = 3.30$ min; (c) $t^* = 3.33$ min.
Squares and full lines represent the less retained component; triangles and dashed lines for the more retained species.

The agreement between model and experimental results is reasonable except for the concentration profile of the less retained species in the second zone. Moreover, from the analysis of the internal profiles obtained we conclude that the flow-rate used in section I was too low. In fact, being the flow-rate in the first section lower than its critical value, the more retained component is not efficiently desorbed and it is recycled with the solid phase to section IV, contaminating the raffinate stream.

The experimental performances presented in *Table 5.17* also show a lower extract purity, which are not predicted by the simulated results. Model and experimental purities are compared in *Figure 5.29.*

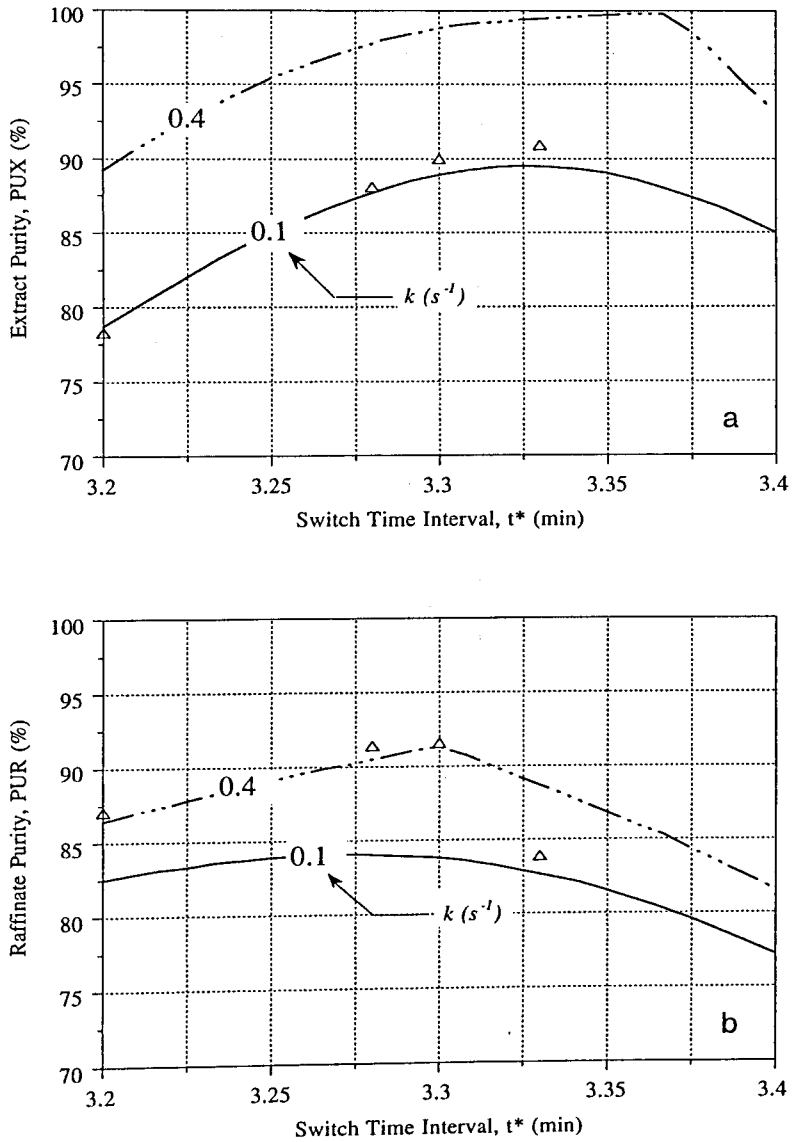


Figure 5.29. Purity performances. Comparison between experimental (points) and simulated (lines) results: (a) Extract purity; (b) Raffinate purity.

For example, for a switch time interval of $t^* = 3.30$ min, the experimental purities obtained were 90.0 and 91.6% for extract and raffinate, respectively, while the model predictions using the steady-state TMB package are 98.9 and 91.3%. This could be eventually due to experimental conditions such as small variations in flow-rates or column packings. *Figure 5.30* shows the recycling pump flow-rates measured by the flowmeter of the SMB pilot unit during the last 10 cycles of the experimental operation with $t^* = 3.30$ min. *Figure 5.31* shows the recycling flow-rate (recycling pump flow-rate in section IV) if the inlet and outlet flow-rates are constant and equal to the theoretical values presented in *Table 5.16*. From the values presented, we conclude that the errors between the measured and the theoretical recycling flow-rate ($Q^*_{RF} = Q^*_{IV} = 23.20$ ml/min) are in the range of $\pm 3$ %.

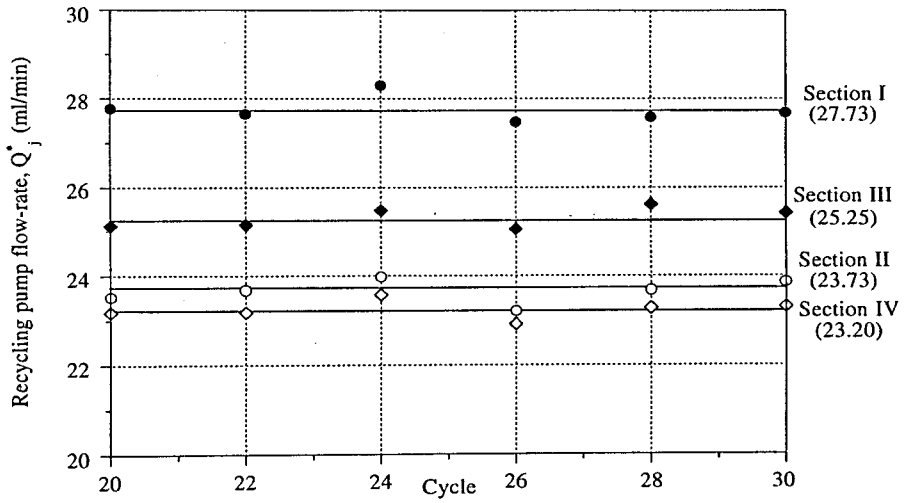


Figure 5.30. Measured recycling pump flow-rates during the SMB operation. Points are experimental measurements, lines are chosen operating conditions.

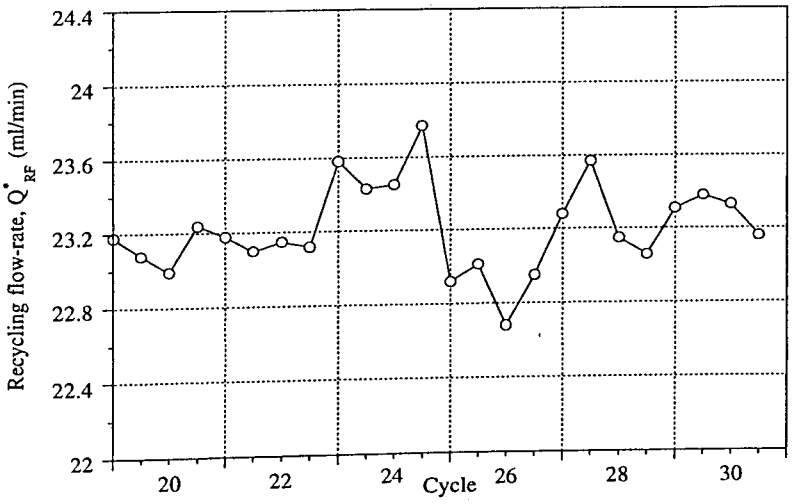


Figure 5.31. Measured recycling flow-rate.

The discrepancies between experimental and model predictions can also be related with an inaccurate description of the competitive binary adsorption equilibrium or of the mechanism of adsorption/desorption. As it is shown in *Figure 5.32*, the model does not predict adequately the behaviour of both species in terms of its concentrations in the extract and raffinate streams, if only mass transfer resistances are considered.

Nevertheless, the model predicts very well the drastic changes in the internal concentration profiles of both components in section III, due to small changes in the switch time interval (see *Figure 5.28*).

To finish our experimental studies in the SMB pilot unit for the chiral epoxide system, we decided to evaluate the internal concentration profiles at different moments of a switch time interval. These internal profiles were evaluated after cyclic steady-state was achieved (after more than 30 full cycles of continuous operation). The operating conditions used were the same of those presented before in *Table 5.19* for $t^* = 3.30$ min.

Simulations with the same operating conditions were also carried out using the SMB model presented previously in this work (see *Section 3.2* of *Chapter 3*), in order to predict the dynamic behaviour of the SMB internal concentration profiles during each switch time interval.

*Table 5.20* presents the experimental and predicted purities and recoveries obtained. Two models are compared: the steady-state TMB model and the SMB model with 8-columns (2 per section). The discrepancies between the experimental and model predictions for the extract purity remain.

*Figure 5.33* shows the internal concentration profiles at different moments of a switch time interval and after the cyclic steady-state was achieved: at the beginning, 25, 50, 75%, and at the end of a switch time interval. The model predictions obtained with the SMB model are also presented. Despite some discrepancies, the SMB model predicts well the dynamic behaviour of the SMB internal concentration profiles during each switch time interval.

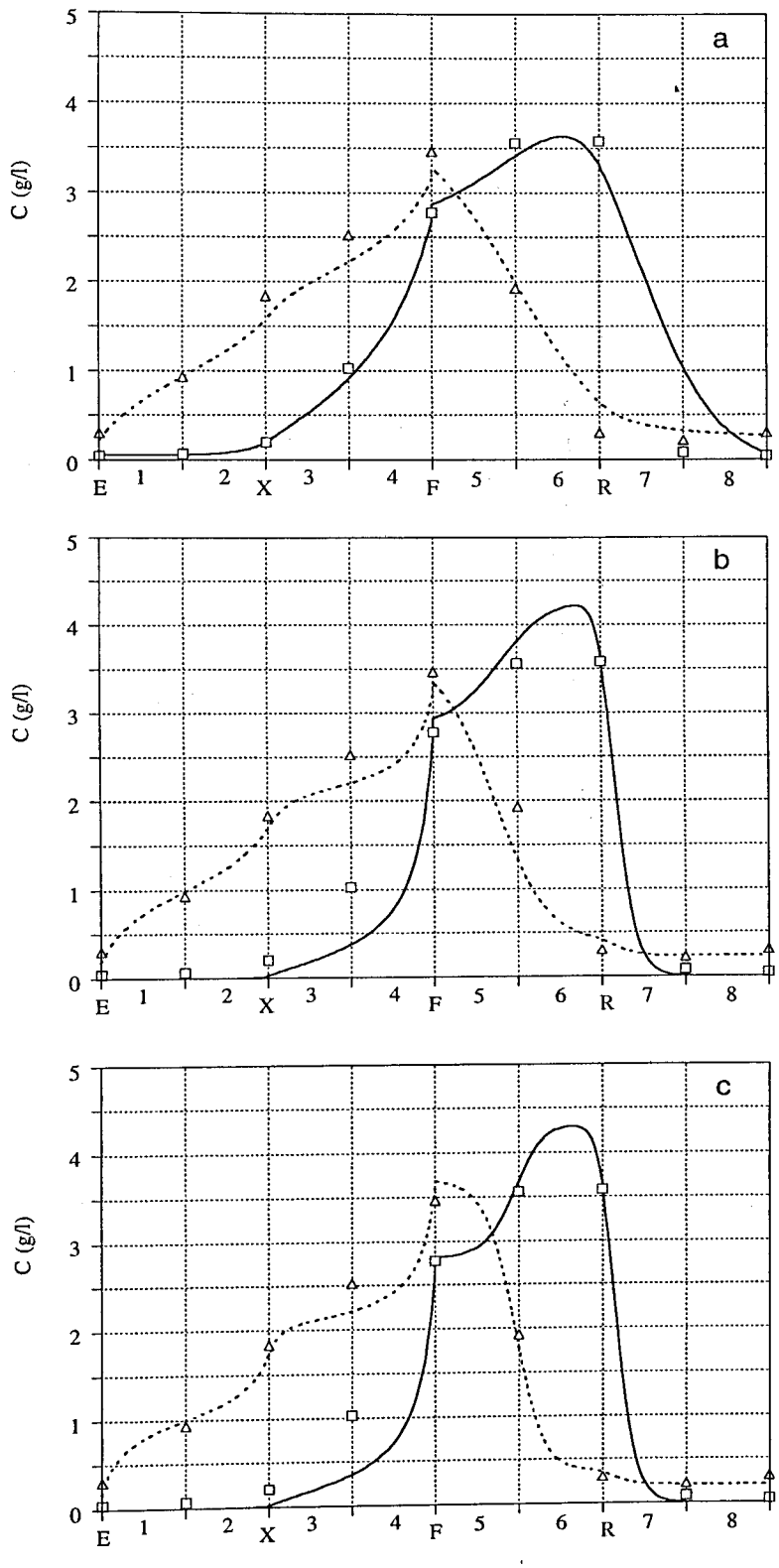


Figure 5.32. Internal concentration profiles: experimental (points) and simulated (lines) results: (a) $k_A = k_B = 0.1$; (b) $k_A = 0.4$ , $k_B = 0.2$; (c) $k_A = k_B = 0.4$ $s^{-1}$. Solid line and squares for the less retained component, dashed line and triangles for the more retained component. (Operating conditions as in *Figure 5.28b*).

Table 5.20. Comparison between the experimental and predicted performance parameters (Operating conditions as in *Table 5.19*, $t^* = 3.30$ min).

| Performance Parameter | Extract Purity PUX (%) | Raffinate Purity PUR (%) | Extract Recovery RCX (%) | Raffinate Recovery RCR (%) |
|---|---|---|---|---|
| Experimental | 90.0 | 91.6 | 94.5 | 90.7 |
| Predicted SMB model | 98.0 | 90.8 | 89.5 | 98.7 |
| Predicted TMB model | 98.9 | 91.3 | 90.5 | 99.0 |

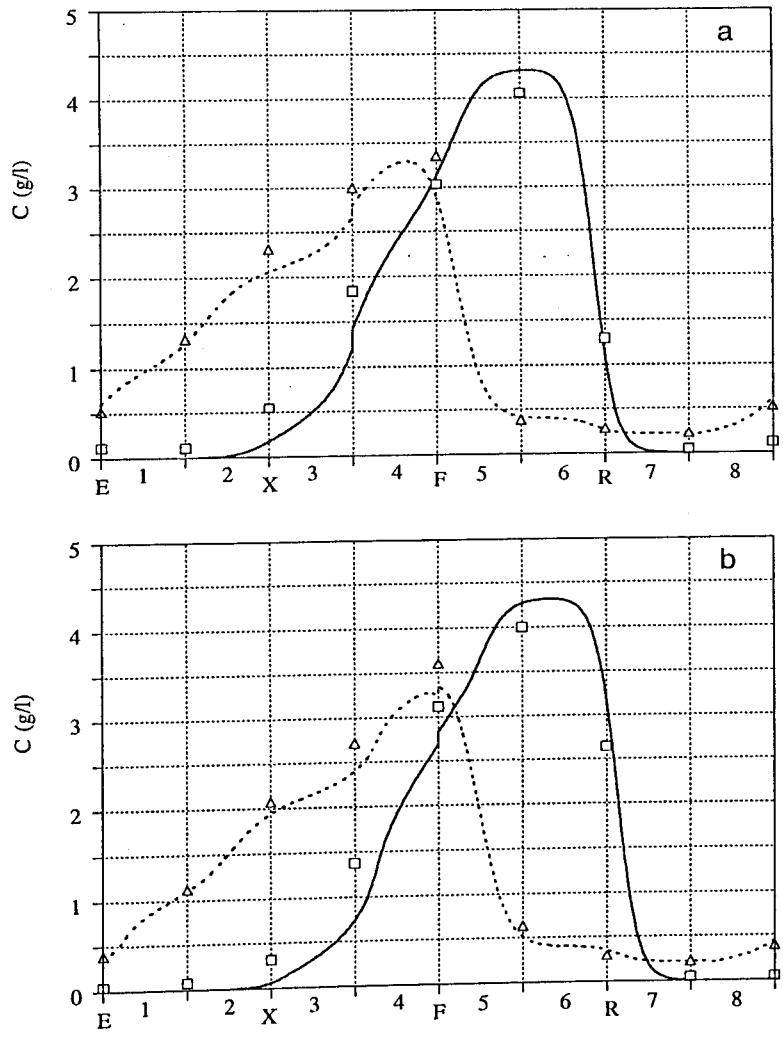

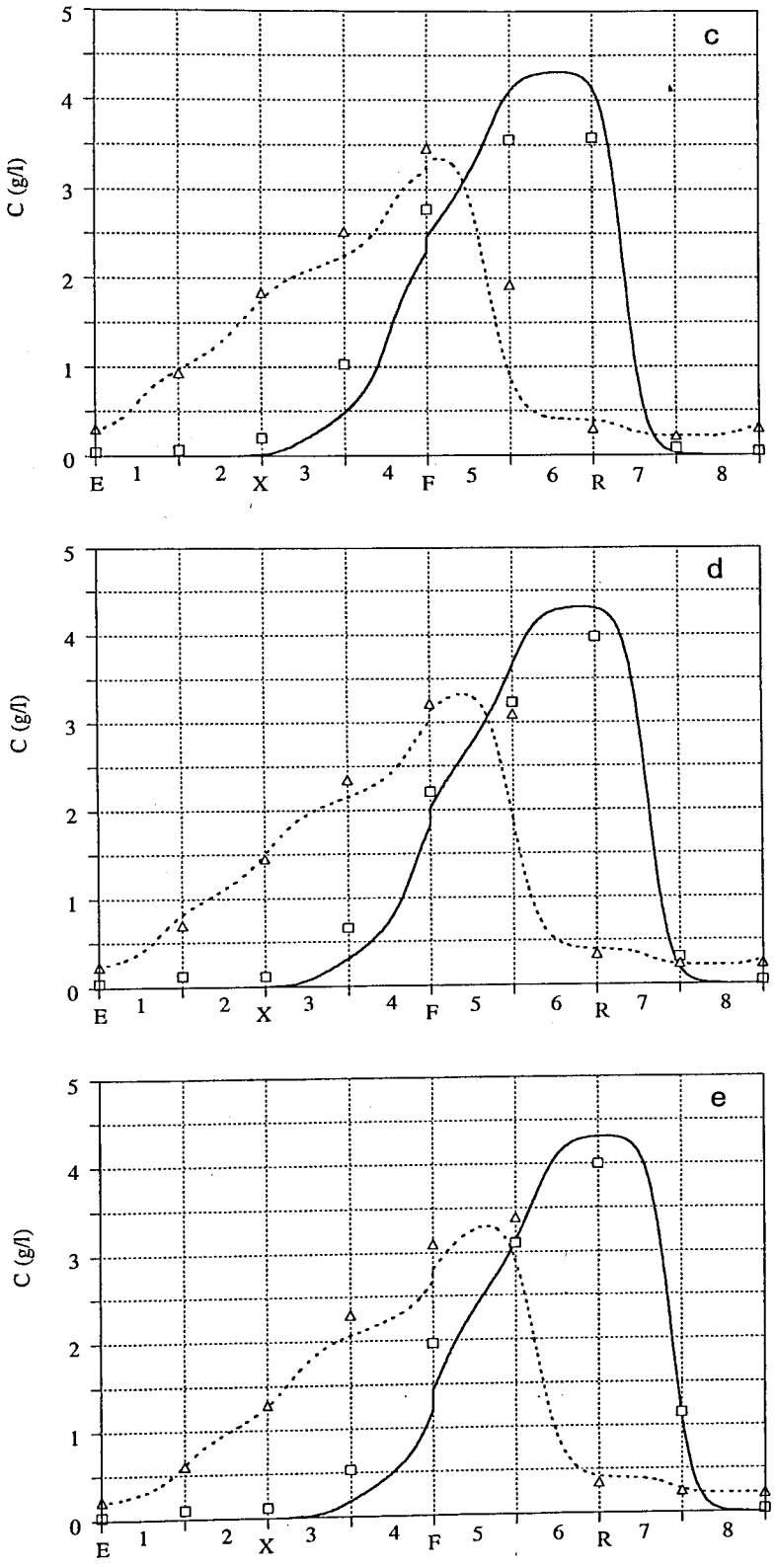


Figure 5.33. Experimental (points) vs simulated (lines) internal concentration profiles evaluated at (a) beginning, (b) 25%, (c) 50%, (d) 75%, and (e) end of a switch time interval. (Operating conditions as in *Table 5.19*, $t^* = 3.30$ min).

## 5.3.7 Additional Simulation Results

Some additional model simulations were carried out to complement the study of the chiral epoxide system. In this section, a similar approach to the one used for the bi-naphthol system in *Section 4.9* is presented. We suggest a higher flow-rate in section I, since we concluded that the one used experimentally was too low. Choosing the higher internal liquid flow-rate, $Q_I^* = 31.00$ ml/min, we will use *Equations 4.66* and *4.67* to evaluate the switch time interval and recycling flow-rate.

As it was explained in *Chapter 4*, the section I, located between the eluent and extract nodes, must provide the complete regeneration of the adsorbent phase, so the solid coming out this zone is recycled to section IV completely clean of the two components. In other words, both components A and B must move upwards, following the liquid phase. Because component B is the more retained species, we have to consider only the constraint considering this component.

The worst situation concerning the constraint in section I appears when dealing with low concentrations of the two enantiomers because it leads to bigger retention times. Since the function of section I is to completely regenerate the adsorbent phase, at the beginning of this zone, concentrations of both enantiomers must be the lowest possible. Hence, the choice of the switch time interval must be done taking into account the initial slope of the proposed isotherm. The linear retention time of a component $i$ in zone $j$ is given by the following equation:

$$t_{ij} = \frac{\varepsilon V_c}{Q_j^*}\left(1 + \frac{1-\varepsilon}{\varepsilon} K_i\right) \tag{5.13}$$

where $K_i$ is the initial slope of the isotherm for component $i$. Considering that the SMB system in study is constituted by 9.9 cm (length) x 2.6 cm (diameter) columns ($V_c = 52.56$ ml), $\varepsilon = 0.4$, $K_B = m + Qb_B = 2.543$, and using the maximum SMB flow-rate chosen, $Q_I^* = 31.00$ ml/min, the retention time of the more retained component in section I is $t_{BI} = 3.27$ min. Hence, the switch time interval for the SMB operation must be greater than the retention time of the more retained component in section I, if we want to fulfill the constraint previously presented for this zone. The value chosen for the switch time interval was $t^* = 3.3$ min, which corresponds to a TMB solid flow-rate of $Q_s = (1-\varepsilon)V_c / t^* = 9.56$ ml of solid/min and is equal to the value used for the

experimental operation of the SMB pilot unit where 90% pure extract and raffinate were obtained. These results show once more that, in our experimental runs, a too low liquid flow-rate in section I was used ($Q_I^* = 27.73$ instead of $Q_I^* = 31.00$ ml/min).

The function of section IV, located between the raffinate and eluent nodes, is to regenerate the liquid phase, so that it can be recycled to section I as pure eluent. In other words, both components A and B must move downwards, following the solid phase. Because component A is the less retained species, we have to consider only the constraint considering this component; i.e., if the constraint is fulfilled for species A, the constraint considering the more retained component B will be always met.

Following the procedure explained in *Chapter 4*, the worst situation concerning the constraint in section IV appears when dealing with non-linear behaviour: it leads to lower retention times, and we must prevent that the less retained component reaches the end of this zone before the jump of the inlet/outlet lines in the SMB operation. Since the switch time interval was already chosen and, in a situation of enantiomer separation, the concentration of the more retained component along the section IV is near zero, we suggested the choice of the liquid flow-rate in section IV by using the following equation:

$$Q_{IV}^* = \frac{\varepsilon V_c}{t^*}\left(1 + \frac{1-\varepsilon}{\varepsilon}\frac{\Delta q_A^{*F}}{\Delta C_A^F}\right) \tag{5.14}$$

where $\Delta q_A^{*F} / \Delta C_A^F$ is the slope of the chord linking points $(C_A^F, q_A^{*F})$ and $(0,0)$ with $C_B = 0$. Considering that feed concentration used for this system is 5 g/l of each enantiomer and $\Delta q_A^{*F} / \Delta C_A^F = m + Qb_A / (1 + b_A C_A^F) = 1.794$, *Equation 5.14* gives $Q_{IV}^* = 23.51$ ml/min.

To complete the choice of the operating conditions, we will use the TMB model developed in this work to predict the SMB performance in a range of possible liquid flow-rates in sections II and III. As it was explained in *Chapter 4*, the conditions for enantiomer separation can be defined alternatively in terms of the $\gamma_j$ model parameters, which are directly related with the TMB (SMB) operating variables (fluid and solid interstitial velocities in the four sections of the TMB unit). Since the $\gamma$ values for sections I and IV were already fixed guaranteeing that constraints concerning these zones were fulfilled, a region for enantiomer separation can be defined in a $\gamma_{III} - \gamma_{II}$ plane.

*Table 5.21* summarizes the SMB operating conditions (and equivalent TMB conditions) used in the design of the $\gamma_{III} - \gamma_{II}$ plot. *Figure 5.34* presents the separation region obtained for the chiral epoxide system. Three regions are displayed: the region of complete separation obtained by the Equilibrium Theory and the regions of almost complete separation (99.5% pure extract and raffinate) for the cases where the mass transfer coefficient is $k = 1$ and $k = 0.4$ $s^{-1}$. The regions for these two last cases were obtained numerically by using the steady-state TMB model. The region of complete separation considering mass transfer resistance negligible was evaluated following the equations presented in *Chapter 4* (*Table 4.2*) and were obtained by Morbidelli and co-workers (Mazzotti *et al.*, 1997).

Table 5.21. Operating conditions and model parameters for the $\gamma_{III} - \gamma_{II}$ plot.

| SMB | Equivalent TMB |
|---|---|
| Column diameter: $D_c = 2.6$ cm<br>Column length: $L_c = 9.9$ cm<br>Configuration: 2-2-2-2 | Section length: $L_j = 2L_c = 19.8$ cm |
| Bed porosity: $\varepsilon = 0.4$<br>Peclet number: $Pe = 1000$ | Peclet number: $Pe_j = 2Pe = 2000$ |
| Feed concentration:<br>$C_A^F = C_B^F = 5$ g/l | |
| Switch time interval:<br>$t^* = 3.3$ min | Solid flow-rate:<br>$Q_s = (1-\varepsilon)V_c / t^* = 9.56$ ml/min |
| Flow-rate in zone I:<br>$Q_I^* = 31$ ml/min<br><br>Flow-rate in zone IV:<br>$Q_{IV}^* = 23.51$ ml/min | Flow-rate in zone I:<br>$Q_I = Q_I^* - Q_s\varepsilon/(1-\varepsilon) = 24.63$ ml/min<br>$\gamma_I = 3.8657$<br>Flow-rate in zone IV:<br>$Q_{IV} = Q_{IV}^* - Q_s\varepsilon/(1-\varepsilon) = 17.14$ ml/min<br>$\gamma_{IV} = 2.6901$ |

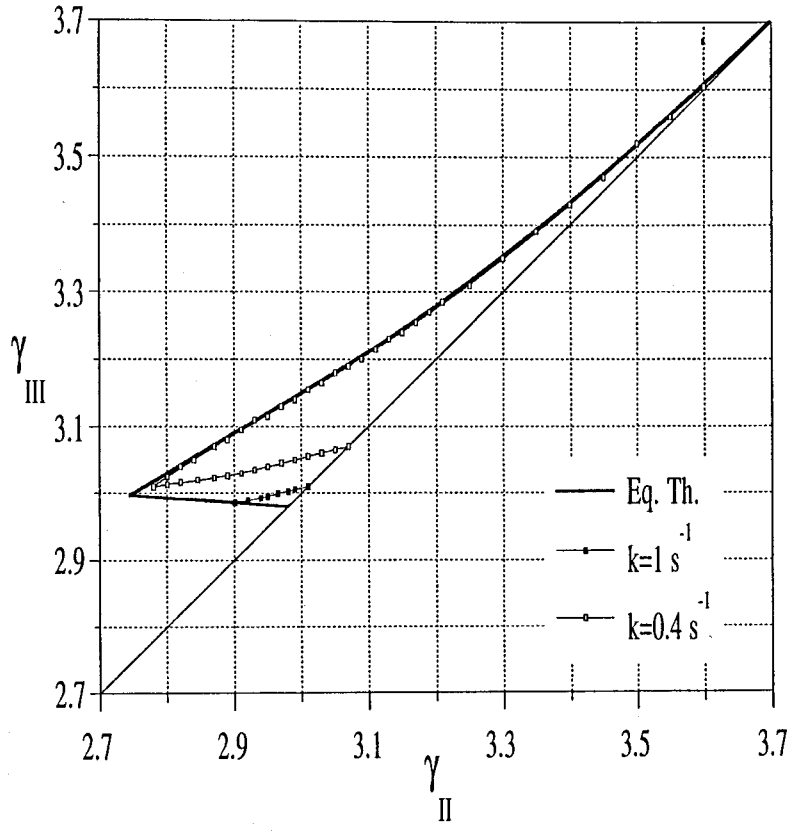


Figure 5.34. Separation regions in a $\gamma_{III} - \gamma_{II}$ plot: Equilibrium Theory (100%, line), mass transfer coefficient $k = 1$ $s^{-1}$ (99.5%, closed squares), $k = 0.4$ $s^{-1}$ (99.5%, open squares) (Operating conditions as in *Table 5.21*).

From *Figure 5.34* we conclude that the case with $k = 0.4$ $s^{-1}$ (open squares) is close to the situation where mass transfer resistance is negligible, besides the differences that appear in the range of low $\gamma_{III}$ values. These differences are due to mass transfer resistances as we can easily conclude by comparing the separation regions obtained for the cases with $k = 0.4$ and $k = 1$ $s^{-1}$.

If mass transfer resistance is important, the region of complete separation can be significantly reduced from the one obtained by the Equilibrium Theory. For example, for a mass transfer coefficient of $k = 0.1$ $s^{-1}$, there is no separation region where extract and raffinate are 99.5% pure. *Figure 5.35* compares the separation regions obtained for mass transfer coefficients of $k = 0.4$ and $k = 0.1$ $s^{-1}$ considering a purity criterion of 90% (extract and raffinate at least 90% pure).

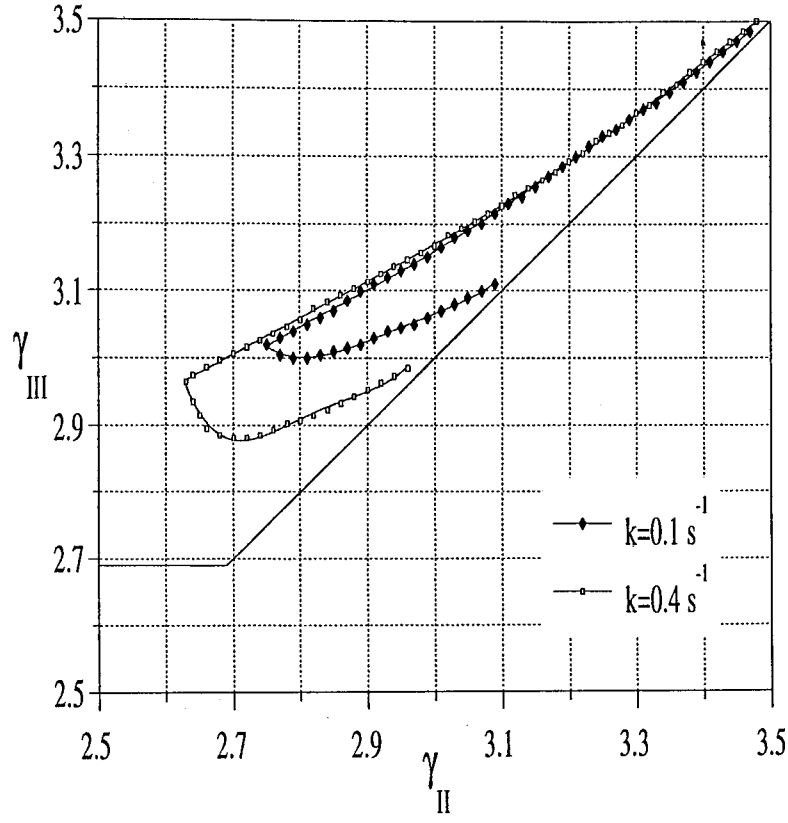


Figure 5.35. Influence of the mass transfer resistance on the separation region. $\gamma_{III} - \gamma_{II}$ plot for a 90% purity criterion: open squares for mass transfer coefficient $k = 0.4$ $s^{-1}$; closed squares for $k = 0.1$ $s^{-1}$. (Operating conditions as in *Table 5.21*).

For practical purposes, it is desirable to work with variables directly related with the SMB unit. Instead of presenting the separation region in a $\gamma_{III} - \gamma_{II}$ plot, we can report the same information in a $Q_X$ versus $Q_F$ plot as it was suggested in *Chapter 4*. *Equations 5.15* and *5.16* present the conversion rules between the TMB operating conditions and feed and extract flow-rates:

$$Q_F = \frac{\varepsilon}{1-\varepsilon}(\gamma_{III} - \gamma_{II})Q_s \tag{5.15}$$

$$Q_X = \frac{\varepsilon}{1-\varepsilon}(\gamma_I - \gamma_{II})Q_s \tag{5.16}$$

Since the liquid flow-rates in sections I and IV are constant in this study, the eluent flow-rate is also constant and equal to $Q_E = Q_I^* - Q_{IV}^* = Q_I - Q_{IV} = 7.49$ ml/min. The raffinate flow-rate can be evaluated by $Q_R = Q_E + Q_F - Q_X$.

*Figure 5.36* presents the same separation regions defined in *Figure 5.34*. Even using a higher eluent flow-rate ($Q_E = 7.49$ instead of $Q_E = 4.53$ ml/min), a feed flow-rate of $Q_F = 1.52$ ml/min (the one used experimentally) corresponds to a situation where the system robustness is very low. If we want to increase system robustness, a lower feed flow-rate should be used, for example, $Q_F = 1.00$ ml/min.

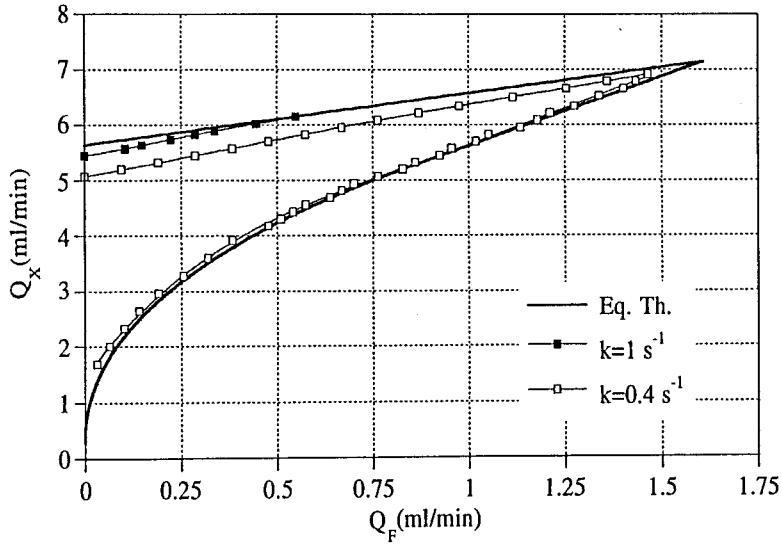


Figure 5.36. Separation regions in a $Q_X$ versus $Q_F$ plot: Equilibrium Theory (100%, line), mass transfer coefficient $k = 0.4$ s$^{-1}$ (99.5%, open squares), $k = 1$ s$^{-1}$ (99.5%, closed squares) (Operating conditions as in *Table 5.21*).

To restrict the values of possible extract flow-rates that lead to the best SMB performance, we can use the optimization procedure suggested in *Chapter 4* (*Equation 4.68*). It consists on the evaluation, for a given feed flow-rate, of the extract flow-rate that leads to equal purities for extract and raffinate. The results obtained are presented in *Figure 5.37* for the case with the mass transfer coefficient $k = 0.4$ s$^{-1}$.

*Figure 5.38* shows the purities of both extract and raffinate obtained with the optimization procedure suggested. Observing *Figure 5.38*, we can conclude that, for the operating conditions presented in *Table 5.21*, the purity of the outlet streams starts to decrease for feed flow-rates greater than 1.3 ml/min. For higher feed flow-rates, complete separation of the two enantiomers will require a higher eluent flow-rate, which will violate the constraint for maximum liquid flow-rate in section I.

*Figure 5.39* presents the solvent consumption and adsorbent productivity obtained as a function of the feed flow-rate. Of course, this figure should not be used without looking for *Figure 5.38*: the increase of the feed flow-rate leads to better solvent consumption and productivity performances, but it is followed by a decrease in both purities and recoveries of extract and raffinate. Furthermore, the higher the feed flow-rate, the smaller the range of extract flow-rates that leads to both enantiomers separation (see *Figure 5.36*); i.e., the system robustness also decreases with the increase of the feed flow-rate.

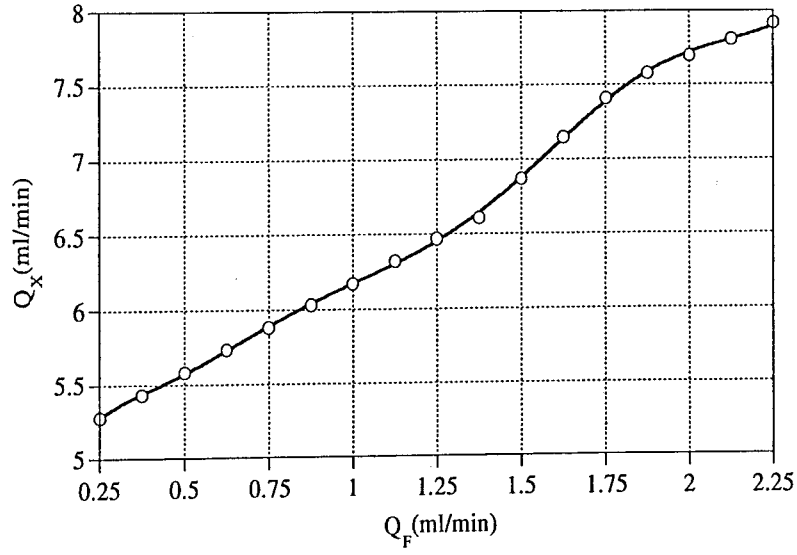


Figure 5.37. Optimum extract and feed flow-rates: path of equal extract and raffinate purities. (Operating conditions as in *Table 5.21*, $k = 0.4$ $s^{-1}$, $Q_E = 7.49$ ml/min, $Q_R = Q_E + Q_F - Q_X$).

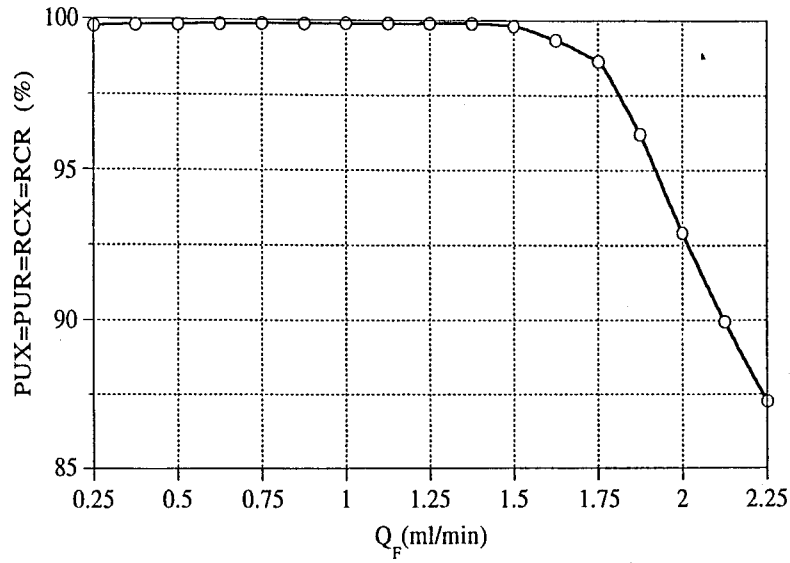


Figure 5.38. Optimum purities and recoveries as a function of the feed flow-rate (Same conditions as in *Figure 5.37*).

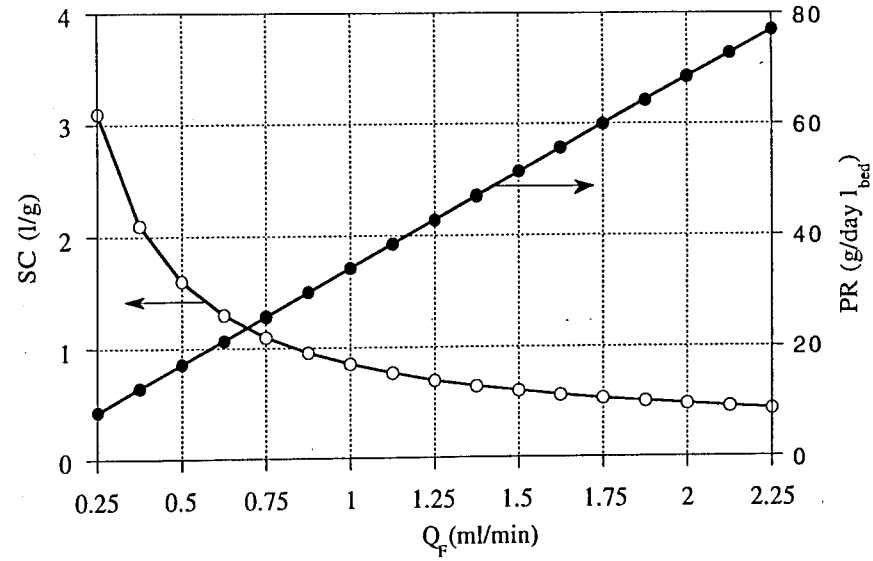




Figure 5.39. Solvent consumption (open circles) and adsorbent productivity (closed circles), obtained for the equal purities optimization procedure, as a function of the feed flow-rate (Same conditions as in *Figure 5.37*).

In conclusion, the set of *Figures 5.37*, *5.38* and *5.39* provides a practical tool for choosing the best SMB operating conditions as a function of the feed flow-rate for the chiral epoxide system. The same procedure can be applied to other feed concentration to optimize it. We believe that these simulation results can be used in future experimental work to obtain a better purity performance than the one presented in the last section.

### 5.3.8 New Experimental Runs on the SMB Pilot Unit

Following the model simulations presented in the last section, we carried out a new set of experimental runs in our SMB pilot unit for the chiral epoxide system. We decided to use the same switch time interval used in the previous experimental work and simulations ($t^* = 3.30$ min), but using an internal liquid flow-rate that is 10% higher than the one obtained with *Equation 5.13*: $Q_I^* = 33.74$ ml/min instead of $Q_I^* = 30.67$ ml/min.

The recycling flow-rate was also chosen in the same way we did in our simulation runs. *Equation 5.14* was used, but a recycling flow-rate 10% lower than the one obtained through this equation was considered: $Q_{IV}^* = 21.38$ ml/min instead of $Q_{IV}^* = 23.51$ ml/min. This is supposed to prevent that small variations in the experimental flow-rates and small differences among the eight SMB columns result in a decrease on the purity performance due to the internal liquid flow-rates in Sections I and IV. Since the internal liquid flow-rates in these sections are fixed, the eluent flow-rate is also fixed and equal to $Q_E = Q_I^* - Q_{IV}^* = 12.36$ ml/min.

Also following the conclusions met in the last section, we decided to use a feed flow-rate of $Q_F = 1.00$ ml/min. *Table 5.22* summarizes the SMB operating conditions (and equivalent TMB conditions) used in our last experimental runs for the chiral epoxide system.

To complete the choice of the SMB operating conditions we must choose the extract and raffinate flow-rates. The steady-state TMB package was used to evaluate the SMB performance as a function of the extract flow-rate. The results are presented in *Figure 5.40*. A complete separation of both enantiomers (purities at least 99.9%) can be obtained in a range of extract flow-rates between $Q_X = 8.36$ and $Q_X = 8.95$ ml/min ($Q_R = Q_E + Q_F - Q_X = 13.36 - Q_X$).

Our first run was carried out with an extract flow-rate of $Q_X = 8.64$ ml/min (and a raffinate flow-rate of $Q_R = 4.72$ ml/min), which were experimentally checked by weighing the outlet liquid provided by the extract and raffinate pumps of the SMB pilot unit. *Table 5.23*summarizes the SMB operating conditions.

Table 5.22. Operating conditions and model parameters for the new experimental runs for the chiral epoxide system.

| SMB | Equivalent TMB |
|---|---|
| Column diameter: $D_c = 2.6$ cm<br>Column length: $L_c = 9.9$ cm<br>Configuration: 2-2-2-2 | Section length: $L_j = 2L_c = 19.8$ cm |
| Bed porosity: $\varepsilon = 0.4$<br>Peclet number: $Pe = 1000$<br>Mass transfer coefficient: $k = 0.4$ s$^{-1}$ | Peclet number: $Pe_j = 2Pe = 2000$ |
| Feed concentration: $C_A^F = C_B^F = 5$ g/l | |
| Switch time interval: $t^* = 3.3$ min | Solid flow-rate: $Q_s = (1-\varepsilon)V_c / t^* = 9.56$ ml/min |
| Eluent flow-rate: $Q_E = 12.36$ ml/min<br>Feed flow-rate: $Q_F = 1.00$ ml/min | |
| Flow-rate in zone I: $Q_I^* = 33.74$ ml/min<br>Flow-rate in zone IV: $Q_{IV}^* = 23.51$ ml/min | Flow-rate in zone I: $Q_I = Q_I^* - Q_s\varepsilon/(1-\varepsilon) = 27.37$ ml/min<br>$\gamma_I = 4.2957$<br>Flow-rate in zone IV: $Q_{IV} = Q_{IV}^* - Q_s\varepsilon/(1-\varepsilon) = 15.01$ ml/min<br>$\gamma_{IV} = 2.3558$ |

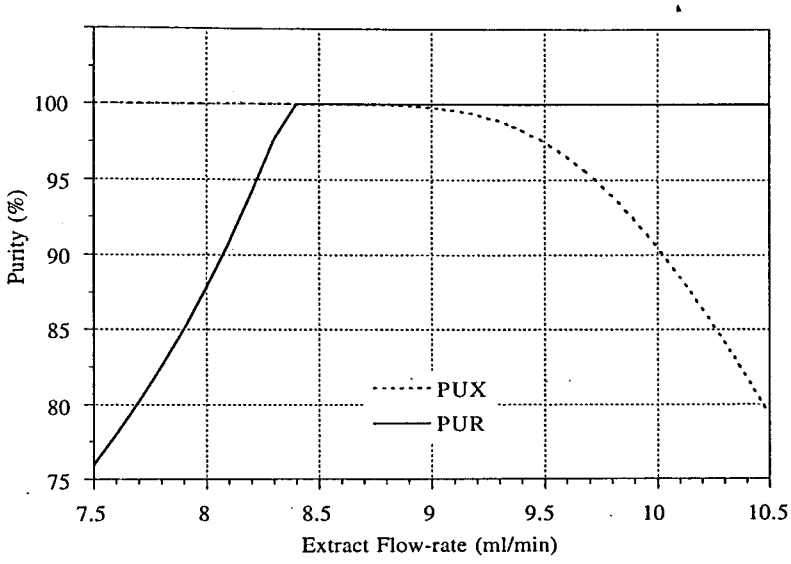


Figure 5.40. Effect of the extract (and raffinate) flow-rates on the purity performance.
(Other operating conditions as in *Table 5.22*).

Table 5.23. Experimental SMB operating conditions for the chiral epoxide system - First run.

| Inlet / Outlet Flow-rates (ml/min) | Internal Liquid Flow-rates (ml/min) | Ratio between fluid and solid interstitial velocities |
|---|---|---|
| $Q_E = 12.36$ | $Q_I^* = 33.74$ | $\gamma_I = 4.2957$ |
| $Q_X = 8.64$ | $Q_{II}^* = 25.10$ | $\gamma_{II} = 2.9396$ |
| $Q_F = 1.00$ | $Q_{III}^* = 26.10$ | $\gamma_{III} = 3.0966$ |
| $Q_R = 4.72$ | $Q_{IV}^* = 21.38$ | $\gamma_{IV} = 2.3558$ |

Experimentally, we obtained a raffinate purity close to 100% ($PUR = 99.6\%$), but the extract purity was a little lower ($PUX = 97.5\%$). The internal concentration profiles were evaluated at cyclic steady-state (after 20 full cycles of continuous operation). Also evaluated were the average concentrations of both species in both extract and raffinate during a full cycle.

The steady-state TMB package was used to compare the theoretical and experimental internal concentration profiles. *Figure 5.41* shows the results obtained. The agreement between experimental and model results is good (see *Figure 5.41b*). Also shown are the predictions of the internal concentration profiles for extract flow-rates of $Q_X = 8.50$ (*Figure 5.41a*) and $Q_X = 8.78$ ml/min (*Figure 5.41c*), which represents a variation of only 1.6% from the experimental value ($Q_X = 8.64$ ml/min).

The agreement between experimental and model predictions of the concentrations plateaus in Sections II and III occurs for an extract flow-rate of $Q_X = 8.50$ (*Figure 5.41a*). Nevertheless, a discrepancy occurs for the internal concentration profile of the less retained species in Section II. In fact, experimental concentrations of this component are higher than the predicted ones, and a 97.5% pure extract was experimentally obtained, instead of a 100% pure as it is predicted by modeling (with $k = 0.4$ $s^{-1}$). This discrepancy remains if we use the SMB package ($PUX = 99.9\%$, $PUR = 100\%$).

*Figure 5.42* shows the transient evolution on the concentration of both species in the extract and raffinate. Average concentrations over a full cycle were evaluated experimentally for cycles 3, 6, 9, 12, 15, and 18. Also shown are the corresponding SMB model predictions. The agreement between them is good and we can conclude that steady-state, in terms of extract and raffinate concentrations, is obtained after 10 full cycles.

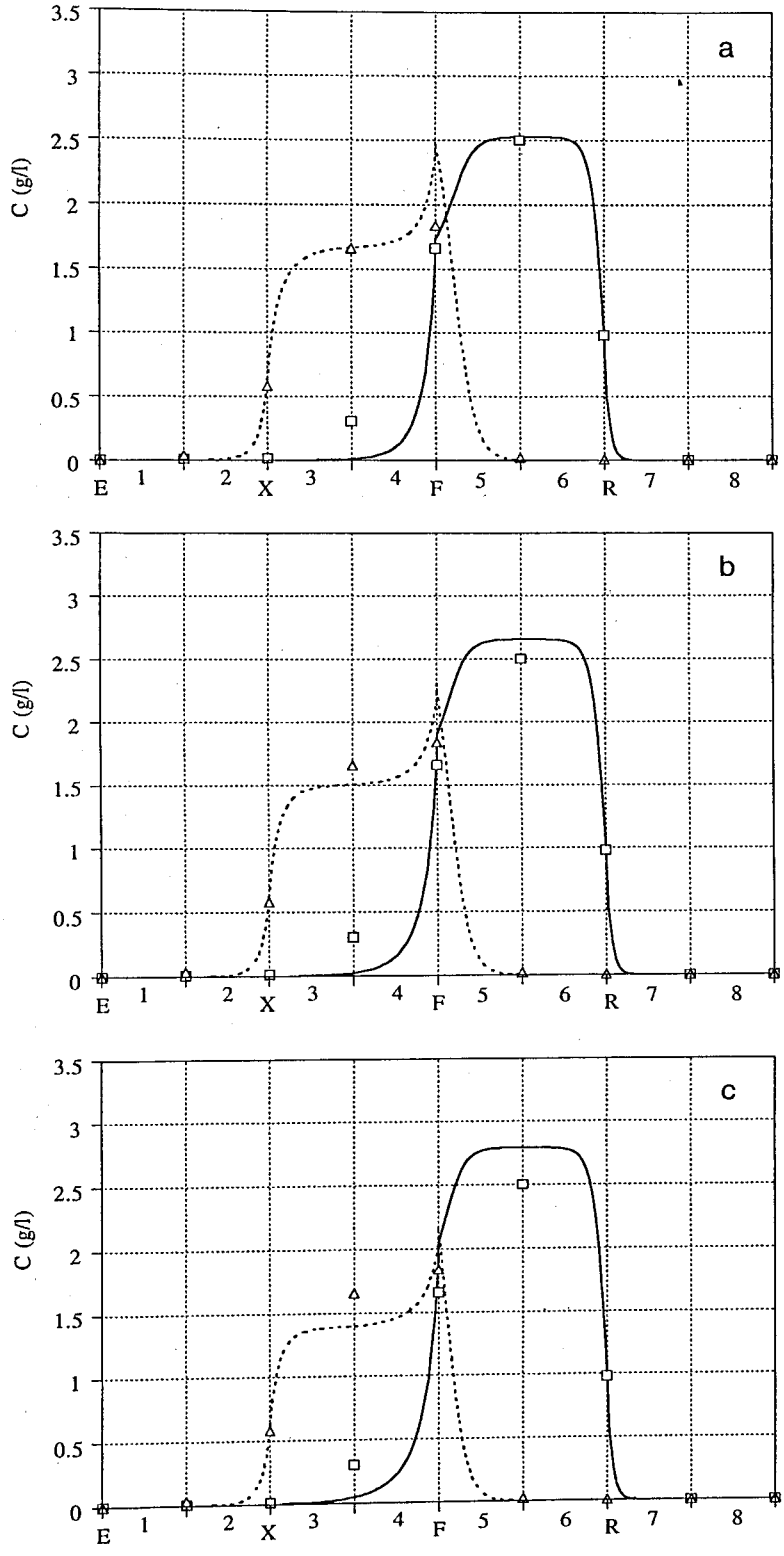


Figure 5.41. Internal concentration profiles: comparison between experimental (points) and simulated (lines) results: (a) $Q_X = 8.50$; (b) $Q_X = 8.64$; (c) $Q_X = 8.78$ ml/min. Squares and full lines represent the less retained component; triangles and dashed lines for the more retained species.

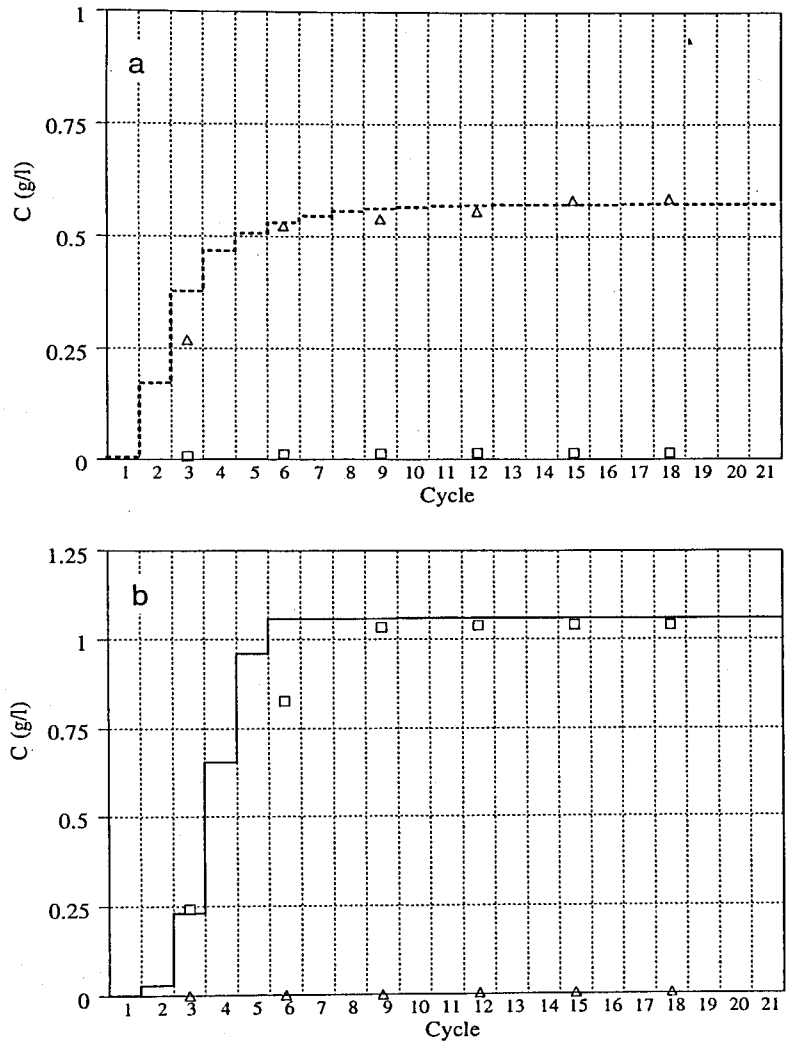


Figure 5.42. Transient evolution of the concentration of both species in the extract (a) and raffinate (b). Points are experimental results; lines are SMB model predictions (average concentrations over each full cycle).

In order to increase the extract purity, we decided to carry out a last run with a lower extract flow-rate. We assume that the internal liquid flow-rates in Sections I and IV were well chosen, which can be supported by the fact that concentrations of both species at the beginning of Section I and at the end of Section IV are zero. In this way, if the extract purity is not 100%, that is because part of the less retained component is carried with the solid in Section II, contaminating the extract stream. To avoid this, we must increase the internal liquid flow-rate in Section II, which corresponds to decreasing the extract flow-rate. The raffinate flow-rate is increased in the same amount. These modifications in the SMB operating conditions lead to higher internal

liquid flow-rates in the two central sections, but keep constant the internal liquid flow-rates in Sections I and IV, and so the ratios between fluid and solid interstitial velocities in these zones.

For the last experimental run we chose an extract flow-rate of $Q_X = 8.37$ ml/min (and a raffinate flow-rate of $Q_R = 4.99$ ml/min), which were checked experimentally. *Table 5.24* summarizes the SMB operating conditions.

Table 5.24. Experimental SMB operating conditions for the chiral epoxide system - Second run.

| Inlet / Outlet Flow-rates (ml/min) | Internal Liquid Flow-rates (ml/min) | Ratio between fluid and solid interstitial velocities |
|---|---|---|
| $Q_E = 12.36$ | $Q_I^* = 33.74$ | $\gamma_I = 4.2957$ |
| $Q_X = 8.37$ | $Q_{II}^* = 25.37$ | $\gamma_{II} = 2.9820$ |
| $Q_F = 1.00$ | $Q_{III}^* = 26.37$ | $\gamma_{III} = 3.1390$ |
| $Q_R = 4.99$ | $Q_{IV}^* = 21.38$ | $\gamma_{IV} = 2.3558$ |

Experimentally, we obtained purities of 98% for both extract and raffinate ($PUX = 98.3\%$, $PUR = 98.0\%$). The model predictions are 100% pure extract and raffinate, using the TMB approach, and $PUX = 99.9\%$ and $PUR = 100\%$ for the SMB model.

The internal concentration profiles were evaluated at cyclic steady-state, after 20 full cycles of continuous operation. The steady-state TMB package was used to compare the theoretical and experimental internal concentration profiles. *Figure 5.43* shows the results obtained. The agreement between experimental and model results is good (see *Figure 5.43c*), except for the concentration profiles of both species in Section III. However, this is due to small variations in the internal liquid flow-rates as it is shown in *Figures 5.43a* to *5.43c*. In fact, drastic variations in the internal concentration profiles of both species can be found due to very small variations in the extract flow-rate; from $Q_X = 8.35$ (*Figure 5.43a*) to $Q_X = 8.37$ ml/min (*Figure 5.43c*). The agreement between experimental and model results is good for an extract flow-rate of $Q_X = 8.36$ ml/min (*Figure 5.43b*), which represents a 0.12% variation from the experimental flow-rate measured.

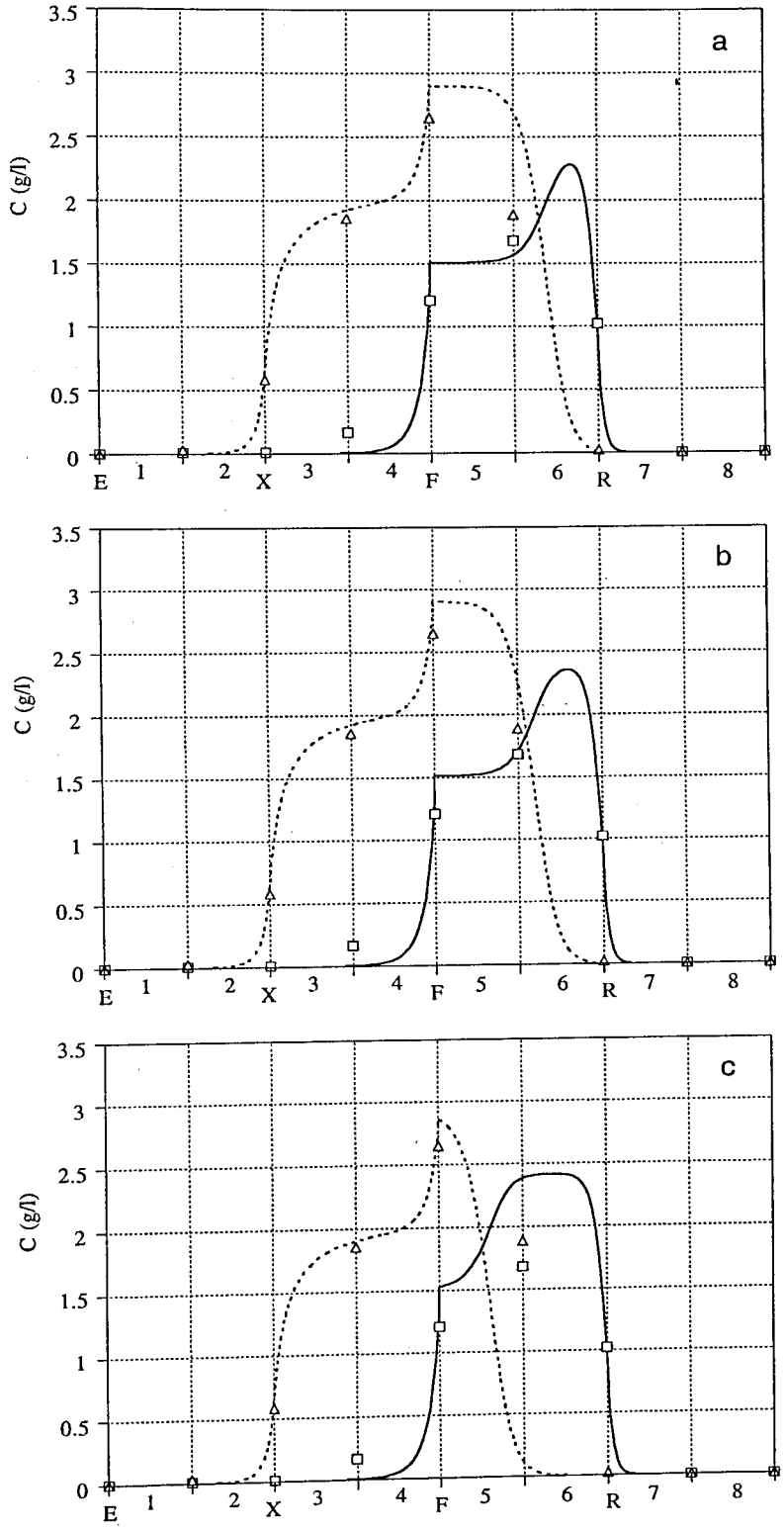


Figure 5.43. Internal concentration profiles: comparison between experimental (points) and simulated (lines) results: (a) $Q_X = 8.35$; (b) $Q_X = 8.36$; (c) $Q_X = 8.37$ ml/min. Squares and full lines represent the less retained component; triangles and dashed lines for the more retained species.

Keeping the same operating conditions summarized in *Table 5.22*, i.e., the same switch time interval, and recycling, eluent and feed flow-rates, we do not expect to obtain a better purity performance than the one obtained in the last run, since the extract and raffinate experimental purities are equal.

This last set of experimental runs in our SMB pilot unit allowed us to achieve a better purity performance: 98% pure extract and raffinate, against 91%. However, it must be mentioned that these last operating conditions lead to lower productivity and higher solvent consumption performances. *Table 5.25* compares the two sets of experimental runs for the chiral epoxide system in terms of all performance parameters.

Table 5.25. Comparison between the two sets of experimental runs for the chiral epoxide system.
(Flow-rates in ml/min, Productivity in grams of racemic mixture processed per day and per liter of bed, Solvent Consumption in liters of mobile phase per gram of racemic mixture processed).

| Run | $Q_E$ | $Q_F$ | $Q^*_{RF}$ | *PUX* | *PUR* | *RCX* | *RCR* | *PR* | *SC* |
|---|---|---|---|---|---|---|---|---|---|
| First Set | 4.53 | 1.52 | 23.20 | 90.0 | 91.6 | 94.5 | 90.7 | 52.1 | 0.40 |
| Second Set | 12.36 | 1.00 | 21.38 | 98.3 | 98.0 | 97.9 | 98.7 | 34.2 | 1.34 |

## 5.4 Conclusions

The *Licosep 12-26* SMB pilot plant was used to carry out the separation of enantiomers of two systems: the bi-naphthol and the chiral epoxide enantiomers.

The competitive adsorption isotherms were experimentally determined for the chiral epoxide system, and a SMB column was used to estimate the axial dispersion and mass transfer coefficients.

The SMB operating conditions were evaluated by using the simulation packages developed in *Chapters 3* and *4* together with the basic data measured experimentally. Experimental results and model predictions were compared in terms of process performance, steady-state internal concentration profiles and transient evolution of the concentration of both species in the extract and raffinate streams.

The agreement between the experimental and model results presented is reasonable, although the experimental purities are a little lower than the ones predicted by modeling. This could be due to several factors, such as flow-rates variations, or an inaccurate description of the binary adsorption equilibrium.

## 5.5 References

Blaschke, G., "Chromatographic Resolution of Chiral Drugs on Polyamides and Cellulose Triacetate," *J. Liq. Chromatogr.* **9**, 341-368 (1986).

Dingenen, J., Somers, I., Pauwels, F., and Van Loon, A., "Enantiomer Separations: Limitations and Possibilities of Preparative Chromatography," *Proceedings of the 9th International Symposium on Preparative and Industrial Chromatography*, M. Perrut, ed., Société Française de Chemie, Nancy, France, p. 359-373 (1992).

Francotte, E., Wolf, R.M., Lohmann, D., and Mueller, R., "Chromatographic Resolution of Racemates on Chiral Stationary Phases. I. Influence of the Supramolecular Structure of Cellulose Triacetate," *J. Chromatogr.* **347**, 24-36 (1985).

Francotte, E. and Junker-Buchheit, A., "Preparative Chromatographic Separation of Enantiomers," *J. Chromatogr.* **576**, 1-45 (1992).

Francotte, E., "Preparative Chromatographic Resolution of Racemates," *Simulated Moving Bed: Basics and Applications*, R.-M. Nicoud, ed., Institut National Polytechnique de Lorraine, Nancy, France, p. 35-53 (1993).

Francotte, E., "Chromatography as a Separation Tool for the Preparative Resolution of Racemic Compounds," *Chiral Separations. Applications and Technology*, S. Ahuja, ed., American Chemical Society, p. 271-308 (1996).

Francotte, E., "Preparation of Drug Enantiomers by Chromatographic Resolution on Chiral Stationary Phases," *The Impact of Stereochemistry on Drug Development and Use*, H.Y. Aboul-Enein, and I.W. Wainer, eds., Chemical Analysis Series, Volume 42, John Wiley & Sons, England, p. 633-683 (1997).

Hesse, G., and Hagel, R., "Eine Vollständige Racemattrennung durch Elutions-Chromatographie an Cellulose-tri-acetat," *Chromatographia* **6**, 277-280 (1973).

Hesse, G., and Hagel, R., "Über Inclusions-Chromatographie und ein neues Retentionsprinzip für Benzolderivate," *Chromatographia* **9**, 62-68 (1976).

Hotier, G., and Nicoud, R.-M., "Chromatographic Simulated Mobile Bed Separation Process with Dead Volume Correction Using Period Desynchronization," U.S. Patent No. 5,578,215 (1996a).

Hotier, G., and Nicoud, R.-M., "Chromatographic Simulated Mobile Bed Separation Process with Dead Volume Correction Using Length Reduction," U.S. Patent No. 5,578,216 (1996b).

Ichida, A., and Shibata, T, "Cellulose Derivatives as Stationary Chiral Phases," *Chromatographic Chiral Separations*, M. Zief, and L.J. Crane, eds., Chromatographic Science Series, Volume 40, Marcel Dekker, New York, USA, p. 219-243 (1988).

Isaksson, R., Erlandsson, P., Hanson, L., Holmberg, A., and Berner, S., "Triacetylcellulose as a Chiral Stationary Phase for High-Performance Liquid Chromatography," *J. Chromatogr.* **498**, 257-280 (1990).

Jacobson, S., Golshan-Shirazi, S., and Guiochon, G., "Isotherm Selection for Band Profile Simulations in Preparative Chromatography," *AIChE J.* **37**, 836-844 (1991).

Koller, H., Rimböck, K.-H., and Mannschreck, A., "High-Pressure Liquid Chromatography on Triacetylcelulose. Characterization of a Sorbent for the Separation of Enantiomers," *J. Chromatogr.* **282**, 89-94 (1983).

Küsters, E., Gerber, G., and Antia, F.D., "Enantioseparation of a Chiral Epoxide by Simulated Moving Bed Chromatography using Chiralcel-OD," *Chromatographia* **40**, 387-393 (1995).

Lim, B.G., Ching, C.B., and Tan, R., "Determination of Competitive Adsorption Isotherms of Enantiomers on a Dual-site Adsorbent," *Sep. Technol.* **5**, 213-228 (1995).

Mazzotti, M., Storti, G., and Morbidelli, M., "Optimal Operation of Simulated Moving Bed Units for Nonlinear Chromatographic Separations," *J. Chromatogr. A* **769**, 3-24 (1997).

Nicoud, R.-M., Fuchs, G., Küsters, E., Antia, F., Reuille, R., and Schmid, E., "Preparative Scale Enantioseparation of a Chiral Epoxide - A Comparison of Liquid Chromatography and Simulated Moving-Bed Adsorption Technology," Proceedings of the 3rd International Symposium on Chiral Discrimination, Tübigen, Germany (1992).

Nicoud, R.-M., Fuchs, G., Adam, P., Bailly, M., Küsters, E., Antia, F., Reuille, R., and Schmid, E., "Preparative Scale Enantioseparation of a Chiral Epoxide: Comparison of Liquid Chromatography and Simulated Moving Bed Adsorption Technology," *Chirality* **5**, 267-271 (1993a).

Nicoud, R.-M., and Seidel-Morgenstern, A., "Adsorption Isotherms: Experimental Determination and Application to Preparative Chromatography," *Simulated Moving Bed: Basics and Applications*, R.-M. Nicoud, ed., Institut National Polytechnique de Lorraine, Nancy, France, p. 4-34 (1993).

Nicoud, R.-M., Bailly, M., Kinkel, J.N., Devant, R.M., Hampe, Th.R., and Küsters, E., "Simulated Moving Bed (SMB): Applications for Enantiomer Separations on Chiral Stationary Phases," *Simulated Moving Bed: Basics and Applications*, R.-M. Nicoud, ed., Institut National Polytechnique de Lorraine, Nancy, France, p. 65-88 (1993b).

Nicoud, R.-M., "A Packing Procedure Suitable for High Flow Rate and High Stability Columns Using Cellulose Triacetate," *LC-GC Int.* **6**, 636-637 (1993).

Oguni, K., Oda, H., and Ichida, A., "Development of Chiral Stationary Phases Consisting of Polysaccharide Derivatives," *J. Chromatogr.* **694**, 91-100 (1995).

Okamoto, Y., "Separate Optical Isomers by Chiral HPLC," *CHEMTECH* March, 176-181 (1987).

Pais, L.S., Loureiro, J.M., and Rodrigues, A.E., "Separation of 1,1'-bi-2-naphthol Enantiomers by Continuous Chromatography in Simulated Moving Bed," *Chem. Engng Sci.* **52**, 245-257 (1997a).

Pais, L.S., Loureiro, J.M., and Rodrigues, A.E., "Modeling, Simulation and Operation of a Simulated Moving Bed for Continuous Chromatographic Separation of 1,1'-bi-2-naphthol Enantiomers," *J. Chromatogr. A* **769**, 25-35 (1997b).

Pais, L.S., Loureiro, J.M., and Rodrigues, A.E., "Modeling Strategies for Enantiomers Separation by SMB Chromatography," *AIChE J.* **44**, 561-569 (1998a).

Pais, L.S., Loureiro, J.M., and Rodrigues, A.E., "Separation of Enantiomers of a Chiral Epoxide by Simulated Moving Bed Chromatography," *J. Chromatogr. A* **827**, 215-233 (1998b).

Peterson, M.A., and Lipkowitz, K.B., "Structure and Dynamics of Cellulose Triacetate," *J. Molecular Structure (Theochem)* **395-396**, 411-423 (1997).

Reid, R., Prausnitz, J., and Poling, B., *The Properties of Gases and Liquids*, 4th Edition, McGraw-Hill (1987).

Rimböck, K.-H., Kastner, F., and Mannschreck, A., "Liquid Chromatography on Triacetylcelulose. Preparative Separation of Enantiomers on an Axially Compressed Column," *J. Chromatogr.* **329**, 307-310 (1985).

Rizzi, A.M., "Band Broadening in High-Performance Liquid Chromatographic Separations of Enantiomers with Swollen Microcrystalline Cellulose Triacetate Packings. I.-Influence of Capacity Factor, Analyte Structure, Flow Velocity and Column Loading," *J. Chromatogr.* **478**, 71-86 (1989).

Ruthven, D.M., *Principles of Adsorption and Adsorption Processes*, John Wiley & Sons, New York, USA (1984).

Seidel-Morgenstern, A., and Guiochon, G., "Modelling of the Competitive Isotherms and the Chromatographic Separation of Two Enantiomers," *Chem. Engng Sci.* **48**, 2787-2797 (1993a).

Seidel-Morgenstern, A., and Guiochon, G., "Thermodynamics of the Adsorption of Tröger's Base Enantiomers from Ethanol on Cellulose Triacetate," *J. Chromatogr.* **631**, 37-47 (1993b).

*Separex*, "A Moving-Bed Chromatograph for Separating Chirals," *Chem. Engng* November, 21 (1992).

*Separex*, "Licosep 12-26 Instruction Manual," Version 1.1 (1994a).

*Separex*, "Purification of Optical Isomers with Continuous Chromatography," 12-Monthly Progress Report, Period: 01/12/93 - 30/11/94 (1994b).

*Separex*, Personal communication (1995).

Shibata, T., Okamoto, I., and Ishii, K., "Chromatographic Optical Resolution on Polysaccharides and their Derivatives," *J. Liq. Chromatogr.* **9**, 313-340 (1986).

Zief, M., "Preparative Enantiomeric Separation," *Chromatographic Chiral Separations*, M. Zief, and L.J. Crane, eds., Chromatographic Science Series, Volume 40, Marcel Dekker, New York, USA, p.337-353 (1988).

Chapter 6

# Conclusions and Suggestions for Future Work

Simulated Moving Bed (SMB) is one of the most powerful and promising techniques for preparative scale chromatography. The simulated countercurrent contact between the solid and the liquid phases maximizes the mass transfer driving force, leading to a significant reduction in mobile and stationary phases consumption when compared with elution chromatography.

The concept of the Simulated Moving Bed was introduced by *UOP* (*Universal Oil Products*) in the early sixties and was applied to numerous hydrocarbon separations. In the seventies, SMB processes have been applied in the carbohydrate industry, namely for the production of high-fructose corn syrup. The SMB technology developed by *UOP* became generally known as the *Sorbex* processes and, nowadays, more than one hundred industrial units are working according to this principle.

With the expiration of the *UOP* patents on SMB technology, other companies developed these chromatographic equipments. This is the case of *Separex* (now *Novasep*), which, in cooperation with the *Institut Français du Pétrole*, developed a commercial SMB plant where the unique rotary valve, used in the *Sorbex* technology, was replaced by a combination of commonly used chromatographic columns and commercial valves.

In the nineties, the SMB technology has found new applications in the areas of fine chemistry and pharmaceuticals. For these applications, we notice that the SMB units are generally smaller and more flexible. For the pharmaceutical industry, it is

crucial that this kind of units can perform fast campaign operations to obtain pure drugs for preliminary biological tests. However, the use of SMB technology is not limited to laboratory tests and, recently, the first industrial units have been built for pharmaceutical applications. SMB technology is particularly appropriate for chiral separations. The resolution of enantiomers is usually a binary separation problem characterized by low selectivities and high costs of eluent and chiral stationary phases.

Modeling and simulation of a chemical engineering process always attracted a special attention since it could lead to significant savings in time and materials. Particularly, the simulation of a Simulated Moving Bed is of crucial importance because the evaluation of the liquid flow-rates at the different sections of the unit, as well as the switch time interval, must be carefully done in order to obtain the desired separation.

The aim of this work was to study by modeling the behaviour of a SMB process, with applications to chiral separations. The problem of modeling a Simulated Moving Bed separation process was analyzed by two different strategies: one, by simulating the system directly, taking into account its intermittent behaviour; other by representing its operation in terms of a true countercurrent system. The first model represents the real SMB and considers the periodic switch of the injection and collection points. The second is developed by assuming the equivalence with the true moving bed, where solid and fluid phases flow in opposite directions.

A comparative study was carried out between these two strategies of modeling. The mathematical models developed were based in the following assumptions: an axially dispersed plug flow model was used to describe the fluid phase flow; the countercurrent solid flow in the TMB approach was represented by a plug flow assumption; the adsorbent particles were considered as homogeneous material and mass transfer between fluid and solid was described by the linear driving force (LDF) approximation. Both models could handle any kind of adsorption equilibrium isotherm.

From the comparative study, we concluded that the prediction of the performance of a SMB operation, and so its flow-rate optimization, can be safely done by using the TMB approach, even when we are dealing with a SMB unit with only two columns per section. Although small differences appear between these two strategies of modeling, they are significant only when a SMB unit with one column per section is considered. Nevertheless, the SMB model will be always useful to characterize the dynamic cyclic behaviour of the internal concentration profiles as it was shown in the

experimental section of this work.

To predict the steady-state performance of a Simulated Moving Bed separation process, one can use the TMB model with obvious advantages in computing time savings. Moreover, if we are interested in characterizing only the steady-state operation, we can develop a steady-state TMB model which is simpler to implement. This strategy was followed in this work to study the influence of the various operating variables and model parameters on the SMB performance.

The effect of the model parameters and operating variables on the SMB performance was analyzed in terms of four parameters: purity, recovery, solvent consumption, and adsorbent productivity. We have shown the influence of the switch time interval, recycling flow-rate, and inlet and outlet flow-rates (eluent, extract, feed, and raffinate). Moreover, these effects were analyzed in terms of the net fluxes of both species in the different sections of the unit.

Also studied was the influence of axial dispersion and mass transfer resistance on the SMB performance. For the system considered, we found that the influence of the axial dispersion on the SMB performance is negligible for Peclet numbers higher than 500, which was the case of the two systems experimentally studied. In what concerns the mass transfer resistance, we concluded that it can affect significantly the performance of the SMB operation. This influence was shown in terms of purity and recovery performances, as well as in terms of the steady-state internal concentration profiles.

The behaviour of a SMB can be systematically analyzed in terms of the net fluxes of species through the unit, which depend on the fluid and equivalent solid velocities, adsorption equilibria, and other model parameters such as axial dispersion and mass transfer resistances.

For the case of a binary system with linear adsorption isotherms and considering negligible dispersion and mass transfer phenomena, very simple formulas can be derived to evaluate the better SMB operating conditions. For non-linear systems, however, the evaluation of the better flow-rates is not straightforward. Moreover, it is well known that, for the majority of the binary systems (chiral mixtures included), the adsorption behaviour must be described with more complex models, such as, the non-linear competitive adsorption isotherm. For this kind of systems, the adsorbed concentration of a component in equilibrium with its concentration in the liquid phase depends not only on its own but also on all other species concentrations. It means that

the ratio between the adsorbed-phase and fluid-phase concentrations that influences the net fluxes of both components in the TMB operation is no longer constant but concentration-dependent.

We used the simulation package developed in this work to predict the separation regions of both enantiomers. These regions are a set of possible values of the net fluxes ratios in Sections II and III of a SMB unit that lead to the separation of both enantiomers, providing that the net fluxes ratios in Sections I and IV are conveniently chosen.

A special focus was put in the study of the influence of mass transfer resistance in these separation regions. We concluded that the mass transfer resistance can reduce significantly the possible set of operating conditions that lead to the desired separation. Moreover, mass transfer resistance can alter the better SMB operating conditions, being this influence emphasized when a higher purity requirement is desired.

The steady-state TMB package was used to predict the better SMB operating conditions and a simple optimization procedure was suggested and tested in the experimental part of this work with reasonable results.

The experimental operation of a Simulated Moving Bed unit was implemented in a *Licosep 12-26* SMB pilot unit (*Novasep, France*), available at the *LSRE*. Two chiral systems were considered: the bi-naphthol and the chiral epoxide enantiomers.

For the bi-naphthol system purities and recoveries higher than 95% were obtained for both extract and raffinate. A 450 ml inventory of stationary phase was used, which corresponds to an adsorbent productivity of 68 grams of racemic mixture processed per day and per liter of bed. The solvent consumption was 1.2 liter per gram of racemic mixture processed.

For the chiral epoxide system, a first set of experimental runs led to purities and recoveries higher than 90%. The inventory of stationary phase used was 420 ml, which corresponds to an adsorbent productivity of 52 grams of racemic mixture per day and per liter of bed, and a solvent consumption of 0.4 liter of mobile phase per gram of racemic mixture processed. In a second set of experimental runs, we obtained 98% pure extract and raffinate, with a productivity of 34 grams per day and per liter of bed, and a solvent consumption of 1.3 liter per gram.

For the chiral epoxide system, a set of independent experiments was carried out to evaluate the model parameters for later use with the simulation packages. In this

way, we experimentally determined and modeled the competitive adsorption isotherms, and evaluated the mass transfer coefficient and Peclet number.

The experimental results obtained in the *Licosep 12-26* SMB pilot unit were reported in terms of process performance, steady-state internal concentration profiles, and transient evolution of the concentration of both species in the extract and raffinate streams. The simulation packages developed in the previous chapters, namely the steady-state TMB model, was used to compare experimental results and model predictions. The dynamic behaviour of the internal concentration profiles under cyclic steady-state operation was also evaluated, and the SMB model was used to compare predicted and experimental profiles.

Generally, the agreement between experimental and model predictions was reasonable, although some discrepancies appeared. They could be due to several factors, such as, experimental flow-rate variations, columns that are not precisely equal, or inaccurate description of the binary adsorption equilibria.

One almost systematic discrepancy appeared between the experimental results and model predictions of the internal concentration profiles of one or the other species in Section II of the SMB unit. Namely, for the less retained component, experimental concentrations in this section were higher than the ones predicted by modeling. This fact influenced the composition of the extract stream, and lower experimental purities were found. The reasons previously described can be used to justify these discrepancies. Alternatively, other models can be used to describe the behaviour of the SMB process, namely a model that takes into account a slow adsorption/desorption kinetic law. This can be carried out in future work.

As it was stated at the beginning of this section, Simulated Moving Bed is one of the most powerful techniques for preparative scale chromatography. Many developments have been made in the last years, namely in what concerns the adsorbent media allowing one to perform difficult separations. The influence of the structure of the adsorbent particles can be an interesting field of study. Because SMB usually works at high flow-rates when compared to common elution chromatography, the use of large-pore materials can improve the performance of the SMB operation.

The simulation packages presented in this work can be useful in the development of control strategies for SMB operation. The study of the influence of the operating variables on the SMB performance shown in this work, can be used to carry out an on-line optimization procedure of the best operating conditions. The dynamic

SMB simulation package can also be helpful to control systems where a low number of columns are used.

Another field of future application of the SMB technology will be the production of high valuable products, such as, amino acids, cosmetics, perfumes and aromas. In the last years, the SMB units have also been adapted to applications that involve reactions. Coupling reaction and separation can be worthwhile, specially when the reaction conversion is limited by equilibrium.

# Appendices

# Appendix A: Influence of the Linear Velocity Upon Plate Height. Experimental Results of Elution Chromatography.

The influence of the linear velocity upon plate height was examined for the microcrystalline cellulose triacetate stationary phase used for the chiral epoxide system. A non-retained compound was used to carry out this study: the 1,3,5-tri-*tert.*-butylbenzene (*Sigma, St. Louis, USA*). The results obtained were presented in *Figure 5.17* (*Chapter 5, Section 5.3.4*). This appendix presents the experimental data used to draw *Figure 5.17.*

Several experiments of elution chromatography were carried out in a HPLC system (*Gilson, Villiers le Bel, France*), using one SMB column at different flow-rates. The outlet concentration was followed by UV detection at 220 nm. *Table A.1* and *Figure A.1* present the results obtained.

The real flow-rate was derived from the weight of a collection vessel measured along the duration of each experiment. The linear velocity was evaluated by

$$v = \frac{Q}{\varepsilon A_c} \tag{A.1}$$

where $Q$ is the flow-rate, $\varepsilon$ is the bed porosity (considered as $\varepsilon = 0.4$), and $A_c$ is the cross section area of the SMB column ($D_c = 2.6$ cm, $A_c = 5.31$ cm$^2$).

The plate height was evaluated by

$$H = \frac{\sigma^2}{t_r^2} L_c \tag{A.2}$$

where $L_c$ is the length of the SMB column ($L_c = 9.9$ cm), $t_r$ and $\sigma^2$ are, respectively, the mean and variance of the eluted peak. They are evaluated through

$$t_r = \frac{\mu_1}{\mu_0} \tag{A.3}$$

and

$$\sigma^2 = \frac{\mu_2}{\mu_0} - \left(\frac{\mu_1}{\mu_0}\right)^2 \tag{A.4}$$

with

$$\mu_0 = \int_{t_i}^{t_f} r(t)dt \tag{A.5}$$

$$\mu_1 = \int_{t_i}^{t_f} r(t)tdt \tag{A.6}$$

$$\mu_2 = \int_{t_i}^{t_f} r(t)t^2dt \tag{A.7}$$

where $r(t)$ is the UV response.

Table A.1. Elution chromatography: experimental results with one SMB column at various flow-rates.
Adsorbent: microcrystalline cellulose triacetate. Mobile phase: methanol.
Solute: 50 µg of the non-retained compound (1,3,5-tri-*tert.*-butylbenzene).

| RUN | Flow-rate $Q$ (ml/min) | Linear velocity $v$ (mm/sec) | Mean $t_r$ (min) | Variance $\sigma^2$ (min$^2$) | Plate height $H$ (µm) |
|---|---|---|---|---|---|
| a | 0.97 | 0.076 | 35.87 | 5.06 | 389 |
| b | 0.97 | 0.076 | 36.12 | 4.77 | 362 |
| c | 1.93 | 0.152 | 18.22 | 0.989 | 295 |
| d | 1.94 | 0.152 | 18.23 | 0.966 | 288 |
| e | 3.86 | 0.303 | 9.172 | 0.261 | 308 |
| f | 3.86 | 0.303 | 9.171 | 0.254 | 299 |
| g | 7.00 | 0.550 | 5.065 | 0.0893 | 345 |
| h | 7.00 | 0.550 | 5.065 | 0.0903 | 349 |
| i | 15.28 | 1.200 | 2.322 | 0.0298 | 547 |
| j | 15.35 | 1.204 | 2.293 | 0.0280 | 528 |
| k | 19.05 | 1.495 | 1.862 | 0.0221 | 632 |
| l | 19.08 | 1.498 | 1.861 | 0.0214 | 611 |
| m | 22.75 | 1.786 | 1.560 | 0.0163 | 664 |
| n | 22.75 | 1.786 | 1.558 | 0.0163 | 664 |

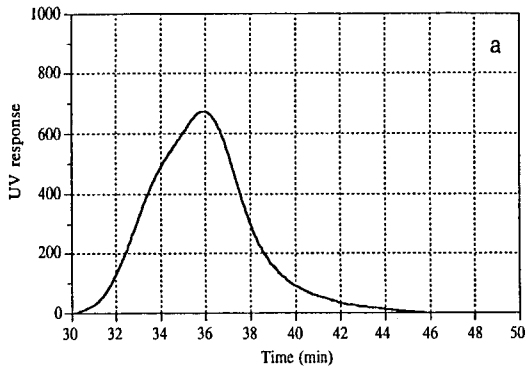
a
UV response
Time (min)

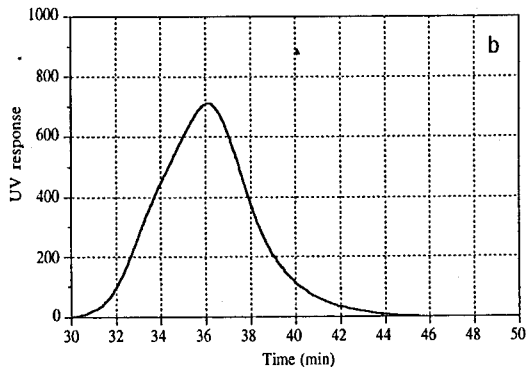
b
UV response
Time (min)

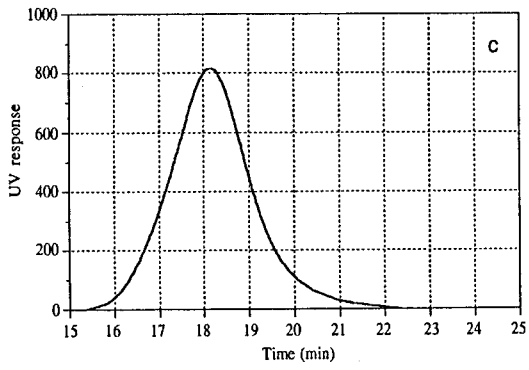
c
UV response
Time (min)

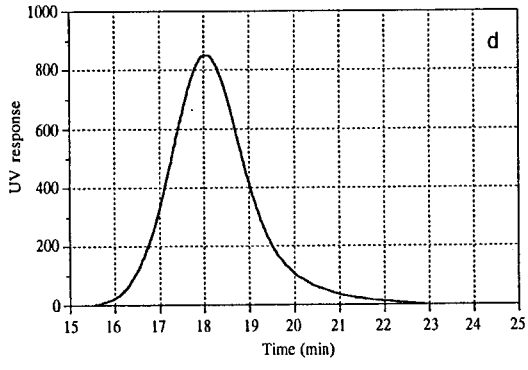
d
UV response
Time (min)

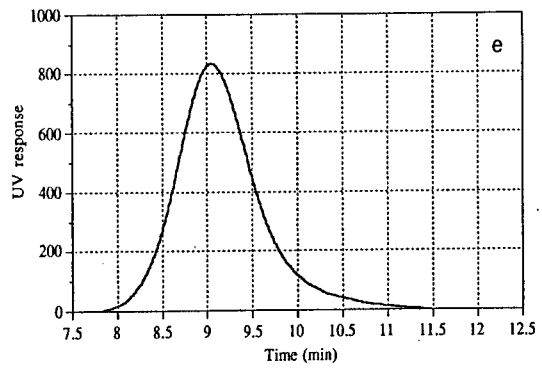
e
UV response
Time (min)

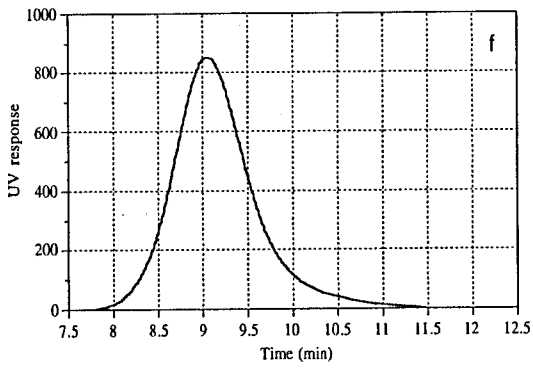
f
UV response
Time (min)

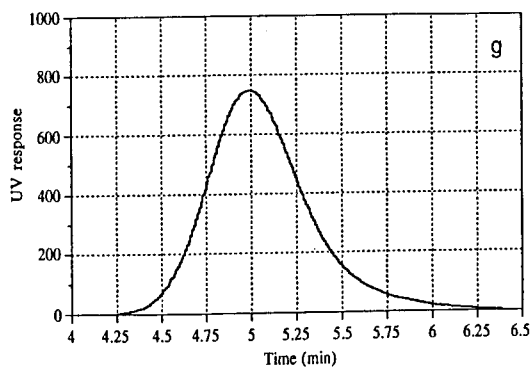
g
UV response
Time (min)

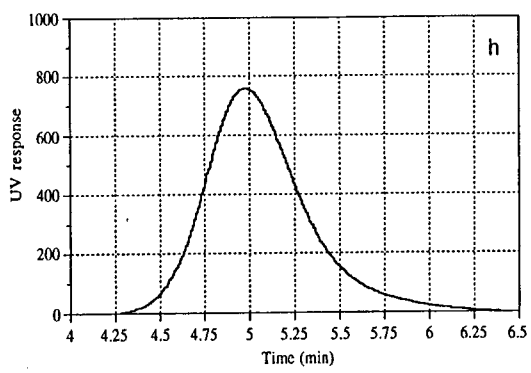
h
UV response
Time (min)

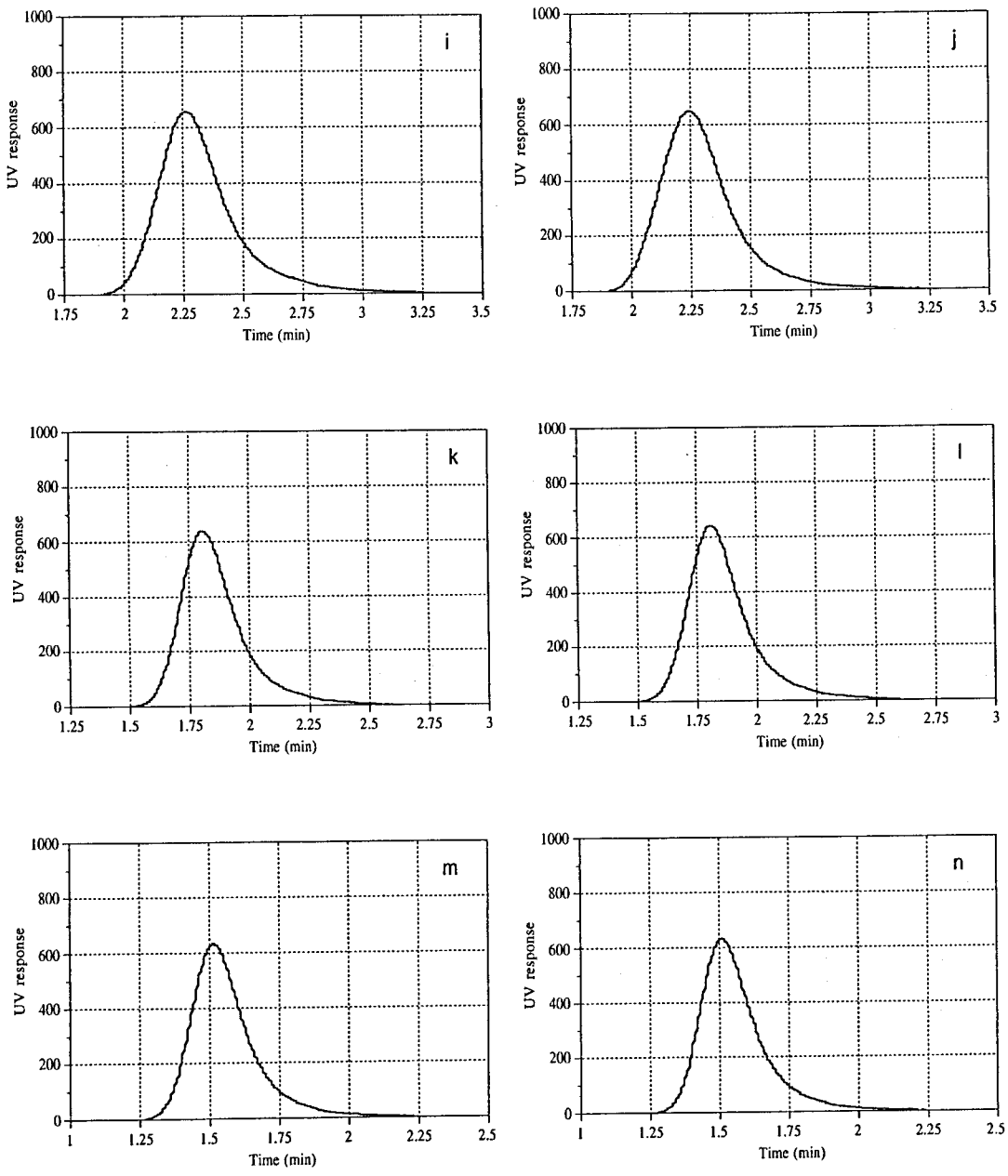


Figure A.1. Elution chromatography: experimental results with one SMB column at various flow-rates (see *Table A.1*). Solute: 50 µg of the non-retained compound (1,3,5-tri-*tert.*-butylbenzene).

# Appendix B: Calibration of the Recycling Pump and of the Flowmeter

The text presented in this appendix was provided by the *Separex* group. It describes the methodology followed to calibrate the recycling pump and the flowmeter of the *Licosep 12-26* SMB pilot unit, using the *manual screen* option of the *Licosep* control software.

The purpose of the experiments described below is to calibrate the recycling pump and the flowmeter. These experiments would better be performed each time a new eluent is used. The parameters $a$, $b$, $c$ and $d$ of the following calibration curves are sought:

$$V = a + bQ_t \tag{B.1}$$

for the recycling pump, and

$$Q_f = c + dI \tag{B.2}$$

for the flowmeter, where $V$ is the electric voltage applied to the recycling pump to get the flow-rate $Q_t$; $Q_f$ is the flow-rate given by the flowmeter and is derived from the electric current $I$ induced by the turbine flowmeter.

The SMB system should be configured as described in *Figure B.1*.

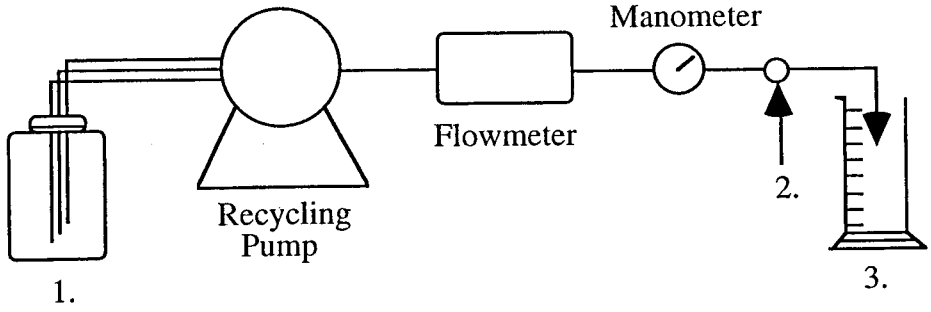


Legend: 1.Vessel filled with the eluent at the separation temperature
2.Valve to set the pump discharge pressure (SMB working pressure)
3.Collection vessel (to be weighed before and after the experiment)

Figure B.1. Experimental configuration of the SMB system for the calibration of the recycling pump and of the flowmeter.

1. Disconnect the inlet of each recycling pump head and connect it to the eluent tank with a large pipe (a 1/4" pipe is suitable). This operation is supposed to lead to a pressure drop as low as possible in the aspiration pipes, and so to avoid cavitation.

2. Connect a manometer to a valve in order to be able to adjust the recycling pump discharge pressure which must be chosen close to the SMB working pressure.

To perform an experiment simply means to run the recycling pump after setting its flow-rate to a value chosen in the range studied. When in the *manual screen*, choose *Pump: flow* in the *Manual pump mode* array and press *F10*. The steps to be followed are:

1. Choose the recycling pump flow-rate. Press *ALT* and *F1* simultaneously and then press *F10* to start the pump.

2. Wait a little bit until the pump is working in steady state and click on the button *ON*. The mean value of the indication given by the flowmeter is calculated from the time *ON* is pressed on to the time *OFF* is pressed on. In the meantime, evaluate the real flow-rate $Q_m$. $Q_m$ is derived from the weight of a collection vessel measured before and after the experiment and from the duration of the collection.

3. At the end of the experiment, check the voltage which was applied to the recycling pump and the mean value of the indication given by the flowmeter.

The voltage applied to the recycling pump $V$ can be read directly from the *manual screen* or, alternatively, can be estimated from the theoretical (expected) flow-rate of the pump $Q_t$ and from the values $a_{old}$ and $b_{old}$ of the $a$ and $b$ parameters used by the software at the time of the experiment:

$$V = a_{old} + b_{old} Q_t \tag{B.3}$$

The $a_{old}$ and $b_{old}$ values can be found in the *manual screen* or in the file C:\LICOSEP\PAR_LICO.INI. This file is made of five lines which are, successively, $a$, $b$, $c$, $d$ and the system dead volume.

The intensity of the current induced by the flowmeter wheel $I$ is calculated from the indication given by the flowmeter $Q_f$ and from the values $c_{old}$ and $d_{old}$ of the $c$ and $d$ parameters used by the software at the time of the experiment:

$$I = \frac{Q_f - c_{old}}{d_{old}} \tag{B.4}$$

The flow-rate given by the flowmeter $Q_f$ is the mean value calculated from the time the button *ON* is pressed on to the time the button *OFF* is pressed on.

At this stage, a set $\{Q_m, V, I\}$ of experimental data is available.

4. Repeat points 1 to 3 to get a new experimental point. To stop the pump, press *ALT* and *F2* simultaneously.

When all the required experiments have been performed, the new values $a_{new}$, $b_{new}$, $c_{new}$ and $d_{new}$ of the $a$, $b$, $c$ and $d$ parameters are just derived from a linear regression involving respectively $(Q_m, V)$ and $(I, Q_m)$. The old values of the parameters should be replaced by the new ones in the *manual screen* and are automatically saved in the PAR_LICO.INI file after we press *F10* and leave the screen.

# Appendix C: Experimental Determination of the Internal Concentration Profiles in a *Licosep 12-26*

The text presented in this appendix describes the methodology followed to determine the internal concentration profiles of the *Licosep 12-26* SMB pilot unit, described in the *Licosep 12-26 Instruction Manual* (*Separex*, 1994).

The SMB internal concentration profiles are determined in such a way as to represent the concentration profiles which could be met in an equivalent TMB. The *Licosep 12-26* internal concentration profiles are determined thanks to the 6-port valve which allows to withdraw samples from the system. To build up complete internal profiles, one full cycle is necessary, one sample being collected at each half-time period.

*Figure C.1* shows typical SMB internal concentration profiles in the case of an 8-column configuration. In this figure, the abscissa gives the positions of the points where the concentrations were measured, relatively to the inlet and outlet lines of an equivalent TMB, the eluent line being at position 1.

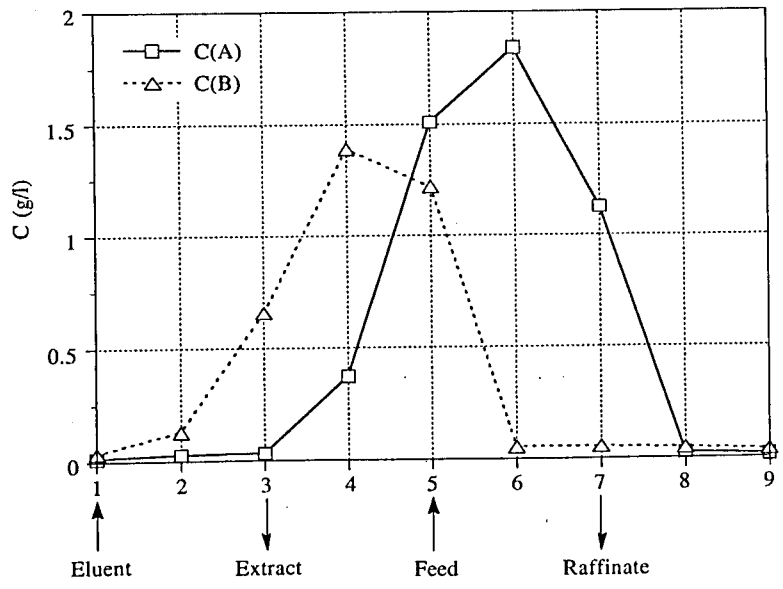


Figure C.1. Typical SMB internal concentration profiles (8-column configuration).

For each position Ei of the eluent line, the sample withdrawn through the 6-port valve leads to the concentration at a different abscissa of *Figure C.1*. In *Table C.1* the eluent line position and its corresponding abscissa in *Figure C.1* are given.

Table C.1. Relation between the position of the eluent line and the abscissa in *Figure C.1*.

| Eluent line position | E1 | E2 | E3 | E4 | E5 | E6 | E7 | E8 |
|---|---|---|---|---|---|---|---|---|
| Abscissa in *Figure B.1* | 1 | 8 | 7 | 6 | 5 | 4 | 3 | 2 |

Consequently, starting when the eluent is at position E1, the sample recovered at the half-time period gives the concentration of the two components for an abscissa equal to 1. The sample collected at the next period gives the concentration for an abscissa equal to 8 and so on. Each sample must of course be analysed to reach the individual concentrations of the two components.

To understand the meaning of the abscissa in *Figure C.1*, it must be kept in mind that the 6-port valve is fixed whereas the injection and collection points of the SMB move. The valve will appear successively in sections IV, III, II and I. The abscissa in *Figure C.1* is related to the number of columns standing between the valve and the eluent line.

The procedure to withdraw a sample from the *Licosep 12-26* through the 6-port valve involves the following steps:

1. The valve being in its *load* position, wash and fill the injection loop (1 ml) with the eluent using the adapted syringe;

2. Switch the valve to its *inject* position;

3. Pump air through the valve, using an empty syringe, to dry its internal tubings and thus avoid an undesirable later dilution of the sample withdrawn;

4. When at the half-time period, switch the valve to its *load* position. The sample sought is now trapped in the injection loop;

5. Put a vial at the purge outlet of the valve and pump air through the valve to make the sample flow out from the waste exit.

As it was pointed out at the beginning of *Chapter 5*, the recycling pump used in the *Licosep 12-26* introduces a dead volume $V_d$, which delays the concentrations leaving the last and entering the first columns. For the recycling pump used (a three-head membrane pump, *Milroyal, Pont St. Pierre, France*) this dead volume is equal to 21 ml. The *Separex* group proposed a dead volume correction accomplished by using a period desynchronization: the injection or collection lines which have passed the last column, during a given cycle, are shifted with a delay equal to

$$t_d = \frac{21}{\frac{(Q_I^* + Q_{II}^* + Q_{III}^* + Q_{IV}^*)}{4}} \qquad \text{(C.1)}$$

Hence, the concentration waves leaving the last column do not enter immediately in the first one; it will enter with a delay equal to $t_d$ (*equation C.1*). On the other hand, the 6-port valve used to withdraw samples from the *Licosep 12-26* is located after the recycling pump and just before the inlet of the first column. Hence, excepting at the beginning of a new full cycle (when the eluent inlet is at the inlet of the first column), a new fraction does not begin at the beginning of a new switch time interval, but only $t_d$ minutes later. This fact must be taken into account in the withdrawal of samples in the 6-port valve. *Table C.2* presents the right moments for the withdrawal of samples at half-time period.

Table C.2. Moments of withdrawal of samples at half-time period.
(*Licosep 12-26* with 8 columns, $t_{1/2} = t^* / 2$).

| Eluent line position | E1 | E2 to E8 |
|---|---|---|
| Moment of withdrawal | $t_{1/2}$ | $t_{1/2} + t_d$ |

FACULDADE DE ENGENHARIA

Rua dos Bragas 4099 PORTO CODEX PORTUGAL
Telef.: 351 2 323201 • Fax: 351 2 319280 • Telex: 27323 FEUP P